JAAVSO

Volume 42
Number 1
2014

The Journal of the American Association of Variable Star Observers

125-Day Spectral Record of the Bright Nova Delphini 2013 (V339 Del)

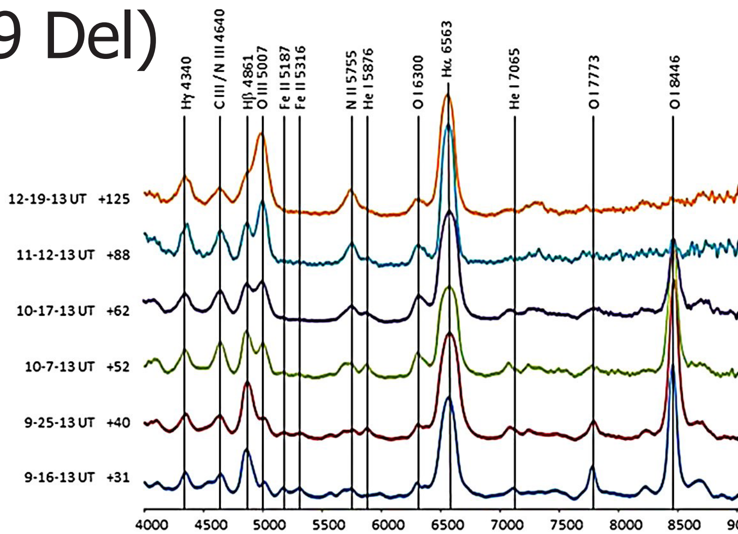

N Del 2013 spectra for days +31 through +125. The appearance of the forbidden lines of N II and O III accompany the disappearance of O I at the transition to the nebular phase.

Also in this issue...

- Amplitude Variations in Pulsating Red Supergiants
- New R CrB and DY Per Star Candidates
- Multicolor CCD Photometry and Analysis of Three Pulsating Variable Stars

Complete table of contents inside...

THE AMERICAN ASSOCIATION OF VARIABLE STAR OBSERVERS
AAVSO
FOUNDED 1911

49 Bay State Road
Cambridge, MA 02138
U. S. A.

ISSN 0271-9053

JAAVSO

The Journal of
The American Association
of Variable Star Observers

Volume 42
Number 1
2014

49 Bay State Road
Cambridge, MA 02138
U. S. A.

ISSN 0271-9053

The *Journal of the American Association of Variable Star Observers* is a refereed scientific journal published by the American Association of Variable Star Observers, 49 Bay State Road, Cambridge, Massachusetts 02138, USA. The *Journal* is made available to all AAVSO members and subscribers.

In order to speed the dissemination of scientific results, selected papers that have been refereed and accepted for publication in the *Journal* will be posted on the internet at the *eJAAVSO* website as soon as they have been typeset and edited. These electronic representations of the *JAAVSO* articles are automatically indexed and included in the NASA Astrophysics Data System (ADS). *eJAAVSO* papers may be referenced as *J. Amer. Assoc. Var. Star Obs., in press,* until they appear in the concatonated electronic issue of *JAAVSO*. The *Journal* cannot supply reprints of papers.

Page Charges

Unsolicited papers by non-Members will be assessed a charge of $15 per published page.

Instructions for Submissions

The *Journal* welcomes papers from all persons concerned with the study of variable stars and topics specifically related to variability. All manuscripts should be written in a style designed to provide clear expositions of the topic. Contributors are strongly encouraged to submit digitized text in MS WORD, LATEX+POSTSCRIPT, or plain-text format. Manuscripts may be mailed electronically to journal@aavso.org or submitted by postal mail to *JAAVSO*, 49 Bay State Road, Cambridge, MA 02138, USA.

Manuscripts must be submitted according to the following guidelines, or they will be returned to the author for correction:

Manuscripts must be:
1) original, unpublished material;
2) written in English;
3) accompanied by an abstract of no more than 100 words.
4) not more than 2,500–3,000 words in length (10–12 pages double-spaced).

Figures for publication must:
1) be camera-ready or in a high-contrast, high-resolution, standard digitized image format;
2) have all coordinates labeled with division marks on all four sides;
3) be accompanied by a caption that clearly explains all symbols and significance, so that the reader can understand the figure without reference to the text.

Maximum published figure space is 4.5" by 7". When submitting original figures, be sure to allow for reduction in size by making all symbols, letters, and division marks sufficiently large.

Photographs and halftone images will be considered for publication if they directly illustrate the text.

Tables should be:
1) provided separate from the main body of the text;
2) numbered sequentially and referred to by Arabic number in the text, e.g., Table 1.

References:
1) References should relate directly to the text.
2) References should be keyed into the text with the author's last name and the year of publication, e.g., (Smith 1974; Jones 1974) or Smith (1974) and Jones (1974).
3) In the case of three or more joint authors, the text reference should be written as follows: (Smith *et al.* 1976).
4) All references must be listed at the end of the text in alphabetical order by the author's last name and the year of publication, according to the following format:
   Brown, J., and Green, E. B. 1974, *Astrophys. J.*, **200**, 765.
   Thomas, K. 1982, *Phys. Rep.*, **33**, 96.
5) Abbreviations used in references should be based on recent issues of the Journal or the listing provided at the beginning of *Astronomy and Astrophysics Abstracts* (Springer-Verlag).

Miscellaneous:
1) Equations should be written on a separate line and given a sequential Arabic number in parentheses near the right-hand margin. Equations should be referred to in the text as, e.g., equation (1).
2) Magnitude will be assumed to be visual unless otherwise specified.
3) Manuscripts may be submitted to referees for review without obligation of publication.

Journal of the American Association of Variable Star Observers
Volume 42, Number 1, 2014

Table of Contents continued on following pages

Table of Contents continued on next page

Amplitude Variations in Pulsating Red Supergiants

John R. Percy
Viraja C. Khatu
Department of Astronomy and Astrophysics, University of Toronto, Toronto, ON M5S 3H4, Canada; john.percy@utoronto.ca

Received October 16, 2013; revised December 5, 2013; accepted December 6, 2013

Abstract We have used long-term AAVSO visual observations and Fourier and wavelet analysis to identify periods and to study long-term amplitude variations in forty-four red supergiants. Of these, twelve stars had data which were too sparse and/or had low amplitude and/or were without conspicuous peaks in the Fourier spectrum; six stars had only a long (2,500–4,000 days) period without significant amplitude variation. The other twenty-six stars had one or two periods, either "short" (hundreds of days) or "long" (thousands of days), whose amplitudes varied by up to a factor of 8, but more typically 2 to 4. The median timescale of the amplitude variation was 18 periods. We interpret the shorter periods as due to pulsation, and the longer periods as analogous to the "long secondary periods" found in pulsating red giants. We discuss possible explanations for the amplitude variations, including the effects of pulsation, rotation, convection cells, and stochastically-excited pulsations.

1. Introduction

Red supergiant stars are extreme and complex objects. Several dozen of them have been intensively studied over the years, on account of their brightness, complexity, and evolutionary importance. Long-term spectroscopic and photometric observations of individual objects such as α Ori (Betelgeuse; Kervella *et al.* 2013), α Sco (Antares; Pugh and Gray 2013a, 2013b), and α Her (Moravveji *et al.* 2010) show complex variability on several time scales, ranging from hundreds to thousands of days.

Kiss *et al.* (2006) have used long-term visual observations from the AAVSO International Database (AID) to study the variability of forty-six pulsating red supergiant stars. They found periods in most of them, and two periods in eighteen stars. The periods divide into two groups: periods of a few hundred days which are probably due to pulsation, and periods of a few thousand days which correspond to the "long secondary periods" (LSPs) in pulsating red giants; the nature of these LSPs is uncertain (Nicholls *et al.* 2009). The shapes of the peaks in the individual power spectra of these stars suggest that pulsation and convection interact strongly, in the sense that the pulsations may be stochastically-excited. The power spectra also exhibit strong 1/f noise, suggestive of irregular photometric variability caused by large convection cells, analogous to the granulation seen in the Sun, but much larger. Percy and Sato (2009) used self-correlation analysis to determine or confirm LSPs in many of these same stars, using the same visual data.

Percy and Abachi (2013), hereinafter Paper 1, have recently used long-term visual observations from the AID to study *amplitude variations* in several samples of pulsating red *giants*: twenty-nine single-mode and thirty double-mode SR stars, ten Mira stars, and the LSPs in twenty-six SR stars. In each case, the amplitude varied significantly, on a time scale (L) which was about 30 to 45 times the pulsation period (P) or the LSP. The fact that L/P is approximately constant for these different groups of stars may be a clue to the origin of the amplitude variations. It suggests that either there is a causal relation between the two processes, or they are both linked to some property of the stars, such as its radius. Christensen-Dalsgaard *et al.* (2001) have pointed out that the pulsations of SR stars may be stochastically-excited, in which case amplitude variations may be due to growth and decay of pulsation modes. In the present paper, we extend Paper 1 to forty-four pulsating red *supergiant* stars.

2. Data and analysis

We used visual observations, from the AAVSO International Database, of the red supergiant variables listed in Table 1. See section 3.2. for remarks on some of these. Our data extend a few years longer than those of Kiss *et al.* (2006).

Paper 1 discussed some of the limitations of visual data which must be kept in mind when analyzing the observations, and interpreting the results. The present study is even more challenging than that of Paper 1, since the periods of red supergiants are even longer than those of red giants, and the timescales of the amplitude variations may be 20 to 40 times these periods.

The data, extending from JD(1) (as given in the table) to about JD 2456300 (except as noted in section 3.2), were analyzed using the VSTAR package (Benn 2013; www.aavso.org/vstar-overview), especially the Fourier (DCDFT) analysis and wavelet (WWZ) analysis routines. As noted by Kiss *et al.* (2006), the peaks in the power spectrum are complex, rather than sharp, and it is not always possible to identify an exact period.

For the wavelet analysis, as in Paper 1, the default values were used for the decay time c (0.001) and time division Δt (50 days). The results are sensitive to the former, but not to the latter. Templeton *et al.* (2005) also used c = 0.001. We used the DCDFT routine to inspect the period spectrum of each star, but we were also guided by the results of Kiss *et al.* (2006) who determined periods for each star, and also listed other periods from the literature. For the WWZ analysis: around each of the true periods, we generated the amplitude as a function of JD graph, and determined the range in amplitude, and the number (N) of cycles of amplitude increase and decrease. As discussed in Paper 1, there was often less than one cycle of amplitude variation, in which case our estimate of N is a crude and possibly unreliable one.

Table 1. Amplitude variability of pulsating red supergiants.

Star	*P(d)*	*JD(1)*	*A Range*	*N*	*L(d)*	*L/P*
SS And*	159	2429500	0.15–0.55	9.5	2789	18
VY CMa*	1440	2440500	0.33–0.52	0.5	41000	26
RT Car*	448	2437000*	0.07–0.31	2.5	6600	15
RT Car*	2060	2437000*	0.07–0.11	<0.5	>39000	>19
BO Car*	330	2439000	0.07–0.27	3.5	5000	15
CL Car*	500	2434800	0.08–0.43	0.5	43400	87
EV Car*	820	2440000	0.10–0.50	0.5	33000	40
TZ Cas	3100	2438000	0.11–0.16	<0.2	>86000	>28
PZ Cas	840	2440000	0.13–0.50	0.5	33000	39
μ Cep*	870	2394500	0.07–0.26	5.0	11800	14
μ Cep*	4525	2394500	0.07–0.09	0.8	80000	18
RW Cyg	645	2416000	0.09–0.19	1.25	32400	50
BC Cyg	700	2439500	0.15–0.51	0.5	33000	46
TV Gem*	426	2431000	0.08–0.29	2.5	9600	23
TV Gem*	2570	2431000	0.16–0.21	<0.2	>96000	>38
α Her*	1550	2425000	0.05–0.09	1.0	31500	20
W Ind*	198	2440000	0.23–0.42	3.75	2933	15
α Ori*	388	2420000	0.03–0.24	5.25	6000	15
α Ori*	2300	2420000	0.08–0.14	0.5	73000	32
S Per*	813	2419000	0.32–0.85	2.25	16670	21
T Per	2500	2410000	0.05–0.10	<0.5	>93000	>37
W Per*	500	2415000	0.20–0.47	3.5	11857	24
W Per*	2875	2415000	0.17–0.19	1.0	41500	14
SU Per	450	2432500	0.07–0.22	2.5	21500	46
SU Per	3300	2432500	0.07–0.22	0.75	32000	10
XX Per*	2400	2422500	0.05–0.10	<0.5	>113000	>47
BU Per*	381	2432500	0.13–0.15	<0.25	>66000	>173
VX Sgr	754	2427500	0.55–1.35	<1.0	>29000	>38
AH Sco	765	2440000	0.38–0.53	1.5	11667	16
α Sco*	1750	2431000	0.10–0.40	0.5	51000	29
CE Tau	1300	2435000	0.06–0.13	0.6	35833	28
W Tri*	680	2431500	0.08–0.11	1.0	25000	37

**See note in section 3.2.*

3. Results

3.1. Summary of results

Interpreting the results is challenging because of the complexity of the stars, the low amplitudes in many stars, and the long time scales involved. Some stars had several low-amplitude peaks in the DCDFT spectra which could not be shown to be significant, unless there was also V data. When the peaks were about a year, and with amplitudes less than 0.1, they might be spurious results of the Ceraski effect (see below). The reality of very long periods was also uncertain if the dataset was short and/or the star showed very long-term irregular variations. In the end, we have been conservative about which stars to include in Table 1, and which to use to draw conclusions.

Table 1 lists the results for each star: the name, period P in days, initial JD, amplitude range, number N, and length L in days of cycles of amplitude variation, and the ratio L/P. An asterisk (*) in the table or in the following paragraphs indicates that there is a note about the star in section 3.2. Especially for the stars with $N \leq 1$, the amplitude range is a lower limit.

The following stars were rejected as supergiants by Kiss *et al.* (2006): UZ CMa, T Cet, IS Gem, and Y Lyn, and are not listed in the table.

Almost all of the stars showed signals at a period of about one year, with an amplitude of a few hundredths of a magnitude. This was most likely due to the Ceraski effect, a physiological effect of the visual observing process. Unless the signal was also present in V data (which would not be subject to this effect), we assumed that the signal was spurious. It is possible, of course, that one or two of these stars had a real low-amplitude period of about a year.

For the following stars, either the data were too sparse, and/or the amplitude was too small, and/or the DCDFT spectrum showed no conspicuous peaks: NO Aur*, CK Car*, IX Car*, W Cep, ST Cep*, AO Cru*, BI Cyg*, WY Gem*, RV Hya*, XY Lyr*, AD Per*, and PP Per*.

The following stars showed possible long (thousands of days) periods, but without any significant variation in amplitude over the timespan of the data: AZ Cyg* (3,600 days), BU Gem (2,500 days), RS Per* (4,000 days), KK Per (3,030 days), PR Per* (3,090 days), and FZ Per* (3,440 days).

Figure 1 shows the light curve and amplitude variation for S Per. Figures 2 and 3 show the light curves and amplitude variations of the "short" and "long" periods of μ Cep and α Ori, respectively. Figure 4 shows the light curve and amplitude variation for VY CMa. Paper 1 shows the amplitude variations for several pulsating red giants; these are similar to those in the red supergiants. The cycles of amplitude change are by no means sinusoidal, but have varying amplitudes themselves.

3.2. Notes on individual stars

SS And In Table 1, we have given results using the literature period of about 120 days, even though that period has an amplitude less than 0.03 in our data. The highest peaks (1,850 ± 100 days) have amplitudes less than 0.05.

NO Aur The star fades noticeably at the end of the (sparse) dataset.

VY CMa The long period is quite conspicuous in the light curve. The DCDFT spectrum includes its aliases.

RT Car A period of about 400± days is present in the V data, as well as in the visual data. The data are sparse after JD 2453000.

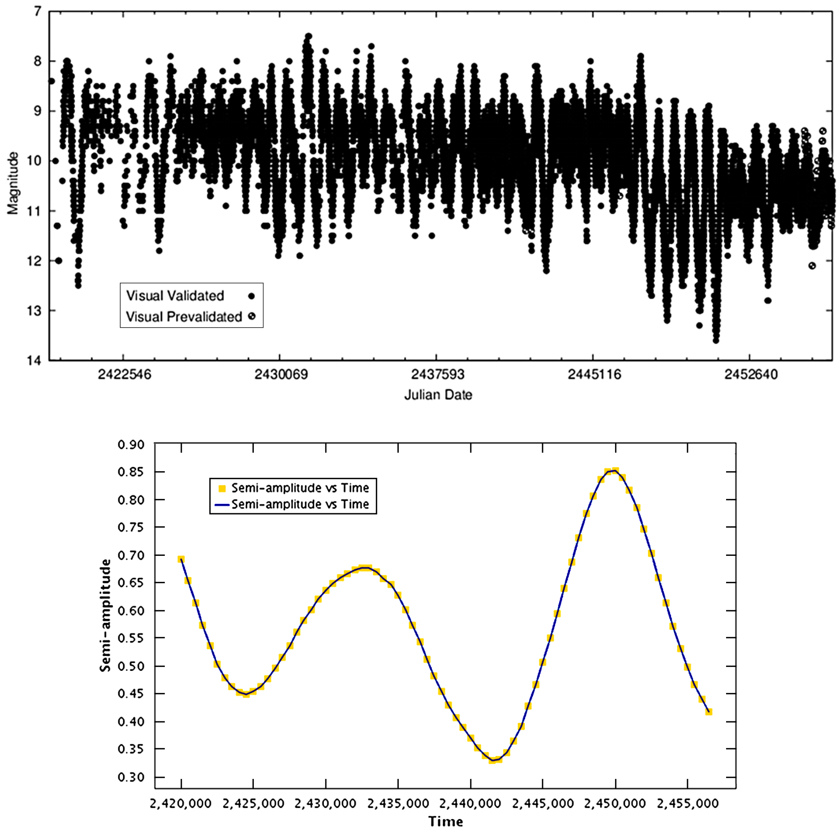

Figure 1. The changing visual amplitude (AAVSO data) of the pulsating red supergiant S Per, with a pulsation period of 813 days. The amplitude varies between 0.35 and 0.85, and there are approximately 2.25 cycles of increase and decrease.

BO Car The 330-day period is sufficiently different from a year that we have accepted it as probably real.

CK Car There is a deep R CrB-like minimum at the start of the dataset, and a possible shallower fading, halfway through the dataset. This makes it difficult to identify any underlying period. There may or may not be a period around 900 to 950 days.

CL Car There are comparable peaks at 500 and 1,350 days which are aliases of each other; the shorter period is the one which seems to be present in the light curve, at least after JD 2452500. The variability before then is not well-defined.

EV Car The data are sparse.

IX Car There is a gap in the data between JD 2441500–2443500. The

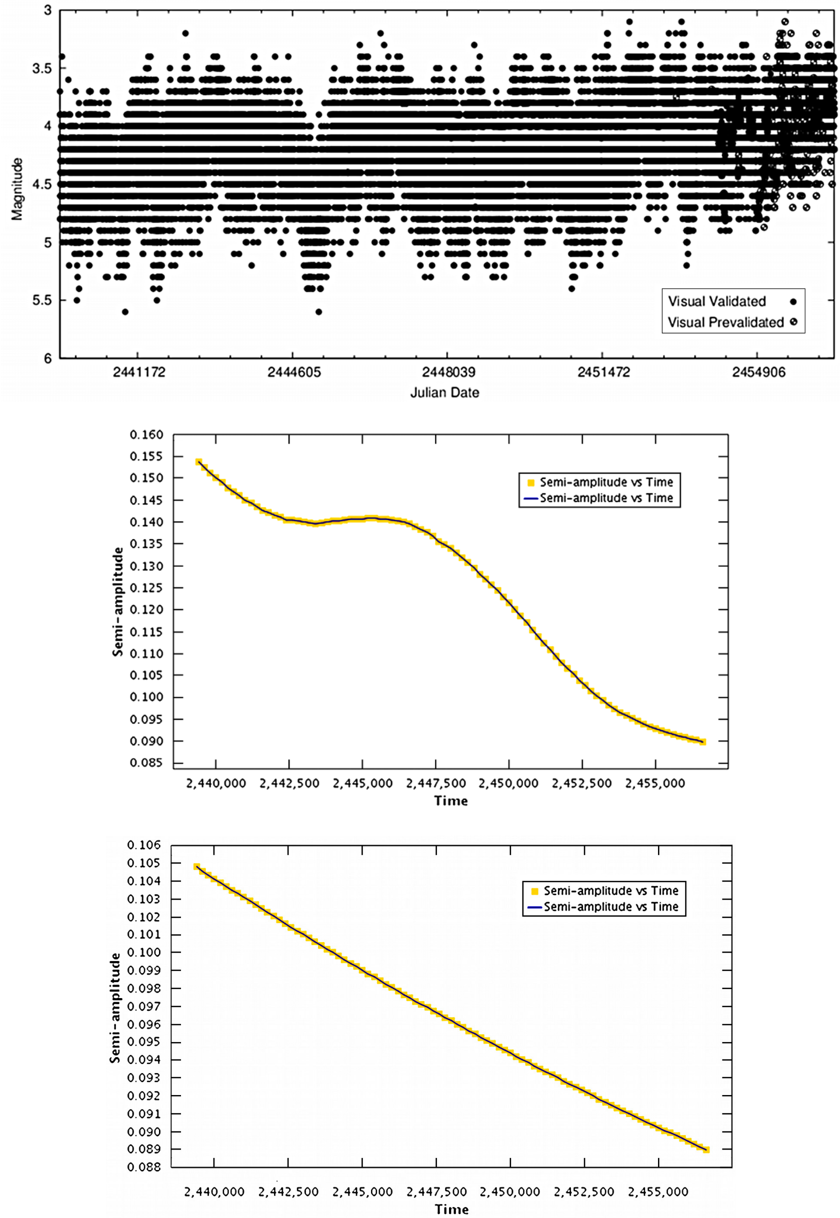

Figure 2. The AAVSO light curve of μ Cep (top), the amplitude of the 870-day period (middle), and the amplitude of the 4,525-day period (bottom).

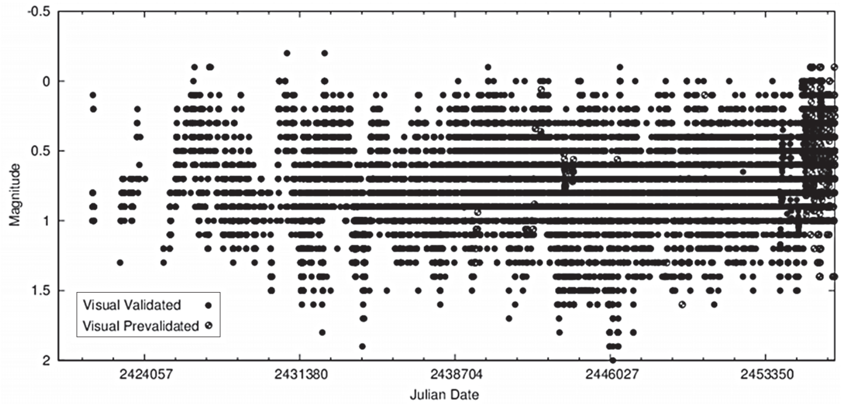

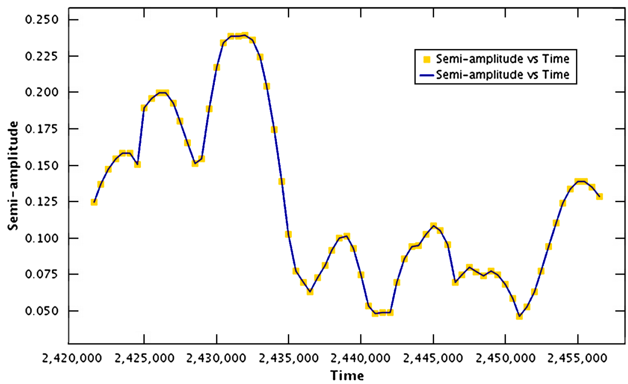

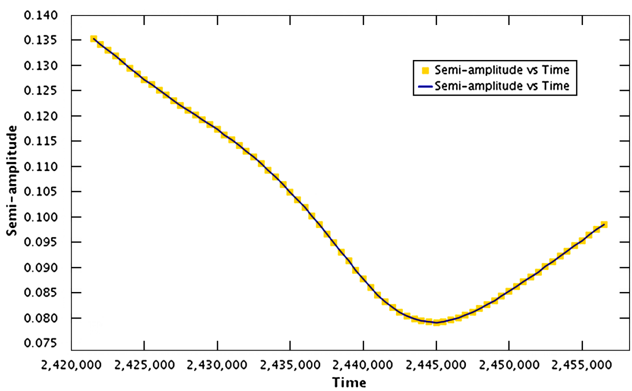

Figure 3. The AAVSO light curve of α Ori (top), the amplitude of the 388-day period (middle), and the amplitude of the 2,300-day period (bottom).

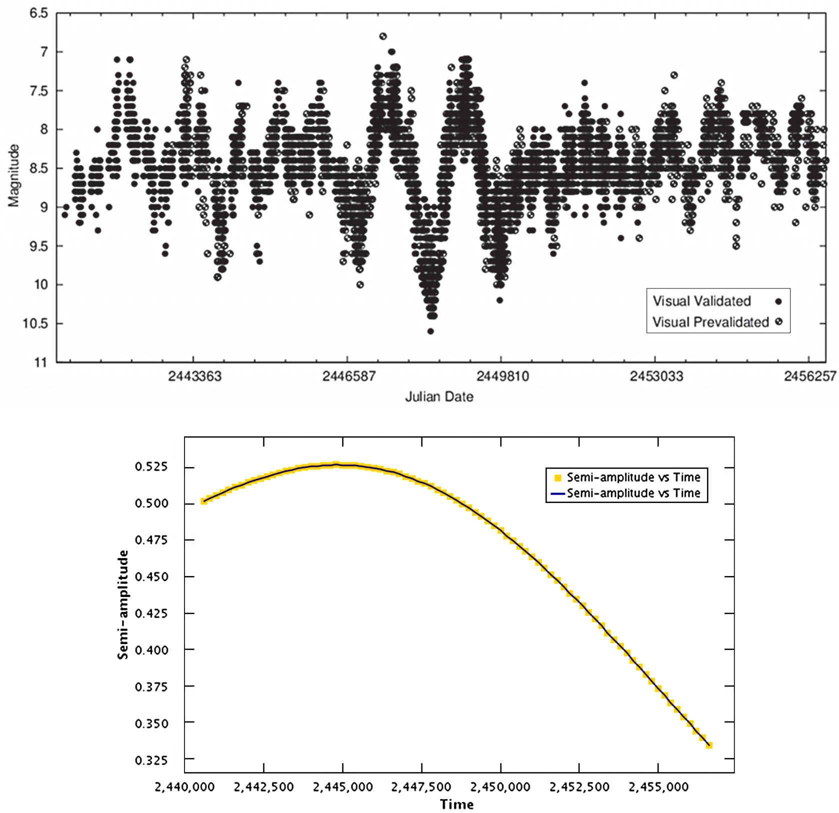

Figure 4. The AAVSO light curve of VY CMa (top), and the amplitude of the 1,440-day period (bottom).

light curve shows a very slow rise and fall from beginning to end. The DCDFT spectrum shows several peaks between 2,000 and 10,000 days which may simply be a mathematical way of representing the very slow variation.

ST Cep The light curve shows very slow variations; the DCDFT spectrum shows several peaks between 2,000 and 10,000 days which may simply be a way of mathematically representing the slow, probably-irregular variations.

μ *Cep* This is a well-observed (visually and photoelectrically) star which is not excessively bright, and therefore much easier to observe than α Ori or α Sco.

AO Cru The 340-day period is close to a year, and of small amplitude; it may well be spurious.

AZ Cyg The light curve shows slow, irregular variations; the DCDFT spectrum shows several peaks between 2,000 and 5,500 days which may simply be a way of mathematically representing the slow, probably-irregular variations. There is no evidence for a significant period around 500 days.

BI Cyg There are many peaks in the range of hundreds and thousands of days, but none stand out.

TV Gem The 426 and 2,550-day periods given by Kiss *et al.* (2006) are aliases of each other.

WY Gem The data are dense, but there are no significant peaks with amplitudes greater than about 0.05 magnitude. This includes the 353-day period reported by Kiss *et al.* (2006), which may be spurious.

α *Her* The period of about 124 days given by Kiss *et al.* (2006) has an amplitude less than 0.03 in our data. The highest peaks are in the range 1,300–1,600 days, and the WWZ results suggest that the long period is in the range 1,500–1,600 days. Moravveji *et al.* (2010) analyzed fifteen years of V-band and three-filter Wing (near infrared) data, and found an LSP of 1,343 days, and other periods around 125 days.

RV Hya The data are very sparse.

W Ind There are very little visual data after JD 2451500, but there are extensive V data. A period of 198 days is present in both datasets.

XY Lyr The literature period of 120 to 122 days has an amplitude less than 0.03 magnitude in our data. The highest peaks, 1850 ± 100 days, have amplitudes less than 0.05 magnitude.

α *Ori* This is the brightest and best-studied pulsating red supergiant, though both visual and photoelectric observations are difficult because of the lack of convenient comparison stars. A workshop about this star has recently been held (Kervalla *et al.* 2013). The period of 388 days (Kiss *et al.* 2006) is present in the V data, but is not prominent in the visual data.

S Per The star fades by about a magnitude towards the end of the dataset.

W Per Our periods agree with the literature periods. The 2,875-day period is clearly visible in the light curve.

RS Per There is a period of 224 days in the V data which does not appear to be present in the visual data.

XX Per The literature periods are 4,100 and 3,150 ± 1,000 days; the latter is not inconsistent with our period of 2,400 days.

AD Per Peaks are at the long period of 3,240 days, and at one year; the latter is not present in the V data, and is probably spurious.

BU Per There is a large gap in the middle of the dataset. There are peaks near a year, which are probably spurious. In the table, we have given results for the 381-day period (which may not be real). There are peaks at 3,700 and 5,500 days (which are possibly aliases of each other); a time scale of about 5,500 days appears to be present in the light curve.

FZ Per The V data do not support a period of about a year, which is present in the visual data, and is almost certainly spurious.

PP Per The only peak is at one year.

PR Per Peaks are at the long period of 3,090 days, and at one year. The amplitude of the long period increases only slightly.

α Sco Both visual and photoelectric observations of this bright star are challenging, because of the lack of convenient comparison stars. The most recent long-term spectroscopic and photometric studies of its variability are by Pugh and Gray (2013a, 2013b). We find evidence in the WWZ analysis for periods in the range of 1000–2000 days.

W Tri The period of about 107 days given by Kiss *et al.* (2006) has an amplitude less than 0.03 in our data. The highest peaks are at 595 and 765 days, both with amplitudes of about 0.07 magnitude. The WWZ contours suggest that both of these periods are present, with variable amplitude, with N ~ 1.0.

4. Discussion

All of the twenty-six stars in Table 1 show amplitude variations although, in some cases, they are small—a few hundredths of a magnitude. They are, of course, lower limits to what might be observed if the dataset was much longer. The timescales of the amplitude variation of the stars for which this timescale is reasonably well-determined—those with one or more cycles of increase and decrease—have a median value of 18 periods, with some uncertainty. This value is similar for the short periods and the long ones. In the pulsating red giants (Paper 1), this ratio was 30–45, which is significantly greater than for the supergiants. As noted above, the cycles of amplitude variation are not sinusoidal, but have varying amplitudes themselves.

Photometric observations of red supergiants in both the Milky Way and the Magellanic Clouds suggest that the "short" period is to be identified with pulsation, and the "long" period with the long secondary periods in red giants. Pugh and Gray (2013b) have identified an additional period of 100 days in α Sco A which is present in long-term spectroscopic observations, but not in photometry. They suggest that it is a convection-driven non-radial p-mode.

Paper 1 raised the hypothesis that the amplitude variations might be associated with the rotation of a star with large-scale convective regions. Both simulations and observations show that red supergiants have such regions on their surfaces (Chiavassa *et al.* 2010). The approximate uniformity of the L/P values suggests that there is some link between the period P and the process which causes the amplitude variations. Stars which are larger pulsate more slowly and rotate more slowly, although the exact relation between these two time scales depends on the distributation of mass and of angular momentum in the star. The rotation period of a star is $2\pi R(\sin i)/(v \sin i)$, where R is the radius and $(v \sin i)$ is the measured projected equatorial rotation velocity. Fadeyev (2012) gives the radii of SU Per and W Per as 780 and 620 solar radii, respectively. The rotation periods are therefore 31,000 $(\sin i)/(v \sin i)$ and 39,000 $(\sin i)/(v \sin i)$ days, respectively. The measured values of $(v \sin i)$ are very uncertain; for α Ori, the value is probably a few km/s (Gray 2000, 2013). If this value also applies to SU Per and W Per, then, using an average value of sin i of 0.7, the rotation periods are not inconsistent with the values of L, which are 21,500 and 11,900 days, respectively, with considerable uncertainty.

Bedding (2013) has suggested a simpler explanation for the amplitude variability in both the red supergiants, and the red giants (Paper 1): amplitude variability is to be expected for stochastic oscillations. Such oscillations are continuously excited by convection at the same time as being damped with a certain e-folding lifetime. Kiss *et al.* (2006) used Lorentzian fits to the power spectra of six red supergiants to estimate their mode lifetimes in days: W Per (1,200), TV Gem (286), α Ori (1,140), α Her (1,060), VY CMa (2,800), and S Per (2,240). These lifetimes are an order of magnitude shorter than the values of L—the lengths of the cycles of amplitude increase and decrease in Table 1.

Amplitude variations are also discussed explicitly by Christensen-Dalsgaard *et al.* (2001) in the context of semiregular (SR) pulsating red *giants*. They determined the rms scatter of the amplitudes of SR variables, using AAVSO visual data, and compared this with the mean amplitudes of the stars. For variables with visual amplitudes less than about 1.5 magnitude, they find that the scatter is proportional to the mean amplitude, which is what would be expected for stochastically-excited pulsations. For larger-amplitude stars, they find that the scatter is independent of the mean amplitude. This might be because the visual amplitudes of these stars are much higher than the bolometric amplitudes, or because a single mode is excited in more luminous stars (rather than two or more modes in the less luminous stars), or because pulsation in the more luminous stars is driven by the standard kappa mechanism, or a mixture of these reasons. The amplitude variations shown in Figure 2 of their paper, for an artificial time series for an oscillation with a period of 82 days, are not unlike those that we observe in pulsating red giants and supergiants. We note also that Fadeyev (2012) has constructed models of red supergiants, and found them to be unstable against fundamental-mode radial pulsation, the driving mechanism being the standard kappa mechanism in the hydrogen and helium ionization zones. The explanation for the complex variability behavior of red supergiants may therefore be a mixture of processes.

Our paper also has an important education application: author VK is an astronomical sciences major at the University of Toronto, and this is her first formal research project—a useful contribution to science, and an interesting (we hope) example, for observers, of how their observations contribute to both science and education.

5. Conclusions

We have identified one or two periods in twenty-six of forty-four red supergiants, using Fourier analysis of sustained, systematic visual observations. All these periods have amplitudes which vary by factors of up to 8 (but more typically 2 to 4) on time scales which are typically about 20 times the period.

The "short" periods (hundreds of days) are presumably due to pulsation. The "long" periods are analogous to the long secondary periods in red giants; their cause is not known for sure. But there is observational and theoretical evidence for large-scale convection in these stars, so a combination of pulsation, convection, and rotation may combine to produce the complex variations that are observed in these stars.

6. Acknowledgements

We thank the hundreds of AAVSO observers who made the observations which were used in this project, and we thank the AAVSO staff for processing and archiving the measurements. We also thank the team which developed the VSTAR package, and made it user-friendly and publicly available. We are especially grateful to the referee, Professor Tim Bedding, for his comments on the manuscript, and his suggestion of a plausible explanation for the amplitude variations. This project made use of the SIMBAD database, which is operated by CDS, Strasbourg, France.

References

Bedding, T. R. 2013, private communication (November 18).

Benn, D. 2013, VSTAR data analysis software (http://www.aavso.org/node/803).

Chiavassa, A., Haubois, X., Young, J. S., Plez, B., Josselin, E., Perrin, G., and Freytag, B. 2010, *Astron. Astrophys.*, **515A**, 12.

Christensen-Dalsgaard, J., Kjeldsen, H., and Mattei, J. A. 2001, *Astrophys. J.*, 562, L141.

Fadeyev, Y. A. 2012, *Astron. Lett.*, **38**, 260.

Gray, D. F. 2000, *Astrophys. J.*, **532**, 487.

Gray, D. F. 2013, private communication (September 24).

Kervella, P., Le Bertre, T., and Perrin, G. (eds.). 2013, *Betelgeuse Workshop 2012*, EAS Publ. Ser. 60, EDP Sciences, Les Ulis, France.

Kiss, L. L., Szabó, G. M., and Bedding, T. R. 2006, *Mon. Not. Roy. Astron. Soc.*, **372**, 1721.

Moravveji, E., Guinan, E. F., Wasatonic, R., Sobouti, Y., and Nasiri, S. 2010, *Astron. Space Sci.*, **328**, 113.

Nicholls, C. P., Wood, P. R., Cioni, M.-R. L., and Soszyński, I. 2009, *Mon. Not. Roy. Astron. Soc.*, **399**, 2063.

Percy, J. R., and Abachi, R. 2013, *J. Amer. Assoc. Var. Star Obs.*, in press (http://www.aaavso.org/sites/default/files/jaavso/ej243.pdf).

Percy, J. R., and Sato, H. 2009, *J. Roy. Astron. Soc. Canada*, **103**, 11.

Pugh, T., and Gray, D. F. 2013a, *Astron. J.*, **145**, 38.

Pugh, T., and Gray, D. F. 2013b, *Astrophys. J.*, **777**, 10.

Templeton, M. R., Mattei, J. A., and Willson, L. A. 2005, *Astron. J.*, **130**, 776.

New R Coronae Borealis and DY Persei Star Candidates and Other Related Objects Found in Photometric Surveys

Sebastián Otero
AAVSO Headquarters, 49 Bay State Road, Cambridge, MA 02138; address email correspondence to sebastian@aavso.org

Stefan Hümmerich
Stiftstr. 4, Braubach, D-56338, Germany

Klaus Bernhard
Kafkaweg 5, Linz, 4030, Austria

Igor Soszyński
Warsaw University Observatory, Al. Ujazdowskie 4, 00-478 Warszawa, Poland

Received January 29, 2014; revised April 7, 2014, and May 6, 2014; accepted May 7, 2014

Abstract We have carried out a search for new R Coronae Borealis (RCB) variables using the publicly accessible data from various photometric sky surveys and—whenever available—AAVSO visual data. Candidates were selected from Tisserand's "Catalogue enriched with R CrB stars" and by a visual inspection of light curves from the ASAS-3, MACHO, NSVS and OGLE surveys. We have identified two new RCB stars, four RCB candidates, and one DY Persei (DYPer) star candidate. Our identification was based mainly on photometric variability, color-color diagrams, and further information drawn from various catalogue sources; spectroscopic classifications were also reported in our analysis whenever available. Additionally, we present a sample of interesting stars which—although showing similar photometric variability—can be ruled out as RCB and DYPer stars or have been rejected as such on spectroscopic grounds in recent studies. Although not useful in the investigation of the aforementioned groups of variables, these objects defy an easy classification and might be interesting targets for follow-up studies which we encourage for all stars presented in this paper.

1. Introduction

R Coronae Borealis (hereafter RCB) stars are a rare class of variables characterized by peculiar chemical composition (notably hydrogen deficiency and carbon overabundance) and unusual photometric variability (irregular and unpredictable fading events). They are a poorly understood class of variables and controversy about their origin is still going on, with recent evidence favoring the Double Degenerate (DD) over the Final Helium Shell Flash (FF) scenario (see, for example, Clayton (2012)).

In order to better understand these enigmatic objects, it is imperative to increase the sample of known RCB stars. With the advent of photometric surveys, progress has been made in this respect. Furthermore, it has been shown that near- and mid-infrared color-color diagrams and cuts are a viable and efficient method of identifying new RCB candidates (see, for example, Feast (1997); Alcock *et al.* (2001); Tisserand *et al.* (2004); and Tisserand (2012)). At the time of this writing, the number of confirmed RCB stars has increased to 76 galactic and 22 extragalactic objects (Tisserand *et al.* 2013b).

Among the RCB variables, DY Persei (hereafter DYPer) stars have been of special interest for being situated at the lower end of the temperature scale. Recently, however, evidence has been mounting that DYPer stars might have more in common with ordinary carbon stars than with other RCB variables (see, for example, Tisserand *et al.* (2009) and Soszyński *et al.* (2009)). In addition to their lower temperatures, they generally show slower declines with smaller amplitudes and roughly symmetric recoveries. Furthermore, they are fainter on average and their pulsational periods tend to be longer than those of typical RCB stars. They are further set aside by a relatively high amount of ^{13}C in their spectra—an isotope of carbon, whose shortage or absence is one of the defining characteristics of classical RCB stars (see, for example, Lloyd Evans (2010)). However, the characterization of the DYPer stars still suffers from an insufficient sample size. Increasing the number of known DYPer stars is therefore an important task.

This paper presents two new RCB stars, four RCB candidates, and one DYPer candidate that have been found using data from various photometric surveys. To achieve this, two different approaches were taken. Firstly, candidates from the VizieR online version of the “Catalogue enriched with R CrB stars” (Tisserand 2012) were investigated using data from various sky surveys and catalogues. Secondly, preselected light curves from the ASAS-3 (Pojmański 2002), MACHO (Alcock *et al.* 1997), NSVS (Woźniak *et al.* 2004b), and OGLE (Udalski *et al.* 1997) surveys were inspected visually for stars showing conspicuous fading events. It is important to note that, for the present paper, the identification of a star as a possible RCB or DYPer candidate has been based primarily on the object’s photometric behavior. Further information drawn from color-color diagrams and various catalogue sources has also been included in the analysis.

Additionally, we present a choice sample of interesting stars which—although showing similar photometric variability—can be ruled out as RCB and DYPer stars or have been rejected as such on spectroscopic grounds in recent studies. Although not useful in the investigation of the aforementioned groups of variables, these objects defy an easy classification and might be interesting targets for follow-up studies.

2. Target stars

2.1. Overview

An overview providing essential data of all variables studied in this paper is given in Table 1. Objects have been sorted by proposed type (RCB / RCB: / DYPer: / SR:) and then by right ascension. Each object is discussed in detail below. For a general definition of variability types, refer to the Variable Star Type Designations in VSX (Otero *et al.* 2013), which are based on the *General Catalogue of Variable Stars* (GCVS; Samus *et al.* 2007–2013) variability types documentation with expansions and revisions from the literature.

2.2. Near- and mid-infrared color-color diagrams

Color-color diagrams have been successfully employed in the investigation of RCB variables (see, for example, Feast (1997), Alcock *et al.* (2001), Tisserand *et al.* (2004), and Tisserand (2012)). We have used near- and mid-infrared color-color diagrams, based on data from the 2MASS and WISE (Cutri *et al.* 2012) catalogues, to investigate all stars presented in this paper.

2.2.1. (J–H) vs. (H–K) diagram

As dust forms and disperses, the colors of RCB stars change. Feast (1997) employed (J–H) vs. (H–K) diagrams and found them to be valuable tools in the investigation of RCB color evolution. Furthermore, they can be used to effectively identify RCB stars and discriminate them from the related DYPer variables (see, for example, Alcock *et al.* (2001) and Tisserand *et al.* (2004)).

A (J–H) vs. (H–K) diagram for all stars presented in this paper is shown in Figure 1. The solid line indicates the colors of SMC carbon stars, as computed by Westerlund *et al.* (1991) and employed in this particular context by Tisserand *et al.* (2004). The dashed line indicates the loci of a combination of two blackbodies, representing the photosphere of the star (~5500 K) and the dust shell (~900 K), as devised by Feast (1997). The flux ranges from "all star" (lower end) to "all shell" (upper end).

As becomes obvious from Figure 1, the present sample is separated into two distinct groups. The two RCB stars and the RCB candidates (denoted by colored squares) roughly follow the dashed line that outlines their possible range in color that is due to the amount of circumstellar dust. The DYPer candidate, on the other hand, is situated near the expected loci of classical carbon stars, which also holds true for the set of miscellaneous variables which have been shown to undergo significant fading events but have been ruled out as RCB or DYPer stars on various grounds (section 3). The displacement of OGLE-II BUL-SC18 64562 towards redder colors might be explained by the heavy extinction in this specific region towards the Galactic Bulge.

Table 1. Essential data on all variables studied in this paper, sorted by proposed type and right ascension.

Identifiers	*R.A. (J2000)*	*Dec. (J2000)*	*Type*	*Range*	*Period*	*Remarks*
ASAS J050232–7218.9 OGLE-IV LMC507.21.5 GSC 09169-00810 2MASS J05023226–7218534	05 02 32.270	–72 18 53.58	RCB	13.5–<18.1 V	43.1 d	In the LMC, Spectral type C2,2Hd. J–K = 0.46; B–V = 1.34.
AO Her IRAS 17343+5026 2MASS J17353628+5024398	17 35 36.284	+50 24 39.88	RCB	10.7–<19.6: V		Spectroscopically confirmed. J–K = 3.59; B–V = 1.86.
NSVS J0051273+645649 GSC 04025-00779 IRAS 00483+6440	00 51 28.114	+64 56 51.72	RCB:	13.2–15.0: V	29.8 d	J–K = 1.76; B–V = 1.48.
IRAS 04519+3553 2MASS J04552045+3558079	04 55 20.456	+35 58 07.98	RCB:	>12.5–<16.0 CV	438 d	J–K = 4.18. Large amplitude pulsations?
IZ Sgr GSC 06279-00870 IRAS 18335–2101	18 36 31.256	–20 59 15.49	RCB:	12.2–<17.0 V 13.3–19.1 B >12.9–<17.6 R		Reported spectral type of M6 erroneous? J–K = 3.00.
NSVS 1461135 GSC 04282-00656 IRAS 23004+6300	23 02 28.518	+63 16 31.04	RCB:	12.8–14.2 R1		J–K = 1.47; B–V = 0.63.

Table continued on next page

Table 1. Essential data on all variables studied in this paper, cont.

Identifiers	*R.A. (J2000)*	*Dec. (J2000)*	*Type*	*Range*	*Period*	*Remarks*
MACHO 128.21543.435	18 06 31.549	–28 34 30.14	DYPer:	17.9–20.5: V	75.6 d	J–K = 1.71.
EROS2–cg6143l34028				15.0–17.15 R_c	66.4 d	
2MASS J18063154–2834301				12.7–<14.4 I_c		
ASAS J095221–4329.8	09 52 21.381	–43 29 40.52	SR:	10.4–13.0 V	~65 d	Spectral type M6;
CD–42 5700						“strong TiO, VO; H?”
IRAS 09503–4315						J–K = 1.29; B–V = 1.78.
ASAS J123034–7703.9	12 30 34.218	–77 03 52.75	SR:	10.0–12.7 V	~273 d	Si emission at 9.7 μm.
GSC 09416-00380						J–K = 1.67, B–V = 2.26.
IRAS 12274–7647						
OGLE-II BUL-SC18 64562	18 06 46.557	–27 22 06.31	SR:	13.4:–15.8: I_c	~60 d	J–K = 2.47, V–I = 4.92.
OGLE-BLG-LPV-210930						
OGLE-IV BLG518.06.142574						
2MASS J18064655–2722063						
NSV 12817	20 09 03.882	–49 41 25.57	SR:	10.5 – 12.3 V	50.93 d	J–K = 1.20, B–V = 1.58.
CD–50 12825						
IRAS 20054–4950						

Note: Positional data were taken from 2MASS (Skrutskie et al. 2006; IRAS 04519+3553, IZ Sgr, MACHO 128.21543.435, OGLE–II BUL–SC18 64562) and UCAC4 (Zacharias et al. 2012; all other objects).

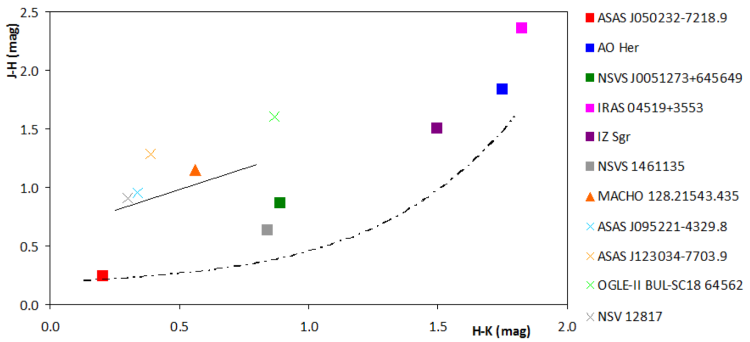

Figure 1. (J–H) vs. (H–K) diagram for all stars presented in this paper, as indicated in the legend on the right side. In order to facilitate discrimination, RCB stars and RCB candidates are denoted by squares, the proposed DYPer variable by a triangle and the non-RCB faders of section 3 by crosses. Data were drawn from the 2MASS catalogue. The solid line illustrates the colors of SMC carbon stars (Westerlund *et al.* 1991). The dashed line indicates the loci of a combination of two blackbodies, representing the photosphere of the star (~5500 K) and the dust shell (~900 K), as devised by Feast (1997).

Our findings are in very good agreement with the results of other researchers (see in particular Figure 9 of Alcock *et al.* (2001) and Figure 7 of Tisserand *et al.* (2004)), which provides additional support that the proposed classifications for the stars of the present sample, which will be enlarged on in the following sections, are valid.

2.2.2 (W2–W3) vs. (W3–W4) diagram

Tisserand (2012) employed mid-infrared color-color cuts based on WISE photometry to identify new RCB candidates. WISE surveyed the whole sky in the four infrared bands W1, W2, W3, and W4, which are centered at 3.4, 4.6, 12, and 22 μm, respectively (Wright *et al.* 2010). Following his approach, we have plotted a (W2–W3) vs. (W3–W4) diagram for all stars presented in this paper (Figure 2). The dashed line indicates selection cut (1) of Tisserand (2012) which effectively identifies objects with a clear shell signal (see in particular Figure 6). Because of the known bias for bright objects in the WISE W2-band, which leads to the overestimation of the brightness by up to one magnitude (see, for example, Tisserand (2012)), we have corrected the corresponding W2 magnitudes for IRAS 04519+3553 and ASAS J123034-7703.9 (Tisserand 2014; private communication). Unfortunately, WISE contamination flags indicate an uncertain value in the W2-band for ASAS J123034-7703.9.

Most RCB stars and candidates presented in this paper are well inside the denoted region on the diagram, with the exception of NSVS 1461135. The latter object's position is reminiscent of the position of MV Sgr in the respective diagram of Tisserand (2012) which shows the star well outside the expected location of RCB variables. According to the aforementioned author, MV Sgr and

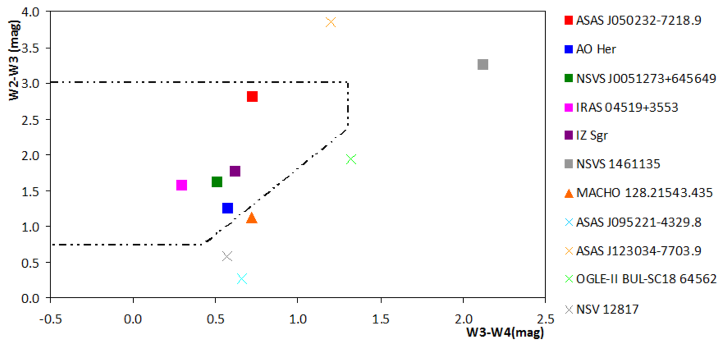

Figure 2. (W2–W3) vs. (W3–W4) diagram for all stars presented in this paper, as indicated in the legend on the right side. In order to facilitate discrimination, RCB stars and RCB candidates are denoted by squares, the proposed DYPer variable by a triangle, and the non-RCB faders of section 3 by crosses. Data were drawn from the WISE catalogue. The dashed line indicates selection cut (1) of Tisserand (2012).

DY Cen—the other obvious outlier in this work—do not resemble the majority of RCB stars in that they are hot (>12000 K) and surrounded by multiple shells. It would be highly interesting to investigate if this also holds true for NSVS 1461135; however, this is beyond the scope of the present paper.

2.3. New RCB stars

2.3.1. ASAS J050232-7218.9 (GSC 09169-00810)

ASAS J050232-7218.9 (GSC 09169-00810)—situated in the Large Magellanic Cloud (LMC)—is a star from the "Catalogue enriched with R CrB stars" (Tisserand 2012) that we confirm as an RCB star. The light curves of the star are shown in Figures 3 and 4.

During the first ~500 days of ASAS-3 coverage, the star's light curve is characterized by short-term variability and mean magnitude shifts between 13.6 and 14.6 magnitude (V). The short-term light changes suggest pulsational variability on a time scale of 43.1 days, although the period is rather ill-defined due to the star's brightness lying near the limiting magnitude of the survey (~14.5 magnitude (V)).

After HJD 2453000, the ASAS-3 system failed to record the star for about 1,300 days, suggesting that the object might have faded out of the survey's range during the indicated timespan. This interpretation is supported by sporadic measurements after HJD 2454438 which show the star below 15 magnitude (V). Recent data from the AAVSO Photometric All-Sky Survey (APASS; Henden *et al.* 2012) show the star at 15.65 magnitude (V) at HJD 2455557.

The reality of these isolated faint datapoints is proven by measurements from the fourth phase of the OGLE project (OGLE-IV; Udalski *et al.* 2008) which show the star recovering slowly from a low state at around 2455400

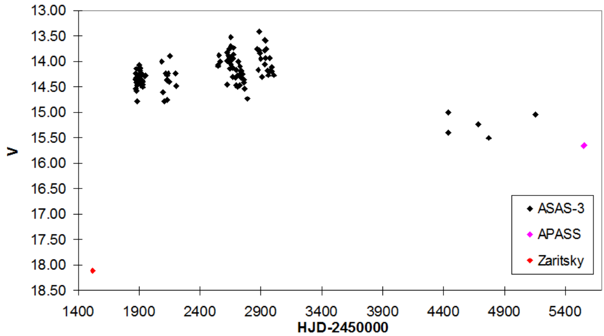

Figure 3. Light curve of ASAS J050232–7218.9, based on ASAS-3 data, APASS data, and data from the Magellanic Clouds Photometric Survey (Zaritsky *et al.* 2004).

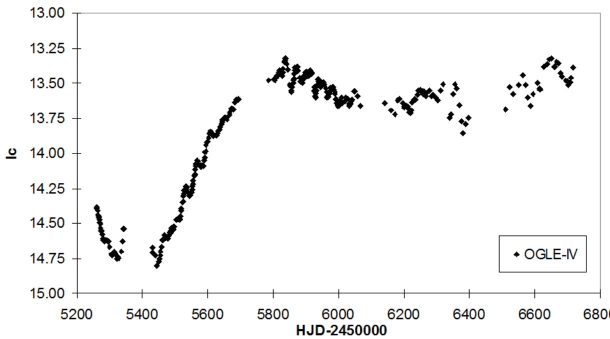

Figure 4. Light curve of ASAS J050232–7218.9, based on OGLE-IV data.

(Figure 4). During the rest of OGLE-IV coverage, which extends up to the present, the light curve is characterized by changes in mean magnitude and semiregular pulsations with a rather unstable period of ~35 days. Additional proof that ASAS J050232-7218.9 is capable of deep fadings comes from the Magellanic Clouds Photometric Survey (Zaritsky *et al.* 2004), in which the object is listed with a V magnitude of 18.1. This measurement was taken at HJD 2451517 (Zaritsky 2014).

Color measurements from 2MASS (J–K = 0.46) and APASS (B–V = 1.34) are in agreement with values found for other RCB stars, which also holds true for the star's position in the near- and mid-infrared two-color diagrams (section 2.2). Finally, and most importantly, the star has been observed spectroscopically in the past. It had been classified as an R-type carbon star by Hartwick and Cowley (1988) and was found to be a hydrogen-deficient carbon star (classified as C2,2Hd) in Richer *et al.* (1979). The other three hydrogen-deficient stars published in the latter paper were subsequently confirmed as RCB stars (EROS2-LMC-RCB-2, EROS2-LMC-RCB-3, and EROS2-LMC-RCB-5;

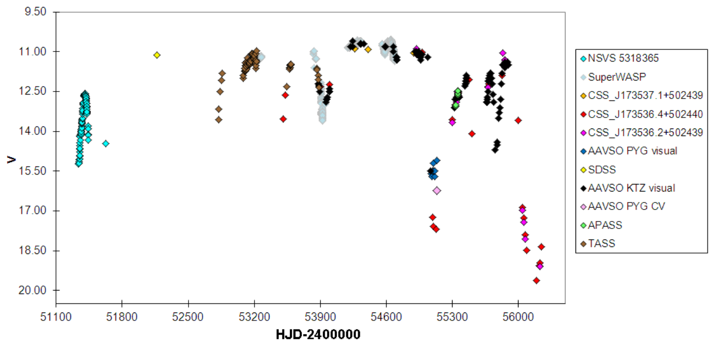

Figure 5. Light curve of AO Her, based on data from various sky surveys, as indicated in the legend.

Tisserand *et al.* 2009). We now confirm the remaining one, ASAS J050232-7218.9, as an RCB variable on grounds of its photometric behavior.

2.3.2. AO Her (2MASS J17353628+5024398)

AO Her (2MASS J17353628+5024398) was discovered in 1924 by Woods at Harvard Observatory (Woods 1924). In an early study of the star, Böhme (1937) comments on AO Her's flat and broad maxima and characterizes its periodicity as semiregular at best. He lists five times of maxima which have been deduced from 80 observations spread among about 3,000 days (between JD 2425688 and JD 2428717), emphasizing their uncertainty because of the star's light curve properties. In the specified period, AO Her's photographic brightness lay between 11.4 magnitude (p) on JD 2427645 and <13.0 magnitude (p) outside of maximum observations. The star has been poorly studied during the following decades but it has been included into the RCB-enriched catalogue of Tisserand (2012). A combination of all available data gives proof of several significant fading events during the covered timespan (Figure 5).

Data from the NSVS show AO Her rising from 15.4 magnitude (ROTSE-I) to about 12.5 magnitude (ROTSE-I) at around HJD 2451400, after which it drops back to around 14.4 magnitude (ROTSE-I). ROTSE-I magnitudes from the NSVS are unfiltered and calibrated with V magnitudes (see Akerlof *et al.* 2000) but are probably much brighter than the visual scale in this case, especially as AO Her is a red object. However, we did not shift NSVS data as there are no contemporaneous V measurements of AO Her to allow a reliable calibration. The NSVS light curve suggests the typical behavior of a red variable, supporting the classification given in the original paper.

There follows a large gap in available data for AO Her between HJD 2451600 and HJD 2452800, with only a single measurement from the Sloan Digital Sky Survey (SDSS; Adelman-McCarthy *et al.* 2011) which shows the star at around 11.0 magnitude (V). The situation improves significantly with the onset of The Amateur Sky Survey (TASS; Richmond 2007) and the SuperWASP project (SWASP; Butters *et al.* 2010) and—at around HJD 2453900—regular visual observations made by AAVSO observers (AAVSO 2013) that have been calibrated with the APASS V scale.

In addition to several minor drops of about 2 to 3 magnitudes (V), two major declines are recorded. The first one took place at around HJD 2455150, when AO Her was as faint as 17.7 magnitude (V). At the end of the covered timespan, data from the Catalina Sky Survey (CSS; Drake *et al.* 2009)—shifted ~1 magnitude to match the V scale from APASS and AAVSO visual data—show the star at its faintest, recovering from below 19.6 magnitude (V) on HJD 2456195, indicating that AO Her's amplitude exceeds 9 magnitudes (V).

In summary, it can be stated that AO Her exhibits light curve properties typical of RCB stars, in particular the sudden and dramatic fadings characteristic of this kind of variable stars. Additionally, color measurements from 2MASS (J–K = 3.59) and APASS (B–V = 1.86) are indicative of infrared excess, and the position of AO Her in the two-color diagrams is characteristic of an RCB star. The classification of AO Her as a bona fide RCB star seems, therefore, justified.

At the time of this writing, AO Her has been confirmed spectroscopically as an RCB variable by Tisserand *et al.* (2013a) with the FLOYDS spectrograph on the 2-m LCOGT/Faulkes Telescope North. Their results, along with data from a planned monitoring campaign, will be published in a future paper.

2.4. RCB / DYPer candidates

2.4.1. NSVS J0051273+645649 (GSC 04025-00779)

The variability of NSVS J0051273+645649 (GSC 04025-00779) was discovered during a search for red variables in the Northern Sky Variability Survey (NSVS) by Woźniak *et al.* (2004a). We have identified the star as a likely RCB variable by investigation of candidates from the RCB-enriched catalogue of Tisserand (2012). The light curve of the star (shifted to the APASS V zero point) is shown in Figure 6.

The light curve of NSVS J0051273+645649 is characterized by semiregular pulsations with a predominant period of 29.8 days (Figure 7) and a significant fading event at around HJD 2451500. The star faded by about 1.5 magnitudes (ROTSE-I), showing signs of a slow recovery during the rest of NSVS coverage, which is typical of RCB stars.

Color measurements from 2MASS (J–K = 1.76) and APASS (B–V = 1.48) give evidence of infrared excess. In addition, the star's B–V index is too blue to qualify it as a DYPer variable. The proposed classification is also supported by the star's position in the near- and mid-infrared two-color diagrams (section 2.2). We therefore conclude that NSVS J0051273+645649 is a likely RCB candidate worthy of follow-up investigations.

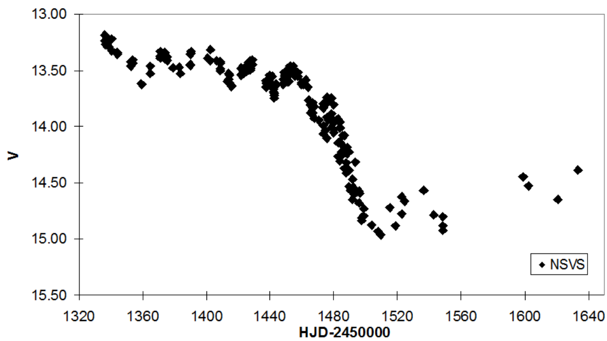

Figure 6. Light curve of NSVS J0051273+645649, based on NSVS data; ROTSE-I magnitudes from NSVS were shifted to the V scale.

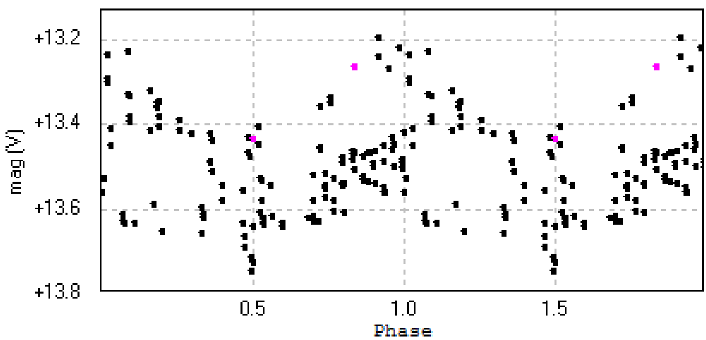

Figure 7. Semiregular pulsations of NSVS J0051273+645649; the phase plot has been based on NSVS data (2451335 < HJD < 2451464; black points) and APASS data (pink points) and folded with a period of P = 29.8 days. ROTSE-I magnitudes from NSVS were shifted to the V scale.

2.4.2. IRAS 04519+3553 (2MASS J04552045+3558079)

IRAS 04519+3553 (2MASS J04552045+3558079) is another large amplitude variable from the RCB-enriched catalogue of Tisserand (2012) which has exhibited conspicuous fading events in the past. Timeseries photometry for this object is available from the CSS; unfortunately, the light curve is sparsely sampled, consisting of 160 datapoints only, and frequently interrupted by observational gaps. Thus, the exact shape of the light curve is open to conjecture during some parts of the coverage (Figure 8).

Despite the above-mentioned difficulties, there are indications of several fadings during the covered timespan. Four closely spaced measurements at the beginning of CSS coverage show the star at ~12.5 magnitude (CV). However, following a gap of ~200 days, the star is found rising from below 14.1 magnitude (CV), which suggests that a drop in brightness has occurred during the observational gap. A more conspicuous fading event is centered around

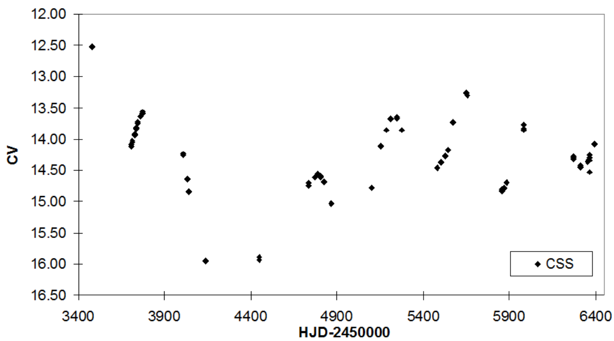

Figure 8. Light curve of IRAS 04519+3553, based on CSS data.

HJD 2454300, with the star dropping sharply from 14.25 magnitude (CV) to about 16.0 magnitude (CV). Again, an observational gap in the data leaves the amplitude and the exact shape of the minimum open to conjecture. Another possible fading event might have taken place around HJD 2455000.

During the rest of CSS coverage, the light curve is reminiscent of large amplitude pulsations, which is unusual for an RCB variable. An analysis of the available data yields a period of P~438 days, a value commonly observed, for example, in carbon-rich semiregular variables that are also sometimes prone to fading events. However, similar pulsations have been reported in RCB stars—for example, EROS2-CG-RCB-12 (Tisserand *et al.* 2008) and EROS2-LMC-RCB-8 (Tisserand *et al.* 2009)—albeit with shorter periods. It remains up to debate whether these light curve features are actually pulsations or connected to small-scale fading events (see Tisserand *et al.* 2009).

A classification as a classic carbon star would also agree with the observed J–K index of 4.18 (2MASS). However, the star's position in the near- and mid-infrared two-color diagrams of section 2.2 is in agreement with a classification as an RCB variable and provides evidence against the former assumption. The star is situated in the "all shell" region of the (J–H) vs. (H–K) diagram (Figure 1). Together with the observed J–K index of 4.18, which is indicative of infrared excess, this implies that 2MASS observations (epoch: HJD 2451093.8724) were made during an obscuration event when the object was deeply enshrouded in dust.

Measurements from the GSC2.3 catalogue and CMC14 (Evans *et al.* 2002; transformed to V) indicate a V magnitude of 18.15 magnitude (epoch: HJD 2447860.5) and 18.3 magnitude (epoch: HJD 2452649.5), respectively. However, it is not possible to tell if the star was in a faint state at the time of the measurements or if it is intrinsically faint at visual wavelengths, which would imply that IRAS 04519+3553 is a very red object even at maximum. This would account for the large difference between the object's brightness in

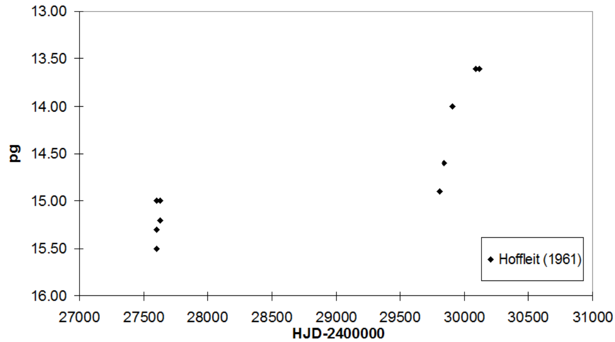

Figure 9. Light curve of IZ Sgr, based on data from Hoffleit (1961).

V and Catalina unfiltered photometry, which is calibrated against V magnitudes but strongly dependent on source color, being more sensitive to the red portion of the spectrum.

Taking into account the above-mentioned evidence, we are unable to arrive at a conclusive classification for IRAS 04519+3553, which we consider a likely RCB candidate. Long-term photometric monitoring and spectroscopic studies are encouraged.

2.4.3. IZ Sgr (GSC 06279-00870)

The star was discovered as HV 4148 by Woods (1928) and later designated as IZ Sgr in the *General Catalogue of Variable Stars* (GCVS; Samus *et al.*, 2007–2013). It was included in an investigation of 45 variable stars by Hoffleit (1961), who commented on the object's invisibility on the majority of the available plate material; positive observations of IZ Sgr were possible on only a dozen of several hundred plates reaching to below 15th magnitude (pg) that were available to Hoffleit (Figure 9).

An investigation of ASAS-3 data presents a similar picture. Except for two bright phases—one Mira-like hump at around HJD 2452100 and one rather broad maximum from about HJD 2453050 to HJD 2453450—the star remained constantly below the survey's detection limit (Figure 10). Therefore, it is evident that IZ Sgr is capable of unpredictable steep rises and drops in magnitude; additionally, a classification as a Mira variable can be excluded. The light curve also shows indications of pulsational variability, in particular during the rise to maximum light near HJD 2453100.

Measurements from various catalogues indicate a large range for IZ Sgr (for example: B = 13.3 (YB6)–19.1 (USNO-B1.0); R = >12.9 (USNO-A2.0)–<17.6 (USNO-B1.0)). Furthermore, there is no entry for IZ Sgr in CMC14 or SPM4.0 (Girard *et al.* 2011), while the 17.8 magnitude (V) star SPM4.0 6551155866, which lies only 7" away, is recorded in both catalogues. This suggests that IZ

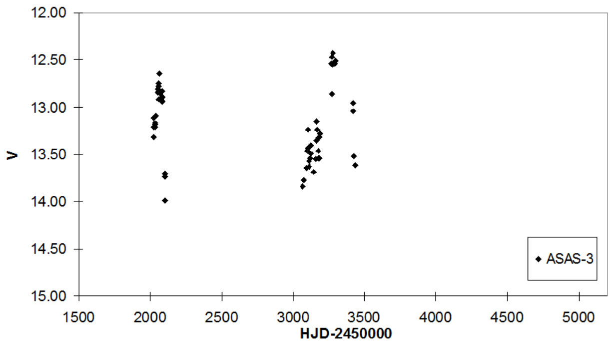

Figure 10. Light curve of IZ Sgr, based on ASAS-3 data.

Sgr might even drop to below 17.8 magnitude (V). The observed amplitude and behavior of IZ Sgr are rather extreme and do not resemble the variations seen in most irregular L-type variables.

Additionally, Tisserand *et al.* (2013b) reported that the star was too faint for spectroscopic follow-up. The star was about V = 17 magnitude during June and July 2012 (Tisserand 2014).

Although its listed spectral type of M6 (Houk 1967) is not in agreement with a classification as an RCB variable, the star's position in the near- and mid-infrared two color diagrams is consistent with its classification as an RCB variable (section 2.2). Considering the possibility that the assigned spectral type might be in error, we strongly encourage further photometric and spectroscopic investigations to gain an insight into the nature of IZ Sgr, which we consider a strong RCB candidate.

2.4.4. NSVS 1461135 (GSC 04282-00656)

The variability of NSVS 1461135 (GSC 04282-00656), which is situated in the field of the open cluster [KPR2005] 125 (Zejda *et al.* 2012), was discovered during a search for variable Asymptotic Giant Branch (AGB) stars in the NSVS database by Usatov and Nosulchik (2008), who classified it as a candidate Mira variable. The star's light curve is characterized by rather irregular pulsations and a significant fading at around HJD 2451375 (Figure 11). The fast decline and slow recovery from this event is reminiscent of the photometric behavior of RCB stars, although the amplitude is small (~1.2 magnitude (ROTSE-I)).

The (unfiltered) ROTSE-I magnitudes of NSVS 1461135 are similar to the V magnitudes that have been gleaned from various catalogues (for example: 13.56 magnitude (UCAC3) and 13.10 magnitude (TASS)), which would be highly unusual for a red object. Furthermore, from two APASS observations at 12.93 magnitude (V) and 12.95 magnitude (V), we derive a color index of B–V = 0.63, which also suggests a yellow star and, in combination with the object's J–K

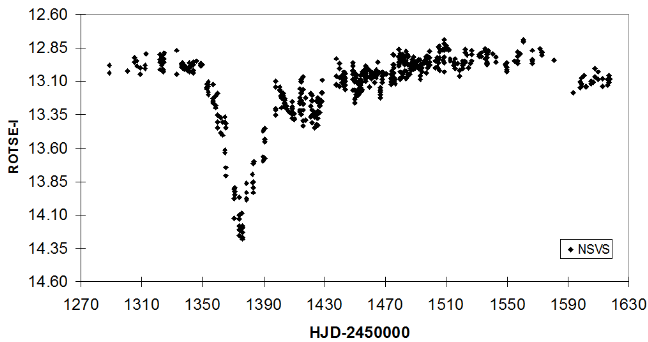

Figure 11. Light curve of NSVS 1461135, based on NSVS data.

index of 1.47 (2MASS), is indicative of infrared excess. This is in agreement with an RCB classification and strong evidence against NSVS 1461135 being a DYPer variable, which is also supported by its position in the near-infrared two-color diagram (section 2.2.1). The star's deviant position in the mid-infrared two-color diagram does not necessarily disqualify NSVS 1461135 as an RCB candidate, as similar results have been reported in the literature (section 2.2.2).

However, the observed range is not large; the faintest recorded magnitude is 14.2 (V), which we derived from SDSS photometry. A classification as a different type of variable—notably a long-period eclipsing binary star like the symbiotic systems V5569 Sgr and V1413 Aql—is not excluded. Further photometric and spectroscopic analyses are advised to arrive at a conclusive classification.

2.4.5. MACHO 128.21543.435 (2MASS J18063154-2834301)

During a search for new Mira variables in the MACHO Galactic Bulge fields (see, for example, Hümmerich and Bernhard 2012), MACHO 128.21543.435 (2MASS J18063154-2834301) was found to exhibit significant fading events during the covered timespan. Additional data were procured from the EROS-2 project (Renault *et al.* 1998; Tisserand and Marquette 2014). The light curve of the star is shown in Figure 12. The transformation of MACHO instrumental magnitudes to the Kron-Cousins system was done by using Equation (2) of Alcock *et al.* (1999). EROS-2 data have been transformed to Johnson V and Cousins I_c using Equation (4) of Tisserand *et al.* (2007).

The first obscuration event took place around HJD 2449200, with the star dropping from about 15.0 magnitude (R_c) to 17.15 magnitude (R_c). A second decline occurred around HJD 2450800; the minimum magnitude is open to conjecture because of an observational gap in the data. Although both declines are only partially covered by MACHO, they suggest the symmetric fading events and sharp minima of a DYPer star. Another fading event was recorded

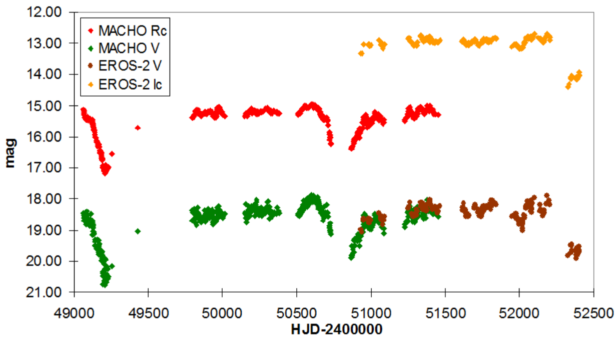

Figure 12. VR_cI_c light curve of MACHO 128.21543.435, based on data from the MACHO and EROS-2 projects. Obvious outliers have been removed by visual inspection.

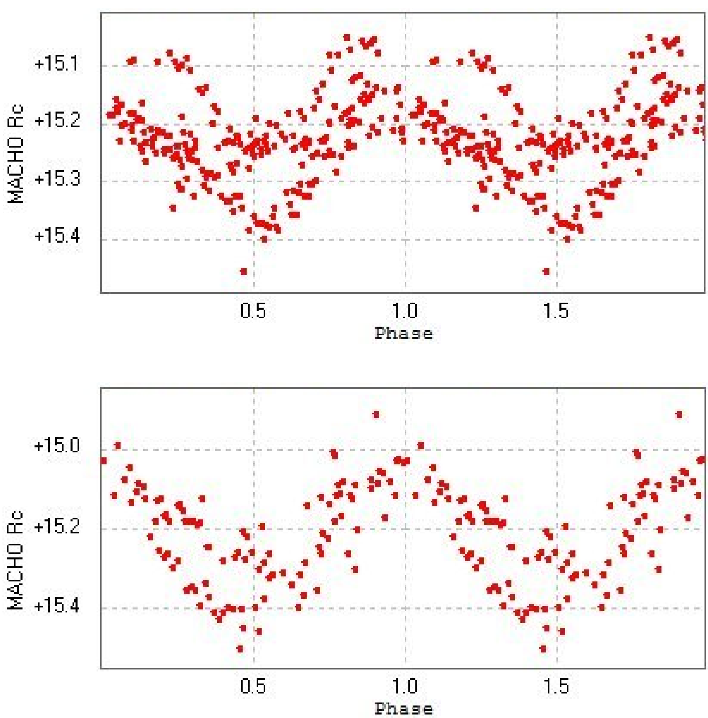

Figure 13. Semiregular pulsations of MACHO 128.21543.435; the phase plots have been based on MACHO R_c data. Phase plot 1 (top panel) is folded with P = 75.6 days (2449794 < HJD < 2450380), phase plot 2 (bottom panel) is folded with P = 66.4 days (2451229 < HJD < 2451454).

by the EROS-2 project and took place at around HJD 2452300. Again, the amplitude of the fading can only be estimated due to an observational gap in the data; it exceeds at least 1.5 magnitudes in both V and I_c, though.

Outside these obscurations, the light curve is characterized by semiregular pulsations. A period of 75.6 days is predominant in the timespan from HJD 2449794 to HJD 2450380, which then changes to 66.4 days in the data from HJD 2451229 to HJD 2451454 (Figure 13).

Judging from its light curve properties (notably the symmetric fadings with rapid declines and sharp minima) and its position in the near-infrared two-color diagram (section 2.2.1), which is in agreement with that of the DYPer star candidates of, for example, Alcock *et al.* (2001) and Tisserand *et al.* (2004), we conclude that MACHO 128.21543.435 is a promising DYPer candidate. However, spectroscopy is needed for a conclusive classification.

3. Photometrically-related objects of interest

All objects presented in this section show photometric behavior similar to RCB stars—namely, significant, unpredictable fading events and semiregular pulsations. Considering spectra, color information, and/or light curve peculiarities, it is evident, though, that these objects are not RCB variables; in fact, some of them have been rejected as such on spectroscopic grounds in recent investigations.

Most of the stars are likely to be ordinary red giants or carbon stars undergoing obscuration events; however, some of them are not easy to assign to a type and their peculiar behavior might merit more detailed follow-up studies. The common link behind the range of observed behavior in these objects seems to be dust ejection on significant scales. It would be highly interesting to investigate what—if anything—differentiates these objects from standard, non-fading semiregular red giant stars. It is possible that long term photometric coverage of red giants would considerably increase the number of these stars, whose behavior might be due to short-lived evolutionary processes.

3.1. Notes on individual stars

3.1.1. ASAS J123034-7703.9 (GSC 09416-00380)

ASAS J123034-7703.9 (GSC 09416-00380) is listed in the *ASAS Catalog of Variable Stars* (ACVS; Pojmański *et al.* 2005) as a miscellaneous variable star (type "MISC") and was proposed as an RCB candidate by Hümmerich (2011). It exhibits a significant obscuration event in its light curve, dropping about two full magnitudes (V) at around HJD 2453000 and remaining in this faint state for the rest of ASAS-3 coverage (Figure 14).

The star's light curve is further characterized by large-amplitude pulsations with a period of about 273 days that are strongly affected by the fading event, during which the pulsational amplitude shrinks to about 0.2 magnitude (V).

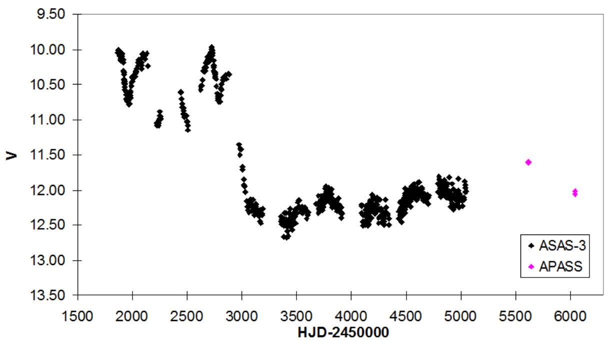

Figure 14. Light curve of ASAS J123034–7703.9, based on ASAS-3 and APASS data. Obvious outliers have been removed by visual inspection.

Color measurements from 2MASS (J–K = 1.67) and APASS (B–V = 2.26) indicate that ASAS J123034-7703.9 is a red object which is also very bright in the near infrared (J = 3.38; H = 2.10; K = 1.71 (2MASS)). In the near-infrared two-color diagram, ASAS J123034-7703.9 is positioned near the loci of classical carbon stars (section 2.2). The star's position in the (W2–W3) vs. (W3–W4) diagram hints at the existence of a cool circumstellar dust shell (Figure 2), which is in agreement with the observed prolonged obscuration event.

Amplitude and period of the pulsations as well as color information are typical of a red giant star. Additional information comes from an IRAS Low Resolution Spectrum (Joint IRAS Science Working Group 1987) that shows Si emission at 9.7 µm (Figure 15), which is known to originate from the circumstellar environments of oxygen-rich AGB stars (for example, Kwok *et al.* 1997). Thus, a classification as RCB or DYPer variable seems highly unlikely; in fact, Miller *et al.* (2012) identified ASAS J123034-7703.9 as a potential candidate but ultimately rejected it on grounds of the aforementioned IRAS spectrum and the classification in Kwok *et al.* (Miller 2012).

It seems that ASAS J123034-7703.9 is another example of a red giant undergoing a significant fading event because of an episode of dust formation, as has been shown, for example, for L2 Pup (Bedding *et al.* 2002). It is interesting to note that the amplitude of the pulsational variations of ASAS J123034-7703.9 has been affected much more strongly by the obscuration event than in the case of L2 Pup. The light curve of L2 Pup from 1980 to the present time is shown in Figure 16.

3.1.2. OGLE-II BUL-SC18 64562 (2MASS J18064655-2722063)

During an investigation of variable objects with high amplitudes from the OGLE Galactic Bulge fields using OGLE-II data (Udalski *et al.* 1997; Szymański 2005), a significant fading event was discovered in the light curve of OGLE-II BUL-SC18 64562 (2MASS J18064655-2722063). As shown in Figure 17, the

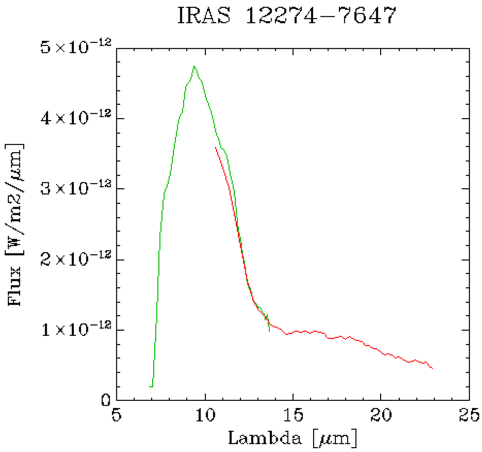

Figure 15. IRAS low resolution spectrum of ASAS J123034–7703.9 showing Si emission (Joint IRAS Science Working Group 1987).

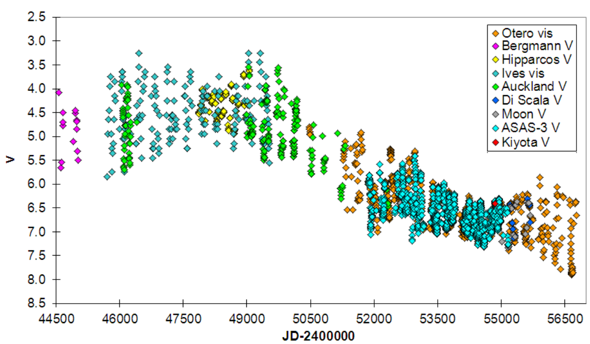

Figure 16. Light curve of L2 Pup, based on various data sources, as indicated in the legend.

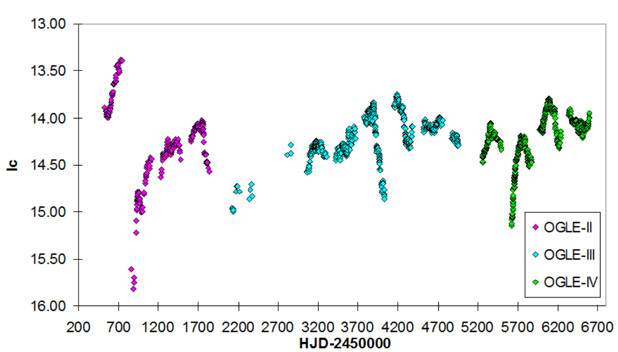

Figure 17. Light curve of OGLE-II BUL-SC18 64562, based on OGLE-II, OGLE-III, and OGLE-IV data.

star was measured at ~13.4 magnitude (I_c) before an observational gap at around HJD 2450800, during which it apparently dropped by more than 2 magnitudes (I_c). The object was next detected at HJD 2450860 with a brightness of around 16.0 magnitude (I_c). It started to rise to 14.5 magnitude (I_c) shortly after, at which brightness it remained during the remainder of OGLE-II coverage.

Additional data were procured from the *OGLE-III Catalog of Long-Period Variables (LPVs) in the Galactic Bulge* (Soszyński *et al.* 2013), which lists the object as an OGLE small amplitude red giant (OSARG), and from OGLE-IV. In addition to a long-term mean magnitude shift, three more fading events were revealed at around HJD 2452000, HJD 2454000, and HJD 2455600, albeit of much smaller scale. The light curve is further characterized by low-amplitude pulsations of a rather irregular nature, although a period of ~60 days is recognizable during parts of the coverage, for example, around HJD 2451300, HJD 2453800 and HJD 2456500.

OGLE-II BUL-SC18 64562 is a very red object with color indices of V–I = 4.92 (Udalski *et al.* 2002) and J–K = 2.47 (2MASS). It is positioned among the classical carbon stars in the (J–H) vs. (H–K) diagram (section 2.2.1), thus joining the ranks of red variables undergoing significant obscuration events. Further photometric and spectroscopic studies are encouraged.

3.1.3. NSV 12817 (CD-50 12825) and ASAS J095221-4329.8 (CD-42 5700)

CD-50 12825 was announced as a variable star by Friedrich and Schöffel (1971) and entered in the *New Catalogue of Suspected Variable Stars* (Kholopov *et al.* 1982) as NSV 12817. The star shows semi-regular pulsations with a predominant period of 50.93 days and several fading events during the coverage of ASAS-3 (Figure 18). Apart from several minor drops in brightness, which have been covered to various degrees, there is a major one with an amplitude of ~1.5 magnitude (V) around HJD 2454300. The symmetric declines and recoveries of the fadings are reminiscent of the behavior of DYPer stars (see, for example, Tisserand (2012)).

An object showing similar photometric variability is ASAS J095221-4329.8 (CD-42 5700), which entered the ACVS as a MISC-type variable. It is also characterized by several minor fadings and a major drop with an amplitude of about 2 magnitudes (V) at around HJD 2452200. Furthermore, the star exhibits semiregular pulsations, with a predominant period of ~65 days, which seem to continue during the obscuration phases (Figure 19).

Both objects show similar colors. The color indices of NSV 12817 (J–K = 1.20 (2MASS), B–V = 1.58 (APASS)) are indicative of a red star. ASAS J095221-4329.8 is classified as M6 in Tisserand *et al.* (2013b), which is in good agreement with its color indices of J–K = 1.29 (2MASS) and B–V = 1.78 (APASS).

The position of both stars in the near- and mid-infrared two-color diagrams is in accordance with that of the DYPer candidates of Alcock *et al.* (2001).

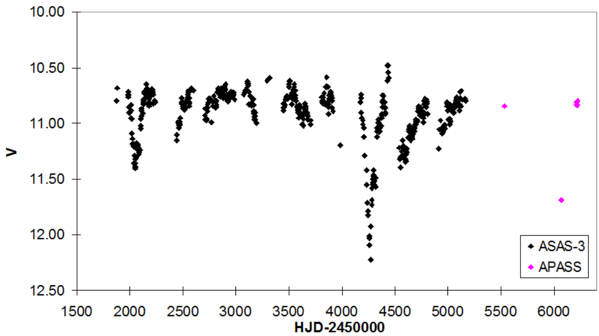

Figure 18. Light curve of NSV 12817, based on ASAS-3 and APASS data. Obvious outliers have been removed by visual inspection.

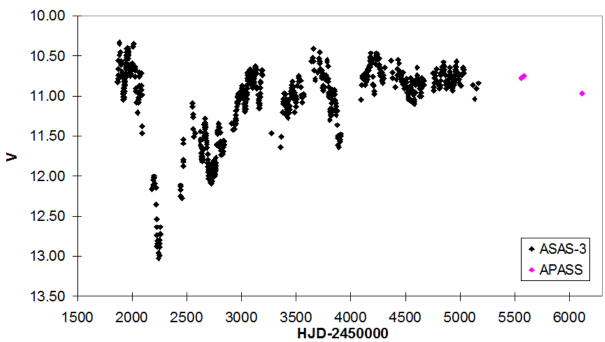

Figure 19. Light curve of ASAS J095221–4329.8, based on ASAS-3 and APASS data. Obvious outliers have been removed by visual inspection.

In fact, ASAS J095221-4329.8 was proposed as a possible DYPer variable by Hümmerich (2011) but rejected as such on spectroscopic grounds by Miller *et al.* (2012), who did not detect carbon compounds but strong titanium oxide bands (TiO), vanadium oxide (VO) and possibly hydrogen ("strong TiO, VO; H?"; see Miller *et al.* (2012), especially their Table 5). Both objects seem to be further examples of semiregular red giant stars that merit attention because of their significant fading events.

4. Acknowledgements

We thank the anonymous referee for valuable comments and suggestions that greatly improved the paper. We acknowledge with thanks the variable star observations from the AAVSO International Database contributed by observers worldwide and used in this research. This research has made use of the SIMBAD and VizieR databases operated at the Centre de Données Astronomiques (Strasbourg) in France. This work has also made use of EROS-2 data, which were kindly provided by the EROS collaboration. The EROS (Expérience pour la Recherche d'Objets Sombres) project was funded by the CEA and the IN2P3 and INSU CNRS institutes. Furthermore, this research has employed data products from the Two Micron All Sky Survey, which is a joint project of the University of Massachusetts and the Infrared Processing and Analysis Center/California Institute of Technology, funded by the National Aeronautics and Space Administration and the National Science Foundation, and the Wide-field Infrared Survey Explorer, which is a joint project of the University of California, Los Angeles, and the Jet Propulsion Laboratory/California Institute of Technology, funded by the National Aeronautics and Space Administration.

References

AAVSO. 2013, observations from the AAVSO International Database (http://www.aavso.org).

Adelman-McCarthy, J. K., *et al.* 2011, *The SDSS Photometric Catalog, Release 8*, VizieR On-line Data Catalog: II/306 (http://cdsarc.u-strasbg.fr/viz-bin/Cat?II/306).

Akerlof, C., *et al.* 2000, *Astron. J.*, **119**, 190.

Alcock, C., *et al.* 1997, *Astrophys. J.*, **486**, 697.

Alcock, C., *et al.* 1999, *Publ. Astron. Soc. Pacific*, **111**, 1539.

Alcock, C., *et al.* 2001, *Astrophys. J.*, **554**, 298.

Bedding, T. R., Zijlstra, A. A., Jones, A., Marang, F., Matsuura, M., Retter, A., Whitelock, P. A., and Yamamura, I. 2002, *Mon. Not. Roy. Astron. Soc*, **337**, 79.

Böhme, S. 1937, *Astron. Nachr.*, **264**, 269.

Butters, O. W., *et al.* 2010, *Astron. Astrophys.*, **520**, L10.

Clayton, G. C. 2012, *J. Amer. Assoc. Var. Star Obs*, **40**, 1, 539.

Cutri, R. M., *et al.* 2012, WISE All-Sky Data Release, VizieR On-line Data Catalog: II/311 (http://cdsarc.u-strasbg.fr/viz-bin/Cat?II/311).

Drake, A. J., *et al.* 2009, *Astrophys. J.*, **696**, 870.

Evans, D. W., Irwin, M. J., and Helmer, L. 2002, *Astron. Astrophys.*, **395**, 347.

Feast, M. W. 1997, *Mon. Not. Roy. Astron. Soc.*, **285**, 339.

Friedrich, D., and Schöffel, E. 1971, *Inf. Bull. Var. Stars*, No. 558, 1.

Girard, T. M., *et al.* 2011, *Astron. J.*, **142**, 15.

Hartwick, F. D. A., and Cowley, A. P. 1988, *Astrophys. J.*, **334**, 135.

Henden, A. A., *et al.* 2012, AAVSO All-Sky Photometric Survey, data release 3 (http://www.aavso.org/apass).

Hoffleit, D. 1961, *Astron. J.*, **66**, 188.

Houk, N. 1967, *Inf. Bull. Var. Stars*, No. 228, 1.

Hümmerich, S. 2011, *BAV Rundbrief*, **60**, 252.

Hümmerich, S., and Bernhard, K. 2012, *Open Eur. J. Var. Stars*, **149**, 1.
Joint IRAS Science Working Group. 1987, *IRAS Low Resolution Spectra* (LRS), NASA RP-1190 (1987), VizieR On-line Data Catalog, III/197 (http://cdsarc.u-strasbg.fr/viz-bin/Cat?III/197).
Kholopov, P. N., *et al.* 1982, *New Catalogue of Suspected Variable Stars*, Moscow.
Kwok, S., Volk, K., and Bidelman, W. P. 1997, *Astrophys. J., Suppl. Ser.*, **112**, 557.
Lloyd Evans, T. 2010, *J. Astrophys. Astron.*, **31**, 177.
Miller, A. A. 2012, private communication.
Miller, A. A., Richards, J. W., Bloom, J. S., Cenko, S. B., Silverman, J. M., Starr, D. L., and Stassun, K. G. 2012, *Astrophys. J.*, **755**, 98.
Otero, S., Watson, C., and Wils, P. 2013, "Variable Star Type Designations in VSX" (http://www.aavso.org/vsx/index.php?view=about.vartypes).
Pojmański, G. 2002, *Acta Astron.*, **52**, 397.
Pojmański, G., Pilecki, B., and Szczygiel, D. 2005, *Acta Astron.*, **55**, 275.
Renault, C., et al. 1998, *Astron. Astrophys.*, **329**, 522.
Richer, H. B., Olander, N., and Westerlund, B. E. 1979, *Astrophys. J.*, **230**, 724.
Richmond, M. W. 2007, *Publ. Astron. Soc. Pacific*, **119**, 1083.
Samus, N. N., *et al.* 2007–2013, *General Catalogue of Variable Stars*, VizieR On-line Data Catalog (http://cdsarc.u-strasbg.fr/viz-bin/Cat?B/gcvs).
Skrutskie, M. F., *et al.* 2006, *Astron. J.*, **131**, 1163.
Soszyński, I., *et al.* 2009, *Acta Astron.*, **59**, 335.
Soszyński, I., *et al.* 2013, *Acta Astron.*, **63**, 21.
Szymański, M. K. 2005, *Acta Astron.*, **55**, 43.
Tisserand, P. 2012, *Astron. Astrophys.*, **539**, 51.
Tisserand, P. 2014, private communication.
Tisserand, P., Clayton, G. C., and Welch, D. L. 2013a, private communication.
Tisserand, P., Clayton, G. C., Welch, D. L., Pilecki, B., Wyrzykowski, L., and Kilkenny, D. 2013b, *Astron. Astrophys.*, **551**, A77.
Tisserand, P., and Marquette, J. B. 2014, private communication.
Tisserand, P., *et al.* 2004, *Astron. Astrophys.*, **424**, 245.
Tisserand, P., *et al.* 2007, *Astron. Astrophys.*, **469**, 387.
Tisserand, P., *et al.* 2008, *Astron. Astrophys.*, **481**, 673.
Tisserand, P., *et al.* 2009, *Astron. Astrophys.*, **501**, 985.
Udalski, A., Kubiak, M., and Szymański, M. 1997, *Acta Astron.*, **47**, 319.
Udalski, A., *et al.* 2002, *Acta Astron.*, **52**, 217.
Udalski, A., Szymański, M. K., Soszyński, I., and Poleski, R. 2008, *Acta Astron.*, **58**, 69.
Usatov, M., and Nosulchik, A. 2008, *Open Eur. J. Var. Stars*, **88**, 1.
Westerlund, B. E., Azzopardi, M., Rebeirot, E., and Breysacher, J. 1991, *Astron. Astrophys., Suppl. Ser.*, **91**, 425.
Woods, I. E. 1924, *Bull. Harvard Coll. Obs.*, No. 807, 4.
Woods, I. E. 1928, *Bull. Harvard Coll. Obs.*, No. 854, 5.

Woźniak, P. R., Williams, S. J., Vestrand, W. T., and Gupta, V. 2004a, *Astron. J.*, **128**, 2965.

Woźniak, P. R., *et al.* 2004b, *Astron. J.*, **127**, 2436.

Wright, E. L., *et al.* 2010, *Astron. J.*, **140**, 1868.

Zacharias, N., Finch, C. T., Girard, T. M., Henden, A., Bartlett, J. L., Monet, D. G., and Zacharias, M. I. 2012, *The Fourth U.S. Naval Observatory CCD Astrograph Catalog (UCAC4)*, VizieR On-line Data Catalog (http://cdsarc.u-strasbg.fr/viz-bin/Cat?I/322).

Zaritsky, D. 2014, private communication.

Zaritsky, D., Harris, J., Thompson, I. B., and Grebel, E. K. 2004, *Astron. J.*, **128**, 1606.

Zejda, M., Paunzen, E., Baumann, B., Mikulášek, Z., and Liška, J. 2012, *Astron. Astrophys.*, **548**, A97.

New Light Elements for the High Amplitude δ Scuti Star BS Aquarii

Roy Andrew Axelsen
P.O. Box 706, Kenmore, Queensland 4069, Australia; reaxelsen@gmail.com

Received January 13, 2014; revised February 19, 2014; accepted March 3, 2014

Abstract DSLR photometry of the monoperiodic, high amplitude δ Scuti star BS Aquarii yielded five times of maximum in September and October 2013. These data were analyzed with twenty-two times of maximum obtained by other observers from 1973 to 1995. New light elements were calculated, revealing a period of 0.197822765 day (±0.000000010) at HJD 2456543.0250 (±0.0005). These light elements represent a linear ephemeris, with no significant change in the period of the star from 1973 to 2013. The data do not support the previous suggestion in the literature of an unseen companion affecting the O–C diagram.

1. Introduction

BS Aqr is a 9th magnitude high-amplitude monoperiodic δ Scuti star with a period of 4.75 hours and an amplitude of 0.45 magnitude in V. Its variability was first identified by Hoffmeister (1931), and Andrews (1936) identified it as a pulsating variable star. Fifty-six times of maximum obtained by various observers between 1935 to 1995 have been reported in earlier literature. Examination of O–C diagrams of those data reveal that the period decreased between the 1930s and 1973, after which it increased.

Yang *et al.* (1993) fitted a quadratic function to the O–C data calculated from times of maximum up until 1984, but inspection reveals that the fit is not good. Fu *et al.* (1997) added a single time of maximum from observations in 1995, and applied a quadratic function with additional trigonometric terms, which resulted in a curve providing a better fit than the quadratic function alone. These authors suggested that the results could be explained by the effects of an unseen companion to BS Aqr.

The most recent data in the literature are those of Rodriguez *et al.* (1998), who added six times of maximum obtained between 1992 and 1995. The present paper reports five new times of maximum obtained in September and October 2013, presents O–C diagrams of the new data and previous times of maximum from the literature, and calculates a new linear ephemeris based on times of maximum obtained from 1973 to 2013.

2. Observations

DSLR photometry was performed on RAW images taken with a Canon EOS 500D DSLR camera imaging through a refracting telescope with an aperture of 80mm at f/7.5, mounted on a Losmandy GM8 German equatorial mount. Photometric data reduction from instrumental magnitudes utilized the software package AIP4WIN (Berry and Burnell 2011). The comparison and check stars were HD 223049 and HD 223293, respectively. Transformed magnitudes in V were calculated using transformation coefficients for the blue and green channels of the DSLR sensor, obtained from images of standard stars in the E regions (Menzies *et al.* 1989).

Transformation coefficients were obtained from DSLR images of a field containing E region stars E408, E417, E426, E432, E433, and E434. The catalogue B–V color indices of these stars ranged from –0.018 to 0.984. Transformation coefficients represented the slopes of the plots of b–v (y axis) against B–V, and B–b (y axis) against B–V, where b and v are the instrumental magnitudes for signals from the blue and green channels, respectively, of the DSLR sensor, and B–V is the catalogue color index of each star.

The time of maximum of each light curve was taken as the time in Julian days of the maximum value of a sixth-order polynomial function fitted to each light curve by the period analysis software PERANSO (Vanmunster 2013), and converted to HJD prior to the plotting of O–C diagrams.

3. Analysis

Figure 1 is an example of a light curve from one night's observations with a sixth-order polynomial expression fitted to the central part of the data by the software program PERANSO, for the determination of the time of maximum. The light curve has the typical pattern of a high-amplitude δ Scuti star, characterized by a fast rise to maximum light, and a slower fall toward the minimum. Table 1 lists the times of maximum light of BS Aqr in Julian days (JD) for each of the five light curves obtained by the author in 2013, calculated using PERANSO, and showing the confidence limits assigned by that program. Those confidence limits cover a range of ±2.3 minutes to ±3.2 minutes.

All published times of maximum from the literature and from our observations are shown in Table 2, together with O–C values based on the period determined by Fu *et al.* (1997) of 0.197822612 day, and with T_0 being the first time of maximum determined by us (maximum 57 in Table 2). The O–C diagram plotted from all of those observations is shown in Figure 2, upper plot. The earlier data are somewhat scattered. Then, there was a decrease in the period of the star to 1973 (the letter "A" on the diagram is placed beneath the group of 1973 observations), after which the period increased. Because of the patterns revealed by visual inspection of this O–C diagram, it was decided to analyze the

Table 1. Times of maximum (TOM) in Julian days (JD) of BS Aqr determined by the author during 2013.

TOM (JD)	Confidence Limits
2456543.020917	0.00157
2456544.997666	0.00186
2456561.020382	0.00215
2456570.123946	0.00223
2456592.080070	0.00158

Table 2. Times of maximum (TOM) of BS Aqr from 1935 to 2013 in heliocentric Julian days (HJD), calculated O–C (observed minus computed) values, and the list of publications representing the source of the data.

Max	TOM (HJD)	Cycles	O–C	Primary Source*
1	2428095.3380	–143804	–0.00572	1
2	2429111.7450	–138666	–0.01130	2
3	2429899.2660	–134685	–0.02212	3
4	2430187.3040	–133229	–0.01385	3
5	2433027.4460	–118872	–0.01109	3
6	2433862.4600	–114651	–0.00633	3
7	2433888.3650	–114520	–0.01609	3
8	2434211.4220	–112887	–0.00342	3
9	2434400.3350	–111932	–0.01101	3
10	2434961.3660	–109096	–0.00494	3
11	2435631.3920	–105709	–0.00413	3
12	2435696.4720	–105380	–0.00777	3
13	2436040.0771	–103643	–0.02054	4
14	2436300.4260	–102327	–0.00620	3
15	2436458.0904	–101530	–0.00642	5
16	2436460.8540	–101516	–0.01234	5
17	2436461.8475	–101511	–0.00795	5
18	2436874.1120	–99427	–0.00578	4
19	2437561.3491	–95953	–0.00443	6
20	2437561.5445	–95952	–0.00685	6
21	2437562.5345	–95947	–0.00597	6
22	2437563.5242	–95942	–0.00538	6
23	2437564.5156	–95937	–0.00309	6
24	2437582.5180	–95846	–0.00255	6
25	2437583.3105	–95842	–0.00134	6
26	2437584.2934	–95837	–0.00755	6

Table continued on next page

Table 2. Times of maximum (TOM) of BS Aqr from 1935 to 2013, cont.

Max	*TOM (HJD)*	*Cycles*	*O–C*	*Primary Source**
27	2437584.4924	–95836	–0.00638	6
28	2437911.4916	–94183	–0.00795	6
29	2437932.4617	–94077	–0.00705	6
30	2437933.4552	–94072	–0.00266	6
31	2437934.4383	–94067	–0.00868	6
32	2437946.3083	–94007	–0.00803	6
33	2437947.2960	–94002	–0.00945	6
34	2439087.1561	–88240	–0.00324	7
35	2441946.6714	–73785	–0.01379	8
36	2441946.8693	–73784	–0.01372	8
37	2441947.6620	–73780	–0.01231	8
38	2441947.8603	–73779	–0.01183	8
39	2441948.6500	–73775	–0.01342	8
40	2441948.8489	–73774	–0.01234	8
41	2441949.6400	–73770	–0.01253	8
42	2441950.6300	–73765	–0.01165	8
43	2441950.8295	–73764	–0.00997	8
44	2445612.7240	–55253	–0.00984	9
45	2445620.6380	–55213	–0.00874	9
46	2445625.5830	–55188	–0.00931	9
47	2445637.6470	–55127	–0.01249	9
48	2445644.5720	–55092	–0.01128	9
49	2445997.0920	–53310	–0.01117	10
50	2450072.0441	–32711	–0.00706	11
51	2448912.8046	–38571	–0.00605	12
52	2449606.7644	–35063	–0.00798	12
53	2449606.9621	–35062	–0.00810	12
54	2449607.9513	–35057	–0.00801	12
55	2449956.5150	–33295	–0.00775	12
56	2449957.5048	–33290	–0.00707	12
57	2456543.0266	0	0.00000	13
58	2456545.0034	10	–0.00146	13
59	2456561.0261	91	–0.00241	13
60	2456570.1294	137	0.00110	13
61	2456592.0845	248	–0.00213	13

**Primary sources: 1. Andrews (1936); 2. Ashbrook (1943); 3. Satanova (1961); 4. Kinman (1961); 5. Spinrad (1959); 6. Tremko and Sajtak (1964); 7. Harding and Penston (1966); 8. Elst (1976); 9. Meylan* et al. *(1986); 1 10. Yang et al. (1993); 11. Fu et al. (1997); 12. Rodriguez* et al.*(1998); 13. Present paper.*

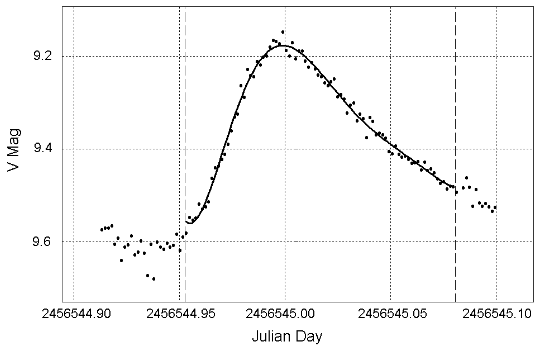

Figure 1. An example of a light curve of BS Aqr from a single night's observations, with a fitted sixth-order polynomial expression using the sofware program PERANSO (Vanmunster 2013), from which the time of maximum is calculated.

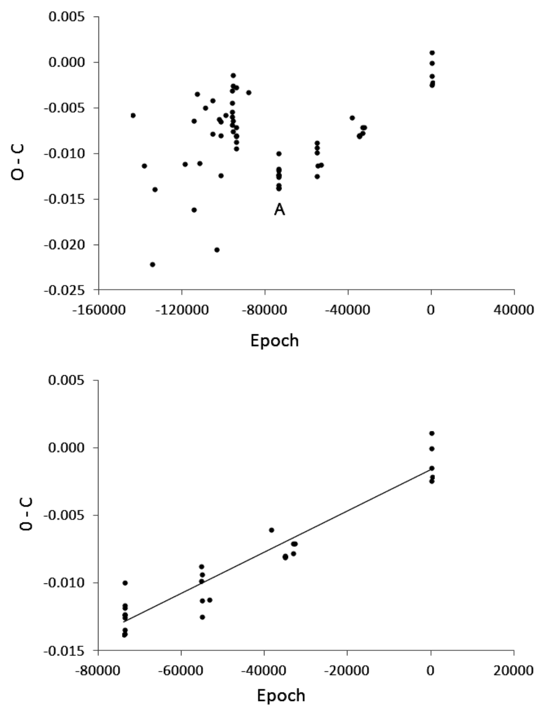

Figure 2. Upper plot: O–C diagram of all times of maximum of BS Aqr from the literature and obtained by the present author, spanning the period 1935 to 2013. The group of observations immediately above the letter "A" were made in 1973. Lower plot: O–C diagram of times of maximum of BS Aqr obtained between 1973 and 2013. Twenty-two times of maximum were obtained from the literature for observations between 1973 and 1995, and five times of maximum were obtained by the author in 2013. The straight line fitted to the data represents a least squares linear expression.

data from 1973 to 2013 separately, which yielded the O–C diagram in Figure 2, lower plot. This diagram represents a plot of the data for maxima 35 to 61 from Table 2, and includes a line which is the least squares linear fit to the data. Although a curve representing a quadratic function was initially plotted (instead of a linear function), the 95% confidence limit of the quadratic term was almost identical to the quadratic term itself, implying that the higher order term could be disregarded as insignificant. If a linear fit is accepted for the data from 1973 to 2013, this result implies that the period of the star has been constant over this time.

The generic formula for the linear function shown in Figure 2, lower plot, is:

$$\text{O–C} = aE + c \tag{1}$$

where E is the epoch (cycle number), a is the slope of the line, and c is a constant.

The values for this formula from the data upon which Figure 2, lower plot, is based, are as follows, with 95% confidence limits in brackets:

$$a = 0.0000001526\ (\pm\ 0.0000000096) \tag{2}$$

$$c = 0.00158\ (\pm\ 0.00051) \tag{3}$$

The light elements of the star are determined by a plot of times of maximum (y axis) against epoch (x axis). The values for the epochs are scaled so that the earliest of our personal observations (maximum 57 near the end of Table 2) represents T_0.

A linear function fitted to this plot represents the light elements of the star, and has the general formula:

$$T_{max} = aE + T_0 \tag{4}$$

where T_{max} is the time of maximum light, E is the epoch number, T_0 is the time of maximum light when E is zero, and the slope a is the period (in days) of the star. The values are as follows, with 95% confidence limits in brackets:

$$a = 0.197822765\ (\pm\ 0.000000010) \tag{5}$$

$$T_0 = 2456543.0250\ (\pm\ 0.0005) \tag{6}$$

4. Conclusions

Observations of the times of maximum of BS Aqr span 78 years, from 1935 to 2013, with a gap of 18 years between the most recently published previous data obtained in1995 and the data obtained by us in 2013. It is therefore timely to report an update of the behavior of this star. The observations and analysis reported in this paper indicate that there has been no significant change in the period from 1973 to 2013. Fu *et al.* (1997) suggested that the O–C diagram calculated by them could be explained by the light time effect of an as-yet undiscovered companion to BS Aqr, and inspection of their Figure 1(b) illustrates that possibility. However, the data obtained by us do not support that suggestion.

References

Andrews, L. B. 1936, *Bull. Harvard Coll. Obs.*, No. 902, 27.

Ashbrook, J. 1943, *Bull. Harvard Coll. Obs.*, No. 917, 10.

Berry, R., and Burnell, J. 2011, "Astronomical Image Processing for Windows," AIP4WIN version 2.4.0, provided with *The Handbook of Astronomical Image Processing*, Willmann-Bell, Richmond, VA.

Elst, E. W. 1976, *Astron. Astrophys., Suppl. Ser.*, **23**, 419.

Fu, J.-N., Jiang, S.-Y., Gu, S.-H., and Qiu, Y.-L. 1997, *Inf. Bull. Var. Stars*, No. 4518, 1.

Harding, G. A., and Penston, M. J. 1966, *Royal Obs. Bull.*, Series E, No. 115, 279.

Hoffmeister, C. 1931, *Astron. Nachr.*, **242**, 129.

Kinman, T. D. 1961, *Royal Obs. Bull.*, Series E, No. 37, 151.

Menzies, J. W., Cousins, A. W. J., Banfield, R. M., and Laing, J. D. 1989, *S. Afr. Astron. Obs. Circ.*, No., 13., 1.

Meylan, G., Burki, G., Rufener, F., Mayor, M., Burnet, M., and Ischi, E. 1986, *Astron. Astrophys., Suppl. Ser.*, **64**, 25.

Rodriguez, E., González-Bedolla, S. F., and López-González, M. J. 1998, *Astron. Astrophys.*, **336**, 911.

Satanova, E.A. 1961, *Perem. Zvezdy*, **13**, 266

Spinrad, H. 1959, *Astrophys. J.*, **130**, 539.

Tremko, J., and Sajtak, D. 1964, *Bull. Astron. Inst. Czechoslovakia*, **15**, 91.

Vanmunster ,T. 2013, Light Curve and Period Analysis Software, PERANSO v.2.50 (http://www.peranso.com/).

Yang, D. W., Tang, Q. Q., Jiang, S. Y., and Wang, H. S. 1993, *Inf. Bul. Var. Stars*, No. 3831, 1.

New Light Elements for the High Amplitude δ Scuti Star RS Gruis

Roy Andrew Axelsen
P.O. Box 706, Kenmore, Queensland 4069, Australia; reaxelsen@gmail.com

Received January 6, 2014; revised March 17 and April 1, 2014; accepted May 2, 2014

Abstract

Photoelectric and DSLR photometry of the monoperiodic high amplitude δ Scuti star RS Gruis yielded 16 times of maximum determined by the author from 2007 to 2013. These data are combined with historical observations obtained from 1952 to 1988 and more recent observations by others from 2003 to 2010. This combined dataset, comprising 50 times of maximum spanning 61 years, was subjected to O–C analysis, which revealed an obvious change in the period of the star between 1988 and 2003. Separate O–C analysis of the data from 2003 to 2013, comprising 28 times of maximum, yielded a quadratic fit, with the pulsational period increasing at the rate of $dP/Pdt = 84.95\,(15.74) \times 10^{-8}\ yr^{-1}$. To our knowledge, this rate of increase in period is the highest ever reported for a Population I high amplitude δ Scuti star with radial pulsation. From a quadratic (second order polynomial) ephemeris, the period was calculated to be 0.14701118 (0.00000011) d at HJD 2452920 (in October 2003) and 0.14701241 (0.00000012) d at HJD 2456497 (in July 2013).

1. Introduction

RS Gru (HD 206379) is a pulsating variable star of high amplitude δ Scuti type, with a period of 0.147 d (3.5 h), and an amplitude of 0.6 magnitude in V, with maximum and minimum magnitudes of approximately 7.9 and 8.5, respectively. The star was first recognized to be variable by Hoffmeister (1956), and Oosterhoff and Walraven (1966) reported that it had a stable light curve. Radial velocity studies were undertaken by Kinman (1961), McNamara and Feltz (1976), and van Citters (1976). Balona and Martin (1978) found that RS Gru was a spectroscopic binary, with a period probably longer than one week, and Joner and Laney (2004) found an orbital period of about two weeks. Derekas *et al.* (2009) finally determined the orbital period of the binary system to be 11.5 days.

Rodríguez *et al.* (1995) fitted a quadratic function to the times of maximum obtained from 1952 to 1988, calculated the period to be 0.147010864 d (0.000000022) at HJD 2447464.7095 (0.004), and determined that the pulsational period of RS Gru had decreased at a rate of $dP/dt = -1.56\,(0.12) \times 10^{-8}$ d yr^{-1}, or $dP/Pdt = -10.6\,(0.8) \times 10^{-8}\ yr^{-1}$.

García (2012) analyzed an enlarged dataset of times of maximum, comprising the historical data studied by Rodríguez (1995) and additional observations covering the years 2003 to 2010 sourced from the AAVSO International Database (AID) and from personal measurements. He performed O–C analysis, determined that the period of RS Gru had increased between 1988 and 2010, and fitted a new cubic regression to the pulsational behavior of the star across the dataset of 37 times of maximum from 1952 to 2010. He also performed Fourier analysis on over 4,000 observations from international databases and from personal measurements, and found a period for the pulsational behavior of the star of 0.14705874 d.

2. Observations

Observations were made by photoelectric photometry from 2007 to 2010, and by DSLR photometry from 2011 to 2013. Two different photoelectric photometers were used, both supplied by Optec Inc, Lowell, Michigan. The data from 2007 was obtained with an SSP-3 model instrument, and in 2009 and 2010 an SSP-5 model instrument with a Hamamatsu R6358 multialkali photomultiplier tube was used. Both photometers were fitted with Johnson V and B photometric filters from Optec Inc, and measurements were taken through a Celestron C9.25 Schmidt-Cassegrain telescope, on a Losmandy GM8 German equatorial mount.

DSLR photometry was performed with a Canon EOS 500D camera imaging through a refracting telescope with an aperture of 80 mm at f/7.5, mounted on a Losmandy GM8 German equatorial mount.

For photoelectric photometry, non-transformed data in V were obtained, since the color indices of the comparison and check stars (HD 206025 and HD 206442 respectively) were similar to that of the variable. For DSLR photometry, RAW images were processed in AIP4WIN (Berry and Burnell 2011) to obtain instrumental magnitudes of the variable, comparison, and check stars. Transformed magnitudes in V were then determined from transformation coefficients for the blue and green channels of the DSLR sensor, obtained from images of standard stars in the E regions (Menzies *et al.* 1989).

A standard method was required for determining the time of maximum light for each night's partial (or complete) light curve. For photoelectric photometry, the numbers of observations before or after the time of maximum were sometimes small, as was the total number of observations on a few nights. As a consequence, it was not possible to obtain a polynomial fit for all observation sets. Therefore, for each observation set that yielded a time of maximum, a center-moving average of each three consecutive observations was plotted against JD, and the time of maximum for each observation set was estimated visually. The time of maximum was then converted to HJD. All 50 times of maximum in HJD from our observations and those in the literature from 1952 to 2013 were tabulated.

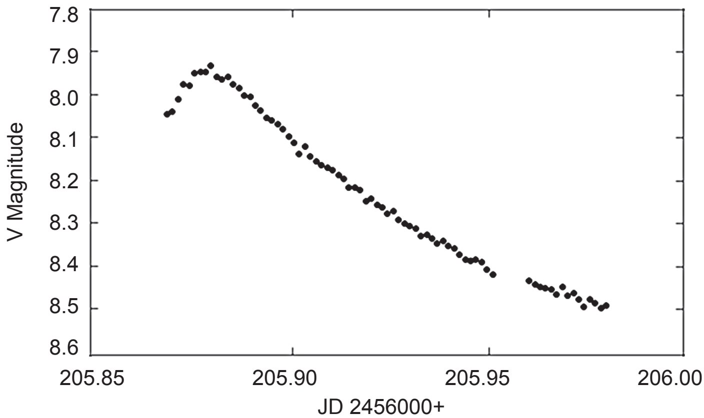

Figure 1. Sample light curve of RS Gru, one night's DSLR photometry data.

Table 1. Times of maximum (TOM) of RS Gru from 1952 to 2013, epochs, and O–C values.

Max	*TOM (HJD)*	*Epoch*	*(O–C)*	*(O–C)c*	*Primary Source**
1	2434325.2940	–89377	–0.026108	0.002786	1
2	2434573.4510	–87689	–0.023447	0.004807	1
3	2436756.5710	–72839	–0.014777	0.007849	2
4	2436760.5380	–72812	–0.017070	0.005545	2
5	2436801.5540	–72533	–0.017101	0.005409	3
6	2436853.3030	–72181	–0.015926	0.006451	3
7	2441538.4027	–40312	–0.005450	0.004848	4
8	2441538.5490	–40311	–0.006161	0.004137	4
9	2441610.4379	–39822	–0.005574	0.004539	4
10	2441611.3200	–39816	–0.005539	0.004571	4
11	2441611.4677	–39815	–0.004850	0.005260	4
12	2441612.3493	–39809	–0.005315	0.004793	4
13	2441915.4856	–37747	–0.005417	0.003910	4
14	2442687.5892	–32495	–0.002874	0.004461	5
15	2443355.4610	–27952	–0.001429	0.004184	6
16	2443355.6092	–27951	–0.000240	0.005373	6
17	2443360.4584	–27918	–0.002399	0.003202	6
18	2443360.6050	–27917	–0.002810	0.002791	6
19	2447464.7095	0	–0.000600	–0.005580	7
20	2447468.5324	26	0.000018	–0.004972	7
21	2447468.6793	27	–0.000093	–0.005084	7
22	2447472.6489	54	0.000213	–0.004787	7
23	2452920.0196	37108	0.030359	0.011315	8

Table continued on next page

Table 1. Times of maximum (TOM) of RS Gru from 1952 to 2013, epochs, and O–C values, cont.

Max	*TOM (HJD)*	*Epoch*	*(O–C)*	*(O–C)c*	*Primary Source**
24	2452921.9311	37121	0.030717	0.011669	8
25	2452922.0772	37122	0.029807	0.010757	8
26	2452923.9905	37135	0.031965	0.012911	8
27	2452925.0188	37142	0.031189	0.012132	8
28	2454373.9645	46998	0.037844	0.015051	9
29	2454374.9929	47005	0.037168	0.014373	9
30	2454387.9307	47093	0.037942	0.015113	9
31	2454417.0373	47291	0.036431	0.013527	10
32	2454417.9191	47297	0.036205	0.013300	9
33	2454417.9216	47297	0.038665	0.015760	10
34	2454423.9464	47338	0.036020	0.013099	10
35	2455059.0379	51658	0.040617	0.016059	9
36	2455059.9208	51664	0.041452	0.016892	9
37	2455391.7254	53921	0.042502	0.017086	11
38	2455394.6654	53941	0.042285	0.016861	11
39	2455422.0115	54127	0.044334	0.018840	9
40	2455423.0401	54134	0.043928	0.018431	9
41	2455481.6920	54533	0.038453	0.012805	11
42	2455482.5796	54539	0.043988	0.018338	11
43	2455766.0212	56467	0.048593	0.022212	9
44	2455767.0489	56474	0.047256	0.020873	9
45	2455768.0779	56481	0.047190	0.020804	9
46	2456196.9130	59398	0.051550	0.024058	9
47	2456205.8798	59459	0.050687	0.023172	9
48	2456496.9639	61439	0.053297	0.025031	9
49	2456497.1119	61440	0.054286	0.026020	9
50	2456497.9929	61446	0.053241	0.024973	9

** Primary Source: 1. Hoffmeister (1956); 2. Oosterhoff and Walraven (1966); 3. Kinman (1961); 4. Dean* et al. *(1977); 5. McNamara and Feltz (1976); 6. Balona and Martin (1978); 7. Rodríguez* et al. *(1995); 8. Derekas* et al. *(2009); 9. Present paper; 10. AAVSO (2013), observer DSI; 11. García (2012).*

Notes: The epochs in the third column and the O–C value in the fourth column were calculated using the quadratic ephemeris of Rodríguez et al. (1995), T_1 *= HJD 2447464.7101, and* P_1 *= 0.147010864 d. The* $(O–C)_c$ *values in column 5 were calculated using the elements from the cubic ephemeris in Equation 1 in the present paper, T = HJD 2447464.71508 and P = 0.147011243 d. Actual (O–C) values are displayed, not residuals from the regression analysis.*

In this paper, each numerical result from our observations and calculations is followed by the standard error in brackets, recognizing that the standard error is half the 95% confidence limits.

3. Analysis

Two analyses were performed. The first involved 50 times of maximum spanning the years 1952 to 2013, and followed as closely as possible the procedures employed by García (2012). In view of the results, a second analysis was performed, using only the data from 2003 to 2013.

A sample light curve of RS Gru obtained during one night by DSLR photometry is shown in Figure 1. Fifty times of maximum from the literature and from our observations are shown in the second column of Table 1. Three of the times of maximum in the paper by García (2012) represent data submitted by us to the AAVSO International Database. They appear as maxima 28, 29, and 30 in Table 2 in García's paper and in Table 1 in the present paper, where the times of maximum shown are those determined by us, so that a consistent method for determining times of maxima was used for all of our own data. Subsequent new times of maximum by us in Table 1 were not previously submitted to the AAVSO International Database. The epochs in the third column and the O–C values in the fourth column of Table 1 were calculated from the ephemeris of Rodríguez *et al.* (1995), namely $T_1 = 2447464.7101$ d and $P_1 = 0.147010864$ d.

Using the times of maximum and the epochs listed in Table 1, we then performed a linear least squares fit, which yielded an ephemeris with the new elements $T_0 = 2447464.7247$ (0.0008) HJD and $P_0 = 0.147011369$ (0.000000016) d. These results are close to those of García (2012). Using the new elements, a cubic (third order polynomial) regression was calculated, from the times of maximum in column two and the epochs in column three of Table 1, yielding the following ephemeris:

$$T_{max} = \text{HJD } 2447464.71508\ (0.00074) + 0.147011243\ (0.000000020)E + 4.220\ (0.298) \times 10^{-12}E^2 + 4.130\ (0.534) \times 10^{-17}E^3 \quad (1)$$

The fifth column in Table 1 contains the O–C values based upon the elements from Equation 1 above (that is, T = 2447464.71508 and P = 0.147011243) and the O–C diagram graphing those values is shown in Figure 2, where the superimposed curve represents a cubic (third order polynomial) expression. The O–C diagram and the superimposed cubic fit are generally similar to the plot in Figure 5 of García (2012). However, examination of García's Figure 5 and our Figure 2 reveals that the cubic expression is not an ideal fit. In view of this, and since our data extend the O–C diagram significantly for recent observation years, it was decided to analyze the more recent (2003 to 2013) data separately.

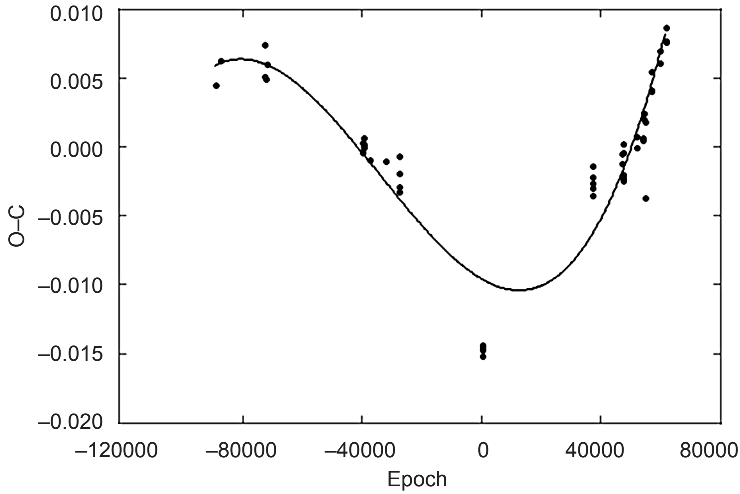

Figure 2. O–C diagram of RS Gru, representing all of the data in Table 1, from observations made between 1952 and 2013. The diagram is based on the elements of Rodriguez *et al.* (1995) T_0 = 2447464.7101 d and P_0 = 0.147010864 d.

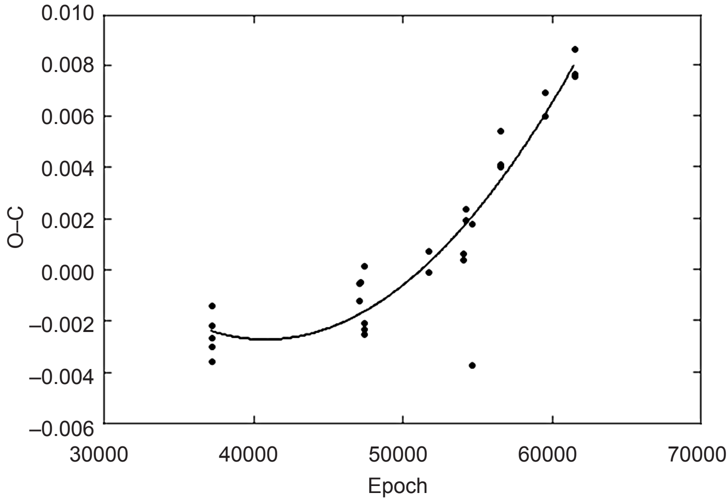

Figure 3. O–C diagram of RS Gru, representing maxima 23–50 of the data in Table 1, from 2003 to 2013. The diagram is based on the same elements as those used for Figure 2. The fitted curve is a quadratic function, the shape of the which (concave up) indicates that the period of RS Gru has been increasing during the years of these observations.

To this end the O–C diagram shown in Figure 3 was plotted, representing the epochs and O–C values in the fourth column of Table 1, for maxima 23 to 50. The curve represents a quadratic (second order polynomial) fit, which we consider to be a better fit to these recent data than that seen in Figure 2. A quadratic ephemeris in the form $T_{max} = T_0 + PE + AE^2$ is given by the following equation, based on an initial epoch of HJD 2452920.0196:

$$T_{max} = \text{HJD } 2452920.02019\ (0.00064) + 0.14701118\ (0.000\,000\,11)E + 2.513\ (0.466) \times 10^{-11}E^2 \quad (2)$$

From the coefficient of the second order term in Equation (2) above, the pulsation period of RS Gru is calculated to be increasing at the rate of dP/dt = 12.29 (2.31) × 10^{-8} d yr^{-1}, or dP/Pdt = 84.95 (14.74) × 10^{-8} yr^{-1}.

The first order term and the constant term (T_0) of Equation (2) indicate that the pulsation period of RS Gru was 0.14701118 (0.00000011) d at HJD 2452920 (7 October 2003). By rescaling the epochs and recalculating the ephemeris, it can also be shown that the pulsation period of RS Gru was 0.14701241 (0.00000012) d at HJD 2456497 (23 July 2013).

4. Conclusions

The present paper confirms the work of others that the pulsational period of RS Gru has increased since the 1988 studies of Rodríguez *et al.*, published in 1995. Furthermore, the O–C diagram of the entire dataset of results from 1952 to 2013, and in particular the separately analyzed results from 2003 to 2013, show that the pulsation period of the star is continually increasing.

In the first of our analyses of O–C values and ephemerides, which attempted to follow as closely as possible the methods of García (2012), the results for the cubic ephemeris seen above in Equation (1) are very close to the results seen in García’s Equation (2).

However, the O–C diagrams in García’s (2012) Figure 5 and our Figure 2 both show that the pulsational period of RS Gru underwent a change after the studies of Rodríguez (1995), whose data are represented by the lowest points on both O–C diagrams. In view of this, and in view of the fact that the cubic function shown on both of these O–C diagrams does not appear to represent an ideal fit, we decided that separate O–C analysis of the recent data from 2003 to 2013 might prove useful.

The results indicate that the pulsational period of RS Gru has been increasing continuously during those years. From the quadratic ephemeris, the period of RS Gru in at HJD 2456497 (23 July 2013) was calculated to be 0.14701241 (0.00000012) d. This figure differs significantly (by approximately 4 seconds) from the period of 0.14705874 d derived by García (2012) from Fourier analysis of more than 4,000 observations from various databases and personal observations made between HJD 2447880 (December 1989) and HJD 2455525 (November 2010). A similar difference is also found if the pulsational period of RS Gru is calculated from the first derivative of the cubic ephemeris during the time span from which the observations for the Fourier analysis were made.

Previous studies by others have shown both increasing and decreasing periods in high amplitude δ Scuti stars (Breger and Pamyatnykh 1998). However, the rate of increase in the period of RS Gru calculated by us for the years 2003 to 2013, dP/Pdt = 84.95 (15.74) $\times 10^{-8}$ yr^{-1}, is substantially greater than that published for any other Population I high amplitude δ Scuti star with radial pulsation, with the next largest figure being dP/Pdt = 15 $\times 10^{-8}$ yr^{-1} for AI Vel, according to Breger and Patmyatnykh (1998).

In view of this unusually high rate of change of the period of RS Gru, and because the data from 2003 to 2013 represent the most concentrated longitudinal series of the times of maximum of this star since it was found to be variable some 60 years ago, continued monitoring of its light curve each season will undoubtedly prove to be valuable.

5. Acknowledgements

The valuable assistance of Timothy Napier-Munn of the Astronomical Association of Queensland with regression analysis is gratefully acknowledged. The inclusion in this paper of the data by AAVSO observer Giorgio Di Scala (DSI; maxima 31, 33, and 34 in Table 1) is gratefully acknowledged.

References

AAVSO. 2013, observations from the AAVSO International Database (http://www.aavso.org).
Balona, L. A., and Martin, W. L. 1978, *Mon. Not. Roy. Astron. Soc.*, **184**, 1.
Berry, R., and Burnell, J. 2011, "Astronomical Image Processing for Windows," version 2.4.0, provided with *The Handbook of Astronomical Image Processing*, Willmann-Bell, Richmond, VA.
Breger, M., and Pamyatnykh, A. A. 1998, *Astron. Astrophys.*, **332**, 958.
Dean, J. F., Cousins, A. W. J., Bywater, R. A., and Warren, P. R. 1977, *Mem. Roy. Astron. Soc.*, **83**, 69.
Derekas, A., *et al.* 2009, *Mon. Not. R. Astron. Soc.*, **394**, 995.
García, J. R. 2012, *J. Amer. Assoc. Var. Star Obs.*, **40**, 272.
Hoffmeister, C. 1956, *Veröff. Sternw. Sonneberg*, **3**, 1.
Joner, M. D., and Laney, C. D. 2004, *Bull. Amer. Astron. Soc.*, **36**, 1429.
Kinman, T. D. 1961, *Roy. Greenwich Obs., Bull.*, **37**, 151.
McNamara, D. H., and Feltz, K. A., Jr. 1976, *Publ. Astron. Soc. Pacific*, **88**, 510.
Menzies, J. W., Cousins, A. W. J., Banfield, R. M., and Laing, J. D. 1989, *S. Afr. Astron. Obs., Circ.*, **13**, 1.

Oosterhoff, P. Th., and Walraven, Th. 1966, *Bull. Astron. Inst. Netherlands*, **18**, 387.

Rodríguez, E., Rolland, A., Costa, V., and Martin, S. 1995, *Mon. Not. Roy. Astron. Soc.*, **277**, 965.

Van Citters, G. W., Jr. 1976, *Astron. J.*, **81**, 766.

Multi-Longitude Observation Campaign of KV Cancri: an RR Lyrae Star with Irregular Blazhko Modulations

Pierre de Ponthière
15 Rue Pré Mathy, Lesve, Profondeville 5170, Belgium; address email correspondence to pierredeponthiere@gmail.com

Michel Bonnardeau
MBCAA Observatory, Le Pavillon, Lalley 38930, France

Franz-Josef (Josch) Hambsch
12 Oude Bleken, Mol, 2400, Belgium

Tom Krajci
P.O. Box 1351, Cloudcroft, NM 88317

Kenneth Menzies
318A Potter Road, Framingham, MA 01701

Richard Sabo
2336 Trailcrest Drive, Bozeman, MT 59718

Received September 9, 2013; revised September 30, 2013; accepted October 3, 2013

Abstract We present the results of multi-longitude observations of KV Cancri, an RR Lyrae star showing an irregular Blazhko effect. With a pulsation period of 0.50208 day, the times of light curve maxima are delayed by 6 minutes per day. This daily delay regularly leads to long periods of time without maximum light curve observations for a given site. To cope with this observing time window problem, we have organized a multi-longitude observation campaign including a telescope of the AAVSONet. From the observed light curves, 92 pulsation maxima have been measured covering about six Blazhko periods. The Fourier analysis of magnitudes at maximum light has revealed a main Blazhko period of 77.6 days and also a secondary period of 40.5 days. A Fourier analysis of (O–C) values did not show the secondary Blazhko period. The frequency spectrum of the complete light curve, from a Fourier analysis and successive pre-whitening with PERIOD04, has shown triplet structures around the two Blazhko modulation frequencies but with slightly different periods (77.8 and 42.4 days). The second Blazhko frequency is statistically not a harmonic of the main Blazhko frequency. Besides the two Blazhko modulations KV Cnc presents other particularities like irregularities from Blazhko cycle to cycle and very fast magnitude variations which can reach a maximum of 2.5 magnitudes per hour over a period of 15 minutes. This campaign shows that regular observations by amateur astronomers remain important. Indeed, such a detailed characterization of the Blazhko effect could not be obtained from large-scale surveys, as cooperative long time-series observations are needed.

1. Introduction

The designation of KV Cnc appeared in the *General Catalogue of Variable Stars* (GCVS; Samus *et al.* 2011) with the 80th Name List of Variable Stars (Kazarovets *et al.* 2011), and previously this star was identified as GSC 1948-1733 and NSVS 7404884. From the Northern Sky Variability Survey data (Wozniak *et al.* 2004), Wils *et al.* (2006) have measured a pulsation period of 0.50202 day and they also provided an uncertain Blazhko period of 42 days.

The current data were gathered during 158 nights between January 2012 and May 2013. During this period of 480 days, a total of 32,280 magnitude measurements covering six Blazhko cycles were collected. The observations were made by the authors using 20-cm to 40-cm telescopes located in Bozeman (Montana), Cloudcroft (New Mexico), Framingham (Massachusetts), Lesve (Belgium), and Rhône-Alpes (France). The numbers of observations for the different locations are respectively 3367, 23614, 2621, 2610, and 92.

The comparison stars are given in Table 1. The star coordinates and magnitudes in B and V bands were obtained from the AAVSO's International Database (AID). Cloudcroft observations have been reduced with C2 as a magnitude reference and C4 as a check star. The other observations have used C1 as a magnitude reference and C3 and C4 as check stars.

Since measurements were performed with V filters only, it was impossible to transform the measurements to the standard system. However, thanks to simultaneous maximum measurements from the instruments in Cloudcroft and Bozeman it has been possible to take account of the magnitude offset due to the color differences of the magnitude reference stars. This offset has been applied to observations based on C1 as reference. Dark and flat field corrections were performed with MAXIMDL software (Diffraction Limited 2004), and aperture photometry was performed using LESVEPHOTOMETRY (de Ponthière 2010), a custom software which also evaluates the SNR and estimates magnitude errors.

Table 1. Comparison stars.

Identification	*R. A. (2000)* h m s	*Dec. (2000)* ° ′ ″	*B*	*V*	*B–V*	
GSC 1948-1556	08 40 05.47	+27 39 12.1	12.526	11.998	0.528	C1
GSC 1948-1451	08 40 09.30	+27 41 19.4	13.627	12.946	0.681	C2
GSC 1948-1631	08 40 34.19	+27 47 50.0	13.972	13.204	0.768	C3
GSC 1948-1548	08 40 00.87	+27 42 35.9	14.110	13.543	0.567	C4

Table 2. List of measured maxima of KV Cnc.

Maximum HJD	*Error*	*O–C (day)*	E	*Magnitude (V)*	*Error*	*Location**
2455943.4189	0.0026	0.0553	–184	12.023	0.01	2
2455944.4178	0.0030	0.0500	–182	12.007	0.01	2
2455960.4523	0.0012	0.0170	–150	11.663	0.01	2
2455962.4642	0.0018	0.0205	–146	11.709	0.012	2
2455967.5064	0.0021	0.0416	–136	11.930	0.003	3
2455970.5282	0.0026	0.0507	–130	11.990	0.005	3
2455971.5335	0.0035	0.0518	–128	11.990	0.004	3
2455978.5639	0.0016	0.0526	–114	12.144	0.004	3
2455984.5914	0.0026	0.0548	–102	12.220	0.004	3
2455989.6193	0.0053	0.0616	–92	12.278	0.005	4
2455992.6310	0.0037	0.0607	–86	12.276	0.006	3
2455996.6553	0.0038	0.0681	–78	12.288	0.004	5
2455997.6525	0.0039	0.0611	–76	12.249	0.005	3
2455998.6595	0.0047	0.0638	–74	12.285	0.005	4
2456000.6733	0.0077	0.0692	–70	12.255	0.005	4
2456004.6854	0.0043	0.0644	–62	12.255	0.005	3
2456008.7018	0.0034	0.0639	–54	12.245	0.005	3
2456008.7032	0.0029	0.0653	–54	12.243	0.004	5
2456008.7041	0.0043	0.0662	–54	12.243	0.005	4
2456009.7026	0.0078	0.0605	–52	12.277	0.005	4
2456009.7085	0.0040	0.0664	–52	12.277	0.004	5
2456011.7174	0.0065	0.0669	–48	12.245	0.005	4
2456011.7219	0.0035	0.0714	–48	12.243	0.004	5
2456013.7404	0.0043	0.0814	–44	12.250	0.005	4
2456015.7505	0.0039	0.0831	–40	12.204	0.005	4
2456016.7472	0.0030	0.0756	–38	12.185	0.006	4
2456021.7383	0.0017	0.0456	–28	11.999	0.005	5
2456023.7350	0.0018	0.0338	–24	11.947	0.007	4
2456028.7337	0.0007	0.0114	–14	11.703	0.004	5
2456029.7368	0.0013	0.0103	–12	11.696	0.005	4
2456030.7368	0.0010	0.0061	–10	11.617	0.019	5
2456031.7412	0.0018	0.0063	–8	11.590	0.039	5
2456033.7459	0.0007	0.0025	–4	11.541	0.006	4
2456034.7501	0.0020	0.0025	–2	11.545	0.006	4
2456035.7518	0.0030	0.0000	0	11.524	0.005	4
2456038.7683	0.0006	0.0038	6	11.614	0.006	4
2456039.7718	0.0005	0.0031	8	11.622	0.004	5
2456039.7740	0.0006	0.0053	8	11.615	0.006	4
2456055.3917	0.0026	0.0576	39	12.106	0.012	2

Table continued on following pages

Table 2. List of measured maxima of KV Cnc, cont.

Maximum HJD	Error	O–C (day)	E	Magnitude (V)	Error	Location*
2456061.4163	0.0052	0.0569	51	12.165	0.016	2
2456202.9511	0.0012	–0.0033	333	11.862	0.006	4
2456205.9689	0.0011	0.0018	339	11.969	0.005	4
2456209.0013	0.0040	0.0215	345	12.051	0.011	5
2456248.6817	0.0039	0.0353	424	12.048	0.011	2
2456254.6918	0.0015	0.0200	436	11.861	0.005	3
2456256.6971	0.0018	0.0169	440	11.815	0.004	3
2456265.7291	0.0013	0.0109	458	11.777	0.004	3
2456268.7406	0.0016	0.0098	464	11.777	0.004	3
2456276.7683	0.0012	0.0037	480	11.724	0.016	3
2456279.7819	0.0015	0.0046	486	11.730	0.013	4
2456280.7878	0.0004	0.0063	488	11.767	0.004	5
2456281.7901	0.0017	0.0044	490	11.740	0.014	4
2456282.7959	0.0013	0.0060	492	11.778	0.01	4
2456287.8229	0.0015	0.0119	502	11.924	0.004	3
2456290.8423	0.0023	0.0186	508	11.960	0.014	4
2456292.8584	0.0031	0.0263	512	12.062	0.006	3
2456294.8715	0.0026	0.0309	516	12.109	0.005	3
2456295.8814	0.0023	0.0366	518	12.106	0.005	3
2456297.9004	0.0045	0.0472	522	12.158	0.007	5
2456300.9255	0.0029	0.0596	528	12.202	0.007	3
2456303.4492	0.0041	0.0728	533	12.168	0.011	2
2456308.9646	0.0043	0.0650	544	12.125	0.019	4
2456308.9684	0.0096	0.0688	544	12.146	0.073	5
2456310.9718	0.0034	0.0637	548	12.106	0.01	4
2456311.9694	0.0030	0.0571	550	12.117	0.011	5
2456311.9742	0.0042	0.0619	550	12.101	0.017	4
2456312.9772	0.0068	0.0607	552	12.079	0.013	4
2456313.9725	0.0027	0.0518	554	12.064	0.011	4
2456314.9747	0.0028	0.0497	556	12.077	0.011	5
2456315.9759	0.0023	0.0467	558	12.028	0.011	4
2456323.4865	0.0041	0.0257	573	11.993	0.02	2
2456323.9876	0.0035	0.0247	574	11.980	0.017	4
2456328.4990	0.0028	0.0171	583	12.007	0.008	3
2456330.5028	0.0016	0.0124	587	11.975	0.004	3
2456334.5124	0.0017	0.0051	595	11.937	0.004	3
2456340.5428	0.0015	0.0102	607	12.000	0.008	1
2456343.5518	0.0015	0.0066	613	11.984	0.009	1
2456351.5974	0.0035	0.0184	629	11.734	0.019	4

Table continued on next page

Table 2. List of measured maxima of KV Cnc, cont.

Maximum HJD	*Error*	*O–C (day)*	E	*Magnitude (V)*	*Error*	*Location**
2456352.6018	0.0036	0.0186	631	11.726	0.022	4
2456353.6024	0.0021	0.0150	633	11.682	0.023	4
2456354.6071	0.0020	0.0154	635	11.679	0.016	4
2456358.6164	0.0019	0.0079	643	11.645	0.016	4
2456363.6383	0.0018	0.0087	653	11.825	0.011	5
2456363.6391	0.0025	0.0095	653	11.784	0.024	4
2456369.6638	0.0015	0.0088	665	12.022	0.004	3
2456374.7017	0.0026	0.0256	675	12.188	0.006	3
2456376.7208	0.0073	0.0363	679	12.257	0.026	5
2456392.8007	0.0072	0.0487	711	12.048	0.014	5
2456400.8163	0.0015	0.0305	727	11.944	0.007	5
2456403.3272	0.0024	0.0309	732	11.868	0.012	2
2456407.3363	0.0025	0.0231	740	11.885	0.01	2
2456418.3574	0.0037	–0.0022	762	11.970	0.012	2

Locations: 1) Rhône–Alpes (France); 2) Lesve (Belgium); 3) Framingham (MA); 4) Cloudcroft (NM); 5) Bozeman (MT)

2. Light curve maxima analysis

The times of maxima of the light curves have been evaluated with custom software (de Ponthière 2010) fitting the light curve with a smoothing spline function (Reinsch 1967). Table 2 provides the list of ninety-two observed maxima and Figures 1a and 1b show the (O–C) and M_{max} (Magnitude at Maximum) values. From an inspection of the (O–C) and M_{max} graphs the Blazhko effect is obviously irregular. The shape of the (O–C) curve during Blazhko cycles does not repeat. During the first observation season, between the dates HJD 2455970 and 2456011, the (O–C) values vary more or less linearly before an abrupt fall. This (O–C) curve variation does not repeat during the next season. The M_{max} graph suggests the presence of a second modulation frequency. The Blazhko effect is itself apparently modulated by a lower frequency component.

A linear regression of all available (O–C) values has provided a pulsation period of 0.5020802 d (1.99171 d^{-1}). The (O–C) values have been re-evaluated with this new pulsation period and the pulsation ephemeris origin has been set to the highest recorded brightness maximum: HJD 2456035.7518. The new derived pulsation elements are:

$$HJD_{Pulsation} = (2456035.7518 \pm 0.0030) + (0.5020802 \pm 0.0000078)\, E_{Pulsation} \quad (1)$$

The derived pulsation period is in good agreement with the value of 0.50202d

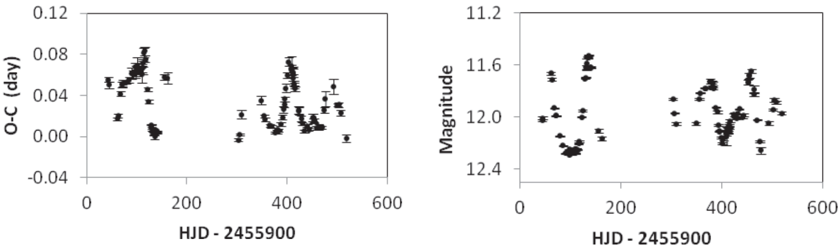

Figure 1. KV Cnc O–C (days, on left) and M_{max} magnitude at maximum (on right).

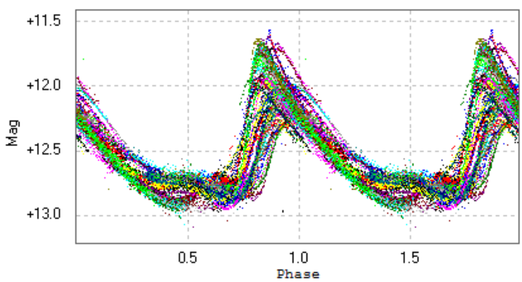

Figure 2. KV Cnc light curve folded with pulsation period of 0.50202 d.

Table 3. Blazhko spectral components from light curve maxima.

Frequency (cycle/days)	*σ(d⁻¹)*	*Period (days)*	*σ(d)*	*Amplitude*	*ϕ (cycle)*	*SNR*
From (O–C) values						
				(days)		
0.01298	$9\ 10^{-5}$	77.02	0.54	0.028	0.926	10.4
From M_{max}						
				(V mag.)		
0.01289	$4\ 10^{-5}$	77.57	0.25	0.245	0.993	22.6
0.02471	$9\ 10^{-5}$	40.48	0.14	0.119	0.398	11.0

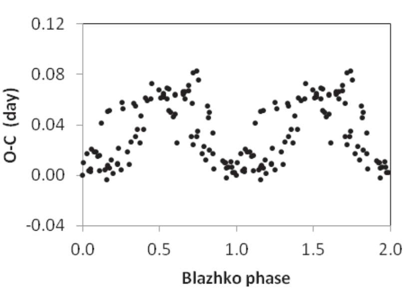

Figure 3. KV Cnc O–C based on Blazhko period of 77.57 days.

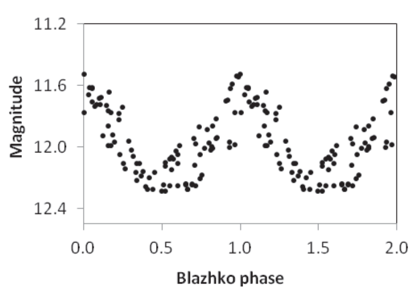

Figure 4. KV Cnc M_{max} based on Blazhko period of 77.57 days.

published by Wils *et al.* (2006). The folded light curve on this pulsation period is shown in Figure 2.

To determine the Blazhko period, Fourier analyses and sine-wave fittings of the (O–C) values and M_{max} (Magnitude at Maximum) values were performed with PERIOD04 (Lenz and Breger 2005). These analyses were limited to the first two frequency components and are given in Table 3. The frequency uncertainties have been evaluated from the Monte Carlo simulation module of PERIOD04. The obtained periods (77.02 ± 0.54 and 77.57 ± 0.25 days) for the main Blazhko effect agree within the errors. Another secondary Blazhko period of 40.48 days is found in the spectrum of M_{max} which is close to the uncertain value of 42 days provided by Wils *et al.* (2006). They probably did not detect the main Blazhko period from the Northern Sky Variability Survey due to the scarcity of the data.

On this basis the best Blazhko ephemeris is

$$HJD_{Blazhko} = 2456035.7518 + (77.57 \pm 0.25)\ E_{Blazhko} \qquad (2)$$

where the origin has been selected as the epoch of the highest recorded maximum.

The (O–C) and M_{max} curves folded with the Blazhko period of 77.02 days are given in Figures 3 and 4. In these diagrams, the scatter of the data is mainly due to the second Blazhko frequency and the irregular behavior from Blazhko cycle to cycle. An attempt at pre-whitening with the secondary Blazhko frequency has not significantly reduced the scatter in the folded (O–C) and M_{max} graphs. Due to an irregular Blazhko effect, the two detected frequency components are not able to precisely model the (O–C) and M_{max} data series.

3. Frequency spectrum analysis of the light curve

In the preceding paragraph, describing the M_{max} analysis, a primary pulsation and two Blazhko frequencies have been identified. It will be shown that these modulating frequencies are clearly present in the spectrum of the complete light curve.

The spectrum of a signal modulated in amplitude and phase is characterized by a pattern of peaks called multiplets at the positions $kf_0 \pm nf_B$ with k and n being integers corresponding respectively to the harmonic and multiplet orders. The frequencies, amplitudes and phases of the multiplets have been obtained with PERIOD04 by performing a succession of Fourier analyses, pre-whitenings and sine-wave fittings. Only the harmonic and multiplet components having a signal to noise ratio (SNR) greater than 4 have been retained as significant signals. Table 5 provides the complete list of Fourier components with their amplitudes, phases, and uncertainties. Besides the pulsation frequency f_0 and harmonics nf_0, two series of triplets, $nf_0 \pm f_B$ and $nf_0 \pm f_{B2}$, based on the principal and secondary Blazhko frequencies f_B and f_{B2} have been found. The Blazhko frequencies and corresponding periods are tabulated in Table 4 with their

Table 4. Blazhko frequencies and periods derived from triplets.

Component	*Derived from*	*Frequency (d^{-1})*	*σ(d^{-1})*	*Period (d)*	*σ(d)*
f_0	—	1.991689	1.7×10^{-6}	0.5020864	4×10^{-7}
f_B	$f_0 + f_B$	0.012853	8×10^{-6}	77.80	0.05
f_{B2}	$f_0 + f_{B2}$	0.023593	16×10^{-6}	42.39	0.03

Table 5. Multi–frequency fit results.

Component	*f(d^{-1})*	*σ(f)*	*A_i (mag.)*	*σ(A_i)*	*Φ_i (cycle)*	*σ(Φ_i)*	*SNR*
f_0	1.991689	1.7×10^{-6}	0.3646	0.0008	0.2022	0.0005	118.5
$2\,f_0$	3.983378	—	0.1298	0.0012	0.7825	0.0013	46.0
$3\,f_0$	5.975067	—	0.0818	0.0011	0.4018	0.0018	29.8
$4\,f_0$	7.966757	—	0.0400	0.0009	0.0400	0.0046	16.4
$5\,f_0$	9.958446	—	0.0268	0.0010	0.6656	0.0065	13.5
$6\,f_0$	11.950135	—	0.0203	0.0011	0.3226	0.0082	11.7
$7\,f_0$	13.941824	—	0.0110	0.0009	0.0354	0.0119	7.0
$8\,f_0$	15.933513		0.0055	0.0008	0.7105	0.0230	3.9
f_0+f_B	2.004542	8×10^{-6}	0.0582	0.0011	0.5060	0.0031	18.9
f_0-f_B	1.978836	—	0.0759	0.0009	0.0580	0.0017	24.7
$2\,f_0+f_B$	3.996231	—	0.0482	0.0010	0.1499	0.0040	17.1
$2\,f_0-f_B$	3.970525	—	0.0419	0.0011	0.6413	0.0044	14.8
$3\,f_0+f_B$	5.987920	—	0.0303	0.0011	0.7451	0.0060	11.0
$3\,f_0-f_B$	5.962215	—	0.0214	0.0010	0.2807	0.0076	7.8
$4\,f_0+f_B$	7.979609	—	0.0216	0.0011	0.3640	0.0076	8.9
$4\,f_0-f_B$	7.953904	—	0.0244	0.0011	0.8420	0.0071	9.9
$5\,f_0+f_B$	9.971299	—	0.0130	0.0009	0.9890	0.0116	6.6
$5\,f_0-f_B$	9.945593	—	0.0211	0.0011	0.5055	0.0079	10.7
$6\,f_0+f_B$	11.962988	—	0.0096	0.0008	0.5410	0.0144	5.5
$6\,f_0-f_B$	11.937282	—	0.0150	0.0011	0.1600	0.0119	8.7
$7\,f_0+f_B$	13.954677	—	0.0096	0.0009	0.1890	0.0115	6.1
$7\,f_0-f_B$	13.92897	—	0.0089	0.0007	0.8373	0.0154	5.7
f_0+f_B	2.015282	16×10^{-6}	0.0394	0.0008	0.2681	0.0034	12.8
f_0-f_B	1.968096	—	0.0258	0.0009	0.7453	0.0066	8.4
$2\,f_0+f_B$	4.006971	—	0.0352	0.0009	0.8826	0.0042	12.5
$2\,f_0-f_B$	3.959785	—	0.0124	0.0010	0.1666	0.0113	4.3
$3\,f_0+f_B$	5.998660	—	0.0174	0.0010	0.5395	0.0084	6.4
$3\,f_0-f_B$	5.951475	—	0.0154	0.0009	0.7617	0.0102	5.6

Table 6. KV Cnc harmonic, triplet amplitudes, ratios, and asymmetry parameters.

i	A_i/A_1	A_i^+/A_1	A_i^-/A_1	R_i	Q_i	$R_i\,(f_{B2})$	$Q_i\,(f_{B2})$
1	1.00	0.16	0.21	0.77	–0.13	1.53	0.21
2	0.36	0.13	0.11	1.15	0.07	2.85	0.48
3	0.22	0.08	0.06	1.42	0.17	1.13	0.06
4	0.11	0.06	0.07	0.89	–0.06	—	—
5	0.07	0.04	0.06	0.62	–0.24	—	—
6	0.06	0.03	0.04	0.64	–0.22	—	—
7	0.03	0.03	0.02	1.08	0.04	—	—
8	0.02	—	—	—	—	—	—

uncertainties. These Blazhko periods are close to the values obtained with M_{max} analysis given in Table 3.

During the sine-wave fitting, the fundamental frequency f_0 and largest triplets $f_0 + f_B$ and $f_0 + f_{B2}$ have been left unconstrained and the other frequencies have been entered as combinations of these three frequencies. The uncertainties of frequencies, amplitudes, and phases have been estimated by Monte Carlo simulations. The amplitude and phase uncertainties have been multiplied by a factor of two as it is known that the Monte Carlo simulations underestimate these uncertainties (Kolenberg *et al.* 2009). The two Blazhko modulation frequencies f_B (0.012853) and f_{B2} (0.023593) are statistically ($\sigma = 16 \times 10^{-6}$) not in resonance, provided that the n:m resonance ratios with n or m greater than 10 are not taken into account. For CZ Lacertae (Sódor *et al.* 2011) and V784 Ophiuchi (de Ponthière *et al.* 2013) 5:4 and 5:6 resonance ratios have been found.

Table 6 lists for each harmonic the amplitude ratios A_i/A_1 and the ratios usually used to characterize the Blazhko effect, that is, A_i^+/A_1 ; A_i^-/A_1 ; $R_i = A_i^+/A_i^-$; and asymmetries $Q_i = (A_i^+ - A_i^-)/(A_i^+ + A_i^-)$. In the present case the side lobe A_i^- is larger than A_i^+ which leads to a negative value (–0.13) for the Q_i asymmetry ratio. It is not unusual but for the majority of the Blazhko stars, this asymmetry ratio is positive (see figure 10 of Alcock *et al.* 2003). The R_i and Q_i ratios for triplets around the secondary Blazhko frequency f_{B2} are also given in Table 6. The asymmetry ratios Q_i for f_{B2} are positive.

4. Light curve variations over Blazhko cycle

Subdividing the data set into temporal subsets is a classical method to visualize and analyze the light curve variations over the Blazhko cycle. Ten temporal subsets corresponding to the different Blazhko phase intervals Ψ_i (i = 0, 9) have been created using the epoch of the highest recorded maximum (2456035.7518) as the origin of the first subset. The folded light curves for the ten subsets are presented in Figure 5. Over the subsets, the number of data points varies between 1916 and 5678. Other than a lack of coverage in two

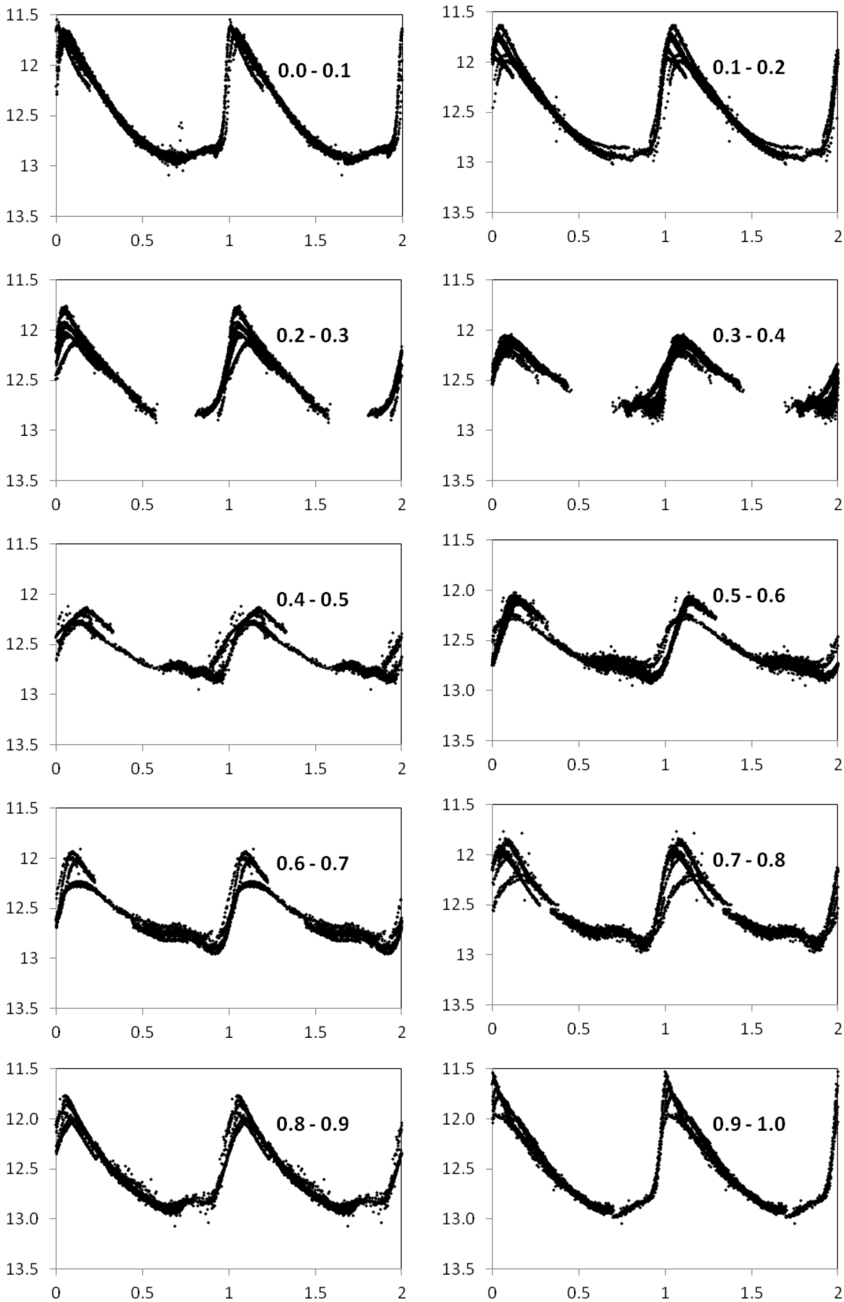

Figure 5. KV Cnc light curves for different temporal subsets (magnitude vs. pulsation phase) based on a Blazhko period of 77.80 days.

Table 7. KV Cnc Fourier coefficients over Blazhko cycle based on period of 77.80 days.

Ψ (cycle)	A_1 (mag.)	A_2 (mag.)	A_3 (mag.)	A_4 (mag.)	Φ_1 (rad.)	Φ_{21} (rad.)	Φ_{31} (rad.)	Φ_{41} (rad.)
0.0–0.1	0.503	0.190	0.117	0.082	1.410	2.315	4.860	1.300
0.1–0.2	0.467	0.187	0.133	0.082	1.356	2.430	5.207	1.953
0.2–0.3	0.420	0.090	0.096	0.076	1.142	2.487	4.463	1.278
0.3–0.4	0.215	0.201	0.068	0.093	0.398	4.022	4.811	3.762
0.4–0.5	0.244	0.099	0.036	0.021	1.206	2.213	5.651	1.804
0.5–0.6	0.296	0.133	0.068	0.033	1.148	2.308	5.326	1.332
0.6–0.7	0.279	0.134	0.080	0.039	0.996	2.315	5.350	1.856
0.7–0.8	0.345	0.156	0.094	0.044	0.975	2.216	5.103	1.596
0.8–0.9	0.402	0.141	0.089	0.048	1.309	2.230	4.587	0.987
0.9–1.0	0.482	0.191	0.115	0.075	1.409	2.405	5.124	1.666

subsets when the light curve is at its minimum, the data points are relatively well distributed.

Despite the subdivision over the Blazhko cycle, a scatter still remains on the light curves; this fact has been already pointed out in the light curve maxima analysis. A visual inspection of the light curves in different subsets reveals that the light curve slope is at its steepest value in the two subsets from Blazhko phases 0.9 to 0.1, that is, when the peak to peak magnitude variations and magnitude at maximum are at their maximal values. An astonishing slope of 2.9 magnitudes per hour has been recorded. Generally the RR Lyrae light curves present a bump just before the minimum. For KV Cnc, in the two subsets from 0.9 to 0.1, the bump is replaced by a slightly increasing slope.

Fourier analyses and Least-Square fittings have been performed on the different temporal subsets. For the fundamental and the first four harmonics the amplitudes A_i and the epoch-independent phase differences ($\Phi_{k1} = \Phi_k - k\Phi_{k1}$) are given in Table 7 and plotted in Figure 6. The amplitudes have large uncertainties for the subsets 0.2–0.3 and 0.3–0.4. This is due to the lack of coverage at light curve minimum as shown in Figure 5. These amplitude uncertainties probably impact the epoch-independent phase differences especially in the subset 0.3–0.4 where the phase differences seem to be dubious. As expected the A_1 amplitudes of the fundamental frequency have lower values for Blazhko phases 0.4 to 0.7, that is, when the light curve amplitude variations on the pulsation are weaker.

5. Conclusions

Blazhko modulations have been detected by measurements of (O–C) values and magnitude of light curve maxima and confirmed by complete light curve Fourier analysis. The Blazhko periods obtained by the complete light curve

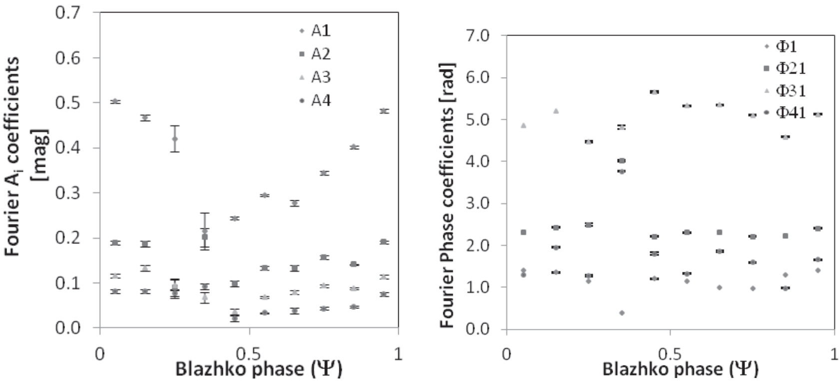

Figure 6. (left): KV Cnc Fourier A_i amplitude (mag.) for the ten temporal subsets based on a Blazhko period of 77.80 days. (right): Fourier Φ_1 and Φk_i phase (rad.) for the ten temporal subsets based on a Blazhko period of 77.80 days.

analysis are reported as their period uncertainties are lower. The main Blazhko period ($1/f_B$) is 77.80 ± 0.05 days. The secondary Blazhko period ($1/f_{B2}$) is 42.39 ± 0.03 days. These two Blazhko modulations are not in resonance. Regular and coordinated multi-longitude observations by amateurs have been needed to cope with the problem of observation time windows created by the pulsation period of 0.50208 day. Amateur astronomers observing RR Lyrae stars have the tendency to restrict their observations near the maximum of light curve which is indeed important. However, the problems encountered in the Fourier analysis in Blazhko subsets were due to a lack of data during the minimum part of the pulsation cycle. Observers are encouraged to also image during pulsation phases other than near the maximum.

6. Acknowledgements

Dr. A. Henden, Director of the AAVSO, and the AAVSO are acknowledged for the use of AAVSOnet telescopes at Cloudcroft (New Mexico). The authors thank the referee for constructive comments which have helped to clarify and improve the paper. This work has made use of The International Variable Star Index (VSX) maintained by the AAVSO and of the SIMBAD astronomical database (http://simbad.u-strasbg.fr).

References

Alcock, C., *et al.* 2003, *Astrophys. J.*, 598, 597.

de Ponthière, P. 2010, LESVEPHOTOMETRY, automatic photometry software (http://www.dppobservatory.net).

de Ponthière, P., *et al.* 2013, *J. Amer. Assoc. Var. Star Obs.*, **41**, 214.

Diffraction Limited. 2004, MAXIMDL image processing software (http://www.cyanogen.com).

Kazarovets, E. V., *et al.* 2011, *Inf. Bull. Var. Stars,* No. 6008, 1.

Kolenberg, K., *et al.* 2009, *Mon. Not. Roy. Astron. Soc.*, **396**, 263.

Lenz, P., and Breger, M. 2005, *Commun. Asteroseismology*, **146**, 53.

Reinsch, C. H. 1967, *Numer. Math.*, **10**, 177.

Samus, N. N., *et al.* 2011, *General Catalogue of Variable Stars* (GCVS database, Version 2011 January, http://www.sai.msu.su/gcvs/gcvs/index.htm).

Sódor, Á. *et al.* 2011, *Mon. Not. Roy. Astron. Soc.*, **411**, 1585.

Wils, P., Lloyd, C., and Bernhard, K. 2006, *Mon. Not. Roy. Astron. Soc.*, **368**, 1757.

Wozniak, P., *et al.* 2004, *Astron. J.*, **127**, 2436.

Multicolor CCD Photometry and Period Analysis of Three Pulsating Variable Stars

Kevin B. Alton
UnderOak Observatory, 70 Summit Avenue, Cedar Knolls, NJ 07927; mail@underoakobservatory.com

Received November 21, 2013; revised January 14, 2014; accepted January 28, 2014

Abstract Multicolor CCD photometry of three pulsating variable stars, RR Leo, TYC 790-1124-1, and V337 Ori has lead to period solutions using Fourier methods on light curves acquired at UnderOak Observatory (UO). New photometric data from RR Leo largely corroborate findings previously reported for this well-studied RRab variable. An O–C diagram period analysis using a rich historical record of time-of-maximum light data produced an updated quadratic ephemeris for RR Leo. Although not compelling, underlying sinusoidal variability in the quadratic residuals suggest that this intrinsic variable may also have a gravitationally bound cohort. Light curves from the poorly studied HADS variable TYC 790-1124-1 were remarkably symmetrical; this behavior was observed during a single campaign in 2011 which lasted only one month. Fortunately, starting nearly a decade ago photometric data were also captured by the ASAS survey between 2002 and 2009; the combined results reveal that the fundamental period and light curve shape for TYC 790-1124-1 has substantively remained unchanged. V337 Ori has only been studied by two other investigative groups within the past three years; their results and the two most prominent pulsation frequencies at 4.96877 and 6.72 c/d detected in the UO light curves are in good agreement. Notably, this HADS exhibits significant cycle-to-cycle amplitude variability which may be related to these and other pulsation modes not detected in the present study.

1. Introduction

CCD images in three passbands (B, V, and I_c) were used to produce new light curves for the intrinsically variable stars RR Leo, V337 Ori, and TYC 790-1124-1. Light curves for RR Leo, an RR Lyrae pulsator, have been available in the literature for over eighty years using data derived from photographic plates (Allen and Marsh 1932). Thereafter multi-color CCD-based light curves of this RRab variable have been published by Liu and Janes (1989) and Ekmekçi *et al.* (2012). By contrast, light curves and period analyses for V337 Ori (Khruslov 2011; Wils *et al.* 2012) and TYC 790-1124-1 (Pojmański *et al.* 2005), both high-amplitude δ Scuti (HADS) variables, were only published within the last decade from data collected during the ASAS (Pojmański 2002), NSVS (Woźniak *et al.* 2004), and/or SuperWASP surveys (Butters *et al.* 2010).

2. Image acquisition and data reduction

All images were acquired at UnderOak Observatory (UO) in Morris County, New Jersey, using a 20-cm catadioptric telescope outfitted with an SBIG ST-402ME CCD camera. Automated multi-bandwidth imaging was performed with SBIG photometric B, V, and I_c filters manufactured to match the Bessell prescription. The computer clock was updated automatically via the U.S. Naval Observatory Time Server immediately prior to each session and all observations recorded as UTC. Image acquisition (object frames, darks, and flats) was performed using CCDSOFT 5 (Software Bisque 2011) while calibration and registration were accomplished with AIP4WIN v2.3.1 (Berry and Burnell 2008). Exposure time for B-filtered images was 90 seconds, whereas V- and I-filtered data were collected within 60 seconds with a thermoelectrically cooled camera. Darks (n > 10) were time- and temperature-matched with object frames; the median of all darks collected nightly was subtracted from each object frame. As necessary, new twilight sky-flats (bias- and dark-corrected) in each band-pass were collected (n > 15) after any change in the optical train orientation; final object images were corrected by standard flats division. Further photometric reduction was performed with MPO CANOPUS v10.3.0.2 (Minor Planet Observer 2010) to ultimately calculate ephemerides (HJD from UTC) and the fundamental period of variability (Henden and Kaitchuck 1990). To minimize the need for air mass corrections due to differential refraction and color extinction, 1) comparison stars were always within the same field-of-view (~7.9 × 11.8 arcmin) for each target image, 2) every effort was made to select comparison stars which were as close to the color index (B–V) of each target as possible, and 3) only data from stars positioned above 30° altitude (airmass < 2.0) were included in light curves.

The mean derived magnitude for each comparison star varied between ± 0.025 (V and I_c) and ± 0.04 (B) mag. Over each session, Comp/Cavg values remained essentially constant, indicating comparison stars did not exhibit any variable behavior beyond that which would be expected from experimental error. As an example, this is illustrated (Figure 1) where the nearly parallel fit of the four comparison stars (B-bandpass) used to derive magnitudes for TYC 790-1124-1 also suggests that did they did not need to be color-corrected (air mass = 1.134 to 1.996). This finding is particularly relevant since, compared to V- and I-passbands, the B-filtered data are the most affected by air mass differences. Similar results were also obtained with the comparison stars used for V337 Ori and RR Leo (Table 1). Instrumental readings were reduced to catalog-based magnitudes using the "Derivedmags" feature and the MPOSC3 reference catalog built into MPO CANOPUS. When using more than one comparison star, a separate derived magnitude is computed for each target-comparison pair and the mean becomes the derived magnitude for the target. Almost all stars in the MPOSC3 reference catalog have $BVRI_c$ magnitudes derived from

Table 1. Astrometric coordinates (J2000) and MPOSC3 catalog magnitudes (B, V, and I_c) for RR Leo, TYC 790 1124 01, V337 Ori, and the corresponding comparison stars (C1–C4) used in this study.

Star Identification	*R.A.* h m s	*Dec.* ° ′ ″	*MPOSC3*[a] *B mag.*	*MPOSC3*[a] *V mag.*	*MPOSC3*[a] I_c *mag.*	*MPOSC3*[a] *(B–V)*
RR Leo	10 07 43.47	23 59 30.4	9.78–11.56[b]	9.69–11.12[b]	9.61–10.59[b]	0.01–0.43[b]
C1	10 07 41.56	24 04 50.1	12.47	11.84	11.13	0.63
C2	10 07 33.83	24 03 13.4	13.77	13.25	12.64	0.52
C3	10 07 51.06	24 05 26.9	14.12	13.55	12.89	0.57
TYC 790–1124–01	07 44 51.02	13 15 03.6	10.44–10.80[b]	10.05–10.32[b]	9.63–9.80[b]	0.35–0.51[b]
C1	07 44 42.71	13 17 39.8	12.00	11.31	10.54	0.69
C2	07 44 31.16	13 16 53.0	13.46	12.52	11.54	0.93
C3	07 44 30.35	13 12 18.8	14.00	13.34	12.60	0.66
C4	07 45 12.14	13 17 07.1	11.42	10.42	9.38	1.00
V337 Ori	05 59 20.58	20 02 07.5	10.93–11.78[b]	10.56–11.23[b]	10.20–10.64[b]	0.22–0.71[b]
C1	05 59 01.98	19 56 17.1	12.36	11.76	11.08	0.60
C2	05 59 28.07	19 57 34.8	12.75	12.36	11.88	0.39
C3	05 59 24.43	19 57 40.7	13.42	12.16	10.88	1.25
C4	05 59 08.10	20 02 10.7	13.21	12.18	11.12	1.03

Notes: a. MPOSC3 is a hybrid catalog which includes a large subset of the Carlsberg Meridian Catalog (CMC-14) as well as data from the Sloan Digital Sky Survey (SDSS). b. Range of values determined at UO for each variable.

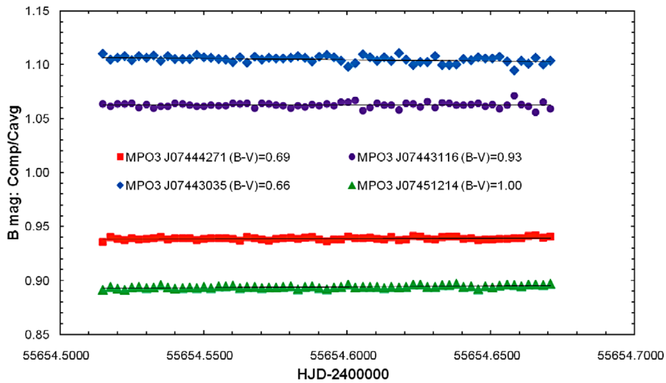

Figure 1. Representative plot showing behavior of comparison stars (B mag.: Comp/Cavg) used for TYC 790-1124-1 during a session when the air mass ranged from 1.134 to 1.996.

2MASS J–K magnitudes; these have an internal consistency of ±0.05 mag. for V, ±0.08 mag. for B, ±0.03 mag. for I_c, and ±0.05 mag. for B–V (Warner 2007). Thereafter, all light curve data (HJD vs magnitude) from each target were further analyzed by discrete Fourier transform (PERIOD04, Lenz and Breger 2005) and/or by the Lomb-Scargle method (PERANSO v2.5, Vanmunster 2013). During the 2009 campaign photometric sessions (V and I_c) for RR Leo occurred between 10 April 2009 and 02 May 2009; two years later imaging of this target in three colors (B, V, and I_c) was completed between 21 April 2011 and 02 June 2011. Photometric data for V337 Ori were collected between 14 Jan 2011 and 24 Feb 2011, while imaging of TYC 790-1124-1 was conducted during a one-month period starting on 03 March 2011.

3. Results and discussion

Photometric data (JD vs magnitude) from this study have been uploaded to the AAVSO International Database (AID; AAVSO 2013) and are also available electronically by request (mail@underoakobservatory.com). Times of maximum acquired at UO were estimated using the polynomial extremum fit feature in PERANSO; mean values (B, V, and I_c) are summarized in Table 2. Discrete Fourier transform analysis (spectral window = 50 c/d) was used to determine the fundamental pulsating frequency for each variable star followed by successive pre-whitening to tease out other potential oscillations. Only independent oscillations with S/N > 4 and above the passband error detection limits are presented; those derived from harmonics or combination frequencies are not tabulated (Table 3). In all cases, uncertainties in frequency, amplitude, and phase were estimated by the Monte Carlo simulation (n ≥ 400) routine built into PERIOD04.

Table 2. Mean times of maximum (HJD from UTC) for the pulsating variables RR Leo, TYC 790-1124-1, and V337 Ori as determined at UnderOak Observatory using B, V, and I_c passbands.

Star Identification	*Mean ToMx* (HJD)*	*(±SD)*
RR Leo	2454949.6032	0.0023
	2454973.5807	0.0021
	2455714.6146	0.0021
TYC 790-1124-1	2455623.6431	0.0054
	2455628.6812	0.0050
	2455645.5858	0.0056
	2455648.6441	0.0057
	2455649.5408	0.0049
	2455654.5778	0.0055
V337 Ori	2455575.6836	0.0011
	2455576.6959	0.0036
	2455584.5327	0.0030
	2455585.5403	0.0013
	2455585.7473	0.0018
	2455592.5906	0.0034
	2455596.6171	0.0042
	2455601.6435	0.0021
	2455603.6569	0.0025
	2455605.6703	0.0045
	2455608.6902	0.0020
	2455616.5385	0.0029

* *Times of maximum and associated error estimated using best fit polynomial (PERANSO, Vanmunster 2013).*

3.1. RR Leo

Folded light curves from 2009 and 2011 (Figure 2) exhibited a fundamental period of 0.452405 ± 0.000001 d which is similar to that reported by Le Borgne *et al.* (2007c). A well-fit ($r^2 > 0.994$) quadratic relationship between observed-minus-calculated residuals and time which spans over 110 years of observation was observed in the so-called “O–C diagram” for RR Leo (Figure 3). As was similarly shown by Olah and Szeidl (1978) and Le Borgne *et al.* (2007c), the plot describes an upwardly-turned parabola, thereby suggesting that the period of this system is slowly increasing with time. Along with new values reported herein, data (Table 4) in Figures 3 and 4 include those reported by Olah and Szeidl (1978), Le Borgne *et al.* (2007c), and time-of-maximum light values published since 2007. When using the GCVS linear elements (Samus *et al.* 2012) a discontinuous curve resulted which could be easily remedied by period-

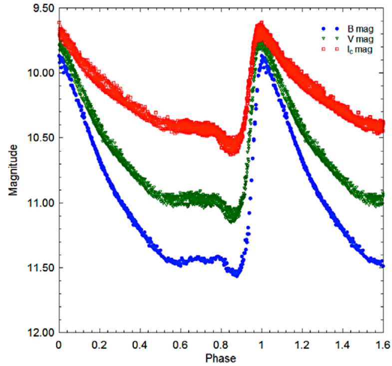

Figure 2. Folded multi-color light curves (P = 0.452405 d) from RR Leo acquired at UO in 2009 and 2011.

shifting data collected prior to 1936. Non-linear regression analysis using a scaled Levenberg-Marquardt algorithm (Press *et al.* 1992) as implemented in QTIPLOT (v0.9.8.9; Vasilief 2013) revealed that the time-to-maximum residual data from the initial timing in 1898 until 2012 could be fit ($r^2 > 0.997$) by a quadratic expression as follows:

$$C = c + a_1 E + a_2 E^2 \tag{1}$$

Accordingly, the coefficients (± error) for each solved term in Equation 1 are as follows:

$$C = -6.480 (\pm 0.490) \times 10^{-3} - 9.052 (\pm 0.154) \times 10^{-7} E + 1.881 (\pm 0.006) \times 10^{-10} E^2, \tag{2}$$

and lead to the updated quadratic ephemeris for RR Leo:

$$\text{Max HJD} = 2456285.5459 (\pm 0.0005) + 0.4524032 (\pm 0.0000002) E + 1.881 (\pm 0.006) \times 10^{-10} E^2. \tag{3}$$

In this case, the period rate of increase ($\Delta p/p = 2a_2 = 3.763 (\pm 0.012) \times 10^{-10}$) for RR Leo has lasted for at least 114 years. The period increase rate ($dP/dt = 8.32 (\pm 0.03) \times 10^{-10}\ d d^{-1}$) compares favorably to the same value ($8.26 (\pm 0.04) \times 10^{-10}\ d d^{-1}$) calculated by Le Borgne *et al.* (2007c). As first suggested by Olah and Szeidl (1978), the residuals (Figure 4) after fitting the quadratic model appear to exhibit behavior consistent with cyclic variation and could be fit by a quadratic expression modulated with a sinusoidal term as follows:

$$C = c + a_1 E + a_2 E^2 + a_3 \sin (a_4 E + a_5) \tag{4}$$

Accordingly, the coefficients (±error) for each solved term in Equation 4 are:

Table 3. Independent frequencies detected in RR Leo, TYC 790-1124-1, and V337 Ori light curves by discrete Fourier transform analysis.

Star Identification		*Frequency c/d*	*Semi-Amplitude Magnitude*	*S/N*[b]	*Phase*
RR Leo (B mag)	f_1	2.2102 (2)[a]	0.593 (8)	285	0.391 (2)
RR Leo (V mag)	f_1	2.213087 (2)	0.429 (2)	153	0.718 (1)
	f_2	3.31987 (3)	0.049 (2)	17.3	0.095 (9)
	f_3	3.09 (2)	0.040 (3)	13.7	0.94 (7)
RR Leo (I_c mag)	f_1	2.2131 (3)	0.295 (7)	297	0.18 (4)
	f_4	2.396 (7)	0.037 (6)	36.9	0.76 (28)
	f_5	4.25 (1)	0.028 (6)	24	0.13 (27)
TYC 790-1124-1 (B mag)	f_1	5.5584 (6)	0.145 (1)	68.9	0.292 (1)
TYC 790-1124-1 (V mag)	f_1	5.5598 (5)	0.109 (9)	102	0.510 (2)
TYC 790-1124-1 (I_c mag)	f_1	5.5586 (6)	0.066 (6)	110	0.61 (1)
V337 Ori (B mag)	f_1	4.96877 (9)	0.287 (6)	138	0.529 (2)
	f_2	6.72 (7)	0.043 (6)	19.5	0.79 (3)
V337 Ori (V mag)	f_1	4.9691 (1)	0.205 (2)	104	0.225 (3)
	f_2	6.72 (7)	0.023 (2)	13.2	0.429 (3)
V337 Ori (I_c mag)	f_1	4.97 (3)	0.121 (4)	136	0.08 (2)

Notes: a. Uncertainty (Monte Carlo simulation) of least significant figure(s) is indicated within parentheses. b. Signal-to-noise (S/N) estimated with box size adjusted to ~1/5 of the measured frequency (PERIOD04, Lenz and Breger 2005).

$$C = -4.49\,(\pm 4.73) \times 10^{-4} + 6.547\,(\pm 2.387) \times 10^{-8}\,E + 1.513\,(\pm 0.774) \times 10^{-12}\,E^2 + 3.751\,(\pm 0.590) \times 10^{-3} \sin[1.400\,(\pm 0.058) \times 10^{-4}\,E + 2.242\,(\pm 0.147)]. \quad (5)$$

The amplitude (0.003751 ± 0.000590 d) of the periodic oscillation is defined by a_3, the coefficient of the sine term. Assuming for the moment that this behavior is associated with another gravitationally bound body, then according to the relationship:

$$P_3 = 2\pi P/\omega, \text{ where the angular frequency, } \omega = a_4 = 1.400\,(\pm 0.058) \times 10^{-4}, \quad (6)$$

its Keplerian orbital period would be 55.6 (±2.3) years.

Further assessment of light curves from RR Leo using PERIOD04 (Table 3) revealed that in addition to its dominant frequency (~2.213 c/d) Fourier analysis

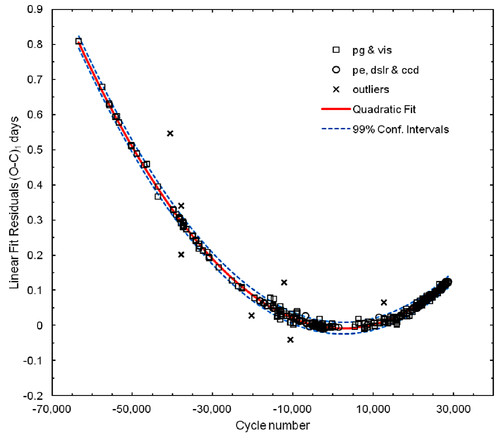

Figure 3. Plot of RR Leo published time-of-maximum data vs epoch using linear elements from Samus *et al.* (2012). Parabolic relation of O–C residuals is well fit by quadratic expression.

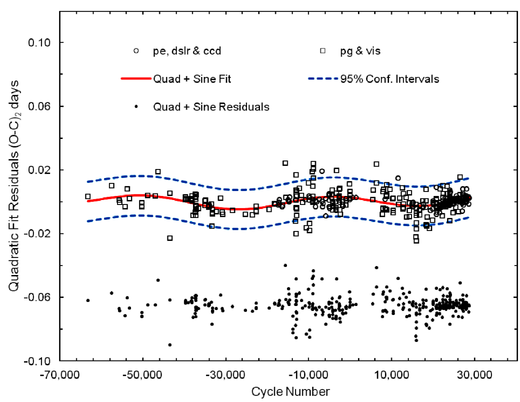

Figure 4. Plot of RR Leo (O–C)$_2$ residuals from quadratic fit of published time-of-maximum data vs epoch data. Apparent cyclic relationship can be fit by quadratic expression modulated with a sinusoidal term. Residuals are offset by a constant amount to keep all data on scale.

uncovered oscillations corresponding to the 1st through 6th harmonics of the fundamental (not shown). Successively pre-whitening spectra with newly detected pulsations also exposed four other potential independent oscillations (Figure 5). None of these values are common to another passband so it is still difficult to judge whether these signals are real without additional data. Curiously, Ekmekçi *et al.* (2012) published a very different set of pulsation frequencies from multicolor (B, V, and R) light curves collected in 2007, none of which agree with the primary pulsation mode observed herein or similarly reported elsewhere (Samus *et al.* 2012; Watson *et al.* 2006–2013). It is not obvious why these differences exist, particularly since this and their investigation used PERIOD04 to analyze light curve data from RR Leo.

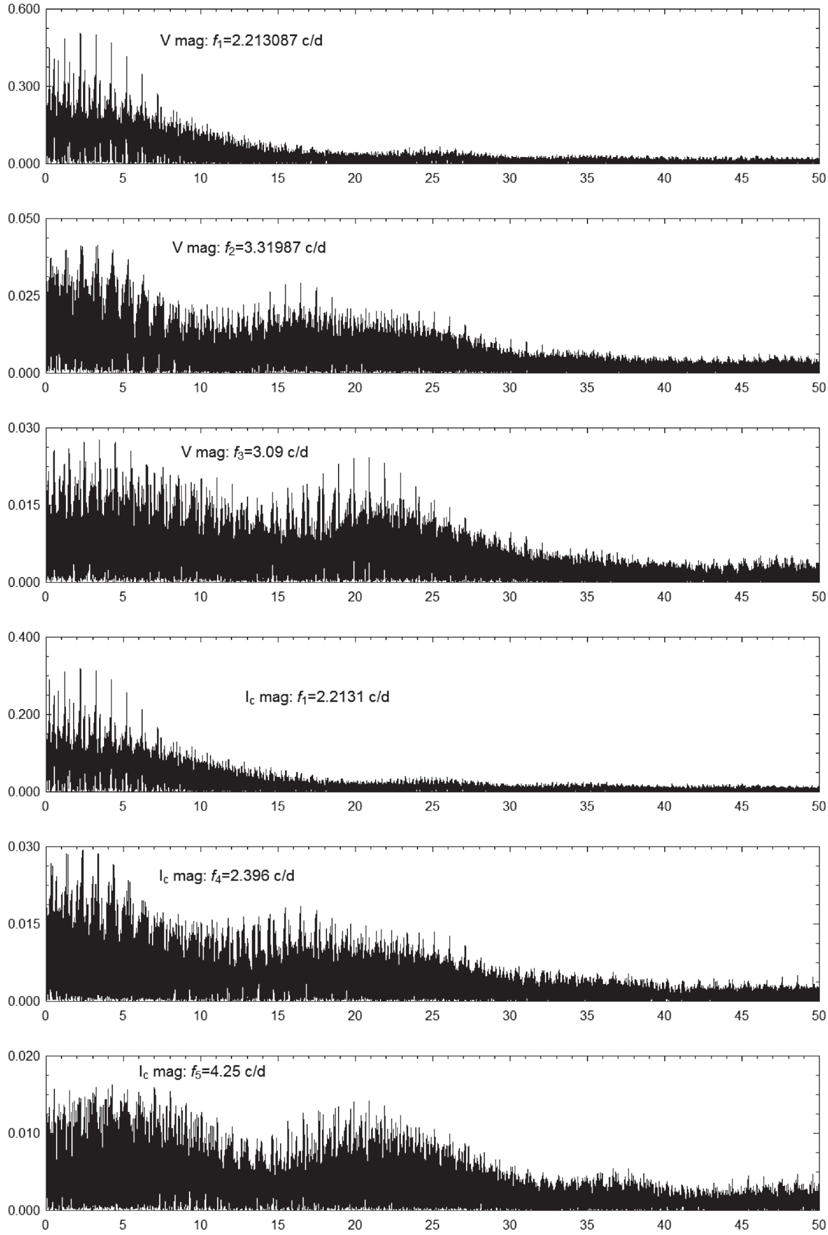

Figure 5. Periodograms showing primary oscillation (f_1 = 2.2131 c/d) of RR Leo and four potential independent pulsations (f_2–f_5) uncovered by successively pre-whitening Fourier spectra from V- and I_c-passband light curves.

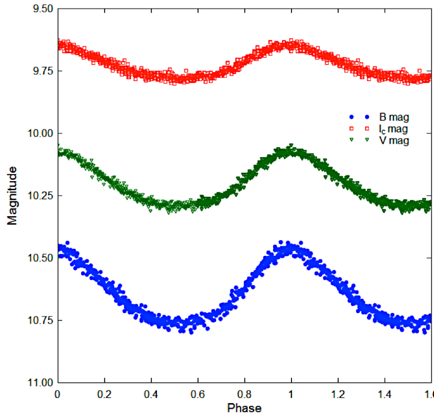

Figure 6. Folded multi-color light curves (P = 0.179846 d) from TYC 790-1124-1 data acquired at UO in 2011.

The observed B–V (~0.42) around phase 0.6 where the color index for RRab variables tend to be fairly constant compares favorably to values reported by Preston (1964) and consistent with a late A or early F spectral class star. In this case, the low interstellar reddening (E(B–V) = 0.0346 ± 0.0035) observed within a 5-arcmin radius of RR Leo (Schlafly and Finkbeiner 2011; Schlegel *et al.* 1998) would not dramatically alter conclusions based upon the observed color index.

3.2 TYC 790-1124-1 (ASAS J074451+1315.0)

Collectively, folded light curves in all passbands from the 2011 campaign at UO (Figure 6) exhibited a primary period of 0.179846 day which is essentially identical to that estimated (0.179846 day) from the ASAS survey (Pojmański *et al.* 2005). Based on these findings, the following linear ephemeris is proposed for this system:

$$\text{Max HJD} = 2455654.5778\,(\pm 0.0055) + 0.179846\,(\pm 0.000006)\,\text{E} \qquad (7)$$

The shape of each (B, V, and I_c) light curve is symmetrical with little variation at minimum or maximum light over the month-long observation period. Discrete Fourier analysis of the UO data revealed (Table 3) a principal pulsation mode at ~5.559 c/d along with a much less intense first harmonic at ~11.12 c/d. All other observations derived from Fourier analysis were below the limits of reliable detection. Pojmański *et al.* (2005) reported the only other light curve (V mag.) for this star (ASAS J074451+1315.0) based upon data collected from the ASAS survey. Combined Fourier analyses of the ASAS (2002–2009) and UO (2011) data using PERANSO 2.5 (Lomb-Scargle method) produced a good fit of the folded V-mag light curves despite greater scatter in the ASAS

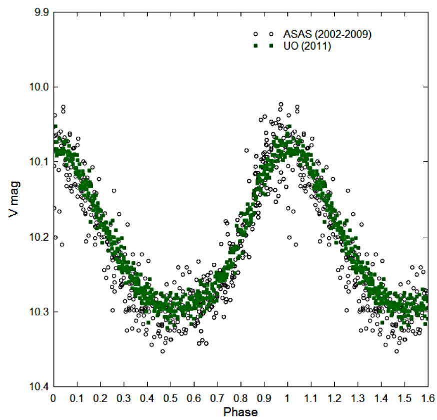

Figure 7. Folded V-mag light curves (P = 0.179846 d) from TYC 790-1124-1 data acquired by the ASAS survey between 2002 and 2009 and at UO in 2011.

data (Figure 7). Individual and combined analyses yielded the same result, suggesting that the fundamental pulsation period (0.179846 ± 0.000006 d) had not appreciably changed during this nine year observation interval (2002–2011). It should be noted that light curves from the RRc subclass of RR Lyrae type pulsating variables are also symmetrical and have been reported with fundamental periods as low as 0.2 day. Arguably, a case could be made to potentially classify TYC 790-1124-1 as an RRc variable rather than a HADS. Poretti (2001a, 2001b) describes three methods to separate monoperiodic RRc and HADs variables according to their fundamental period ($1/f_1$), the semi-amplitudes of the fundamental (A_1) and first harmonic (A_2), and the ratio ($R_{21} = A_2/A_1$) of the semi-amplitudes. A subset of the OGLE (Udalski *et al.* 1992) database used in Poretti's (2001b) paper is conveniently maintained at the CDS website (http://cdsweb.u-strasbg.fr/) so that findings from the present study could be analyzed along with data from stars known to be RRc or HADs variables. Accordingly, three tests were successfully applied using results from the Fourier decomposition and frequency analysis of pulsating (P < 1 d) stars in the OGLE database. In the first relationship, when the amplitude ratio (R_{21}) from I_c-band is plotted against the period (d) of known HADS and RRc variables, clear separation of each population can be seen (Figure 8). Two other examples in which R_{21} and A_1 (Figure 9) or A_1^2 and A_2 (Figure 10) are similarly plotted convincingly show that TYC 790-1124-1 appears in the cluster with other known HADS stars. Based on the B–V color index range (0.35–0.51) observed herein, this pulsator would appear to vary from spectral class F3 to F6, which is not unexpected for a δ Scuti variable star (Lee *et al.* 2008). Interstellar reddening (E(B–V) = 0.0386 ± 0.0022) within a 5-arcmin radius (Schlafly and Finkbeiner 2011; Schlegel *et al.* 1998) would not significantly alter spectral classification of this system based upon the observed color index.

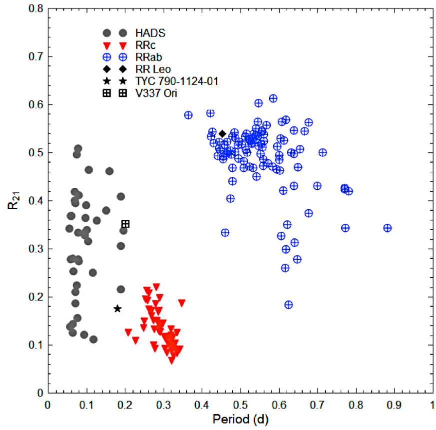

Figure 8. Diagram showing clustering of known HADS, RRc, and RRab pulsators as a function of period (d) and the fundamental to first harmonic amplitude ratio (R_{21}). Data from RR Leo, TYC 790-1124-1, and V337 Ori are superimposed to illustrate class separation achieved using the approach from Poretti (2001a).

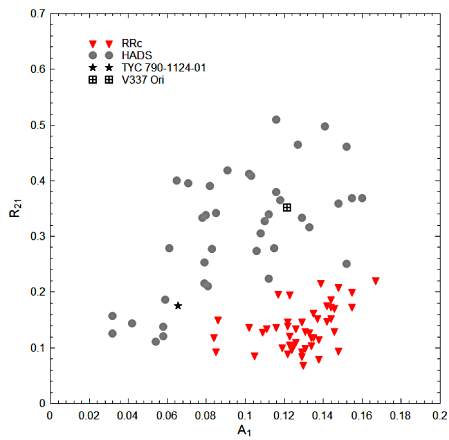

Figure 9. Diagram showing clustering of known HADS and RRc pulsators as a function of the fundamental pulsation mode, semi-amplitude (A_1), and amplitude ratio (R_{21}). Corresponding data from TYC 790-1124-1 and V337 Ori are superimposed to illustrate class separation achieved using the approach from Poretti (2001a).

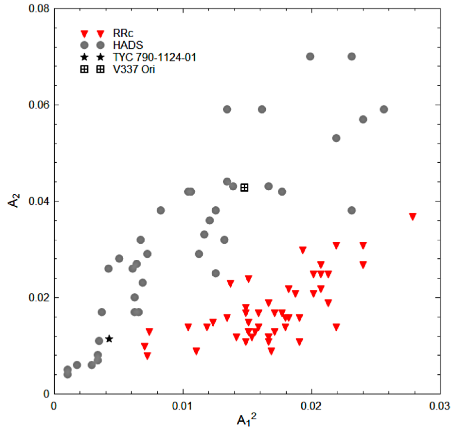

Figure 10. Diagram showing clustering of known HADS and RRc pulsators as a function of the fundamental pulsation, mode semi-amplitude (A_1^2), and the first harmonic semi-amplitude (A_2). Corresponding data from TYC 790-1124-1 and V337 Ori are superimposed to illustrate class separation achieved using the approach from Poretti (2001b).

3.3. V337 Ori (ASAS J055921+2002.1)

Samus and Antipin (2005) corrected the record on this HADS which had previously been misidentified as a nearby irregular red variable (Ahnert 1950; Neckel 1958). Folded light curves from the 2011 campaign at UO (Figure 11) exhibited a primary period of 0.201259 day (4.968722 c/d) which compares favorably with those estimated by other investigators (Samus and Antipin 2005; Khruslov 2011; Wils *et al.* 2012). Linear elements from the latest epoch collected at UO were determined as follows:

$$\text{Max HJD} = 2455616.5385\,(\pm 0.0029) + 0.201259\,(\pm 0.000001)\,\text{E} \qquad (8)$$

Khruslov (2011) and more recently Wils *et al.* (2012) conducted an in-depth analysis on the light curve (V mag.) variation of V337 Ori using Fourier techniques. The time span for observations analyzed by both investigators extended over a longer time period (years) and culled data from three diverse photometric surveys (ASAS, Pojmański 2002; NSVS, Woźniak *et al.* 2004; SuperWASP, Butters *et al.* 2010). Nonetheless, similar to the findings reported herein (Table 3), the fundamental (f_1) pulsation frequency was observed at 4.96877 c/d. This along with other related harmonics (1st–4th) and combinations were also detected during the present four-week campaign in all three passbands. Khruslov (2011) and Wils *et al.* (2012) measured a second oscillation at 6.724 c/d as well as combination frequencies at 11.693 (f_1+f_2) and 1.75509 (f_2-f_1) c/d. Similarly, an independent pulsation at 6.72 c/d was detected in the B- and V-magnitude light curves acquired at UO, but not in the I_c passband (Figure 12). Many other potential oscillations were observed, but none rose above the limits of reliable detection.

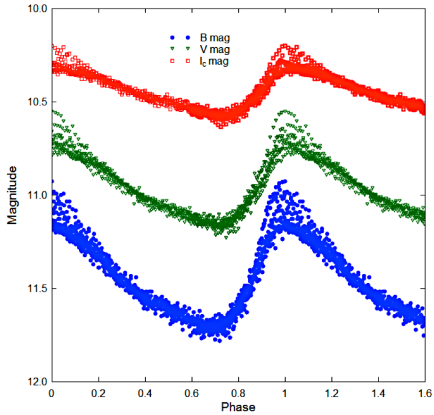

Figure 11. Folded multi-color light curves (P = 0.201259 d) from V337 Ori acquired at UO in 2011.

Although V337 Ori and TYC 790-1124-1 ostensibly share the same HADS classification, the general shape of their light curves is quite different. The overall light curve profile for V337 Ori is not unlike that observed for many RRab pulsators, however, the shorter period (0.201259 d) clearly separates this HADS from its RRab brethren (Figure 8) like RR Leo. As noted earlier, the brightness changes for TYC 790-1124-1 are symmetrical while maximum light is fairly constant over time in each of the three passbands evaluated (Figure 6). By contrast, the light curves for V337 Ori are asymmetrical with significant cycle-to-cycle variability at maximum light. The most extreme change for V337 Ori occurred within a single six-hour session on 24 Jan 2011 where maximum light was captured twice (Figure 13) and varied by 0.185 B-mag. Similarly large brightness changes over a short period of time (hours) have been observed for many other HADS, including GSC 0376-0596 (Buchheim 2006), VX Hya (Templeton *et al.* 2009), and GP And (Zhou and Jiang 2011) where the peak-to-peak variability approached 0.1 V-mag. The evidence thus far from this study and other investigators (Khruslov 2011; Wils *et al.* 2012) demonstrates that a single dominant pulsation frequency occurs at 4.9687 c/d. The weight of evidence from all Fourier analyses suggests that V337 Ori is a multiperiodic HADS with at least one additional independent pulsation mode (6.72 c/d). This, along with potentially two other low-amplitude (~0.017) close-frequency pulsations at 6.48 and 6.61 c/d which nearly met the limits of reliable detection, may account for the observed cycle-to-cycle variability in maximum light. It is unknown which, if any, of the pulsations vary in amplitude with time. Additional high precision light curve data from multiple sites would be helpful in fully characterizing the variable nature of V337 Ori.

V337 Ori is located in the Winter Milky Way where the observed color within a 5-arcmin radius of this variable is significantly reddened (E(B–V) = 1.34 ± 0.06) due to interstellar dust (Schlafly and Finkbeiner 2011;

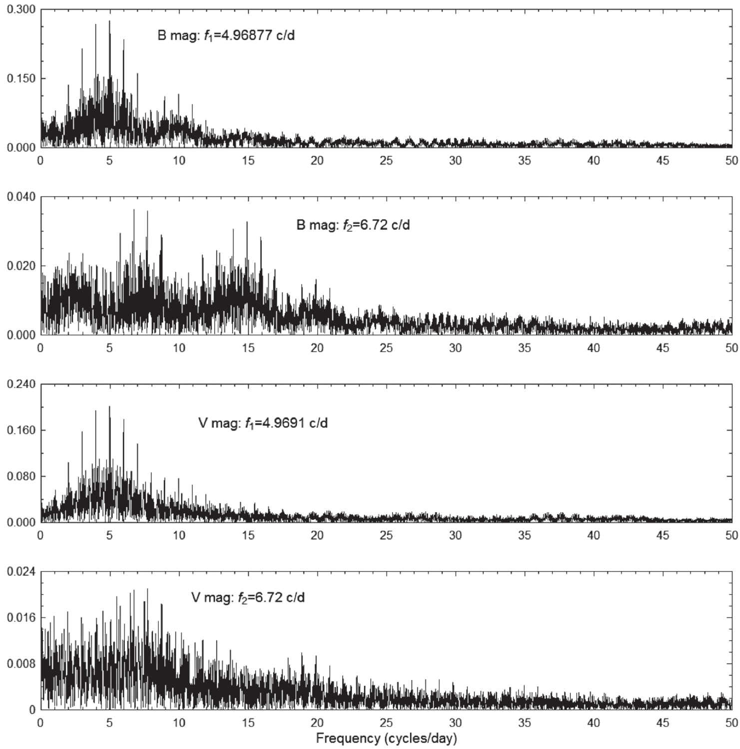

Figure 12. Periodograms showing fundamental mode of oscillation (f_1) for V337 Ori and second independent pulsation (f_2 = 6.72 c/d) exposed after successively pre-whitening the initial Fourier spectra from B- and V-mag light curves.

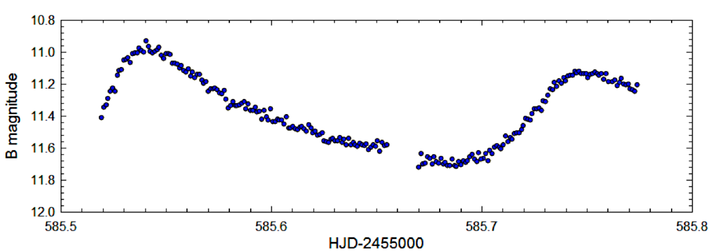

Figure 13. Unfolded light curve data (HJD vs B magnitude) from V337Ori collected during a single night on 24 Jan 2011 showing large cycle-to-cycle amplitude changes (ΔB mag. = 0.185) observed with this HADS pulsator.

Schlegel *et al.* 1998). Estimating the total extinction for V337 Ori is unreliable because of its low Galactic latitude (b = –1.85°) and determining the true intrinsic color is complicated by the fact that its distance is unknown. The observed B–V color index predicts a cooler star (G6) than would be expected for a HADS variable. However, based on the $V–I_c$ (0.12–0.52) color index observed herein which is less susceptible to reddening effects, V337 Ori would appear no cooler than spectral class A3 to F6 and well within the normal range for a HADS variable (Lee *et al.* 2008). Evidence from the 2MASS infrared survey (Skrutskie *et al.* 2006) using the published values in J, K, and H passbands (J–H and J–K color indices) suggests an effective temperature at least as hot as an F6-class star.

4. Summary

New light curve data from RR Leo largely corroborate findings previously reported for this RRab variable. In addition to its dominant frequency (2.21309 c/d), Fourier decomposition potentially uncovered as many as four other independent pulsations. A period analysis using over 110 years of time-of-maximum light data produced a revised quadratic ephemeris for RR Leo. Further evidence from the quadratic residuals suggests an underlying sinusoidal-like variability (~56 y) in the O–C diagram, possibly corresponding to the gravitational influence of a binary partner. Light curves from the HADS pulsator TYC 790-1124-1 remained symmetrical between the first time data for this system were collected (2002) and the 2011 campaign at UO. In addition, the fundamental period of oscillation (0.179846 d) appeared to be constant over this time. V337 Ori exhibits significant cycle-to-cycle amplitude variability; in addition to the fundamental pulsation (~4.969 c/d) strong evidence exists for another independent oscillation at 6.72 c/d. At this time it is unknown whether the rapid light curve changes can be attributed to potential close-frequency pairs which beat or amplitude variability of individual oscillations. Further studies of this system may be necessary to fully characterize all oscillations which lead to these rapid changes in maximum light.

5. Acknowledgements

This research has made use of the SIMBAD database, operated at Centre de Données astronomiques de Strasbourg, France. Times-of-maximum data from the B.R.N.O., *Inf. Bull. Var. Stars*, AAVSO, GEOS, and VSOLJ websites proved invaluable to the period assessment of RR Leo. The diligence and dedication shown by all associated with these organizations is very much appreciated. This research has made use of the International Variable Star Index (VSX) database, operated at AAVSO, Cambridge, Massachusetts. Many thanks to Patrick Wils, Lubos Brat, and an anonymous referee for their helpful discussion and comments on this paper.

Table 4. Recalculated quadratic residuals $(O–C)_2$ for RR Leo times-of-maximum following linear least squares fit of $(O–C)_1$ and cycle number between 1898 Dec 17 and 2012 Dec 24.

Time of Maximum (HJD–2400000)	*Cycle Number*	*$(O–C)_1^*$*	*$(O–C)_2$*	*Reference*
14639.8100	–63344	0.80920	0.00341	Gaposchkin 1934
17257.6800	–57557	0.67917	0.01026	Gaposchkin 1934
18062.4390	–55778	0.63049	0.00112	Luizet 1911
18120.3412	–55650	0.62635	–0.00022	Kukarkin 1928
18756.3730	–54244	0.59317	–0.00306	Luizet 1911
18966.2850	–53780	0.59467	0.00830	Robinson 1930
19202.4170	–53258	0.57737	0.00198	Luizet 1911
20547.7740	–50284	0.51670	0.00194	Jordan 1929
20567.6760	–50240	0.51339	–0.00049	Jordan 1929
20577.6260	–50218	0.51074	–0.00271	Jordan 1929
21220.4560	–48797	0.48986	0.00417	Kukarkin 1933
22023.4200	–47022	0.45575	0.00367	Martin and Plummer 1921
22313.8600	–46380	0.45925	0.01903	Gaposchkin 1934
23588.6125	–43562	0.36743	–0.02255	Kukarkin and Parenago 1931
23588.6404	–43562	0.39533	0.00535	Soloviev 1936b
24922.9000**	–40613	0.54709	0.00535	Gaposchkin 1934
25299.5270	–39780	0.33047	0.00322	Oosterhoff 1930
25304.5020	–39769	0.32915	0.00206	Oosterhoff 1930
25318.5250	–39738	0.32796	0.00136	Oosterhoff 1930
25323.5020	–39727	0.32863	0.00221	Oosterhoff 1930
25335.7160	–39700	0.32801	0.00202	Nielsen 1929
25645.5940	–39015	0.31660	0.00137	Oosterhoff 1930
25920.1880	–38408	0.30787	0.00203	Allen and Marsh 1932
26016.5440	–38195	0.30409	0.00152	Oosterhoff 1930
26030.5700	–38164	0.30590	0.00380	Oosterhoff 1930
26031.4730	–38162	0.30411	0.00205	Oosterhoff 1930
26060.4240	–38098	0.30194	0.00085	Oosterhoff 1930
26143.2000	–37915	0.28997	–0.00834	Zakharov 1953
26146.2800**	–37908	0.20322	–0.09499	Zakharov 1953
26148.2270**	–37904	0.34064	0.0425	Zakharov 1953
26382.5197	–37386	0.29361	0.00328	Zakharov 1953
26387.4973	–37375	0.29489	0.00472	Lause 1931
26397.4484	–37353	0.29333	0.00349	Lause 1931
26406.4862	–37333	0.28327	–0.00627	Lause 1931
26415.5357	–37313	0.28490	–0.00434	Lause 1931
26416.4417	–37311	0.28612	–0.00310	Lause 1931
26417.3513	–37309	0.29093	0.00175	Lause 1931
26420.5077	–37302	0.28058	–0.00850	Lause 1931

Table continued on following pages

Table 4. Recalculated quadratic residuals $(O–C)_2$ for RR Leo times-of-maximum following linear least squares fit of $(O–C)_1$ and cycle number between 1898 Dec 17 and 2012 Dec 24, cont.

Time of Maximum (HJD–2400000)	*Cycle Number*	*$(O–C)_1^*$*	*$(O–C)_2$*	*Reference*
26421.4239	–37300	0.29199	0.00294	Lause 1931
26430.4662	–37280	0.28642	–0.00233	Lause 1931
26440.4186	–37258	0.28617	–0.00225	Lause 1931
26474.3538	–37183	0.29187	0.00457	Lause 1931
26487.4637	–37154	0.28237	–0.00450	Lause 1931
26497.4180	–37132	0.28402	–0.00253	Lause 1931
26764.3200	–36542	0.27397	–0.00386	Detre 1936
27458.2710	–35008	0.25365	–0.00215	Tsesevich 1934
27472.7500	–34976	0.25606	0.00072	Gaposchkin 1934
27498.5360	–34919	0.25564	0.00110	Kanishcheva and Lange 1971
27834.6510	–34176	0.24242	–0.00179	Soloviev 1936a, 1936b
27840.5310	–34163	0.24131	–0.00272	Kooreman 1935
27864.5070	–34110	0.24046	–0.00284	Kooreman 1935
27869.4830	–34099	0.24014	–0.00301	Kooreman 1935
27874.4590	–34088	0.23981	–0.00319	Kooreman 1935
27875.3640	–34086	0.24002	–0.00295	Kooreman 1935
27889.3880	–34055	0.23983	–0.00272	Kooreman 1935
27903.4120	–34024	0.23964	–0.00248	Kooreman 1935
28178.4600	–33416	0.23251	–0.00134	Soloviev and Shakhovskoj 1958
28190.2080	–33390	0.21829	–0.01522	Guriev 1937
28245.4067	–33268	0.22500	–0.00686	Balázs and Detre 1949
28249.4800	–33259	0.22676	–0.00498	Balázs and Detre 1949
28250.3822	–33257	0.22418	–0.00754	Balázs and Detre 1949
28668.3830	–32333	0.21357	–0.00591	Balázs and Detre 1949
29136.6050	–31298	0.20850	0.00235	Soloviev and Shakhovskoj 1958
29312.5725	–30909	0.19501	–0.00624	Balázs and Detre 1949
29371.3806	–30779	0.19198	–0.00764	Balázs and Detre 1949
30440.3598	–28416	0.16581	–0.00535	Balázs and Detre 1949
31888.4332	–25215	0.12826	–0.00771	Balázs and Detre 1949
32615.4126	–23608	0.11163	–0.00812	Balázs and Detre 1949
33010.3456	–22735	0.10528	–0.00607	Balázs and Detre 1949
33011.7061	–22732	0.10860	–0.00272	Ashbrook 1949
33024.3700	–22704	0.10548	–0.00557	Balázs and Detre 1949
34097.3710**	–20332	0.02958	–0.06013	Balázs and Detre 1949
34443.5010	–19567	0.07870	–0.00457	Olah and Szeidl 1978

Table continued on following pages

Table 4. Recalculated quadratic residuals $(O–C)_2$ for RR Leo times-of-maximum following linear least squares fit of $(O–C)_1$ and cycle number between 1898 Dec 17 and 2012 Dec 24, cont.

Time of Maximum (HJD–2400000)	*Cycle Number*	*$(O–C)_1^*$*	*$(O–C)_2$*	*Reference*
35069.6055	–18183	0.07087	–0.00131	Olah and Szeidl 1978
35069.6060	–18183	0.07137	–0.00081	Olah and Szeidl 1978
35127.5109	–18055	0.06993	–0.00126	Olah and Szeidl 1978
35479.4664	–17277	0.06344	–0.00188	Olah and Szeidl 1978
35489.4204	–17255	0.06479	–0.00037	Olah and Szeidl 1978
35542.3512	–17138	0.06558	0.00128	Olah and Szeidl 1978
35561.3490	–17096	0.06286	–0.00113	Olah and Szeidl 1978
35874.3982	–16404	0.05589	–0.00310	Geyer 1961
35925.5190	–16291	0.05625	–0.00195	Olah and Szeidl 1978
36229.5490	–15619	0.07795	0.02440	Huth 1964
36287.4330	–15491	0.05561	0.00292	Huth 1964
36513.6249	–14991	0.05086	0.00149	Olah and Szeidl 1978
36586.4585	–14830	0.04914	0.00082	Olah and Szeidl 1978
36599.5870	–14801	0.05823	0.01010	Huth 1964
36604.5533	–14790	0.04821	0.00014	Olah and Szeidl 1978
36610.4410	–14777	0.05479	0.00681	Ahnert 1959a,b
36614.5064	–14768	0.04865	0.00073	Olah and Szeidl 1978
36667.4640	–14651	0.07624	0.02907	Huth 1964
36672.4142	–14640	0.05011	0.00301	Geyer 1961
37024.3510	–13862	0.02492	–0.01730	Wenske 1980
37028.4250	–13853	0.02738	–0.01478	Wenske 1980
37042.4570	–13822	0.03519	–0.00678	Wenske 1980
37316.6118	–13216	0.03965	0.00131	Olah and Szeidl 1978
37366.3610	–13106	0.02559	–0.01211	Wenske 1980
37375.4010	–13086	0.01772	–0.01986	Wenske 1980
37375.4270	–13086	0.04372	0.00614	Ahnert 1961a,b
37375.4380	–13086	0.05472	0.01714	Huth 1964
37376.3220	–13084	0.03394	–0.00364	Ahnert 1961a,b
37376.3290	–13084	0.04094	0.00336	Ahnert 1961a,b
37399.4010	–13033	0.04088	0.00360	Huth 1964
37399.4050	–13033	0.04488	0.00760	Ahnert 1961b
37403.4700	–13024	0.03834	0.00112	Ahnert 1961b
37432.4290	–12960	0.04417	0.00732	Karetnikov 1961, 1962
37447.3468	–12927	0.03299	–0.00367	Karetnikov 1961, 1962
37454.5845	–12911	0.03240	–0.00417	Karetnikov 1961, 1962
37466.3425	–12885	0.02817	–0.00825	Karetnikov 1961, 1962
37476.3066	–12863	0.03962	0.00332	Karetnikov 1961, 1962
37768.1020	–12218	0.04134	0.00867	Demjanovski 1975

Table continued on following pages

Table 4. Recalculated quadratic residuals $(O–C)_2$ for RR Leo times-of-maximum following linear least squares fit of $(O–C)_1$ and cycle number between 1898 Dec 17 and 2012 Dec 24, cont.

Time of Maximum (HJD–2400000)	*Cycle Number*	*$(O–C)_1^*$*	*$(O–C)_2$*	*Reference*
37780.3990**	–12191	0.12372	0.09120	Demjanovski 1975
38000.6250	–11704	0.03418	0.00430	Demjanovski 1975
38107.3840	–11468	0.02836	–0.00028	Demjanovski 1975
38414.5572	–10789	0.02651	0.00133	Olah and Szeidl 1978
38496.4220	–10608	0.00813	–0.01617	Wenske 1980
38497.7320**	–10605	–0.03905	–0.06333	Demjanovski 1975
38732.5970	–10086	0.03382	0.01203	Demjanovski 1975
38824.8760	–9882	0.02459	0.00375	Fitch *et al.* 1966
38825.7780	–9880	0.02180	0.00097	Fitch *et al.* 1966
38848.3830	–9830	0.00714	–0.01346	Wenske 1980
38852.4500	–9821	0.00260	–0.01796	Wenske 1980
38881.4237	–9757	0.02313	0.00286	Olah and Szeidl 1978
39146.5225	–9171	0.01945	0.00181	Olah and Szeidl 1978
39150.5922	–9162	0.01761	0.00001	Olah and Szeidl 1978
39172.3260	–9114	0.03654	0.01914	Braune *et al.* 1970
39205.3310	–9041	0.01683	–0.00026	Wenske 1980
39228.4130	–8990	0.02677	0.00990	Braune *et al.* 1970
39233.3800	–8979	0.01744	0.00062	Braune *et al.* 1970
39238.3590	–8968	0.02011	0.00334	Braune *et al.* 1970
39257.3710	–8926	0.03160	0.01501	Braune *et al.* 1970
39257.3800	–8926	0.04060	0.02401	Braune *et al.* 1970
39305.3300	–8820	0.03691	0.02077	Braune *et al.* 1970
39503.4564	–8382	0.01504	0.00071	Olah and Szeidl 1978
39507.5280	–8373	0.01510	0.00081	Olah and Szeidl 1978
39536.4770	–8309	0.01093	–0.00310	Wenske 1980
39608.4100	–8150	0.01340	0.00000	Wenske 1980
39906.5364	–7491	0.01261	0.00175	Olah and Szeidl 1978
40220.0600	–6798	0.02765	0.01928	Epstein 1969
40232.7079	–6770	0.00854	0.00027	Olah and Szeidl 1978
40301.4680	–6618	0.00486	–0.00289	Wenske 1980
40321.3750	–6574	0.00655	–0.00105	Wenske 1980
40654.3372	–5838	0.00729	0.00207	Olah and Szeidl 1978
40657.4930	–5831	–0.00367	–0.00886	Wenske 1980
40980.5097	–5117	0.00422	0.00114	Olah and Szeidl 1978
40984.5770	–5108	–0.00002	–0.00308	Wenske 1980
41003.5855	–5066	0.00796	0.00502	Olah and Szeidl 1978
41008.5610	–5055	0.00713	0.00423	Wenske 1980
41028.4580	–5011	–0.00117	–0.00395	Wenske 1980

Table continued on following pages

Table 4. Recalculated quadratic residuals $(O–C)_2$ for RR Leo times-of-maximum following linear least squares fit of $(O–C)_1$ and cycle number between 1898 Dec 17 and 2012 Dec 24, cont.

Time of Maximum (HJD–2400000)	*Cycle Number*	*$(O–C)_1^*$*	*$(O–C)_2$*	*Reference*
41033.4430	–5000	0.00750	0.00475	Wenske 1980
41071.4360	–4916	–0.00054	–0.00305	Wenske 1980
41311.6607	–4385	0.00332	0.00221	Olah and Szeidl 1978
41312.5677	–4383	0.00553	0.00443	Olah and Szeidl 1978
41332.4760	–4339	0.00853	0.00754	Braune and Mundry 1973
41389.4700	–4213	0.00097	0.00030	Wenske 1980
41390.3720	–4211	–0.00181	–0.00248	Wenske 1980
41394.4410	–4202	–0.00435	–0.00500	Braune and Mundry 1973
41394.4450	–4202	–0.00035	–0.00100	Braune and Mundry 1973
41405.3030	–4178	0.00021	–0.00038	Berdnikov 1977
41682.6190	–3565	–0.00089	–0.00002	Olah and Szeidl 1978
41736.4500	–3446	–0.00469	–0.00356	Tsesevich 1974
41751.3770	–3413	–0.00667	–0.00547	Wenske 1980
41771.2830	–3369	–0.00597	–0.00468	Berdnikov 1977
41794.3650	–3318	0.00397	0.00537	Braune *et al.* 1977
41812.4750	–3278	0.01824	0.01973	Braune *et al.* 1977
42019.6515	–2820	–0.00139	0.00104	Olah and Szeidl 1978
42089.3220	–2666	0.00054	0.00327	Braune *et al.* 1977
42095.6600	–2652	0.00503	0.00779	Braune *et al.* 1977
42102.4420	–2637	0.00113	0.00392	Braune *et al.* 1977
42106.5120	–2628	–0.00041	0.00239	Wenske 1980
42145.4180	–2542	–0.00023	0.00273	Wenske 1980
42150.4000	–2531	0.00544	0.00843	Braune *et al.* 1977
42154.4630	–2522	–0.00310	–0.00010	Wenske 1980
42183.4110	–2458	–0.00827	–0.00515	Braune *et al.* 1977
42202.4090	–2416	–0.01079	–0.00759	Braune *et al.* 1977
42443.5415	–1883	–0.00392	0.00019	Olah and Szeidl 1978
42469.3260	–1826	–0.00583	–0.00163	Braune *et al.* 1977
42492.3970	–1775	–0.00689	–0.00261	Wenske 1980
42829.4335	–1030	–0.00340	0.00195	Olah and Szeidl 1978
42840.2870	–1006	–0.00734	–0.00196	Braune *et al.* 1979
42857.4820	–968	–0.00329	0.00214	Wenske 1980
42891.4100	–893	–0.00478	0.00074	Wenske 1980
43213.5140	–181	–0.00481	0.00150	Olah and Szeidl 1978
43224.3810	–157	0.00475	0.01108	Braune *et al.* 1979
43281.3760	–31	–0.00181	0.00464	Braune *et al.* 1979
43295.3980	0	–0.00400	0.00248	Braune *et al.* 1979
43295.4020	0	0.00000	0.00648	Samus *et al.* 2012

Table continued on following pages

Table 4. Recalculated quadratic residuals $(O–C)_2$ for RR Leo times-of-maximum following linear least squares fit of $(O–C)_1$ and cycle number between 1898 Dec 17 and 2012 Dec 24, cont.

Time of Maximum (HJD–2400000)	*Cycle Number*	*$(O–C)_1^*$*	*$(O–C)_2$*	*Reference*
43560.5004	586	–0.00407	0.00287	Szeidl and Pocs 2002
43911.5572	1362	–0.00447	0.00289	Szeidl and Pocs 2002
45757.3220	5442	–0.00434	0.00149	Firmanyuk *et al.* 1985
45812.5203	5564	0.00198	0.00767	Le Borgne 2004
46174.4401	6364	0.00714	0.01176	Le Borgne 2004
46175.3568	6366	0.01905	0.02367	Le Borgne 2004
46826.3220	7805	–0.00971	–0.00762	Braune and Hübscher 1987
46864.3270	7889	–0.00574	–0.00383	Braune and Hübscher 1987
46869.3030	7900	–0.00607	–0.00418	Braune and Hübscher 1987
46877.4460	7918	–0.00615	–0.00430	Braune and Hübscher 1987
46883.3380	7931	0.00474	0.00656	Braune and Hübscher 1987
46910.4830	7991	0.00614	0.00784	Hübscher *et al.* 1990
47121.7456	8458	0.00107	0.00174	Liu and Janes 1989
47124.0020	8463	–0.00450	–0.00383	Liu and Janes 1989
47172.4080	8570	–0.00458	–0.00416	Hübscher and Lichtenknecker 1988
47239.3710	8718	0.00421	0.00428	Hübscher and Lichtenknecker 1988
47262.4340	8769	–0.00485	–0.00490	Hübscher and Lichtenknecker 1988
47263.3470	8771	0.00337	0.00331	Hübscher and Lichtenknecker 1988
47263.3480	8771	0.00437	0.00431	Hübscher and Lichtenknecker 1988
47267.4260	8780	0.01083	0.01075	Hübscher *et al.* 1989
47652.4120	9631	0.01013	0.00787	Aubaud 1990
47966.3690	10325	0.00618	0.00195	Hübscher *et al.* 1990
47970.4410	10334	0.00664	0.00238	Hübscher *et al.* 1990
47989.4340	10376	–0.00088	–0.00527	Hübscher *et al.* 1990
48018.3860	10440	–0.00205	–0.00663	Hübscher *et al.* 1991
48500.2100	11505	0.02308	0.01507	Perryman *et al.* 1997
48604.6970	11736	0.00723	–0.00158	Aubaud 1992
48683.4180	11910	0.01180	0.00237	Hübscher *et al.* 1992
49021.3650	12657	0.02100	0.00880	Hübscher *et al.* 1994
49030.4580**	12677	0.06614	0.05385	Vandenbroere 1997
49044.4240	12708	0.00794	–0.00446	Vandenbroere 1997
49087.4050	12803	0.01158	–0.00119	Hübscher *et al.* 1993
49097.3640	12825	0.01793	0.00507	Vandenbroere 1997

Table continued on following pages

Table 4. Recalculated quadratic residuals $(O–C)_2$ for RR Leo times-of-maximum following linear least squares fit of $(O–C)_1$ and cycle number between 1898 Dec 17 and 2012 Dec 24, cont.

Time of Maximum (HJD–2400000)	*Cycle Number*	*$(O–C)_1^*$*	*$(O–C)_2$*	*Reference*
49101.4270	12834	0.00939	–0.00351	Hübscher *et al.* 1993
49439.3740	13581	0.01859	0.00266	Hübscher *et al.* 1994
49472.3870	13654	0.00688	–0.00936	Hübscher *et al.* 1994
49776.4070	14326	0.01858	–0.00058	Hübscher *et al.* 1995
49781.3750	14337	0.01026	–0.00896	Hübscher *et al.* 1995
49786.3550	14348	0.01393	–0.00533	Hübscher *et al.* 1995
49786.3660	14348	0.02493	0.00567	Hübscher *et al.* 1995
50049.6540	14930	0.02003	–0.00191	Vandenbroere 1998
50097.6090	15036	0.02134	–0.00111	Vandenbroere 1998
50170.4459	15197	0.02292	–0.00030	Agerer and Hübscher 1997
50194.4204	15250	0.02058	–0.00290	Agerer and Hübscher 1997
50489.3650	15902	0.00474	–0.02196	Hübscher *et al.* 1997
50499.3380	15924	0.02509	–0.00172	Vandenbroere 2001
50518.3160	15966	0.00257	–0.02446	Hübscher *et al.* 1997
50518.3320	15966	0.01857	–0.00846	Vandenbroere 2001
50541.3960	16017	0.01051	–0.01678	Vandenbroere1999
50542.3140	16019	0.02373	–0.00357	Vandenbroere 2001
50546.3760	16028	0.01419	–0.01316	Hübscher *et al.* 1997
50546.3820	16028	0.02019	–0.00716	Dahm and Kleikamp 1998
50865.3220	16733	0.02291	–0.00814	Hübscher *et al.* 1998
50896.5410	16802	0.02677	–0.00465	Agerer *et al.* 1999
50897.4450	16804	0.02599	–0.00545	Hübscher *et al.* 1998
50898.3530	16806	0.02920	–0.00225	Agerer *et al.* 1999
51234.4838	17549	0.03178	–0.00380	Agerer and Hübscher 2000
51245.3460	17573	0.03654	0.00082	Hübscher *et al.* 1999
51272.4863	17633	0.03324	–0.00282	Agerer and Hübscher 2000
51278.3690	17646	0.03483	–0.00130	Agerer and Hübscher 2000
51568.3660	18287	0.04772	0.00784	Hübscher *et al.* 2000
51610.4170	18380	0.02615	–0.01430	Hübscher *et al.* 2000
51610.4320	18380	0.04115	0.00070	Hübscher *et al.* 2000
51612.6900	18385	0.03718	–0.00329	Wils *et al.* 2006
51625.3460	18413	0.02617	–0.01447	Hübscher *et al.* 2000
51672.3950	18517	0.02626	–0.01501	Hübscher *et al.* 2000
51677.3770	18528	0.03194	–0.00940	Hübscher *et al.* 2000
51924.3800	19074	0.02820	–0.01651	Hübscher 2001
52052.4202	19357	0.04109	–0.00540	Agerer and Hübscher 2002
52279.5190	19859	0.03846	–0.01129	Hübscher *et al.* 2002
52322.5040	19954	0.04609	–0.00428	Agerer and Hübscher 2003

Table continued on following pages

Table 4. Recalculated quadratic residuals $(O–C)_2$ for RR Leo times-of-maximum following linear least squares fit of $(O–C)_1$ and cycle number between 1898 Dec 17 and 2012 Dec 24, cont.

Time of Maximum (HJD–2400000)	*Cycle Number*	*$(O–C)_1^*$*	*$(O–C)_2$*	*Reference*
52347.3900	20009	0.05046	–0.00027	Agerer and Hübscher 2003
52361.4155	20040	0.05177	0.00083	Agerer and Hübscher 2003
52365.4856	20049	0.05033	–0.00067	Agerer and Hübscher 2003
52366.3899	20051	0.04984	–0.00117	Agerer and Hübscher 2003
52664.5201	20710	0.05286	–0.00261	Agerer and Hübscher 2003
52683.5208	20752	0.05304	–0.00272	Agerer and Hübscher 2003
52694.3772	20776	0.05200	–0.00393	Agerer and Hübscher 2003
52697.5500	20783	0.05805	0.00207	Hübscher *et al.* 2003
52717.4458	20827	0.04854	–0.00774	Agerer and Hübscher 2003
52717.4548	20827	0.05754	0.00126	Hübscher 2005a
52722.4268	20838	0.05321	–0.00314	Agerer and Hübscher 2003
52722.4390	20838	0.06541	0.00906	Hübscher *et al.* 2003
52746.4007	20891	0.05027	–0.00645	Agerer and Hübscher 2003
52751.3823	20902	0.05554	–0.00126	Agerer and Hübscher 2003
52787.5720	20982	0.05378	–0.00358	Le Borgne *et al.* 2008b
53046.3460	21554	0.05881	–0.00261	Le Borgne *et al.* 2004
53047.6990	21557	0.05463	–0.00681	Le Borgne *et al.* 2004
53048.6040	21559	0.05485	–0.00661	Le Borgne *et al.* 2004
53049.5150	21561	0.06106	–0.00041	Le Borgne *et al.* 2004
53050.4200	21563	0.06127	–0.00021	Le Borgne *et al.* 2004
53051.3220	21565	0.05849	–0.00301	Le Borgne *et al.* 2004
53068.5139	21603	0.05944	–0.00233	Hübscher 2005a
53071.6791	21610	0.05789	–0.00393	Samolyk 2010
53092.9420	21657	0.05830	–0.00386	Le Borgne *et al.* 2008b
53101.5400	21676	0.06083	–0.00147	Le Borgne *et al.* 2004
53107.4310	21689	0.07072	0.00832	Hübscher 2005b
53145.4225	21773	0.06118	–0.00183	Hübscher 2005a
53152.6592	21789	0.05959	–0.00354	Samolyk 2010
53332.2570	22186	0.05725	–0.00880	Hirosawa 2012
53357.5980	22242	0.06422	–0.00224	Le Borgne *et al.* 2005a
53362.5750	22253	0.06490	–0.00165	Le Borgne *et al.* 2005a
53386.5640	22306	0.07705	0.01011	Vandenbroere 2005
53405.5534	22348	0.06593	–0.00133	Samolyk 2010
53407.3670	22352	0.06996	0.00267	Hübscher *et al.* 2005a
53438.5810	22421	0.06882	0.00101	Le Borgne *et al.* 2005b
53443.5550	22432	0.06649	–0.00139	Le Borgne *et al.* 2005b
53463.0070	22475	0.06558	–0.00263	Le Borgne *et al.* 2008b
53463.4600	22476	0.06619	–0.00203	Le Borgne *et al.* 2005b

Table continued on following pages

Table 4. Recalculated quadratic residuals $(O–C)_2$ for RR Leo times-of-maximum following linear least squares fit of $(O–C)_1$ and cycle number between 1898 Dec 17 and 2012 Dec 24, cont.

Time of Maximum (HJD–2400000)	*Cycle Number*	*$(O–C)_1^*$*	*$(O–C)_2$*	*Reference*
53463.4613	22476	0.06749	–0.00073	Hübscher *et al.* 2005b
53464.3720	22478	0.06698	–0.00134	Vandenbroere and Denoux 2007
53469.7943	22490	0.06539	–0.00306	Samolyk 2010
53477.0310	22506	0.06781	–0.00066	Hirosawa 2012
53478.3906	22509	0.07091	–0.00087	Hübscher *et al.* 2005b
53674.2800	22942	0.06905	–0.00289	Hirosawa 2012
53683.3260	22962	0.07502	0.00265	Hirosawa 2012
53708.6660	23018	0.07037	–0.00217	Le Borgne *et al.* 2006a
53718.6140	23040	0.07142	–0.00141	Le Borgne *et al.* 2006a
53735.8060	23078	0.06998	–0.00304	Le Borgne *et al.* 2008b
53746.6620	23102	0.07384	0.00075	Le Borgne *et al.* 2006b
53750.2850	23110	0.07179	–0.00147	Hirosawa 2012
53760.6880	23133	0.07396	0.00050	Le Borgne *et al.* 2006b
53772.0000	23158	0.07588	0.00170	Hirosawa 2012
53813.6221	23250	0.07414	–0.00047	Samolyk 2010
53838.5020	23305	0.07282	–0.00188	Le Borgne *et al.* 2006b
53843.4770	23316	0.08484	0.00988	Le Borgne *et al.* 2006b
53876.0570	23388	0.08050	0.00523	Hirosawa 2012
53886.0040	23410	0.07485	–0.00059	Hirosawa 2012
54084.6070	23849	0.07719	–0.00176	Le Borgne *et al.* 2007a
54093.6560	23869	0.07832	–0.00078	Le Borgne *et al.* 2007a
54098.6310	23880	0.07700	–0.00220	Le Borgne *et al.* 2007a
54103.6080	23891	0.07767	–0.00161	Le Borgne *et al.* 2007b
54119.4450	23926	0.08090	0.00134	Le Borgne *et al.* 2007b
54124.4190	23937	0.07858	–0.00108	Le Borgne *et al.* 2007b
54129.3950	23948	0.07825	–0.00149	Le Borgne *et al.* 2007b
54172.3756	24043	0.08149	0.00097	Martignoni 2011
54172.3800	24043	0.08589	0.00537	Vandenbroere and Denoux 2007
54173.7308	24046	0.07951	–0.00103	Samolyk 2010
54175.5410	24050	0.08013	–0.00044	Le Borgne *et al.* 2007b
54181.4301	24063	0.08812	0.00744	Yilmaz *et al.* 2009
54185.9470	24073	0.08109	0.00033	Hirosawa 2012
54195.4457	24094	0.07953	–0.00140	Hübscher 2007
54195.4472	24094	0.08103	0.00010	Hübscher 2007
54200.4271	24105	0.08460	0.00358	Yilmaz *et al.* 2009
54205.3991	24116	0.06918	–0.01194	Hübscher 2007

Table continued on following pages

Table 4. Recalculated quadratic residuals $(O–C)_2$ for RR Leo times-of-maximum following linear least squares fit of $(O–C)_1$ and cycle number between 1898 Dec 17 and 2012 Dec 24, cont.

Time of Maximum (HJD–2400000)	*Cycle Number*	*$(O–C)_1^*$*	*$(O–C)_2$*	*Reference*
54209.4710	24125	0.08028	–0.00084	Le Borgne *et al.* 2007b
54211.2878	24129	0.08064	–0.00055	Yilmaz *et al.* 2009
54213.9950	24135	0.08786	0.00665	Hirosawa 2012
54215.3591	24138	0.08070	–0.00056	Yilmaz *et al.* 2009
54234.3555	24180	0.08762	0.00633	Yilmaz *et al.* 2009
54244.3088	24202	0.08351	0.00187	Yilmaz *et al.* 2009
54486.7925	24738	0.08415	0.00234	Samolyk 2010
54512.5796	24795	0.08504	–0.00122	Hübscher *et al.* 2009b
54514.3920	24799	0.08573	–0.00102	Hübscher *et al.* 2009a
54529.3190	24832	0.08855	0.00177	Hübscher *et al.* 2009a
54532.9320	24840	0.08657	–0.00048	Hirosawa 2012
54535.6518	24846	0.08043	–0.00670	Samolyk 2010
54539.7270	24855	0.08587	–0.00131	Samolyk 2010
54563.7025	24908	0.08953	0.00228	Samolyk 2010
54576.3700	24936	0.08818	0.00048	Le Borgne *et al.* 2008a
54589.4878	24965	0.08867	0.00073	Hübscher *et al.* 2009c
54594.4667	24976	0.08707	–0.00112	Hübscher *et al.* 2009b
54796.6900	25423	0.08964	0.00136	Le Borgne *et al.* 2009a
54800.3050	25431	0.09313	0.00102	Hirosawa 2012
54821.5730	25478	0.08899	–0.00319	Le Borgne *et al.* 2009a
54860.4790	25564	0.09450	0.00191	Le Borgne *et al.* 2009b
54875.8608	25598	0.09468	0.00134	Samolyk 2010
54877.6700	25602	0.09511	0.00147	Le Borgne *et al.* 2009b
54878.5750	25604	0.09495	0.00126	Le Borgne *et al.* 2009b
54885.3610	25619	0.09505	0.00123	Le Borgne *et al.* 2009b
54890.3380	25630	0.09572	0.00181	Le Borgne *et al.* 2010b
54903.4570	25659	0.09532	0.00115	Le Borgne *et al.* 2010b
54905.7194	25664	0.09575	0.00154	Samolyk 2010
54908.4344	25670	0.09639	0.00213	Hübscher *et al.* 2010
54908.4360	25670	0.09799	0.00373	Le Borgne *et al.* 2010b
54913.4100	25681	0.09566	0.00130	Le Borgne *et al.* 2009b
54917.4810	25690	0.09512	0.00069	Le Borgne *et al.* 2009b
54923.8143	25704	0.09492	0.00036	Samolyk 2010
54932.4117	25723	0.09684	0.00212	Hübscher *et al.* 2010
54949.6032	25761	0.09735	0.00229	This study
54973.5807	25814	0.09805	0.00253	This study
55142.3180	26187	0.09265	–0.00619	Hirosawa 2012
55167.6610	26243	0.10163	0.00229	Le Borgne *et al.* 2010a

Table continued on following pages

Table 4. Recalculated quadratic residuals $(O–C)_2$ for RR Leo times-of-maximum following linear least squares fit of $(O–C)_1$ and cycle number between 1898 Dec 17 and 2012 Dec 24, cont.

Time of Maximum (HJD–2400000)	*Cycle Number*	*$(O–C)_1^*$*	*$(O–C)_2$*	*Reference*
55217.8755	26354	0.10047	0.00013	Samolyk 2011
55220.5900	26360	0.10061	0.00022	Le Borgne *et al.* 2010b
55261.7583	26451	0.10112	–0.00009	Samolyk 2011
55276.6882	26484	0.10204	0.00053	Samolyk 2011
55281.6644	26495	0.10192	0.00030	Samolyk 2011
55293.4310	26521	0.10629	0.00444	Vandenbroere and Salmon 2010
55294.3323	26523	0.10280	0.00094	Hübscher and Monninger 2011
55297.4990	26530	0.10275	0.00082	Le Borgne *et al.* 2011
55303.3950	26543	0.11764	0.01559	Vandenbroere and Salmon 2010
55519.6270	27021	0.10564	–0.00079	Le Borgne *et al.* 2011
55521.8901	27026	0.10677	0.00029	Samolyk 2011
55524.6060	27032	0.10831	0.00178	Le Borgne *et al.* 2011
55527.3128	27038	0.10075	–0.00584	Hirosawa 2012
55533.6540	27052	0.10845	0.00173	Le Borgne *et al.* 2011
55576.6330	27147	0.11008	0.00248	Le Borgne *et al.* 2012
55600.6160	27200	0.11624	0.00814	Vandenbroere and Hambsch 2011
55601.5171	27202	0.11255	0.00444	Vandenbroere and Hambsch 2011
55602.4230	27204	0.11367	0.00553	Vandenbroere and Hambsch 2011
55604.6817	27209	0.11040	0.00222	Samolyk 2012
55614.6340	27231	0.11005	0.00166	Le Borgne *et al.* 2012
55631.3740	27268	0.11150	0.00276	Vandenbroere and Hambsch 2011
55643.5860	27295	0.10888	–0.00011	Le Borgne *et al.* 2012
55666.6594	27346	0.11022	0.00076	Samolyk 2012
55668.0140	27349	0.10764	–0.00185	Hirosawa 2012
55669.3740	27352	0.11046	0.00094	Vandenbroere and Hambsch 2011
55714.6146	27452	0.11170	0.00124	This study
55890.6020	27841	0.11813	0.00398	Le Borgne *et al.* 2012
55904.6250	27872	0.11694	0.00249	Le Borgne *et al.* 2012
55905.9802	27875	0.11496	0.00048	Samolyk 2012

Table continued on next page

Table 4. Recalculated quadratic residuals $(O–C)_2$ for RR Leo times-of-maximum following linear least squares fit of $(O–C)_1$ and cycle number between 1898 Dec 17 and 2012 Dec 24, cont.

Time of Maximum (HJD–2400000)	*Cycle Number*	*$(O–C)_1$**	*$(O–C)_2$*	*Reference*
55942.6240	27956	0.11491	–0.00035	Vandenbroere and Le Borgne 2012
55946.6990	27965	0.11837	0.00302	Le Borgne *et al.* 2013
55951.6742	27976	0.11724	0.00179	Le Borgne *et al.* 2013
55961.6271	27998	0.11749	0.00182	Le Borgne *et al.* 2013
55963.8890	28003	0.11742	0.00171	Samolyk 2013
55969.7716	28016	0.11891	0.00307	Samolyk 2013
55976.1036	28030	0.11740	0.00143	Hirosawa 2013
55980.6283	28040	0.11817	0.00210	Le Borgne *et al.* 2013
55987.4147	28055	0.11867	0.00246	Le Borgne *et al.* 2013
55988.3185	28057	0.11768	0.00145	Le Borgne *et al.* 2013
55997.3670	28077	0.11832	0.00189	Vandenbroere and Le Borgne 2012
56000.5320	28084	0.11656	0.00007	Le Borgne *et al.* 2013
56000.9883	28085	0.12047	0.00397	Hirosawa 2013
56002.3450	28088	0.11999	0.00346	Vandenbroere and Le Borgne 2012
56006.4214	28097	0.12485	0.00823	Hübscher *et al.* 2013
56011.3920	28108	0.11912	0.00240	Vandenbroere and Le Borgne 2012
56035.3686	28161	0.11888	0.00164	Le Borgne *et al.* 2013
56250.2570	28636	0.12046	–0.00142	Hirosawa 2013
56251.6186	28639	0.12488	0.00297	Le Borgne *et al.* 2013
56259.3091	28656	0.12470	0.00262	Hirosawa 2013
56285.5483	28714	0.12508	0.00243	Le Borgne *et al.* 2013

*Notes: *$(O–C)_1$ residuals from linear elements reported (GCVS, Samus et al. 2012) for RR Leo. **Value rejected as outlier.*

References

AAVSO. 2013, observations from the AAVSO International Database (http://www.aavso.org).

Agerer, F., Dahm, M., and Hübscher, J. 1999, *Inf. Bull. Var. Stars*, No. 4712, 1.

Agerer, F., and Hübscher, J. 1997, *Inf. Bull. Var. Stars*, No. 4472, 1.

Agerer, F., and Hübscher, J. 2000, *Inf. Bull. Var. Stars*, No. 4912, 1.

Agerer, F., and Hübscher, J. 2002, *Inf. Bull. Var. Stars*, No. 5296, 1.

Agerer, F., and Hübscher, J. 2003, *Inf. Bull. Var. Stars*, No. 5485, 1.

Ahnert, P. 1950, *Mitt. Veränderliche Sterne*, No. 118, 1.

Ahnert, P. 1959a, *Mitt. Veränderliche Sterne*, No. 399, 1.

Ahnert, P. 1959b, *Mitt. Veränderliche Sterne*, No. 419, 1.

Ahnert, P. 1961a, *Mitt. Veränderliche Sterne*, No. 579, 1.

Ahnert, P. 1961b, *Mitt. Veränderliche Sterne*, No. 567, 1.

Allen, L. B., and Marsh, F. E. 1932, *Bull. Harvard Coll. Obs.*, No. 888, 19.

Ashbrook, J. 1949, *Astron. J.*, **54**, 198.

Aubaud, J. 1990, *AFOEV Bull.*, **51**, 1.

Aubaud, J. 1992, *AFOEV Bull.*, **59**, 3.

Balázs, J., and Detre, L. 1949, *Commun. Konkoly Obs.*, No. 21, 1.

Berdnikov, L. N. 1977, *Perem. Zvezdy Prilozh.*, **3**, 329.

Berry, R., and Burnell, J. 2005, *Handbook of Astronomical Image Processing*, Willmann-Bell, Richmond.

Braune, W., and Hübscher, J. 1987, *BAV Mitt.*, No. 46, 1.

Braune, W., Hübscher, J., and Mundry, E. 1970, *Astron. Nachr.*, **292**, 185.

Braune, W., Hübscher, J., and Mundry, E. 1977, *Astron. Nachr.*, **298**, 121.

Braune, W., Hübscher, J., and Mundry, E. 1979, *Astron. Nachr.*, **300**, 165.

Braune, W., and Mundry, E. 1973, *Astron. Nachr.*, **294**, 225.

Buchheim, B. 2006, in *The Society for Astronomical Sciences 25th Annual Symposium on Telescope Science. Held May 23-25, 2006, at Big Bear, CA*, Society for Astronomical Sciences, Rancho Cucamonga, CA, 183.

Butters, O. W., *et al.* 2010, *Astron. Astrophys.*, **520**, L10.

Dahm, M., and Kleikamp, W. 1998, *BAV Rundbrief*, **47**, 67.

Demjanovsky, V. 1975, *Perem. Zvezdy Prilozh.*, **2**, 301.

Detre, L. 1936, *Astron. Nachr.*, **259**, 305.

Ekmekçi, F., Çelik, L., and Şenavci, H. V. 2012, paper presented at the 20th Stellar Pulsation Conference Series on impact of new instrumentation and new insights in stellar pulsations, Granada, 5–9 September 2011.

Epstein, I. 1969, *Astron. J.*, **74**, 1131.

Firmanyuk, B. N., Derevyagin, V. G., and Lysova, L. E. 1985, *Astron. Circ.*, No. 1374, 7.

Fitch, W. S., Wisniewski, W. Z., and Johnson, H. L. 1966, *Commun. Lunar Planet. Lab.*, **5**, 71.

Gaposchkin, S. 1934, *Circ. Harvard Coll. Obs.*, No. 392, 1.

Geyer, E. H. 1961, *Z. Astrofiz.*, **52**, 229.

Guriev, N. 1937, *Tadjik Obs. Circ.*, No. 26, 1.

Henden, A. A., and Kaitchuck, R. H. 1990, *Astronomical Photometry: A Text and Handbook for the Advanced Amateur and Professional Astronomer*, Willmann-Bell, Richmond.

Hirosawa, K. 2012, *Var. Star Bull*. (VSOLJ), No. 52, 6.

Hirosawa, K. 2013, *Var. Star Bull.* (VSOLJ), No. 54, 2.

Hübscher, J. 2001, *BAV Mitt.*, No. 143, 1.

Hübscher, J. 2005a, *Inf. Bull. Var. Stars*, No. 5643, 1.

Hübscher, J. 2005b, *BAV Mitt.*, No. 171, 1.

Hübscher, J. 2007, *Inf. Bull. Var. Stars*, No. 5802, 1.

Hübscher, J., Agerer, F., Busch, H., Goldhahn, H., Hassforther, B., and Dahm, M. 1999, *BAV Mitt.*, No. 122, 1.

Hübscher, J., Agerer, F., Busch, H., Goldhahn, H., Hassforther, B., and Dahm, M. 2000, *BAV Mitt.*, No. 131, 1.

Hübscher, J., Agerer, F., Busch, H., Goldhahn, H., Hassforther, B., Lange, T., and Paschke, A. 2002, *BAV Mitt.*, No. 154, 1.

Hübscher, J., Agerer, F., Frank, P., and Wunder, E. 1994, *BAV Mitt.*, No. 68, 1.

Hübscher, J., Agerer, F., Hassforther, B., and Dahm, M. 1998, *BAV Mitt.*, No. 113, 1.

Hübscher, J., Agerer, F., Hassforther, B., Lange, T., and Paschke, A. 2003, *BAV Mitt.*, No. 157, 1.

Hübscher, J., Agerer, F., and Wunder, E. 1991, *BAV Mitt.*, No. 59, 1.

Hübscher, J., Agerer, F., and Wunder, E. 1992, *BAV Mitt.*, No. 60, 1.

Hübscher, J., Agerer, F., and Wunder, E. 1993, *BAV Mitt.*, No. 62, 1.

Hübscher, J., Agerer, F., and Wunder, E. 1995, *BAV Mitt.*, No. 79, 1.

Hübscher, J., Agerer, F., and Wunder, E. 1997, *BAV Mitt.*, No. 101, 1.

Hübscher, J., Braune, W., and Lehmann, P. B. 2013, *Inf. Bull. Var. Stars*, No. 6048, 1.

Hübscher, J., Lange, T., Paschke, A., Vohla, F., and Walter, F. 2005a, *BAV Mitt.*, No. 174, 1.

Hübscher, J., Lehmann, P. B., Monninger, G., Steinbach, H.-M., and Walter, F. 2010, *Inf. Bull. Var. Stars*, No. 5918, 1.

Hübscher, J., and Lichtenknecker, D. 1988, *BAV Mitt.*, No. 50, 1.

Hübscher, J., Lichtenknecker, D., and Wunder, E. 1989, *BAV Mitt.*, No. 52, 1.

Hübscher, J., Lichtenknecker, D., and Wunder, E. 1990, *BAV Mitt.*, No. 56, 1.

Hübscher, J., and Monninger, G. 2011, *Inf. Bull. Var. Stars*, No. 5959, 1.

Hübscher, J., Paschke, A., and Walter, F. 2005b, *Inf. Bull. Var. Stars*, No. 5657, 1.

Hübscher, J., Steinbach, H.-M., Vohla, F., and Walter, F. 2009a, *BAV Mitt.*, No. 202, 1.

Hübscher, J., Steinbach, H.-M., and Walter, F. 2009b, *Inf. Bull. Var. Stars*, No. 5874, 1.

Hübscher, J., Steinbach, H.-M., and Walter, F. 2009c, *Inf. Bull. Var. Stars*, No. 5889, 1.

Huth, H. 1964, *Mitt. Veränderliche Sterne*, **2**, 112.
Jordan, F. C. 1929, *Publ. Allegheny Obs.*, **7**, 1.
Kanishcheva, R. K., and Lange G. A. 1971, *Perem. Zvedzy Prilozh.*, **1**, 107.
Karetnikov, V. G. 1961, *Astron. Circ.*, No. 225, 13.
Karetnikov, V. G. 1962, *Perem. Zvezdy*, **14**, 238.
Khruslov, A. V. 2011, *Perem. Zvezdy Prilozh.*, **11**, 24.
Kooreman, C. J. 1935, *Bull. Astron. Inst. Netherlands*, **7**, 301.
Kukarkin, B. V. 1928, *Perem. Zvezdy*, **1**, No. 5, 3.
Kukarkin, B. V. 1933, *Perem. Zvezdy*, **4**, 93.
Kukarkin, B. V., and Parenago, P. P. 1931, *Perem. Zvezdy*, **3**, 34.
Lause, P. 1931, *Astron. Nachr.*, **244**, 417.
Le Borgne, J.-F. 2004, *GEOS Circular on RR Type Variables*, No. RR22, 1.
Le Borgne, J.-F., Klotz, A., and Boër, M. 2004, *Inf. Bull. Var. Stars*, No. 5568, 1.
Le Borgne, J.-F., Klotz, A., and Boër, M. 2005a, *Inf. Bull. Var. Stars*, No. 5622, 1.
Le Borgne, J.-F., Klotz, A., and Boër, M. 2005b, *Inf. Bull. Var. Stars*, No. 5650, 1.
Le Borgne, J.-F., Klotz, A., and Boër, M. 2006a, *Inf. Bull. Var. Stars*, No. 5686, 1.
Le Borgne, J.-F., Klotz, A., and Boër, M. 2006b, *Inf. Bull. Var. Stars*, No. 5717, 1.
Le Borgne, J.-F., Klotz, A., and Boër, M. 2007a, *Inf. Bull. Var. Stars*, No. 5767, 1.
Le Borgne, J.-F., Klotz, A., and Boër, M. 2007b, *Inf. Bull. Var. Stars*, No. 5790, 1.
Le Borgne, J.-F., Klotz, A., and Boër, M. 2008a, *Inf. Bull. Var. Stars*, No. 5853, 1.
Le Borgne, J.-F., Klotz, A., and Boër, M. 2009a, *Inf. Bull. Var. Stars*, No. 5877, 1.
Le Borgne, J.-F., Klotz, A., and Boër, M. 2009b, *Inf. Bull. Var. Stars*, No. 5895, 1.
Le Borgne, J.-F., Klotz, A., and Boër, M. 2010a, *Inf. Bull. Var. Stars*, No. 5934, 1.
Le Borgne, J.-F., Klotz, A., and Boër, M. 2011, *Inf. Bull. Var. Stars*, No. 5986, 1.
Le Borgne, J.-F., Klotz, A., and Boër, M. 2012, *Inf. Bull. Var. Stars*, No. 6009, 1.
Le Borgne, J.-F., Klotz, A., and Boër, M. 2013, *Inf. Bull. Var. Stars*, No. 6043, 1.
Le Borgne, J.-F., Klotz, A., and Kugel, F. 2010b, *GEOS Circular on RR Type Variables*, No. RR44, 1.
Le Borgne, J.-F., Vandenbroere, J., Henden, A. A., Butterworth, N., and Dvorak, S. 2008b, *Inf. Bull. Var. Stars*, No. 5854, 1.
Le Borgne, J. F., *et al.* 2007c, *Astron. Astrophys.*, **476**, 307.
Lee, Y.-H., Kim, S.S., Shin, J., and Lee, J. 2008, *Publ. Astron. Soc. Japan*, **60**, 551.
Lenz, P., and Breger, M. 2005, *Commun. Asteroseismology*, **146**, 53.
Liu, T., and Janes, K. A. 1989, *Astron. J., Suppl. Ser.*, **69**, 593.
Luizet, M. 1911, *Bull. Astron.*, **28**, 452.
Martignoni, M. 2011, *Inf. Bull. Var. Stars*, No. 6006, 1.
Martin, C., and Plummer, H. C. 1921, *Mon. Not. Roy. Astron. Soc.*, **81**, 458.
Minor Planet Observer. 2010, MPO Software Suite (http://www.minorplanetobserver.com), BDW Publishing, Colorado Springs.
Neckel, H. 1958, *Astrophys. J.*, **128**, 510.
Nielsen, A.V. 1929, *Astron. Nachr.*, **235**, 177.
Olah, K., and Szeidl, B. 1978, *Commun. Konkoly Obs.*, No. 71, 1.

Oosterhoff, P. T. 1930, *Bull. Astron. Inst. Netherlands*, **6**, 39.
Perryman, M. A. C, *et al.* 1997, *Astron. Astrophys.*, **323**, L49.
Pojmański, G. 2002, *Acta. Astron.*, **52**, 397.
Pojmański, G., Pilecki, B., and Szczygiel, D. 2005, *Acta. Astron.*, **55**, 275.
Poretti, E. 2001a, *Commun. Asteroseismology*, **140**, 40.
Poretti, E. 2001b, *Astron. Astrophys.*, **371**, 986.
Press, W., Teukolsky, S. A., Vetterling, W. T., and Flannery, B. P. 1992, *Numerical Recipes in FORTRAN*, Cambridge Univ. Press, Cambridge.
Preston, G. W. 1964, *Ann. Rev. Astron. Astrophys.*, **2**, 23.
Robinson, L.V. 1930, *Bull. Harvard Coll. Obs.*, No. 876, 23.
Samolyk, G. 2010, *J. Amer. Assoc. Var. Star Obs.*, **38**, 12.
Samolyk, G. 2011, *J. Amer. Assoc. Var. Star Obs.*, **39**, 23.
Samolyk, G. 2012, *J. Amer. Assoc. Var. Star Obs.*, **40**, 923.
Samolyk, G. 2013, *J. Amer. Assoc. Var. Star Obs.*, **41**, 85.
Samus, N. N., and Antipin, S. V. 2005, *Inf. Bull. Var. Stars*, No. 5699, 3.
Samus, N. N., *et al.* 2012, *General Catalogue of Variable Stars* (GCVS; http://www.sai.msu.su/gcvs/gcvs/).
Schlafly, E. F., and Finkbeiner, D. P. 2011, *Astrophys. J.*, **737**, 103.
Schlegel, D. J., Finkbeiner, D. P., and Davis, M. 1998, *Astrophys. J.*, **500**, 525.
Skrutskie, M. F., *et al.* 2006, *Astron. J.*, **131**, 1163.
Software Bisque. 2011, CCDSOFT CCD control software (http://www.bisque.com), Santa Barbara Instrument Group, Santa Barbara, CA.
Soloviev, A. V. 1936a, *Perem. Zvezdy*, **5**, 77.
Soloviev, A. V. 1936b, *Tadjik Obs. Circ.*, No. 15, 1.
Soloviev, A. V., and Shakhovskoj, N. M. 1958, *Tadjik Tr.*, **7**, 45.
Szeidl, B., and Pocs, M. D. 2002, *Inf. Bull. Var. Stars*, No. 5349, 1.
Templeton, M. R., Samolyk, G., Dvorak, S., Poklar, R., Butterworth, N., and Gerner, H. 2009, *Publ. Astron. Soc. Pacific*, **121**, 1076.
Tsesevich, V. P. 1934, *Leningrad Bull.*, No. 4, 1.
Tsesevich, V. P. 1974, *Astron. Tsirk.*, No. 811, 1.
Udalski, A., Szymański, M., Kałużny, J., Kubiak, M., and Mateo, M. 1992, *Acta Astron.*, **42**, 253.
Vandenbroere, J. 1997, *GEOS Circular on RR Type Variables*, No. RR14, 1.
Vandenbroere, J. 1998, *GEOS Circular on RR Type Variables*, No. RR15, 1.
Vandenbroere, J. 1999, *GEOS Circular on RR Type Variables*, No. RR16, 1.
Vandenbroere, J. 2001, *GEOS Circular on RR Type Variables*, No. RR17, 1.
Vandenbroere, J. 2005, *GEOS Circular on RR Type Variables*, No. RR23, 1.
Vandenbroere, J., and Denoux, E. 2007, *GEOS Circular on RR Type Variables*, No. RR30, 1.
Vandenbroere, J., and Hambsch, F.-J. 2011, *GEOS Circular on RR Type Variables*, No. RR47, 1.
Vandenbroere, J., and Le Borgne, J.-F. 2012, *GEOS Circular on RR Type Variables*, No. RR49, 1.

Vandenbroere, J., and Salmon, G. 2010, *GEOS Circular on RR Type Variables*, No. RR45, 1.

Vanmunster, T. 2013, PERANSO (v.2.50) Light Curve and Period Analysis Software (http://www.peranso.com/).

Vasilief, I. 2013, QTIPLOT (v. 0.9.8.9) Data Analysis and Scientific Visualization (http://soft.proindependent.com/qtiplot.html).

Warner, B. 2007, *Minor Planet Bull.*, **34**, 113.

Watson, C., Henden, A. A., and Price, A. 2013, AAVSO International Variable Star Index VSX (Watson+, 2006–2013; http://www.aavso.org/vsx).

Wenske, W. 1980, *BAV Rundbrief*, **29**, 45.

Wils, P., Lloyd, C., and Bernhard, K. 2006, *Mon. Not. Roy. Astron. Soc.*, **368**, 1757.

Wils, P., *et al.* 2012, *Inf. Bull. Var. Stars*, No. 6015, 1.

Woźniak, P. R., *et al.* 2004, *Astron. J.*, **127**, 2436.

Yilmaz, M., *et al.* 2009, *Inf. Bull. Var. Stars*, No. 5887, 1.

Zakharov, G.P. 1953, *Perem. Zvezdy*, **9**, 271.

Zhou, A.-Y., and Jiang, S.-Y. 2011, *Astron. J.*, **142**, 100.

New Variable Stars Discovered by the APACHE Survey. I. Results After the First Observing Season

Mario Damasso
INAF-Astrophysical Observatory of Torino, Via Osservatorio 20, I-10025 Pino Torinese, Italy; Astronomical Observatory of the Autonomous Region of the Aosta Valley, fraz. Lignan 39, 11020 Nus (Aosta), Italy; Dept. of Physics and Astronomy, University of Padova, Vicolo dell'Osservatorio 3, I-35122 Padova, Italy; mario.damasso@studenti.unipd.it and m.damasso@gmail.com

Andrea Bernagozzi
Enzo Bertolini
Paolo Calcidese
Albino Carbognani
Davide Cenadelli
Astronomical Observatory of the Autonomous Region of the Aosta Valley, fraz. Lignan 39, 11020 Nus (Aosta), Italy

Jean Marc Christille
Dept. of Physics, University of Perugia, Via A. Pascoli, 06123 Perugia, Italy; Astronomical Observatory of the Autonomous Region of the Aosta Valley, fraz. Lignan 39, 11020 Nus (Aosta), Italy

Paolo Giacobbe
INAF-Astrophysical Observatory of Torino, Via Osservatorio 20, I-10025 Pino Torinese, Italy; Dept. of Physics, University of Trieste, Via Tiepolo 11, I-34143 Trieste, Italy

Luciano Lanteri
Mario G. Lattanzi
Richard Smart
Allesandro Sozzetti
INAF-Astrophysical Observatory of Torino, Via Osservatorio 20, I-10025 Pino Torinese, Italy

Received December 2, 2013; revised January 7, 2014; accepted January 8, 2014

Abstract We present more than 80 new variable stars discovered during the first observing season of the APACHE survey. APACHE is a project aimed at detecting extrasolar planets transiting nearby, bright M dwarfs by using an array of small-aperture telescopes. Despite the fact that the survey is targeted to a well-defined sample of cool stars, we also reduce and analyze data for all the detected field stars. Since July 2012 dozens of different stellar fields

have been monitored, leading to the detection of several variables for which we propose a classification and estimate a period, when a periodicity is evident in the data. Thanks to the SuperWASP public archive, we have also retrieved and analyzed photometric data collected by the SWASP survey, which helped us to refine the classification and the period estimation of many variables found in the APACHE database. Some of the variables present peculiarities and thus are discussed separately.

1. Introduction

Project APACHE (A PAthway toward the Characterization of Habitable Earths) is a new ground-based photometric survey specifically designed to search for transiting, small-size planets orbiting bright, nearby early-to-mid M dwarfs (Sozzetti *et al.* 2013). The project has been active, since July 2012, at the Astronomical Observatory of the Autonomous Region of the Aosta Valley (OAVdA), located in the Western Italian Alps.

APACHE (http://apacheproject.altervista.org) is a collaboration between OAVdA and INAF-Osservatorio Astrofisico di Torino (INAF-OATo), and it will last for five years. The survey utilizes an array of five automated 40-cm telescopes to monitor hundreds of M dwarfs properly selected from the catalogue of Lépine and Gaidos (2011). In parallel with the search for transit-like signals in the light curves of the M dwarfs, we are also analyzing the photometric data of the huge sample of stars that fall in the fields of view of the telescopes, which are centered on the target cool stars, to look for new variable stars. Here we report a list of variables discovered during the first observing season of APACHE. As demonstrated after the first year of operation, the large photometric database collected by APACHE represents a treasure trove for identifying new variable stars which will be constantly scoured.

2. Instruments and methods

The APACHE survey uses an array composed of identical Carbon Truss 40-cm f/8.4 Ritchey-Chrétien telescopes, each with a GM2000 10MICRON German mount and equipped with a FLI Proline PL1001E-2 CCD Camera and Johnson-Cousins V, R, and I filters. This instrument configuration is characterized by a pixel scale of 1.5 arcsec/pixel and a field of view of $26' \times 26'$. Except for a small number of targets which are monitored in the V band, all the fields are observed using the I_c filter. The complete catalogue of M dwarfs eligible for observations by the APACHE survey is composed of 3,323 targets and has been organized in a ranking list by assigning observing priorities which take into account several factors, for example: the highest priority is given to stars with a reliable spectral classification published in the literature; to those that are known to be slow rotators, based on measurements of their projected rotational velocity v *sin* i; whether they have a low chromospheric activity as measured by the equivalent width of the H-α line and are not known as bright X-ray sources. A slow rotator and a star with a low activity level has to be preferred because, for the spectroscopic follow-up required to measure the mass of a transiting planetary candidate, the measurements of the radial velocity variations are less affected by the line broadening and the intrinsic jitter due to stellar activity.

It is interesting to mention another parameter considered for the definition of the ranking list: the expected number of observations of each target guaranteed by the Gaia satellite, which has been successfully launched and is expected to provide a very relevant contribution to extrasolar science. According to the scanning law of Gaia, it is possible to calculate the number of expected transits over a certain field after the nominal five years of mission. When building the APACHE schedule, we have assumed that targets with a number of Gaia observations greater than 100 have higher priorities because they will be characterized by a very accurate measurements of trigonometric parallax, from which it will be possible to accurately determine fundamental stellar parameters such as the intrinsic luminosity, mass, and radius, which are necessary for a precise study of any hosted planet.

The APACHE observations are carried out in focus, and the exposure times—which are kept fixed during the sessions independently from the seeing—are in the range of 3 to 180 seconds, while the magnitudes of the target M dwarfs vary within 8–16.5 in the V-band and 5.5–13 in the J-band. The APACHE telescopes use a circular observing schedule, with each target being re-pointed typically 20 minutes after the last observation. This cadence should be optimal for collecting enough data points which fall in the portion of the light curve showing a transit, if it is in progress, that usually is expected to last for one to three hours. Each time a target is pointed, three consecutive exposures are taken and usually the average value of the corresponding differential magnitudes is used for light curve analysis. In the course of a night the same field is observed as long as its altitude above the horizon is greater than 30 degrees, while it remains in schedule for typically 60 to 90 days in a row.

After the first observing season nearly 150 different stellar fields have been observed, necessarily characterized by not uniform amounts of data. We have searched for new variable stars especially considering those fields with the major amounts of photometric data. For each field we have visually inspected the differential light curves of all the stars identified, which typically amount to some dozens but in some cases are more than one thousand per field, and processed by the data reduction and analysis pipeline TEEPEE (Transiting ExoplanEt PipElinE), developed by the authors mostly in IDL programming language and tailored specifically to provide the user with optimal light curves of the primary target M dwarfs. The TEEPEE package, indifferently applied to data collected during a single night or over the whole timespan of observations, tests up to twelve different apertures and the best set of comparison stars is automatically determined from a list of dozens among the brightest objects in the field, excluding those too close to the CCD borders. The best aperture and set of reference stars selected at the end of the data processing are the ones which give the smallest RMS for the entire light curve of the object of interest. To save CPU time, this procedure is applied once with regard only to the primary M dwarf targets. Thus the aperture and set of comparisons used for determining the differential light curves of the field stars are those selected for the M dwarfs, which usually represent a good choice. Because, as stated, the number of comparison stars is typically high for each field (more than 10 in several cases), we do not provide the complete list for each variable we discuss here. At our site the seeing conditions can vary sensibly from night to night, and typical values for the FWHM of the APACHE images range within 1.5 to 3 pixels, and the TEEPEE pipeline tests aperture radii in the range 3.5 to 9 pixels.

3. Results

The aim of this work is to provide a list of new variable stars for which we propose tentative classification and—for those showing evidence of periodicity—we produce an estimate of the period. Our conclusions originate only from photometry, and no spectroscopic follow-up has been carried out to improve our knowledge about these objects. For some stars, we considered it interesting to provide a detailed, separate discussion (section 4). The complete list of 86 variables discussed in this work is presented in Table 1. All of them have been searched in the AAVSO VSX database and 83 can be considered as new genuine discoveries. Three objects are already included in the VSX database. One eclipsing binary system is provided without any information about the orbital period, which we have estimated from our data. Another object is classified in VSX as an eclipsing variable without any information about the orbital period, but our data do not confirm this classification, rather the star appears to be an irregular variable of type L. A variable of L type, as read in the VSX database, is reported with a period of 88 days, but this value is not confirmed by our data. In Figure 1 we show the corresponding light curves, with those showing periodicity folded according to the best period found through a Lomb-Scargle (L-S) analysis applied to the APACHE data, except in very few cases (as explained below). For this task we used the IDL version of the L-S algorithm (http://www.arm.ac.uk/ csj/idl/PRIMITIVE/scargle.pro). Almost every APACHE light curve presented here has been obtained using the I_c filter, except where specified in the explanatory notes accompayining Table 1. The magnitudes in V band, where not otherwise specified, are those from the APASS survey, which are reported by the UCAC4 catalogue (Zacharias *et al.* 2012). Several stars appear as having no evidence of periodicity, or with a very poorly defined periodicity which shows only occasionally. Due to this

Table 1. Variable stars discovered by APACHE during the first observing season. For stars with two periods indicated, that in parentheses is the one determined from the APACHE data, while the other is estimated from SuperWASP archive data. The amplitudes of the light curves are measured from APACHE data. Time T_0 corresponds to phase = 0 in the folded light curves.

No.	*Name*	*R.A. (2000)*	*Dec. (2000)*	*Mag. V*	*Period (days)*	*Amplitude (mag.)*	*T_0 (HJD–2455000)*	*Var. Type*	*Note*
1	UCAC4 744-001518	002.6931077	+58.6863575	14.86	7.55 (7.518)	~0.25	1146.3523197	ROT?	(1)
2	UCAC4 743-001636	002.7103159	+58.5618373	10.21	0.10625 (0.09603)	~0.02	1146.3523197	DSCT	(2)
3	UCAC4 758-009639	015.1541895	+61.5753528	14.27	1.20557	~0.6	1146.4105864	E	(3)
4	UCAC4 752-014548	018.8161518	+60.3735250	13.14	1.087	~0.3	1146.3866004	EB	
5	UCAC4 870-000885	018.9877518	+83.9571120	16.77	0.40861	~0.3	1273.2157609	EW	
—	UCAC4 872-000839	021.2561924	+84.2626639	16.17	?	—	RR?	(4)	
6	UCAC4 728-026837	044.2308518	+55.5203950	16.38 (GSC2.3)	?	~0.4	1146.4709166	L	
7	UCAC4 618-013561	062.4040074	+33.4937250	12.83	?	~0.25	1162.5960791	L	
8	UCAC4 713-031969	063.5650233	+52.5300092	14.4	6.22	~0.4	1208.3673785	E	(5)
9	UCAC4 709-034533	074.7646086	+51.7157109	10.77	?	~0.05	1328.2561929	L	
10	UCAC4 610-021265	082.4603353	+31.9110003	13.59	0.80089 (0.80086)	~0.3	1210.5113093	EW	(6)
11	UCAC4 619-030850	092.0415889	+33.6711831	13.01	2.008 (2.009)	~0.27	1205.5239017	EB	(7)
12	UCAC4 521-023140	094.9127039	+14.0543662	12.47	~77?	~0.16	1270.3904921	L	(8)
13	UCAC4 624-036803	105.7816774	+34.7009262	15.90	0.21635 (WASP)	~0.25	1246.5895718	EW	(9)
14	UCAC4 715-044844	105.9254200	+52.8823920	13.22	0.3281 (0.32811)	~0.33	1205.4926955	EW	(10)
15	UCAC4 664-056989	179.4896992	+42.6626264	14.19	0.33651	~0.5	1353.4968403	RRab	(11)
16	UCAC4 609-049172	208.1377689	+31.6871487	13.47	0.35471 (0.35470)	~0.16	1301.7535576	EW	(12)
17	UCAC4 666-060394	232.1916465	+43.0916548	12.79	1.9756 (1.9788)	~0.1	1127.3672611	ROT	(13)
18	UCAC4 633-053996	250.3480433	+36.5047900	12.26	?	~0.1	1367.4885131	L	
19	UCAC4 633-054311	250.4026556	+36.4431934	15.06	?	~0.3	1367.4885131	L	(14)

Table continued on following pages

Table 1. Variable stars discovered by APACHE during the first observing season. For stars with two periods indicated, that in parentheses is the one determined from the APACHE data, while the other is estimated from SuperWASP archive data. The amplitudes of the light curves are measured from APACHE data. Time T_0 corresponds to phase = 0 in the folded light curves, cont.

No.	*Name*	*R.A. (2000)*	*Dec. (2000)*	*Mag. V*	*Period (days)*	*Amplitude (mag.)*	*T_0 (HJD–2455000)*	*Var. Type*	*Note*
20	UCAC4 633-054908	250.4621462	+36.4817620	11.82	?	~0.2	1367.4885131	L	(15)
21	UCAC4 652-057450	253.3608262	+40.3033556	14.83	1.47	~0.45	1420.4785809	EB	
22	UCAC4 592-063874	275.7670439	+28.3080614	14.01(GSC2.3)	~60?	~0.2	1127.3682196	L	
23	UCAC4 533-077928	279.6991892	+16.4103631	15.12	?	~0.5	1166.3294430	L	
24	UCAC4 533-078069	279.8361324	+16.5350567	14.97 (GSC2.3)	?	~0.2	1166.3294430	L	
25	UCAC4 532-076755	279.8824256	+16.3173617	15.15	0.3199	~0.25	1166.3294430	EW	
26	UCAC4 533-078283	280.0367009	+16.5274503	14.58	?	~0.11	1166.3294430	L	
27	UCAC4 723-061541	283.8471103	+54.4308875	14.33	0.38399 (0.38399)	~0.7	1385.4985908	EW	(16)
28	UCAC4 723-061622	284.1744556	+54.5157323	13.34 (GSC2.3)	?	~0.35	1385.4876350	L	
29	UCAC4 479-089263	284.6627689	+05.7352287	11.68	0.744	~0.1	1473.4154161	RRc	(17)
30	UCAC4 491-099556	284.8352648	+08.1355764	N.A.	?	~0.15	1432.4879724	L	(18)
31	2MASS 18592325+0810247	284.846896	+08.173555	N.A.	?	~0.25	1432.4879724	L	(19)
32	UCAC4 491-099593	284.8855603	+08.0666542	16.48 (GSC2.3)	1.251	~0.35	1432.4879724	EW	
33	2MASS 19000738+0805125	285.030765	+08.086826	19.00 (GSC2.3)	?	~0.25	1432.4879724	L	
34	UCAC4 490-094834	285.0720153	+07.9374948	16.58 (GSC2.3)	?	~0.12	1432.4879724	L	
35	UCAC4 729-060138	290.8229630	+55.6600275	12.76	0.6902 (0.688)	~0.08	1434.3738137	ROT	(20)
36	UCAC4 728-061629	290.9937003	+55.5546067	14.81	0.36689 (0.3669)	~0.2	1434.3728183	EW	(21)
37	UCAC4 728-061766	291.4820559	+55.5007378	15.27 (GSC2.3)	0.189029 (0.1890)	~0.1	1434.3738137	DSCT	(22)

Table continued on following pages

Table 1. Variable stars discovered by APACHE during the first observing season. For stars with two periods indicated, that in parentheses is the one determined from the APACHE data, while the other is estimated from SuperWASP archive data. The amplitudes of the light curves are measured from APACHE data. Time T_0 corresponds to phase=0 in the folded light curves, cont.

No.	*Name*	*R.A. (2000)*	*Dec. (2000)*	*Mag. V*	*Period (days)*	*Amplitude (mag.)*	*T_0 (HJD–2455000)*	*Var. Type*	*Note*
38	UCAC4 811-027074	294.4105074	+72.0363334	13.63	?	~0.2	1424.3380554	L	
39	UCAC4 610-092144	297.3880989	+31.8705942	14.72 (NOMAD)	?	~0.1	1127.5857519	L	
40	UCAC4 609-091131	297.4135403	+31.6445878	14.79 (NOMAD)	?	~0.15	1127.5857519	L	
41	UCAC4 609-091297	297.4814474	+31.7204662	17.27 (NOMAD)	?	~0.9	1127.5857519	L	
42	2MASS 19500382+3149132	297.515956	+31.820337	N.A.	?	~0.15	1127.5857519	L	
43	2MASS 19500885+3135499	297.536909	+31.597216	N.A.	?	~0.4	1127.5857519	L	
44	UCAC4 610-092592	297.5731206	+31.9941723	15.53 (NOMAD)	?	~0.2	1127.5857519	L	
45	2MASS 19502059+3152091	297.585806	+31.869217	17.38 (NOMAD)	?	~0.2	1127.5857519	L	
46	2MASS 19502935+3158417	297.622323	+31.978273	N.A.	?	~0.17	1127.5857519	L	
47	UCAC4 610-092815	297.6690953	+31.9639217	15.41 (NOMAD)	0.427	~0.5	1127.5857519	EW	
48	UCAC4 609-091797	297.7097806	+31.6965225	12.70	~40?	~0.13	1127.5857519	L	
49	UCAC4 608-095594	297.7998224	+31.5728037	15.22 (NOMAD)	?	~0.45	1127.5857519	L	
50	2MASS 19511471+3143128	297.811294	+31.720238	17.47	?	~0.14	1127.5857519	L	
51	UCAC4 623-096266	302.9632515	+34.4131084	15.28 (NOMAD)	9.8	~0.45	1416.5074270	PULS	(23)
52	UCAC4 623-096337	303.0224745	+34.4758434	15.87 (NOMAD)	~61?	~0.16	1416.5074270	L	

Table continued on following pages

Table 1. Variable stars discovered by APACHE during the first observing season. For stars with two periods indicated, that in parentheses is the one determined from the APACHE data, while the other is estimated from SuperWASP archive data. The amplitudes of the light curves are measured from APACHE data. Time T_0 corresponds to phase = 0 in the folded light curves, cont.

No.	*Name*	*R.A. (2000)*	*Dec. (2000)*	*Mag. V*	*Period (days)*	*Amplitude (mag.)*	*T_0 (HJD–2455000)*	*Var. Type*	*Note*
53	UCAC4 621-098928	303.0456662	+34.0879998	13.90	0.1365	~0.07	1416.5076083	DSCT?	
54	UCAC4 622-095023	303.0508565	+34.2564675	14.06 (NOMAD)	?	~0.22	1416.5074270	L	(24)
55	UCAC4 622-095081	303.0868139	+34.3034262	17.07 (NOMAD)	~44?	~0.15	1416.5074270	L	
56	UCAC4 622-095314	303.2126174	+34.2968739	16.19 (NOMAD)	?	~0.12	1416.5074270	L	
57	UCAC4 623-096673	303.2543371	+34.4226409	14.72 (NOMAD)	?	~0.25	1416.5074270	L	
58	UCAC4 622-095521	303.3453327	+34.3789689	13.58	?	~0.3	1416.5074270	L	
59	UCAC4 622-095554	303.3731539	+34.3134381	14.99 (NOMAD)	?	~0.05	1416.5074270	L	
60	UCAC4 516-127264	303.6096042	+13.1699259	12.40	0.575	~0.2	1445.5441597	EW	
—	UCAC4 744-062741	306.3905642	+58.6538473	14.09	1.51?	~0.2	1127.3642954	ROT?	(25)
61	UCAC4 744-062753	306.4085277	+58.7603659	14.17 (GSC2.3)	0.4406 (0.4405)	~0.25	1127.3642954	EW	(26)
62	UCAC4 744-062788	306.5188756	+58.7358845	15.2 (GSC2.3)	0.3495	~0.45	1127.3642954	EW	
63	2MASS 20305052+5547074	307.710540	+55.785416	18.64 (GSC2.3)	?	~2.0	1417.5662968	L	
64	UCAC4 729-067019	307.8310009	+55.7983139	15.56 (GSC2.3)	?	~0.6	1417.5664087	L	
65	UCAC4 731-068791	308.1278424	+56.1299364	14.44	?	~0.4	1417.5664087	L	
66	UCAC4 621-112859	314.4579859	+34.1641767	13.84 (NOMAD)	?	~0.15	1432.5597351	L	(27)
67	UCAC4 617-116284	315.4994471	+33.3210739	14.90 (NOMAD)	?	~0.5	1127.3687558	L	
68	UCAC4 598-126361	317.6277274	+29.4905828	12.48	?	~0.2	1443.4864670	L	
69	UCAC4 621-122572	321.8936342	+34.0494003	12.09	0.43635 (0.438)	~0.1	1445.5736404	EW	(28)
70	UCAC4 590-130214	326.9765700	+27.9013675	12.71	~36	~0.2	1135.4185368	L	(29)

Table continued on following pages

Table 1. Variable stars discovered by APACHE during the first observing season. For stars with two periods indicated, that in parentheses is the one determined from the APACHE data, while the other is estimated from SuperWASP archive data. The amplitudes of the light curves are measured from APACHE data. Time T_0 corresponds to phase=0 in the folded light curves, cont.

No.	*Name*	*R.A. (2000)*	*Dec. (2000)*	*Mag. V*	*Period (days)*	*Amplitude (mag.)*	*T_0 (HJD–2455000)*	*Var. Type*	*Note*
71	UCAC4 590-130270	327.0770353	+27.8228681	12.49	1.02500 (1.025)	~0.25	1127.3844791	EW	(30)
72	UCAC4 652-105561	327.4152459	+40.3802687	14.33	?	~0.35	1443.4839005	L	
73	UCAC4 588-128603	330.1270789	+27.4577517	12.72	4.21221 (1.29)	~0.08	1459.5047071	ROT?	(31)
74	UCAC4 789-036290	330.5805324	+67.6531512	16.00 (GSC2.3)	0.17 (0.34)	~0.15	1127.3607291	DSCT (EW)	(32)
75	UCAC4 788-037466	330.9508409	+67.4961639	14.29 (GSC2.3)	0.47	~0.4	1127.3602622	EA	
76	UCAC4 788-037537	331.1173995	+67.4969889	13.66 (GSC2.3)	?	~0.16	1127.3602622	L	
77	UCAC4 788-037577	331.2463553	+67.5745589	15.62 (GSC2.3)	0.36	~0.25	1127.3607291	EW	
78	UCAC4 726-083454	333.0765986	+55.1851717	14.67	?	~0.18	1127.3607291	L	
79	UCAC4 725-086173	333.2373680	+54.9382473	13.34	0.192835	~0.2	1127.3607291	DSCT?	
80	UCAC4 725-086241	333.2829348	+54.8638348	14.33	0.17234	~0.5	1443.4626241	DSCT?	
81	UCAC4 781-040386	333.4526621	+66.1133137	15.43	1.13	~0.2	1127.3604366	EB	
82	UCAC4 726-084171	333.5242624	+55.0744792	12.13	~50	~0.15	1127.3604366	L	
83	UCAC4 859-013147	343.6693409	+81.7063873	12.72	37	~0.17	1385.653719	L	
84	UCAC4 749-082493	352.8942900	+59.7192198	10.64	0.861	~0.2	1146.4200537	EW	

Table continued on next page

Table 1. Variable stars discovered by APACHE during the first observing season, cont.

Notes: (1) Star 1SWASPJ001046.35+584111.0, 1837 points analyzed. APACHE data are less scattered than those of SWASP. (2) Star 1SWASPJ001050.47+583342.6, SWASP data with high scatter, 1969 of 2015 data analyzed (applying a 1-sigma clipping to the original data). (3) Eclipsing binary already known in VSX (Mis V1368) but the orbital period was not reported. (4) The light curve is discussed separately in Figure 2. No SWASP data available for this star. (5) Only the primary minimum detected. (6) Star 1SWASPJ052950.48+315439.8, 7033 of 7110 data points from SWASP analyzed (applying a 3-sigma clipping to the original data). The secondary minimum appears deeper in the light curve from the APACHE survey. Refer to Figure 3 for a comparison between SWASP and APACHE light curves. (7) Star 1SWASPJ060809.97+334016.5, 6223 of 6282 data points from SWASP analyzed (applying a 3-sigma clipping to the original data). The existence of a secondary minimum can be guessed from the APACHE light curve, while is not visible in SWASP data (not shown here). (8) Tentative period, but the phase coverage does not make possible a reliable estimation. (9) Star 1SWASPJ070307.60+344203.60, 4066 of 4305 data points analyzed (applying a 2-sigma clipping to the original data). Even with few data points, this faint star appears to be an eclipsing binary system in the APACHE photometry. From data in the SWASP public archive we derive the best period P=0.21635 days, that in this case we adopted for folding our data because is a far better estimate than that from APACHE data. This star is discussed separately in section 4. (10) Star 1SWASPJ070342.10+525256.8, noisy light curve, 1094 of 1258 data points from SWASP analyzed (applying a 1-sigma clipping to the original data). (11) Star 1SWASPJ115757.51+423945.5, 5509 data points analyzed. From APACHE photometry alone, because the data are few, we could only guess that the star has a short period (<1 day), but a reliable determination was not possible. SWASP photometry helped us in classifying the star's variability and estimating a reliable period. We show part of the APACHE light curve and the SWASP data in Figure 5. (12) Star 1SWASPJ135233.09+314113.8, 7348 of 7425 data points analyzed (applying a 3-sigma clipping to the original data). (13) Star 1SWASPJ152845.99+430530.1, 5387 of 5428 data points analyzed (applying a 3-sigma clipping to the original data). Spotted star. Color indexes B–V = 0.98, V–J = 1.78, V–K = 2.39. Tentantive spectral classification: dK3/dK4. (14) Appears in Kopacki et al. (2003). V from Sandquist et al. (2010). (15) Appears in Kopacki et al. (2003). (16) Star 1SWASPJ185523.32+542551.4, 11972 of 12016 data points analyzed (applying a 3-sigma clipping to the original data). (17) Observations in V band. Color indexes: B–V = 0.95, V–J = 1.7, V–K = 2.33. (18) In on-line archive images it appears as a blended object. Faint, no V available. (19) Faint object in on-line archive images. (20) Star 1SWASP192317.5+553936.2, 12861 of 12919 data points analyzed (applying a 3-sigma clipping to the original data). Results for this star are discussed separately in section 4. (21) Star 1SWASPJ192358.37+553316.9, 12469 of 12596 data points analyzed (applying a 3-sigma clipping to the original data). (22) Star 1SWASPJ192555.70+5530002.9, 12934 photometric points used in the analysis. (23) Undefined type of pulsating star. Modulation possibly due to rotation. We provide a more conservative uncertainty than that calculated as 1/timespan. (24) Star listed in the International Variable Star Index (NSVS J2012124+341522) and classified as L. The reported periodicity of 88 days is not found in our data that clearly show that the possible period should be longer. (25) Star 1SWASPJ202533.73+583913.9, 10637 of 10721 data points analyzed (applying a 3-sigma clipping to the original data). Because of its uncertain classification, this star is discussed separately in section 4. (26) Star 1SWASPJ202538.05+584537.4, 10485 of 10550 data points analyzed (applying a 3-sigma clipping to the original data). The primary minimum is not well sampled in the APACHE light curve. (27) Star listed in the International Variable Star Index (NSV 25408) and classified as an eclipsing binary, but without an estimate of the orbital period. No evidence for eclipses is present in the APACHE data. Rather, the star appears as an irregular variable. Thus we propose a change of variability status for this star. (28) Star 1SWASPJ212734.47+340257.9, 14781 of 14872 data points analyzed (applying a 3-sigma clipping to the original data). (29) Long periodicity, assumed tentatively nearly equal to 36 days by looking at the light curve. (30) Star 1SWASPJ214818.48+274922.0, 14086 of 14151 data points analyzed (applying a 3-sigma clipping to the original data). (31) Star 1SWASPJ220030.52+272728.8, 21352 of 21499 data points analyzed (applying a 3-sigma clipping to the original data). This star is discussed in detail in section 4. Even if the classification remains uncertain, based on SWASP data we suggest this could be a rotating star. (32) Difficult classification, faint star/noisy light curve. We propose two possibilities, with corresponding periodicities.

circumstance, we propose these stars to be classified as a variable of L type. The remainder of our list is composed of periodic variables, mostly eclipsing binary systems and some pulsators, with a classification not always clear. To improve the period estimation and to provide a less ambiguous classification where required, we used the SuperWASP public archive—a precious treasure trove now hosted by the NASA Exoplanet Archive (http://exoplanetarchive.ipac.caltech.edu/index.html)—to recover the light curves of our stars. Nearly 25% of the stars in our sample have thousands of useful SWASP photometric data points that can complement the APACHE dataset with high profit. We performed a L-S analysis to the data from the SWASP survey, specifically using the magnitudes de-trended with the SysRem algorithm (Tamuz *et al.* 2005). In Table 1 we report out of parentheses the best period found from the SWASP data (when available) which usually, because the time span and number of data are greater, can be indicated with a number of significant digits higher than for the period derived from APACHE timeseries (reported in parentheses). In a few cases, we report only the period found from SWASP data, which has been used to obtain the plot in Figure 1. The position of the last significant decimal digit, both for SWASP and APACHE data, is determined in the following way. We start by folding the light curve using the best period found by the L-S algorithm. Then, after removing the last decimal digit, we fold the data with this truncated period and, by visual inspection, we look at any change in the new phased light curve. If no change is evident, this means that the removed digit is not significant, and we reiterate the process by removing the second to last digit, and so on. When a change in the folded light curve is seen, this means that the removed digit is significant and the process comes to an end.

4. Discussion of individual variables

A small subset of variables deserves closer investigation.

4.1. UCAC4 872-000839

The star UCAC4 872-000839 (the first non-numbered object in Table 1) showed in the APACHE photometry and on nightly basis a variability similar to that of a pulsating star that we could not characterize with a well defined period. Figure 2 shows a sample of APACHE light curves of this star collected during single nights. Unfortunately this star is not present in the SWASP archive.

4.2. UCAC4 624-036803

The quite faint star UCAC4 624-036803 (Number 13 in Table 1) appears as an eclipsing binary system already in the APACHE data, and we obtained the best estimate for the orbital period P = 0.21635 day from SWASP data. This value is just below the lower limit of ~ 0.22 day for such systems discussed in Norton *et al.* (2011). This circumstance makes that star an interesting object for

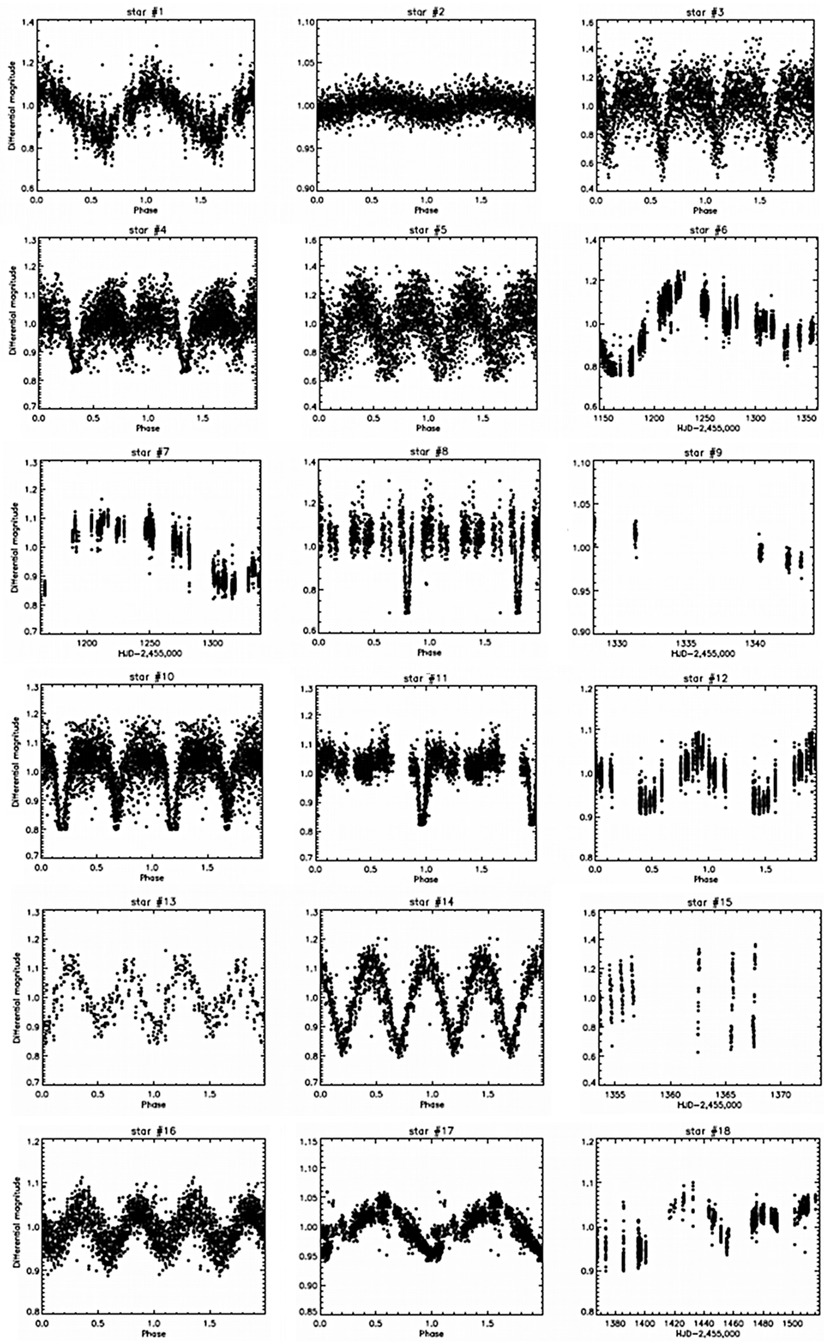

Figure 1. Light curves of the new variables listed in Table 1. They were found during the first observing season of the APACHE survey (figure continued on following pages).

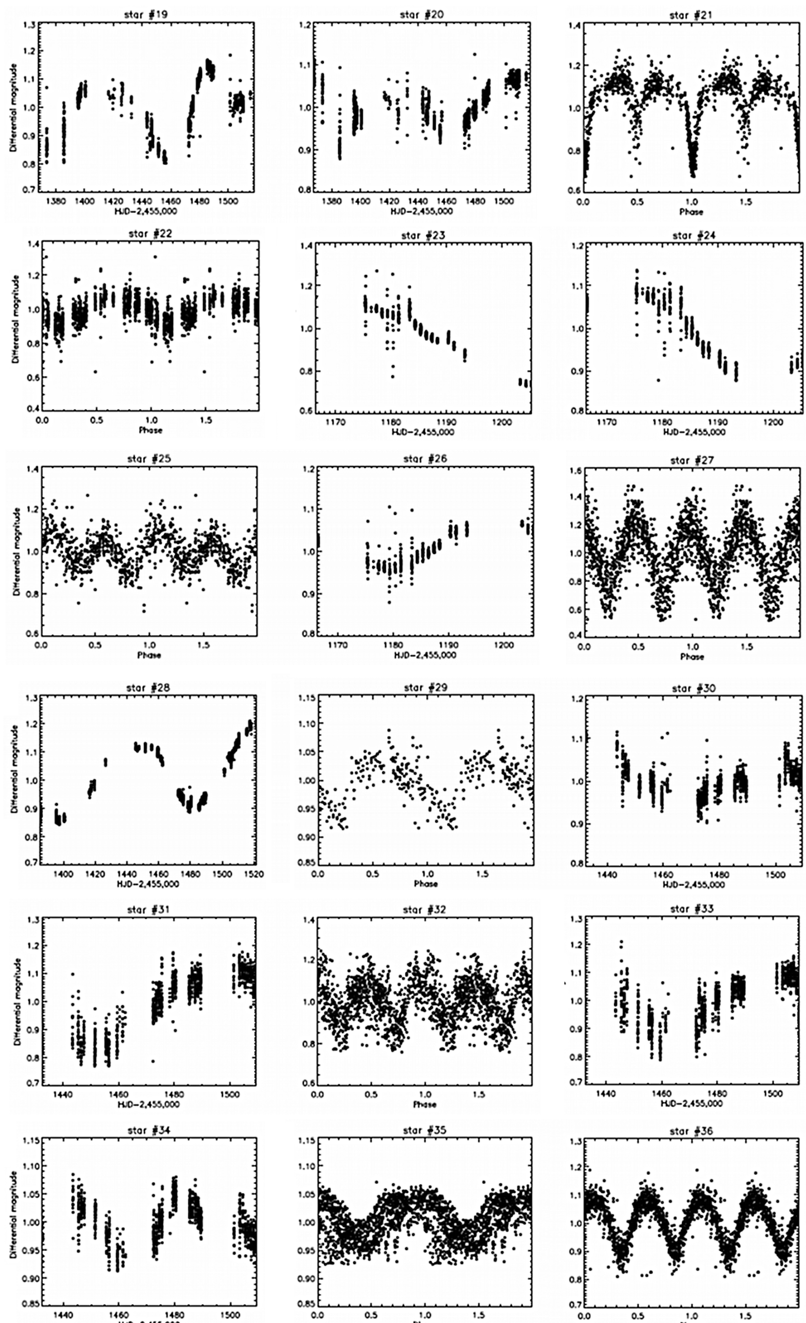

Figure 1. Light curves of the new variables listed in Table 1, continued.

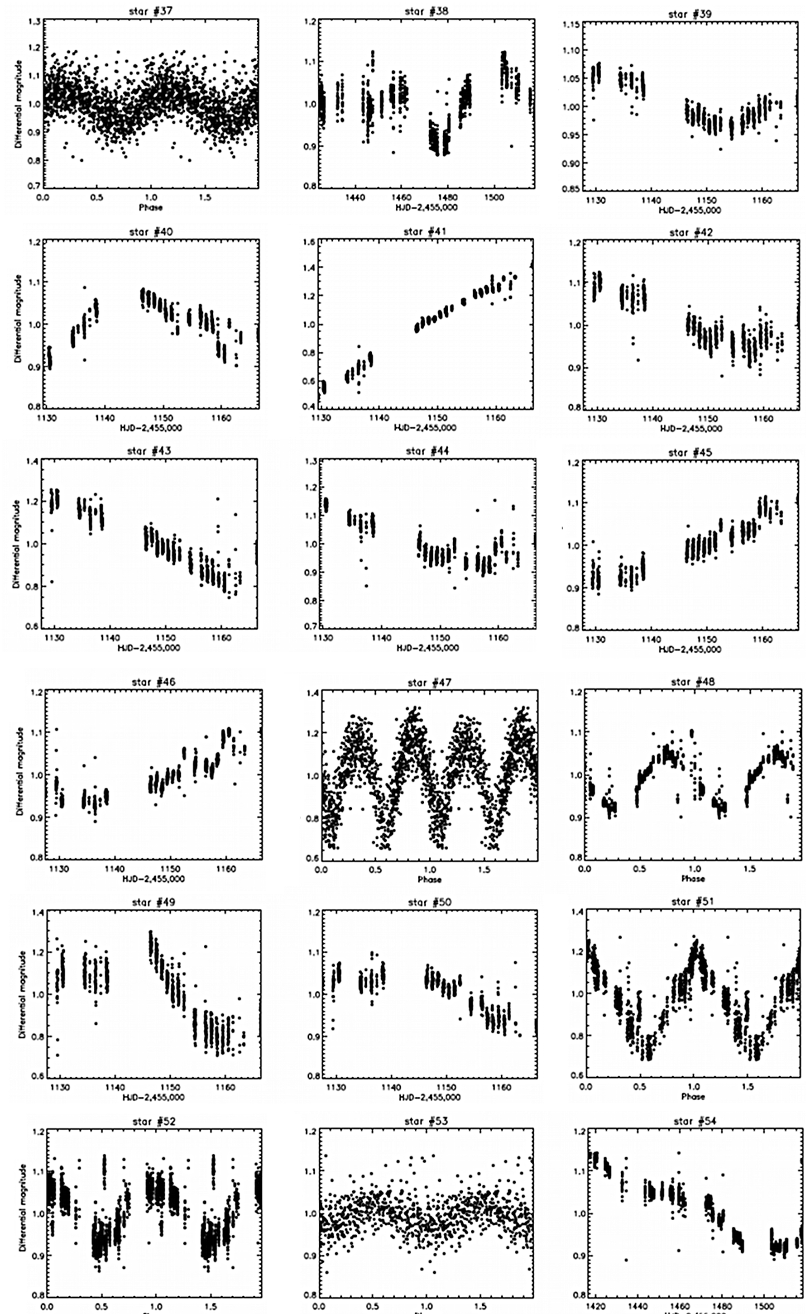

Figure 1. Light curves of the new variables listed in Table 1, continued.

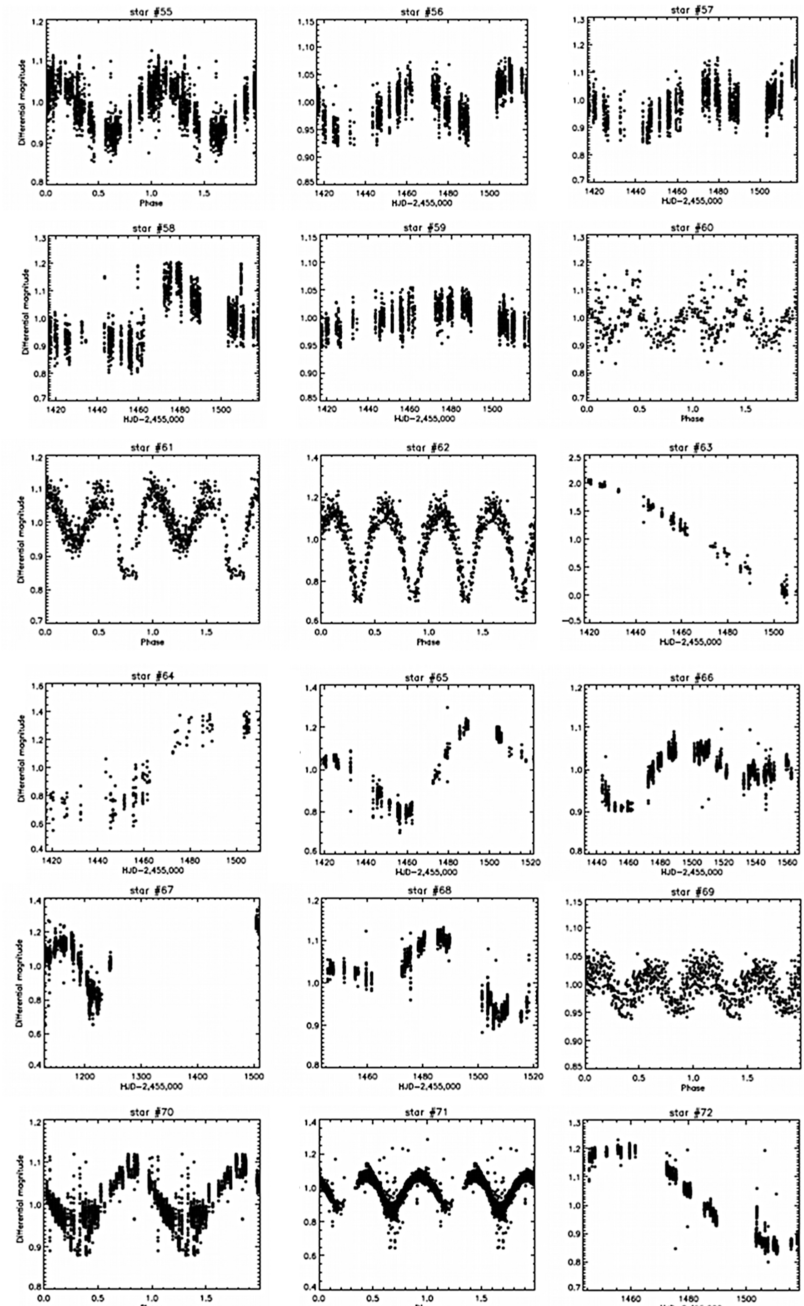

Figure 1. Light curves of the new variables listed in Table 1, continued.

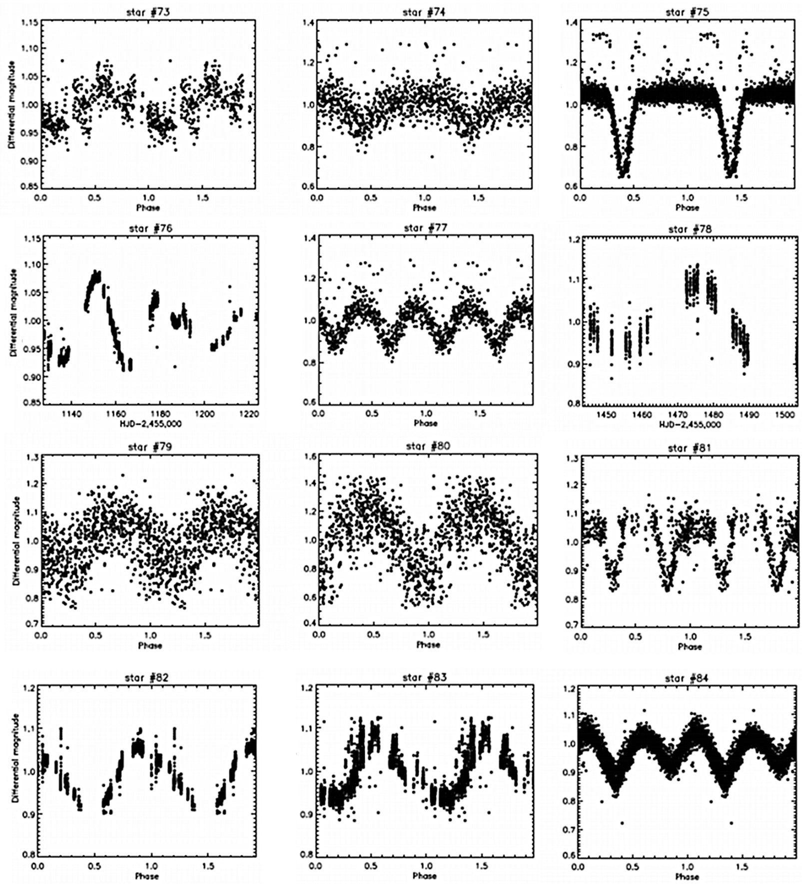

Figure 1. Light curves of the new variables listed in Table 1, continued.

follow-up studies, as we have done for a similar variable (Damasso *et al.* 2012). The highest peak in the L-S periodogram of SWASP data is P = 0.108176 day, which we have doubled to get the most reliable periodicity. The folded SWASP light curve and the corresponding L-S periodogram in the region of interest are shown in Figure 4, while data from the APACHE survey are shown in Figure 1, folded according to the best period found from SWASP photometry.

4.3. UCAC4 664-056989

In the first plot of Figure 5, data for six nights are shown for the star UCAC4 664-056989 (Number 15 in Table 1). It has been observed by APACHE only for a few epochs, and it was not possible to determine a reliable periodicity. By looking at the single-night light curves it can be guessed that the star should be an RR Lyrae-type variable, but a clear classification is not possible. Luckily,

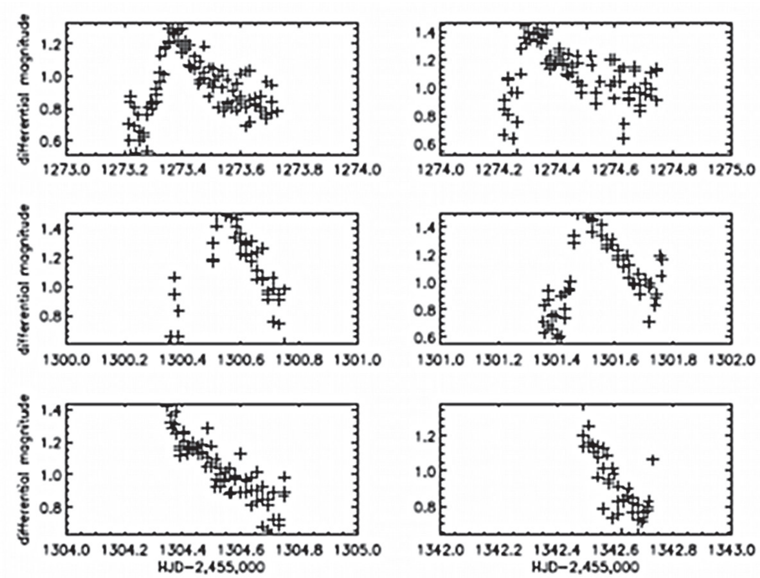

Figure 2. Sample of APACHE light curves of the star UCAC4 872-000839 obtained during six observing nights. Looking at the characteristics of the flux variations, the star can be tentatively and generically classified as a pulsating variable, but lacking a reliable determination of the periodicity. No data from the SWASP archive are available.

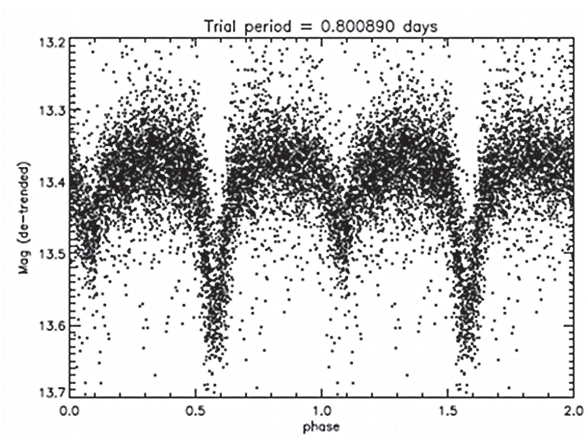

Figure 3. Light curve of the star UCAC4 610-021265 (Number 10 in Table 1) obtained with data from the WASP survey and folded according to the best period found P = 0.80089 day. By comparing this plot with that in Figure 1, it can be seen that the secondary minimum appears deeper in the APACHE data, obtained using an I_c filter. See Note 6 in Table 1.

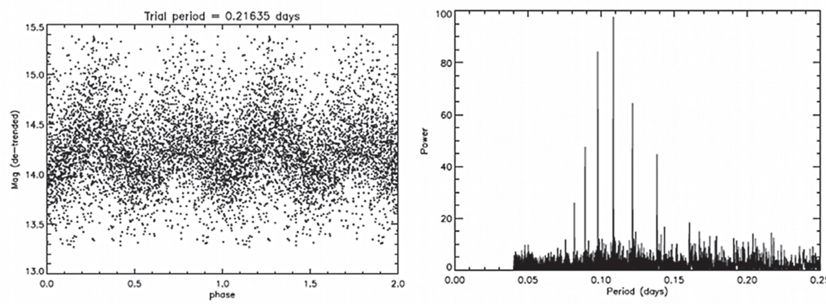

Figure 4. Left: light curve of the star UCAC4 624-036803 (SWASP J070307.60+344203.60; Number 13 in Table 1) obtained from data of the SuperWASP survey. Data are folded according to double the period with the highest peak in the Lomb-Scargle periodogram and rounded to the last significant digit. Right: the Lomb-Scargle periodgram in the range of periods of interest.

this star has been observed by SWASP (1SWASPJ115757.51+423945.5), and we can quite safely propose classification as an RRab variable by looking at the SWASP light curve characteristics.

4.4. UCAC4 729-060138

The star UCAC4 729-060138 (Number 35 in Table 1) has B–V $\simeq$1.0 according to the APASS photometry, and the dust reddening in the star's direction is estimated to be E(B–V) = 0.1 (Schlafly and Finkbeiner 2011), thus suggesting that, assuming the star is a dwarf, it should be a late G to early K type. We propose that this variable should be classified as a rotator. Folding the APACHE data with the best period found (0.688 day) results in a light curve quite scattered in regard to the maximum, maybe indicating a change in amplitude that could be attributed to evolving active regions on the stellar surface. This star is also present in the SWASP database and a L-S analysis resulted in the best period of 0.6902 day. The corresponding folded light curve is showed in Figure 6. The curve from SWASP does not show the kind of amplitude scatter present in the APACHE data.

4.5. UCAC4 744-062741

The star UCAC4 744-062741 (second non-numbered object in Table 1) shows a clear (and with a complicated pattern) variability which was not possible to classify from APACHE photometry alone (first plot in Figure 7). The number of our data is not sufficient to clearly understand whether this is an eclipsing binary system or, generally speaking, a pulsating variable. The analysis of the SWASP light curve results in the most probable period P = 1.5174 days, according to both the L-S and BLS algorithms (Kovács *et al.* 2002), and we show the folded data in the second panel of Figure 7. The analysis of the APACHE data, less numerous than those of SWASP, with the L-S algorithm reveals that the greatest power in the periodogram occurs at P = 1.51 days (third

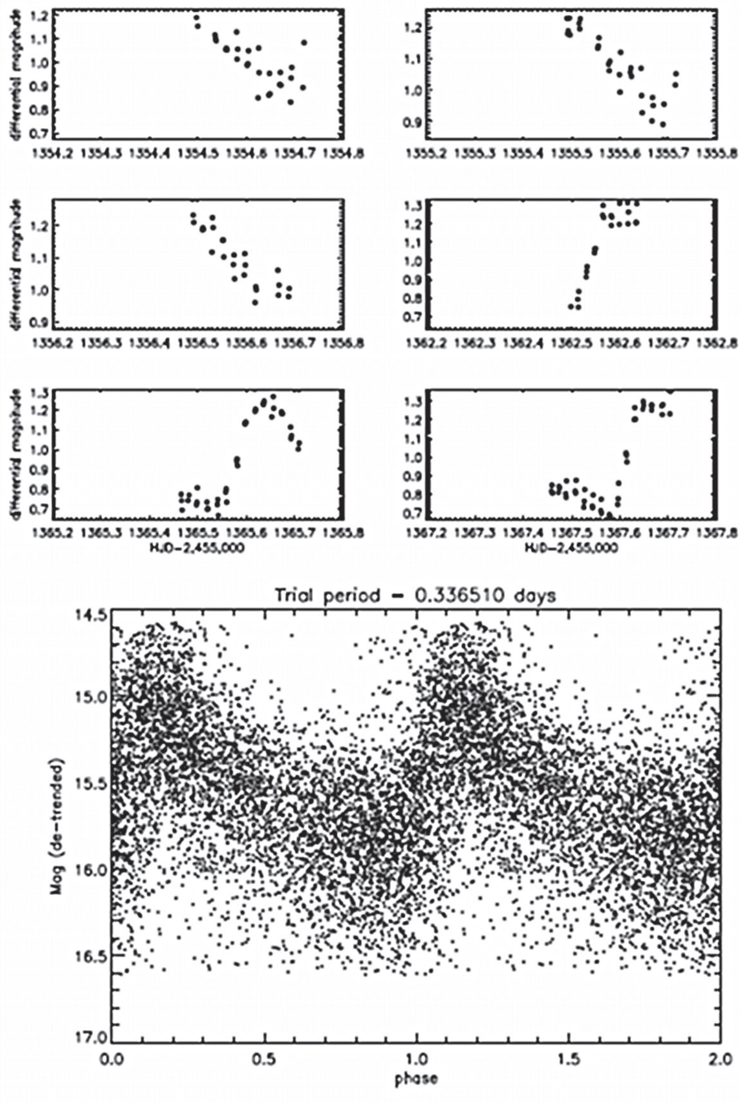

Figure 5. Top: sample of APACHE light curves of the star UCAC4 664-056989 obtained during six observing nights. Looking at the characteristics of the flux variations, the star can be tentatively and generically classified as an RRab variable, but lacking a reliable determination of the periodicity. Bottom: the real nature of this variable is unveiled, and a reliable period estimation made possible, thanks to the data in the SuperWASP archive, shown here. The star indeed appears to be an RRab variable.

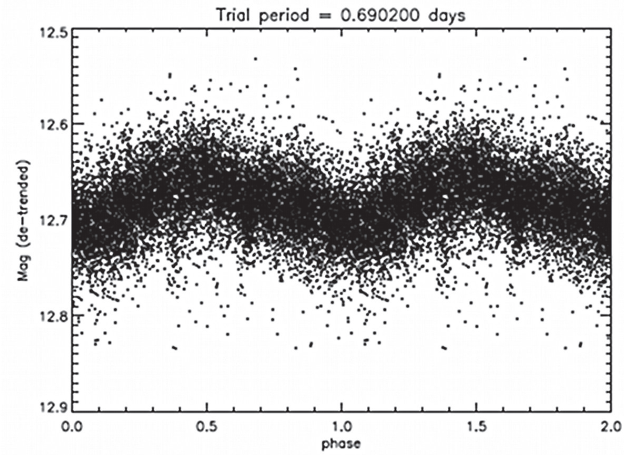

Figure 6. Light curve of the star UCAC4 729-060138 obtained with data from the WASP survey and folded according to the best period found P = 0.6902 day.

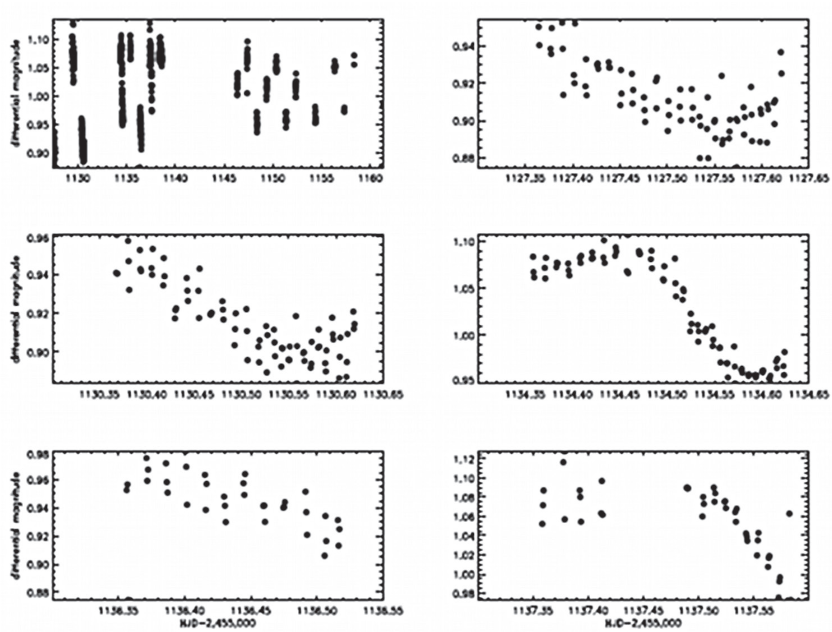

Figure 7. First plot (six panels): sample of APACHE light curves of the star UCAC4 744-062741. The upper left plot shows the light curve during the whole timespan of observations. The other plots show the light curves obtained during five different nights. They correspond to the 1st, 3rd, 4th, 6th, and 7th sub-intervals of the first plot. From our data alone we cannot conclude anything about the variability type of this star. Figure continued on next page.

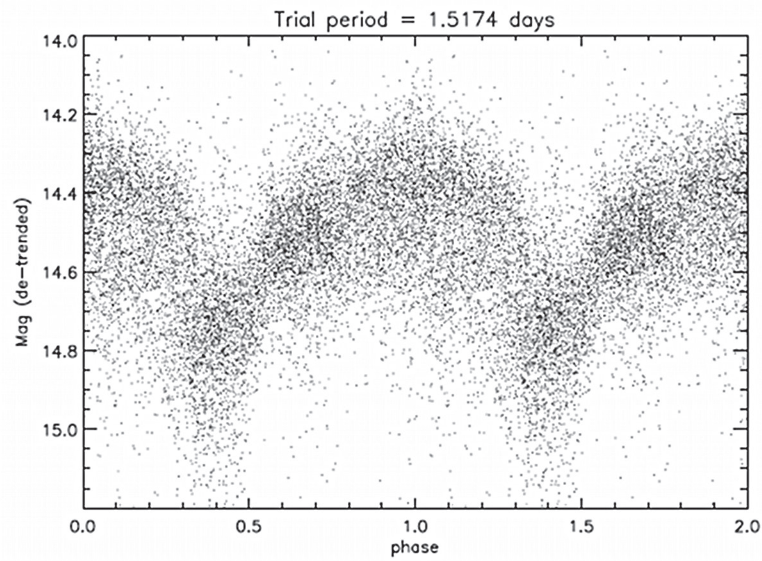

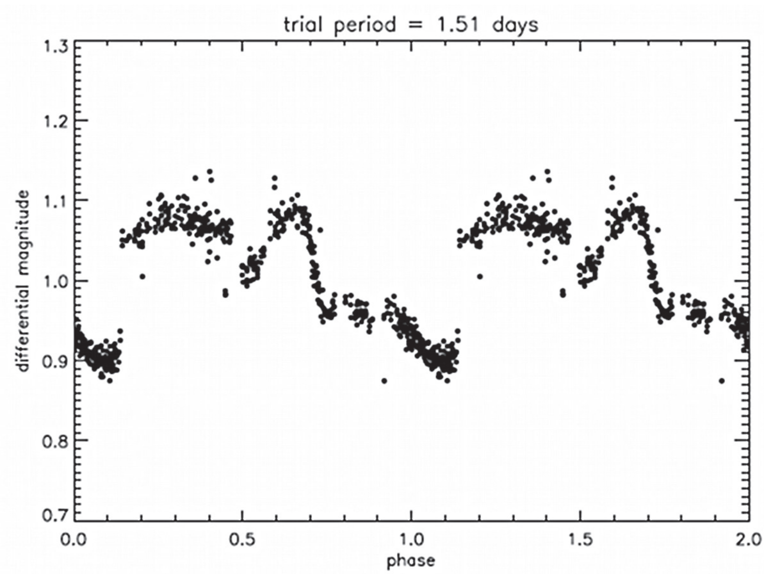

Figure 7 (continued). Second panel: light curve obtained from data of the WASP survey and folded according to the best period P = 1.5174 days found after a Lomb-Scargle analysis. Third panel: light curve from APACHE folded according to the best period P = 1.5 days found after a Lomb-Scargle analysis.

panel of Figure 7). Although the shape of both folded light curves does not allow an immediate explanation, the fact that in effect the same periodicity is obtained from both the datasets would lean towards the interpretation as a modulation due active regions/spots on the stellar surface, and the period of 1.5 days should be considered as the rotation period of the star. Under this hypothesis, the light curve from APACHE, although less sampled, shows less scatter than that from SWASP, and can be useful for observing the details of the flux variations due to features on the stellar atmosphere.

4.6. UCAC4 588-128603

The last object we discuss here is the star UCAC4 588-128603 (Number 73 in Table 1). This star is also included in the SWASP archive. The period analysis of both APACHE and SWASP data results in similar results, but with different significance. We show in Table 2 the first significant periods found by the L-S algorithm applied to the two datasets, in order of their significance. While in Figure 1 (star #73) we show the APACHE data folded according to the period P = 1.29 days (which is the fourth in order of significance found in the SWASP data), in Figure 8 (second and fourth plots) we show the APACHE data folded according to the first and second significant periods estimated from the SWASP data, which could be more reliable due to the high number of SWASP data points. The first and third panels in Figure 8 are the corresponding folded light curves of SWASP. It can be seen that both these APACHE light curves show and interesting modulation that can be related to a particular variability type. In the first case, we should be possibly looking at a rotating star, while if the real period is ~0.8 day this would lean towards a pulsating star (RRc type?). In absence of other information, a defintive conclusion cannot be drawn.

Table 2. Most significant periods found for the star UCAC4 588-128603 by applying the Lomb-Scargle algorithm to the SWASP and APACHE data. The periods are listed in order of decreasing spectral power. Despite the different number of data points from the two surveys, similar periods are retrieved in both datasets, but not in the same order. Values are rounded to the last significant digit.

Lomb-Scargle periods (SWASP) (days)	*Lomb-Scargle periods (APACHE) (days)*
4.21221	1.29
0.80635	4.01
4.16551	0.81
1.30667	0.44
4.26001	—
0.44585	—

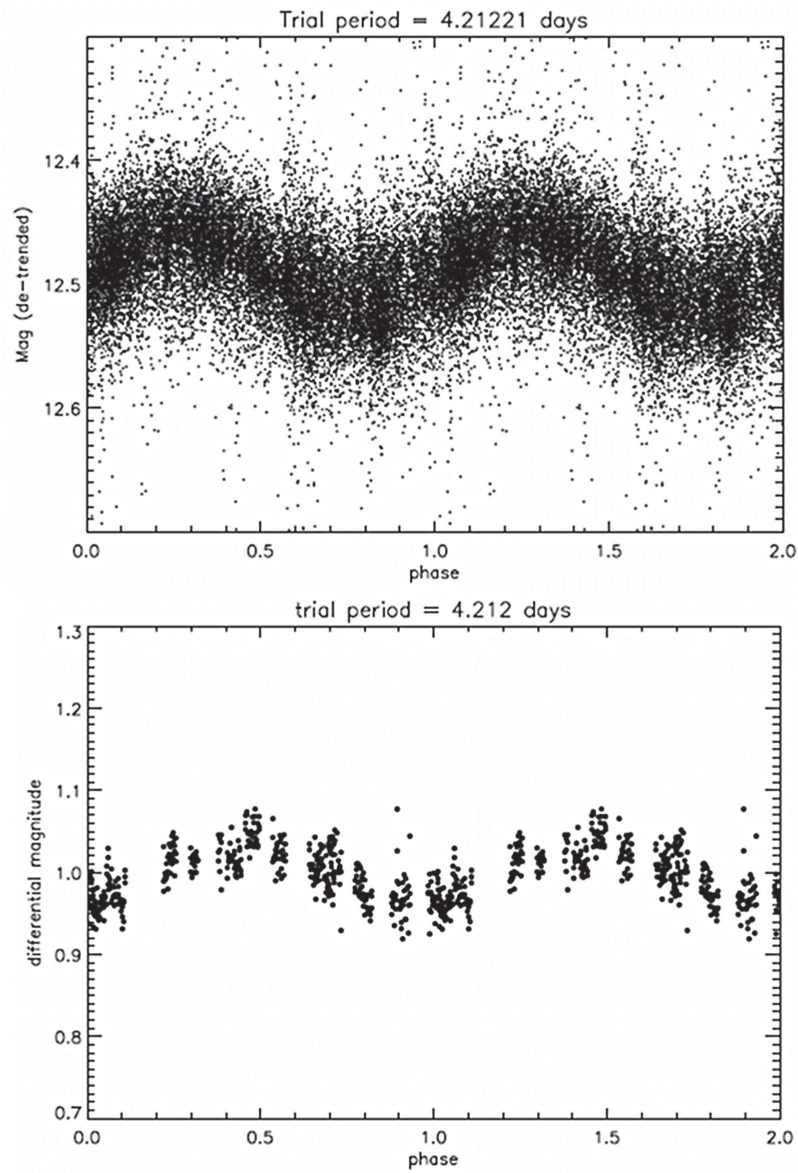

Figure 8. Photometry of the star UCAC4 588-128603 1st and 2nd panels: light curves of SWASP and APACHE surveys, respectively, folded according to the best period P = 4.21221 days found by applying the Lomb-Scargle algorithm to the SWASP time-series. Figure continued on next page.

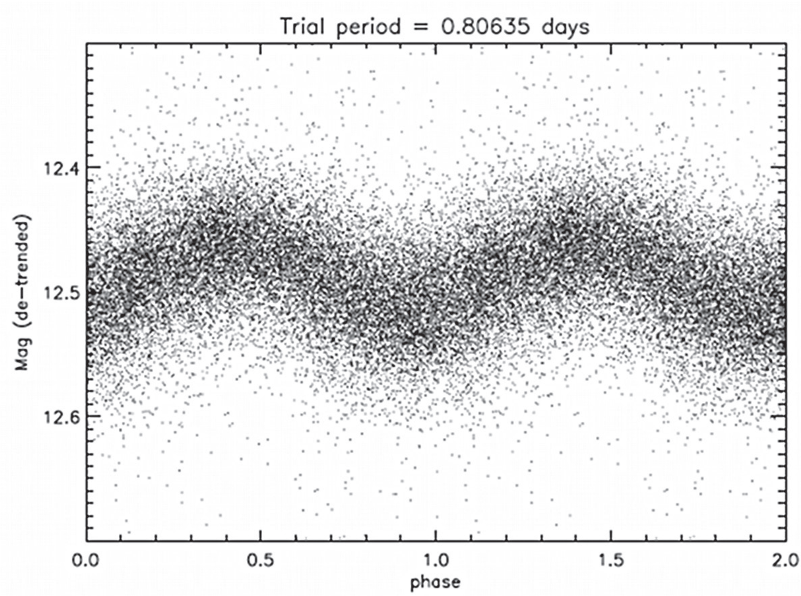

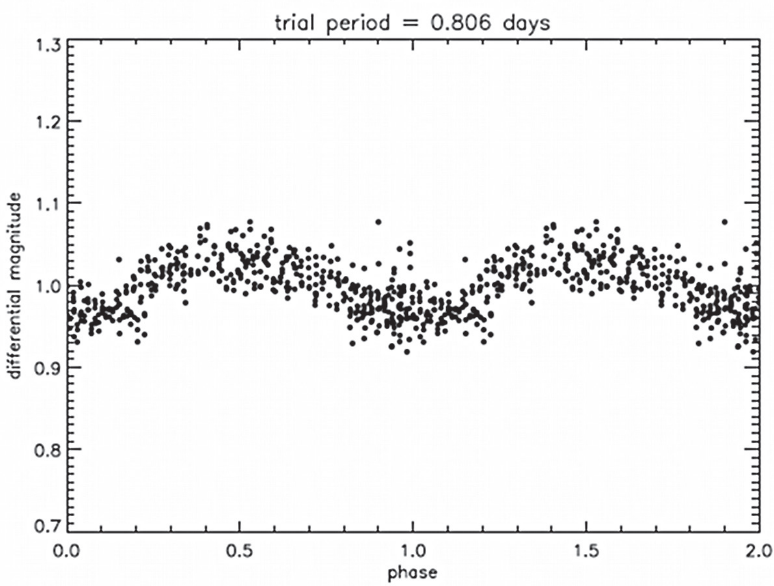

Figure 8 (continued). 3rd and 4th panels: light curves of SWASP and APACHE surveys, respectively, folded according to the second significant period P = 0.80635 day found by applying the Lomb-Scargle algorithm to the WASP time-series.

5. Acknowledgements

We acknowledge the anonymous referee for helpful comments. MD acknowledges the European Union, the Autonomous Region of the Aosta Valley and the Italian Department for Work, Health and Pensions for the grants provided during the first three years of Ph.D. study, and the INAF and ASI for providing the grant for the year 2013 under contract I/058/10/0 (Gaia Mission—The Italian Participation to DPAC).This work made use of the International Variable Star Index (VSX) database, operated at AAVSO (Cambridge, Massachusetts); data from the SuperWASP Public Archive; and the VizieR catalogue access tool (Ochsenbein *et al.* 2000), CDS, Strasbourg, France.

References

Damasso, M., Cenadelli, D., Calcidese, P., Borsato, L., Granata, V., and Nascimbeni, V. 2012, *J. Amer. Assoc. Var. Star Obs.*, **40**, 945.

Kopacki, G., Kołaczkowski, Z., and Pigulski, A. 2003, *Astron. Astrophys.*, **398**, 541.

Kovács, G., Zucker, S., and Mazeh, T. 2002, *Astron. Astrophys.*, **391**, 369.

Lépine, S., and Gaidos, E. 2011, *Astron. J.*, **142**, 138.

Norton, A. J., *et al.* 2011, *Astron. Astrophys.*, **528A**, 90.

Ochsenbein, F., Bauer, P., and Marcout, J. 2000, *Astron. Astrophys., Suppl. Ser.* **143**, 23.

Sandquist, E. L., Gordon, M., Levine, D., and Bolte, M. 2010, *Astron. J.*, **139**, 2374.

Schlafly, E. F., and Finkbeiner, D. P. 2011, *Astrophys. J.*, **737**, 103.

Sozzetti, A., *et al.* 2013, in *Hot Planets and Cool Stars*, ed. R. Saglia, EPJ Web of Conferences 47, id. 03006 (http://publications.edpsciences.org/).

Tamuz, O., Mazeh, T., and Zucker, S. 2005, *Mon. Not. Roy. Astron. Soc.*, **356**, 1466.

Zacharias, N., Finch, C., Girard, T., Henden, A., Bartlett, J., Monet, D., and Zacharias, M. 2012, *The Fourth US Naval Observatory CCD Astrograph Catalog* (UCAC4; http://arxiv.org/abs/1212.6182).

Recent Maxima of 75 Short Period Pulsating Stars

Gerard Samolyk
PO Box 20677; Greenfield WI 53220; gsamolyk@wi.rr.com

Received January 6, 2014; accepted January 6, 2014

Abstract This paper contains times of maxima for 75 short period pulsating stars (primarily RR Lyrae and δ Scuti stars). This represents the CCD observations received by the AAVSO SPP section in 2013.

1. Recent observations

This accompanying list contains times of maxima calculated from CCD observations made by participants in the AAVSO's Short Period Pulsator (SPP) Section. This list will be web-archived and made available through the AAVSO ftp site at ftp:ftp.aavso.org/public/datasets/gsamoj421.txt. The error estimate is included. RR Lyr stars in this list, along with data from earlier AAVSO publications, are included in the GEOS database at: http://rr-lyr.irap.omp.eu/dbrr/dbrr-V1.0_0.php. This database does not include δ Scuti stars. Most of these observations were reduced by the writer or using the PERANSO program (Vanmunster 2007). Pierre de Ponthiére supplied some additional times of maxima. Column F indicates the filter used; "SG" indicates Sloan g.

The linear elements in the *General Catalogue of Variable Stars* (GCVS; Kholopov *et al.* 1985) were used to compute the O–C values for most stars. For a few exceptions where the GCVS elements are missing or are in significant error, light elements from another source are used: RZ Cap (Samolyk 2010), V421 Her (Drake *et al.*, 2013), and GW UMa (Hintz *et al.*, 2001).

References

Drake A. J. *et al.* 2013, *Astrophys. J.*, **763** 32.

de Ponthiére, P. 2013, private communication.

Hintz, E. G., Bush, T. C., and Rose, M. B. 2005, *Astron. J.*, **130**, 2876.

Kholopov, P. N., *et al.* 1985, *General Catalogue of Variable Stars*, 4th ed., Moscow.

Samolyk, G. 2010, *J. Amer. Assoc. Var. Star Obs.*, **38**, 12.

Vanmunster, T. 2007, PERANSO period analysis software (http://www.peranso.com).

Table 1. Recent times of maxima of stars in the AAVSO Short Period Pulsator program.

Star	JD(max) Hel. 2400000 +	Cycle	O–C	F	Observer	Error
SW And	56525.7686	86808	–0.4177	V	K. Menzies	0.0006
SW And	56532.8557	86824	–0.4071	V	R. Sabo	0.0026
SW And	56563.8024	86894	–0.4199	V	K. Menzies	0.0007
SW And	56563.8057	86894	–0.4166	V	G. Samolyk	0.0012
SW And	56575.7456	86921	–0.4183	V	G. Samolyk	0.0013
SW And	56582.3771	86936	–0.4210	V	T. Arranz	0.0007
SW And	56587.6869	86948	–0.4185	V	R. Sabo	0.0014
SW And	56587.6870	86948	–0.4184	B	R. Sabo	0.0013
SW And	56593.4334	86961	–0.4217	V	T. Arranz	0.0008
SW And	56597.4121	86970	–0.4235	V	T. Arranz	0.0007
SW And	56609.3553	86997	–0.4218	V	T. Arranz	0.0007
SW And	56616.4328	87013	–0.4208	V	T. Arranz	0.0011
SW And	56617.3165	87015	–0.4217	V	T. Arranz	0.0007
SW And	56619.5272	87020	–0.4224	V	G. Samolyk	0.0011
SW And	56620.4127	87022	–0.4214	V	T. Arranz	0.0006
SW And	56621.2989	87024	–0.4198	V	T. Arranz	0.0008
SW And	56623.5049	87029	–0.4252	V	T. Arranz	0.0004
SW And	56624.3929	87031	–0.4217	V	T. Arranz	0.0008
SW And	56625.2770	87033	–0.4222	V	T. Arranz	0.0007
SW And	56627.4893	87038	–0.4213	V	T. Arranz	0.0007
SW And	56628.3697	87040	–0.4255	V	T. Arranz	0.0005
SW And	56629.2580	87042	–0.4217	V	T. Arranz	0.0012
SW And	56631.4705	87047	–0.4206	V	T. Arranz	0.0013
SW And	56635.4479	87056	–0.4237	V	T. Arranz	0.0007
SW And	56636.3326	87058	–0.4236	V	T. Arranz	0.0006
SW And	56643.4065	87074	–0.4262	V	T. Arranz	0.0013
XX And	56539.8719	24147	0.2595	V	G. Samolyk	0.0015
XX And	56552.8786	24165	0.2568	V	G. Samolyk	0.0015
XX And	56568.7825	24187	0.2602	V	K. Menzies	0.0009
ZZ And	56493.8806	57103	0.0266	V	R. Sabo	0.0017
ZZ And	56589.8160	57276	0.0278	V	R. Sabo	0.0017
ZZ And	56589.8163	57276	0.0282	I	R. Sabo	0.0034
AT And	56489.8793	22931	–0.0133	V	R. Sabo	0.0025
AT And	56539.8589	23012	–0.0038	V	G. Samolyk	0.0021
AT And	56549.7300	23028	–0.0034	V	G. Samolyk	0.0021
AT And	56567.6170	23057	–0.0069	V	G. Samolyk	0.0020
DM And	55865.3621	31961	0.0683	V	P. de Ponthiére	0.0037
DM And	55875.4443	31977	0.0642	V	P. de Ponthiére	0.0063

Table continued on following pages

Table 1. Recent times of maxima of stars in the AAVSO Short Period Pulsator program, cont.

Star	*JD(max) Hel. 2400000 +*	*Cycle*	*O–C*	*F*	*Observer*	*Error*
DM And	56521.5951	33002	0.0663	V	K. Menzies	0.0022
DM And	56586.5290	33105	0.0702	V	K. Menzies	0.0012
DY And	56315.5307	33515	0.0047	V	K. Menzies	0.0012
GM And	55837.5116	42725	0.0447	V	P. de Ponthiére	0.0035
GM And	55856.5940	42752	0.0446	V	P. de Ponthiére	0.0120
GM And	55886.2794	42794	0.0462	V	P. de Ponthiére	0.0036
GM And	55888.3975	42797	0.0440	V	P. de Ponthiére	0.0021
SW Aqr	56449.8691	68261	–0.0024	V	R. Sabo	0.0009
SW Aqr	56570.6654	68524	–0.0028	V	R. Sabo	0.0009
TZ Aqr	56565.6797	33293	0.0079	V	G. Samolyk	0.0014
YZ Aqr	56610.5659	38494	0.0703	V	G. Samolyk	0.0015
AA Aqr	56609.6308	58896	–0.1455	V	G. Samolyk	0.0018
BO Aqr	56620.5731	21612	0.1911	V	G. Samolyk	0.0019
BR Aqr	56575.7809	39304	–0.1907	V	G. Samolyk	0.0013
CY Aqr	56571.4471	364738	0.0180	V	T. Arranz	0.0002
CY Aqr	56579.5609	364871	0.0137	V	G. Samolyk	0.0007
CY Aqr	56579.6214	364872	0.0132	V	G. Samolyk	0.0008
CY Aqr	56579.6830	364873	0.0138	V	G. Samolyk	0.0007
CY Aqr	56579.7441	364874	0.0138	V	G. Samolyk	0.0007
CY Aqr	56579.8045	364875	0.0132	V	G. Samolyk	0.0004
CY Aqr	56593.5391	365100	0.0142	V	G. Samolyk	0.0006
CY Aqr	56593.5997	365101	0.0137	V	G. Samolyk	0.0004
CY Aqr	56593.6605	365102	0.0135	V	G. Samolyk	0.0006
CY Aqr	56603.6092	365265	0.0130	V	G. Samolyk	0.0004
CY Aqr	56603.6708	365266	0.0134	V	G. Samolyk	0.0004
TZ Aur	56572.9815	93625	0.0133	V	R. Sabo	0.0009
TZ Aur	56603.9264	93704	0.0159	V	G. Samolyk	0.0008
TZ Aur	56655.6262	93836	0.0146	V	G. Samolyk	0.0009
BH Aur	56552.9237	30260	0.0044	V	R. Sabo	0.0022
BH Aur	56563.8689	30284	0.0034	V	N. Simmons	0.0011
BH Aur	56563.8694	30284	0.0039	V	G. Samolyk	0.0013
BH Aur	56574.8173	30308	0.0056	V	G. Samolyk	0.0019
BH Aur	56588.9551	30339	0.0047	V	R. Sabo	0.0013
BH Aur	56588.9556	30339	0.0052	I	R. Sabo	0.0018
BH Aur	56619.9689	30407	0.0044	V	R. Sabo	0.0010
BH Aur	56643.6862	30459	0.0050	V	K. Menzies	0.0013
RS Boo	56376.9058	38709	0.0020	V	R. Sabo	0.0008
RS Boo	56409.7314	38796	–0.0009	V	R. Sabo	0.0009

Table continued on following pages

Table 1. Recent times of maxima of stars in the AAVSO Short Period Pulsator program, cont.

Star	*JD(max) Hel. 2400000 +*	*Cycle*	*O–C*	*F*	*Observer*	*Error*
RS Boo	56449.7265	38902	–0.0037	V	R. Sabo	0.0010
ST Boo	56447.4606	59885	0.0968	V	T. Arranz	0.0014
ST Boo	56457.4216	59901	0.1012	V	T. Arranz	0.0010
ST Boo	56474.8294	59929	0.0848	V	R. Sabo	0.0015
ST Boo	56480.4408	59938	0.0956	V	T. Arranz	0.0012
ST Boo	56490.4029	59954	0.1011	V	T. Arranz	0.0015
ST Boo	56503.4698	59975	0.0998	V	T. Arranz	0.0009
ST Boo	56513.4286	59991	0.1020	V	T. Arranz	0.0011
ST Boo	56518.4107	59999	0.1058	V	T. Arranz	0.0011
ST Boo	56523.3934	60007	0.1101	V	T. Arranz	0.0009
SW Boo	56339.8722	26812	0.3968	V	R. Sabo	0.0012
SW Boo	56361.9526	26855	0.3955	V	R. Sabo	0.0011
SW Boo	56378.9013	26888	0.3977	V	R. Sabo	0.0015
SW Boo	56444.6357	27016	0.4006	V	K. Menzies	0.0011
SZ Boo	56437.6815	55081	0.0131	V	G. Samolyk	0.0026
TV Boo	56356.8737	101572	0.0794	V	R. Sabo	0.0015
TV Boo	56408.7683	101738	0.0891	V	R. Poklar	0.0016
TV Boo	56467.5459	101926	0.1056	V	M. Rodríguez	0.0041
TW Boo	56437.6745	55510	–0.0761	V	G. Samolyk	0.0014
UU Boo	56392.9584	44446	0.2599	V	R. Sabo	0.0008
UU Boo	56400.7280	44463	0.2618	V	R. Poklar	0.0011
UU Boo	56441.3992	44552	0.2671	V	T. Arranz	0.0007
UU Boo	56446.4260	44563	0.2678	V	T. Arranz	0.0007
UU Boo	56456.4795	44585	0.2690	V	T. Arranz	0.0008
UU Boo	56472.4711	44620	0.2684	V	T. Arranz	0.0008
UU Boo	56478.4110	44633	0.2683	V	T. Arranz	0.0008
UU Boo	56483.4357	44644	0.2669	V	T. Arranz	0.0007
UU Boo	56494.4016	44668	0.2667	V	T. Arranz	0.0007
UU Boo	56499.4282	44679	0.2672	V	T. Arranz	0.0009
UU Boo	56504.4522	44690	0.2651	V	T. Arranz	0.0008
UU Boo	56515.4197	44714	0.2665	V	T. Arranz	0.0007
UU Boo	56520.4452	44725	0.2658	V	T. Arranz	0.0007
UY Boo	56401.6570	22379	0.8930	V	R. Poklar	0.0014
UY Boo	56465.4690	22477	0.9230	V	T. Arranz	0.0011
UY Boo	56467.4246	22480	0.9261	V	T. Arranz	0.0011
UY Cam	56603.8054	78784	–0.0973	V	G. Samolyk	0.0033
RW Cnc	56339.6722	30671	0.2177	V	R. Sabo	0.0015
RW Cnc	56356.6295	30702	0.2118	V	R. Sabo	0.0010

Table continued on following pages

Table 1. Recent times of maxima of stars in the AAVSO Short Period Pulsator program, cont.

Star	*JD(max) Hel. 2400000 +*	*Cycle*	*O–C*	*F*	*Observer*	*Error*
RW Cnc	56385.6299	30755	0.2107	V	N. Simmons	0.0008
RW Cnc	56396.5794	30775	0.2162	V	M. Rodríguez	0.0013
RW Cnc	56406.4260	30793	0.2132	V	T. Arranz	0.0008
TT Cnc	56334.6656	29089	0.1190	V	R. Sabo	0.0012
TT Cnc	56361.6898	29137	0.0976	V	R. Sabo	0.0027
VZ Cnc	56340.7877	92190	0.0132	V	G. Samolyk	0.0011
VZ Cnc	56651.8589	93934	0.0181	V	R. Sabo	0.0017
VZ Cnc	56651.8604	93934	0.0196	B	R. Sabo	0.0016
VZ Cnc	56651.8620	93934	0.0212	I	R. Sabo	0.0020
VZ Cnc	56652.0252	93935	0.0061	I	R. Sabo	0.0018
VZ Cnc	56652.0265	93935	0.0074	B	R. Sabo	0.0006
VZ Cnc	56652.0270	93935	0.0079	V	R. Sabo	0.0010
SS CVn	56411.7482	35086	–0.3446	V	R. Poklar	0.0013
RZ Cap	56566.6435	12922	0.0007	V	G. Samolyk	0.0012
YZ Cap	56574.5821	46972	0.0518	V	G. Samolyk	0.0021
RR Cet	56567.8702	42288	0.0122	V	G. Samolyk	0.0014
RU Cet	56557.7861	28538	0.1165	V	G. Samolyk	0.0021
RV Cet	56573.8579	28008	0.2237	V	G. Samolyk	0.0023
RX Cet	56633.5342	28774	0.3273	V	G. Samolyk	0.0013
RZ Cet	56619.6725	44482	–0.2064	V	G. Samolyk	0.0013
UU Cet	56604.6880	25403	–0.1636	V	R. Poklar	0.0026
SZ CrB	56389.7881	44807	–0.0205	V	K. Menzies	0.0014
SZ CrB	56397.8639	44825	–0.0199	V	K. Menzies	0.0018
XX Cyg	56493.7281	89262	0.0039	V	G. Samolyk	0.0008
XX Cyg	56493.8612	89263	0.0021	V	G. Samolyk	0.0006
XZ Cyg	56431.8321	26376	–2.2871	V	G. Samolyk	0.0012
XZ Cyg	56446.7707	26408	–2.2829	V	G. Samolyk	0.0016
XZ Cyg	56460.7759	26438	–2.2787	V	G. Samolyk	0.0013
XZ Cyg	56488.7582	26498	–2.2984	V	G. Samolyk	0.0019
XZ Cyg	56506.4973	26536	–2.2939	V	T. Arranz	0.0009
XZ Cyg	56507.4308	26538	–2.2938	V	T. Arranz	0.0006
XZ Cyg	56514.4354	26553	–2.2897	V	T. Arranz	0.0005
XZ Cyg	56521.4387	26568	–2.2869	V	T. Arranz	0.0007
XZ Cyg	56528.4291	26583	–2.2970	V	T. Arranz	0.0006
XZ Cyg	56529.3618	26585	–2.2977	V	T. Arranz	0.0007
XZ Cyg	56535.4227	26598	–2.3039	V	T. Arranz	0.0007
XZ Cyg	56549.4108	26628	–2.3168	V	T. Arranz	0.0006
XZ Cyg	56550.3513	26630	–2.3097	V	T. Arranz	0.0010

Table continued on following pages

Table 1. Recent times of maxima of stars in the AAVSO Short Period Pulsator program, cont.

Star	*JD(max) Hel. 2400000 +*	*Cycle*	*O–C*	*F*	*Observer*	*Error*
XZ Cyg	56556.4213	26643	–2.3068	V	T. Arranz	0.0008
XZ Cyg	56557.3571	26645	–2.3044	V	T. Arranz	0.0008
XZ Cyg	56570.4201	26673	–2.3090	V	T. Arranz	0.0005
XZ Cyg	56571.3539	26675	–2.3086	V	T. Arranz	0.0006
XZ Cyg	56577.4200	26688	–2.3096	V	T. Arranz	0.0005
XZ Cyg	56578.3544	26690	–2.3086	V	T. Arranz	0.0006
XZ Cyg	56592.3473	26720	–2.3167	V	T. Arranz	0.0010
DM Cyg	56471.8685	33081	0.0738	V	R. Sabo	0.0010
DM Cyg	56484.8846	33112	0.0743	V	R. Sabo	0.0012
DM Cyg	56490.7649	33126	0.0765	V	G. Samolyk	0.0016
DM Cyg	56497.9020	33143	0.0760	V	R. Sabo	0.0022
DM Cyg	56509.6576	33171	0.0755	V	K. Menzies	0.0008
DM Cyg	56537.7899	33238	0.0772	V	R. Sabo	0.0012
DM Cyg	56558.3668	33287	0.0810	V	T. Arranz	0.0008
DM Cyg	56560.4653	33292	0.0802	V	T. Arranz	0.0008
DM Cyg	56574.3196	33325	0.0791	V	T. Arranz	0.0007
DM Cyg	56608.3223	33406	0.0731	V	T. Arranz	0.0007
DM Cyg	56637.2984	33475	0.0789	V	T. Arranz	0.0009
DM Cyg	56642.3384	33487	0.0806	V	T. Arranz	0.0005
RW Dra	56446.7250	38538	0.1987	V	G. Samolyk	0.0012
RW Dra	56449.8202	38545	0.1934	V	R. Sabo	0.0010
XZ Dra	56436.6457	30448	–0.1090	V	N. Simmons	0.0013
SV Eri	56620.7316	29515	0.9219	V	G. Samolyk	0.0021
RX For	56301.6863	27574	–0.0369	V	R. Poklar	0.0034
RR Gem	56382.5990	37819	–0.4956	V	K. Menzies	0.0007
RR Gem	56587.9956	38336	–0.5086	V	R. Sabo	0.0012
RR Gem	56603.8875	38376	–0.5091	V	G. Samolyk	0.0007
TW Her	56436.7001	87316	–0.0166	V	G. Samolyk	0.0007
TW Her	56462.6754	87381	–0.0153	V	N. Simmons	0.0006
TW Her	56545.3942	87588	–0.0137	V	T. Arranz	0.0008
TW Her	56547.3922	87593	–0.0137	V	T. Arranz	0.0007
TW Her	56551.3875	87603	–0.0144	V	T. Arranz	0.0007
TW Her	56553.3854	87608	–0.0145	V	T. Arranz	0.0007
TW Her	56561.3758	87628	–0.0161	V	T. Arranz	0.0005
TW Her	56573.3627	87658	–0.0172	V	T. Arranz	0.0006
TW Her	56575.3620	87663	–0.0159	V	T. Arranz	0.0006
VX Her	56382.9349	76053	–0.0169	V	R. Sabo	0.0008
VX Her	56497.6855	76305	–0.0202	V	G. Samolyk	0.0010

Table continued on following pages

Table 1. Recent times of maxima of stars in the AAVSO Short Period Pulsator program, cont.

Star	*JD(max) Hel. 2400000 +*	*Cycle*	*O–C*	*F*	*Observer*	*Error*
VZ Her	56463.7050	44682	0.0762	V	G. Samolyk	0.0013
AR Her	56431.8485	31868	–1.3508	V	G. Samolyk	0.0015
AR Her	56447.7858	31902	–1.3945	V	G. Samolyk	0.0015
AR Her	56457.6384	31923	–1.4124	V	G. Samolyk	0.0017
AR Her	56462.8464	31934	–1.3748	V	G. Samolyk	0.0011
AR Her	56468.4972	31946	–1.3643	V	T. Arranz	0.0013
AR Her	56469.4292	31948	–1.3723	V	T. Arranz	0.0008
AR Her	56476.4764	31963	–1.3756	V	T. Arranz	0.0010
AR Her	56477.4129	31965	–1.3791	V	T. Arranz	0.0008
AR Her	56484.4358	31980	–1.4066	V	T. Arranz	0.0011
AR Her	56493.4094	31999	–1.3636	V	T. Arranz	0.0006
AR Her	56500.4552	32014	–1.3682	V	T. Arranz	0.0010
AR Her	56508.4261	32031	–1.3878	V	T. Arranz	0.0006
AR Her	56509.3699	32033	–1.3840	V	T. Arranz	0.0007
AR Her	56516.3917	32048	–1.4126	V	T. Arranz	0.0009
AR Her	56532.4223	32082	–1.3630	V	T. Arranz	0.0005
DL Her	56409.9010	30765	0.0417	V	R. Sabo	0.0034
DL Her	56489.7906	30900	0.0615	V	R. Sabo	0.0029
DY Her	56330.9156	154015	–0.0287	V	K. Menzies	0.0006
DY Her	56463.6425	154908	–0.0296	V	G. Samolyk	0.0008
DY Her	56495.4531	155122	–0.0261	V	T. Arranz	0.0007
DY Her	56496.4962	155129	–0.0235	V	T. Arranz	0.0006
DY Her	56497.3858	155135	–0.0256	V	T. Arranz	0.0006
V394 Her	56404.8270	61133	–0.1679	V	K. Menzies	0.0014
V394 Her	56448.4337	61233	–0.1670	V	P. de Ponthiére	0.0015
V394 Her	56451.4869	61240	–0.1662	V	P. de Ponthiére	0.0020
V394 Her	56475.4688	61295	–0.1674	V	P. de Ponthiére	0.0024
V421 Her	56374.7980	5068	0.0744	V	K. Menzies	0.0018
V434 Her	56410.7537	53214	–0.0668	V	K. Menzies	0.0019
V434 Her	56425.6718	53243	–0.0664	V	K. Menzies	0.0017
V434 Her	56440.5893	53272	–0.0666	V	K. Menzies	0.0017
V434 Her	56443.6743	53278	–0.0680	V	K. Menzies	0.0017
V434 Her	56447.7914	53286	–0.0662	V	K. Menzies	0.0015
SZ Hya	56340.7940	29152	–0.2449	V	G. Samolyk	0.0027
SZ Hya	56353.6948	29176	–0.2379	V	R. Poklar	0.0014
SZ Hya	56360.6821	29189	–0.2347	V	R. Sabo	0.0018
SZ Hya	56368.7017	29204	–0.2737	V	R. Poklar	0.0034
SZ Hya	56382.7045	29230	–0.2391	V	R. Sabo	0.0009

Table continued on following pages

Table 1. Recent times of maxima of stars in the AAVSO Short Period Pulsator program, cont.

Star	JD(max) Hel. 2400000 +	Cycle	O–C	F	Observer	Error
UU Hya	56308.7481	32126	0.0089	SG	F.J. Hambsch	0.0011
UU Hya	56309.7928	32128	0.0058	SG	F.J. Hambsch	0.0008
UU Hya	56310.8461	32130	0.0114	SG	F.J. Hambsch	0.0016
UU Hya	56311.8928	32132	0.0104	SG	F.J. Hambsch	0.0011
UU Hya	56312.9463	32134	0.0161	SG	F.J. Hambsch	0.0016
UU Hya	56323.9431	32155	0.0117	SG	F.J. Hambsch	0.0035
UU Hya	56329.6961	32166	0.0021	SG	F.J. Hambsch	0.0022
UU Hya	56330.7410	32168	–0.0007	V	R. Sabo	0.0023
UU Hya	56334.9298	32176	–0.0028	SG	F.J. Hambsch	0.0014
UU Hya	56351.7083	32208	0.0119	V	R. Poklar	0.0013
UU Hya	56353.8113	32212	0.0194	SG	F.J. Hambsch	0.0015
UU Hya	56354.8622	32214	0.0226	SG	F.J. Hambsch	0.0013
UU Hya	56363.7539	32231	0.0085	SG	F.J. Hambsch	0.0022
UU Hya	56364.8003	32233	0.0072	SG	F.J. Hambsch	0.0022
UU Hya	56365.8506	32235	0.0097	SG	F.J. Hambsch	0.0014
RR Leo	56350.6934	28858	0.1255	V	R. Poklar	0.0009
RR Leo	56384.6249	28933	0.1276	V	N. Simmons	0.0009
RR Leo	56415.3889	29001	0.1288	V	T. Arranz	0.0006
RR Leo	56424.4368	29021	0.1288	V	T. Arranz	0.0007
RR Leo	56434.3895	29043	0.1289	V	T. Arranz	0.0007
RR Leo	56438.4606	29052	0.1284	V	T. Arranz	0.0008
RR Leo	56443.4367	29063	0.1282	V	T. Arranz	0.0008
RR Leo	56448.4112	29074	0.1264	V	T. Arranz	0.0008
SS Leo	56363.8655	23282	–0.0868	V	R. Sabo	0.0012
ST Leo	56383.7151	59543	–0.0221	V	R. Poklar	0.0009
TV Leo	56384.6725	28748	0.1160	V	R. Poklar	0.0020
AA Leo	56363.7093	28008	–0.0945	V	R. Poklar	0.0015
AA Leo	56408.6087	28083	–0.0943	V	K. Menzies	0.0013
AA Leo	56414.5950	28093	–0.0946	V	K. Menzies	0.0011
U Lep	56298.6537	25704	0.0435	V	R. Poklar	0.0011
RY Lib	56396.8658	62671	–0.0697	V	F.J. Hambsch	0.0021
RY Lib	56397.8302	62673	–0.0713	V	F.J. Hambsch	0.0019
VY Lib	56387.8223	28549	–0.0350	V	F.J. Hambsch	0.0017
VY Lib	56388.8893	28551	–0.0359	V	F.J. Hambsch	0.0018
VY Lib	56395.8327	28564	–0.0337	V	F.J. Hambsch	0.0017
SZ Lyn	56340.6348	151128	0.0352	V	G. Samolyk	0.0006
SZ Lyn	56381.6173	151468	0.0358	V	N. Simmons	0.0008
SZ Lyn	56574.9515	153072	0.0320	V	G. Samolyk	0.0005

Table continued on following pages

Table 1. Recent times of maxima of stars in the AAVSO Short Period Pulsator program, cont.

Star	*JD(max) Hel. 2400000 +*	*Cycle*	*O–C*	*F*	*Observer*	*Error*
SZ Lyn	56604.8449	153320	0.0327	V	G. Samolyk	0.0007
SZ Lyn	56604.9641	153321	0.0314	V	G. Samolyk	0.0006
SZ Lyn	56615.8127	153411	0.0318	V	G. Samolyk	0.0008
RR Lyr	56457.7231	23876	–0.2308	V	G. Samolyk	0.0011
RR Lyr	56457.7233	23876	–0.2306	V	N. Simmons	0.0013
RZ Lyr	56457.7699	29877	–0.0423	V	N. Simmons	0.0012
RZ Lyr	56457.7718	29877	–0.0404	V	G. Samolyk	0.0014
ST Oph	56464.6937	62258	–0.0223	V	G. Samolyk	0.0012
AE Peg	56128.9017	33659	–0.0542	V	F.J. Hambsch	0.0043
AE Peg	56129.8934	33661	–0.0559	V	F.J. Hambsch	0.0029
AE Peg	56130.8873	33663	–0.0554	V	F.J. Hambsch	0.0034
AE Peg	56131.8788	33665	–0.0574	V	F.J. Hambsch	0.0031
AE Peg	56132.8723	33667	–0.0573	V	F.J. Hambsch	0.0026
AE Peg	56134.8590	33671	–0.0574	V	F.J. Hambsch	0.0027
AE Peg	56140.8218	33683	–0.0551	V	F.J. Hambsch	0.0026
AV Peg	56519.8052	32608	0.1510	V	R. Sabo	0.0008
AV Peg	56537.7677	32654	0.1562	V	G. Samolyk	0.0014
AV Peg	56566.6521	32728	0.1529	V	R. Sabo	0.0012
AV Peg	56574.4640	32748	0.1573	V	T. Arranz	0.0007
AV Peg	56576.4112	32753	0.1527	V	T. Arranz	0.0007
AV Peg	56583.4381	32771	0.1528	V	T. Arranz	0.0007
AV Peg	56608.4231	32835	0.1538	V	T. Arranz	0.0008
AV Peg	56610.3717	32840	0.1506	V	T. Arranz	0.0007
AV Peg	56614.6678	32851	0.1525	V	R. Sabo	0.0009
AV Peg	56619.3485	32863	0.1487	V	T. Arranz	0.0004
AV Peg	56630.2823	32891	0.1520	V	T. Arranz	0.0006
DF Ser	56488.7023	61176	0.0940	V	G. Samolyk	0.0011
RV UMa	56340.9068	24068	0.1277	V	G. Samolyk	0.0024
RV UMa	56403.6239	24202	0.1248	V	N. Simmons	0.0009
AE UMa	56428.4637	242093	–0.0012	V	M. Rodríguez	0.0005
AE UMa	56458.3993	242441	0.0005	V	M. Rodríguez	0.0010
AE UMa	56610.7385	244212	0.0035	V	G. Samolyk	0.0007
AE UMa	56610.8199	244213	–0.0012	V	G. Samolyk	0.0006
AE UMa	56610.9054	244214	–0.0017	V	G. Samolyk	0.0008
AE UMa	56615.7275	244270	0.0035	V	G. Samolyk	0.0005
AE UMa	56615.8091	244271	–0.0009	V	G. Samolyk	0.0005
AE UMa	56615.8948	244272	–0.0013	V	G. Samolyk	0.0008
AE UMa	56615.9849	244273	0.0028	V	G. Samolyk	0.0013

Table continued on next page

Table 1. Recent times of maxima of stars in the AAVSO Short Period Pulsator program, cont.

Star	*JD(max) Hel. 2400000 +*	*Cycle*	*O–C*	*F*	*Observer*	*Error*
AE UMa	56619.7701	244317	0.0033	V	G. Samolyk	0.0008
AE UMa	56620.7171	244328	0.0041	V	G. Samolyk	0.0006
AE UMa	56620.7979	244329	–0.0011	V	G. Samolyk	0.0004
AE UMa	56620.8839	244330	–0.0011	V	G. Samolyk	0.0008
AE UMa	56633.7012	244479	–0.0004	V	G. Samolyk	0.0005
AE UMa	56633.7859	244480	–0.0017	V	G. Samolyk	0.0007
AE UMa	56633.8762	244481	0.0026	V	G. Samolyk	0.0013
AE UMa	56633.9627	244482	0.0031	V	G. Samolyk	0.0007
AE UMa	56655.7221	244735	0.0001	V	G. Samolyk	0.0003
GW UMa	56403.5425	21672	0.0018	V	M. Rodríguez	0.0010
GW UMa	56436.4588	21834	0.0007	V	M. Rodríguez	0.0014

New Observations of Close Eclipsing Binary Systems with δ Scuti Pulsations

Garrison Turner
Big Sandy Community and Technical College, Prestonsburg, KY 41653; gturner0040@kctcs.edu

Ronald Kaitchuck
Ball State University Dept. of Physics and Astronomy, Muncie, IN 47306; rkaitchu@bsu.edu

John Holaday
Purdue University Dept. of Material Engineering, Lafayette, IN, 47907; jholaday@purdue.edu

Received October 23, 2013; revised November 19, 2013; accepted December 6, 2013

Abstract In this paper we present the detection of δ Scuti-type pulsations in three close eclipsing binary systems (EV Ori, FO Ori, X Tri) as part of a photometric observing campaign of fourteen such systems. These observations were done as part of an ongoing effort to find such objects as they are of great value for checking theoretical models of stellar characteristics against empirically determined parameters.

1. Introduction

δ Scuti stars have become of particular importance in the last few decades. They are intrinsic variables with generally low amplitudes (on the order of less than 100 mmag) and short periods (about 0.02 to 0.3 day). See Breger (2000) for a detailed review of the characteristics of δ Scuti stars. These stars allow for the study of their interiors through asteroseismology, thus allowing theoretical models to be checked against observational results. In particular, a recently discovered class of object involves an (Algol-type) binary system in which one of the components is a δ Scuti-type variable (Broglia and Marin 1974; Liakos *et al.* 2012). These objects were termed "oscillating eclipsing Algol-type binary systems," or oEAs by Mkrtichian *et al.* (2004). Close binary systems allow for the determination of characteristics of each component in the system through photometric and spectroscopic observations, while studies of the pulsations allow for detailed asteroseismological studies of the pulsating component.

2. Observations

The targets for observation were chosen from a catalogue of possible oEAs given by Soydugan *et al.* (2006). FO Ori was found to have pulsation while

Table 1. Specifications for the instruments used for observations.

Instrument	*Diameter (m)*	*Focal Ratio*	*Camera*	*Field Scale arc sec/pixel*	*Field of View length (arc min)*	*Field of View width (arc min)*
BSUO Meade	0.4	f/6	SBIG ST-10XME	0.58	21.01	14.1
BSUO Celestron	0.3	f/11	SBIG STL-6303	0.47	24.34	16.26
SARA North	0.9	f/7.5	Apogee U42	0.4	13.86	13.86
SARA South	0.6	f/13.5	Apogee Alta E6	0.6	11.55	11.55

being observed for a separate program (see Kaitchuck *et al.* 2012). X Tri was observed in 2009 but pulsations were not detected in the study (Liakos and Niarchos 2009); however, they were detected in our campaign.

The observations for this project were taken between January and December of 2010. Data were collected with four different telescopes. The Ball State University Observatory (BSUO) houses two of the instruments. These include 0.4-m and 0.3-m diameter telescopes. Ball State University is also part of the SARA consortium which operates a 0.9-m telescope at Kitt Peak National Observatory and a 0.6-m telescope at Cerro Tololo in Chile. The SARA telescopes are of the Cassegrain design, while the BSUO telescopes are Schmidt-Cassegrains. Table 1 gives the specifications of each telescope and the CCD camera used.

Tables 2 and 3 describe the observing program for each star. Included are the target and comparison stars chosen, R.A. and Dec. coordinates (J2000), UT and Julian Dates for each observation session (with heliocentric correction applied), which telescope was used, and the number of images taken in each filter. Coordinates for each were obtained from the SIMBAD database.

All the observations made for this study were done using differential photometry. Because a typical star in the δ Scuti region on the HR diagram is of spectral type A5-F2, the best filters to use to detect pulsations are the B and V (pulsation amplitudes are filter-dependent with the B and V filters providing the highest amplitudes in this case). Images were reduced using the IRAF (Tody 1993) ccdred package, correcting for bias, dark, and flat-field effects. Differential photometry was performed with the AIP4WIN software package (Berry and Burnell 2006). All light curves that indicated eclipse phenomena were fit with quadratic polynomials to flatten the data set before the period analysis was performed. Only the in-eclipse portions of the light curves were fit with polynomials to remove orbital phenomena as the out-of-eclipse portions of the light curve did not need fitting. The errors on the data points represent the standard deviation on the check-comparison observations, as it is believed this is a more accurate representation of the true error rather than the errors calculated by AIP4WIN, which are underestimates.

Table 2. Coordinates for the target, comparison, and check stars.

Target	Target R.A. (J2000) h m s, Dec. (J2000) ° ' "	Comparison	Comparison R.A. (J2000) h m s, Dec. (J2000) ° ' "	Check	Check R.A. (J2000) h m s, Dec. (J2000) ° ' "
AD Her	18 50 00.3 +20 43 16.5	HD 349426	18 50 13.3 +20 45 01.6	TYC 1596-270-1	18 50 18.5 +20 45 30
AT Peg	22 13 23.5 +08 25 30.9	—	22 12 47.9 +08 33 21.4	—	22 12 56.4 +08 31 14.8
CZ Aqr	23 22 20.6 -15 56 20.4	TYC 6396-1024-1	23 22 24.0 -15 59 14.5	TYC 6396-872-1	23 22 34.6 -15 55 20.4
EE Peg	21 40 01.9 +09 11 05.1	—	21 40 17.3 +09 00 34.3	HD 206015	21 39 04.3 +09 03 23.0
EG Cep	20 15 56.8 +76 48 35.7	HD 193834	20 14 43.9 +76 43 11.2	HD 194400	20 17 52.9 +76 40 07.4
EY Ori	05 31 18.4 -05 42 13.5	Parenago 599	05 31 02.2 -05 37 27.5	—	05 30 59.6 -05 39 14.6
FO Ori	05 28 09 +03 37 23	TYC 105-2415-1	05 28 35.4 +03 38 45.0	HD 244077	05 28 19.7 +03 36 25.9
QY Aql	20 09 28.8 +15 18 44.7	HD 354962	20 09 25 +15 17 34	TYC 1618-1054-1	20 09 11 +15 21 49
RR Vul	20 54 47.6 +27 55 05.7	TYC 2179-59-1	20 54 37.7 +27 53 11.2	TYC 2179-613-1	20 54 48.8 +27 57 54.2
SW CMa	07 08 15.2 -22 26 25.3	TYC 5976-1216-1	07 07 54.9 -22 23 26.1	TYC 5976-472-1	07 07 53.8 -22 25 57.2
SY Cen	13 41 51.5 -61 46 10.1	TYC 8991-1036-1	13 42 04.6 -61 44 58.1	TYC 8891-616-1	13 41 52.1 -61 44 35.2
UX Her	17 54 07.8 +16 56 37.8	TYC 1557-1248-1	17 54 06.6 +16 58 14.8	TYC 1557-440-1	17 54 13.0 +17 04 37.8
V805 Aql	19 06 18.2 -11 38 57.3	HD 177707	19 06 16.3 -11 35 39.9	TYC 5715-940-1	19 06 12.6 -11 33 18.3
X Tri	02 00 33.7 +27 53 19.2	HD 122212	02 00 30.6 +27 47 05.9	TYC 1763-2015-1	02 00 37.8 27 55 10.8

3. Analysis and results

3.1. Observational results

Once generated, each light curve was processed and period-searched using the PERANSO (Vanmunster 2007) period analysis software package for periodic

Table 3. UT dates for the observations, start and end times in JD, instrument used, and number of images collected in each filter for each set of observations.

Target	*UT*	*JD Start 2455000*	*JD End 2455000*	*Instrument*	*B*	*V*
AD Her	25-Jun-10	372.7021	372.7669	0.3-m	—	27
	28-Jun-10	375.7534	375.8413	0.9-m	86	86
AT Peg	19-Aug-10	427.6592	427.7383	0.3-m	50	50
CZ Aqr	31-Jul-10	408.7623	408.9127	0.6-m	84	84
	8-Oct-10	477.7341	477.8246	0.6-m	89	84
	13-Oct-10	482.5072	482.6699	0.6-m	45	—
EE Peg	18-Jun-10	365.806	365.8565	0.3-m	—	48
EG Cep	17-Aug-10	425.7196	425.8094	0.3-m	31	31
EY Ori	17-Nov-10	517.7899	517.9638	0.6-m	464	—
	10-Dec-10	540.7472	540.8907	0.9-m	107	
FO Ori	3-Jan-10	199.587	199.9109	0.9-m	199	199
	8-Jan-10	204.6062	204.8927	0.9-m	168	204
	11-Jan-10	207.6431	—	0.9-m	129	180
QY Aql	1-Jul-10	378.7433	378.8872	0.6-m	60	60
	15-Jul-10	392.645	392.7995	0.4-m	—	70
	9-Sep-10	448.6848	448.7857	0.4-m	—	96
RR Vul	6-Oct-10	475.6726	475.7427	0.4-m	—	60
	7-Oct-10	476.5624	476.8155	0.4-m	—	104
SW CMa	7-Apr-10	293.5004	293.6583	0.6-m	—	318
SY Cen	31-May-10	347.4475	347.6513	0.6-m	—	162
UX Her	25-Jun-10	372.6583	372.846	0.4-m	—	93
V805 Aql	18-Jun-10	365.7374	365.7925	0.4-m	—	50
X Tri	6-Oct-10	475.7500	475.8708	0.4-m	—	101
	7-Oct-10	476.6976	476.8154	0.4-m	—	212

behavior between 0.01 and 0.3 day, which encompasses the accepted range of periods found in δ Scuti stars, using the Lomb-Scargle method (Lomb 1976; Scargle 1982).

An object was determined to have strong periodicity if the period window in PERANSO showed a dominant peak above the noise in the Lomb-Scargle statistic (theta) and if this peak was associated to only one (the central) peak of the spectral window (the peaks in the spectral window show how the data were sampled). Only peaks in the period spectrum that were not found to be artifacts of the observing schedule were deemed as possibly due to stellar pulsation.

Table 4. Orbital period P_{orb}, the pulsation period P_{pulse}, uncertainty, and amplitude in mmag for targets showing strong periodicity (Soygugan *et al.* 2006; Brancewicz and Dworak 1980).

Target	P_{orb} *(day)*	P_{pulse} *(day)*	*Uncertainty (day)*	*Amplitude (mmag)*
EY Ori	16.78781	0.103	0.002	10
FO Ori	18.80062	0.0292	0.0002	50
X Tri	0.97151	0.022	0.0002	20
CZ Aqr	0.86281	0.0331	0.0002	12
QY Aql	7.22961	0.1119	0.0024	12

Table 4 gives the results of the observational campaign, indicating the dominant pulsation period, uncertainty, and amplitude (all amplitudes indicated are half-amplitudes). Five objects were found to have strong periodicity, although two (CZ Aqr and QY Aql) were observed with better coverage by Liakos *et al.* (2012) and thus their result contains more certainty in the measurement of the periods. They determined pulsation periods of 0.02849 and 0.09385 day for CZ Aqr and QY Aql, respectively. The discrepancies between the results are likely due to better coverage by Liakos *et al.* (2012). It is difficult to precisely determine pulsation periods with such short time spans as obtained in this study. The remaining three were EY Ori, FO Ori, and X Tri. Figure 1 shows the light curves and Figure 2 shows the power spectra for EY Ori, FO Ori, and X Tri, respectively. Because data in only one filter were taken for EY Ori and X Tri, no other filters could be used for comparison. On the other hand, the power spectrum for the V data for FO Ori is shown in Figure 2, and period-searching the B data produced an identical period shown in Table 4.

3.2. Discussion and conclusion

This present work has sought to contribute to the total number of close eclipsing binary systems with a δ Scuti variable by reporting six new pulsation periods in eclipsing systems from a ground-based campaign. However, further observations on all of these objects is encouraged as short time spans on each object limit the accuracy and the resolution of the frequency analysis, in particular for those δ Scuti stars which undergo multi-periodic pulsations (a general behavior). Due to the uninterrupted data collection of the Kepler and CoRot satellites the numbers in this class of object should increase significantly in just a few years. Eclipsing systems with a pulsating component are important for their use as laboratories in which theoretical stellar models are able to be tested against observational results, thus this type of work has very serious implications for the understanding of stellar processes.

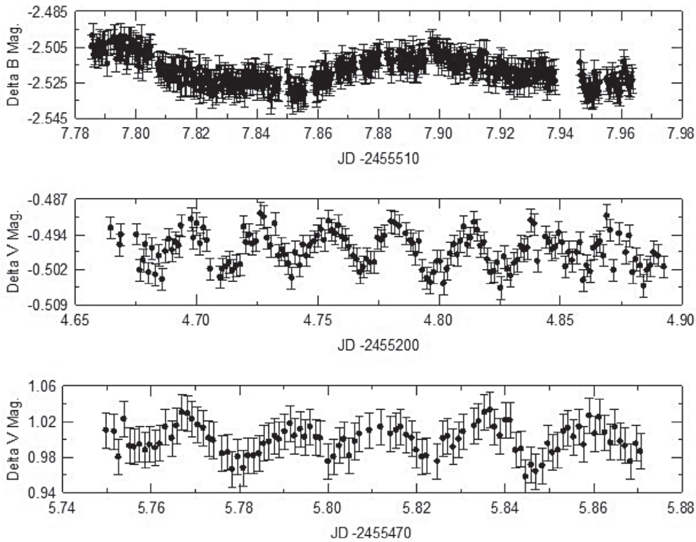

Figure 1. Light curves for EY Ori (top panel), FO Ori (middle panel), and X Tri (bottom panel) on the nights of 17-Nov-2010, 8-Jan-2010, and 6-Oct-2010, respectively. The top panel shows the ΔB magnitudes of EY Ori, while the middle and bottom panels show the ΔV magnitudes of FO Ori and X Tri.

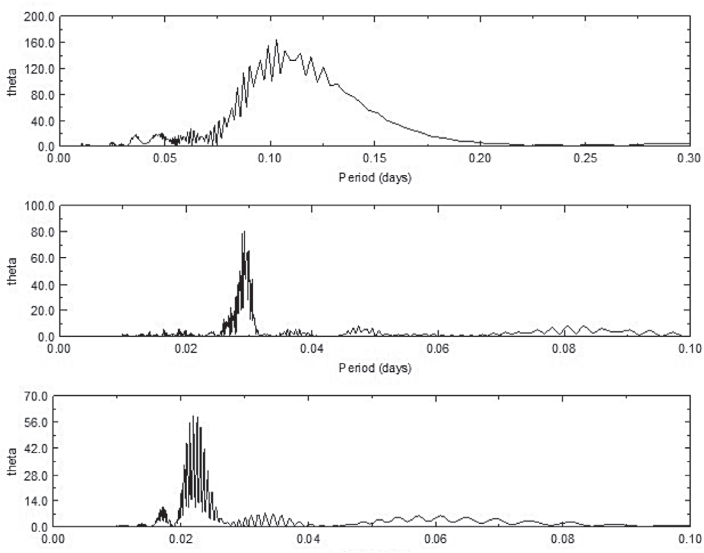

Figure 2. Power spectra for EY Ori (top panel), FO Ori (middle panel), and X Tri (bottom panel). The top panel shows the power spectrum for all of the B images of EY Ori. The middle panel and bottom panels show the power spectrums for the V images of FO Ori and X Tri, respectively.

4. Acknowledgements

This work was funded by the Indiana Space Grant Consortium.

References

Berry, R., and Burnell, J. 2006, “Astronomical Image Processing for Windows,” version 1.4, provided with *The Handbook of Astronomical Image Processing*, Willmann-Bell, Richmond, VA.

Breger, M. 2000, in *Delta Scuti and Related Stars, Reference Handbook and Proceedings of the 6th Vienna Workshop in Astrophysics*, eds. M. Breger and M. H. Montgomery, ASP Conf. Proc. 210, Astron. Soc. Pacific, San Francisco, 3

Brancewicz, H. K., and Dworak, T. Z. 1980, *Acta Astron.*, **30**, 501.

Broglia, P., and Marin, F. 1974, *Astron. Astophys.*, **34**, 89.

Kaitchuck, R., Turner, G., and Childers, J. 2012, *J. Astron. Space Sci.*, **29**, 41.

Liakos, A., and Niarchos, P. 2009 *Commun. Asteroseismology*, **160**, 2.

Liakos, A., Soydugan, E., and Zasche, P. 2012, *Mon. Not. Roy. Astron. Soc.*, **422**, 1250.

Lomb, N. R. 1976, *Astrophys. Space Sci.*, **39**, 447.

Mkrtichian, D. E., *et al.* 2004, *Astron. Astophys.*, **419**, 1015.

Scargle, J. D. 1982, *Astrophys. J.*, **263**, 835.

Soydugan, E., Soydugan, F., Demircan, O., and Ibanoglu, C. 2006, *Mon. Not. Roy. Astron. Soc.*, **370**, 2013.

Tody, D. 1993, in *Astronomical Data Analysis Software and Systems II*, eds. R. J. Hanisch, R. J. V. Brissenden, and J. Barnes, ASP Conf. Ser. 52, Astron. Soc. Pacific, San Francisco, 173.

Vanmunster, T. 2007, Light Curve and Period Analysis Software, PERANSO version 2.50 (http://www.peranso.com).

Three New Eccentric Eclipsing Binary Systems in the OGLE-II Database

Marco Ciocca
Department of Physics and Astronomy, Eastern Kentucky University, 521 Lancaster Avenue, Moore 351, Richmond, KY 40475; marco.ciocca@eku.edu

Stefan Hümmerich
Stiftstr. 4, Braubach, D-56338, Germany; ernham@rz-online.de

Received February 10, 2014; revised April 15, 2014; accepted April 15, 2014

Abstract During a search for new binary stars in the publicly available data from the second phase of the OGLE project (OGLE-II), we have identified three new eclipsing binary systems which exhibit various degrees of eccentricity. We have computed models for all systems using BINARYMAKER3 (BM3) and present model fits, residual plots and basic parameters of the stars, along with detailed information on the BM3 parameters used in the modelling process. Our models—which produce good fits to the observed OGLE-II light curves—provide starting points for further (multicolour photometric and spectroscopic) observations of these interesting binary systems.

1. Introduction

The OGLE I-band database is a searchable database of quality photometric data available to the public. During Phase 2 of the experiment, known as "OGLE-II", I-band observations were made over a period of approximately 1,000 days, resulting in over 10^{10} measurements of more than 40 million stars. This was accomplished by using a filter with a passband near the standard Cousins I_c.

Extended searches for previously unrecorded eclipsing binary systems in the OGLE-II database (Udalski *et al.* 1997; Szymański 2005) have led to the discovery of many previously unrecorded eclipsing binaries (cf. Hümmerich and Bernhard 2012; Ciocca 2013). In the present paper, we present details for three eclipsing binary stars exhibiting various degrees of eccentricity. We have computed preliminary models for all systems using BINARYMAKER3 (Bradstreet and Steelman 2004; hereafter BM3). Because OGLE-II photometry is limited to one passband (near Cousins I_c), these models of necessity include a number of assumptions and are limited in the range of information they provide. However, they still reveal a plethora of information and might serve as starting points for further investigations of these interesting systems.

2. Essential data

We have derived magnitude ranges, periods, and epochs of the present objects from an analysis of OGLE-II I-band data. Calculation of periods and epochs were done using PERIOD04 (Lenz and Breger 2005) and PERANSO (Vanmunster 2011). An overview providing essential data of all systems studied in this paper is given in Table 1.

3. Notes on individual objects

3.1. OGLEII CAR-SC3 83135

The OGLE-II database provides 410 observations for this object collected over a time span of 1,265 days. Light curve and phase plot of OGLEII CAR-SC3 83135 (period P = 1.599808 days and eccentricity e = 0.02) are shown in Figure 1.

A visual inspection of the light curve suggests a slight displacement of the secondary minimum from phase $\phi = 0.5$, which becomes more evident when zooming on the corresponding part of the phase plot (compare Figure 2). The secondary minimum actually occurs at phase $\phi = 0.52$, which is indicative of a slightly elliptical orbit. Furthermore, the observed rise in magnitude between phases $\sim 0.1 < \phi < \sim 0.4$ and the corresponding decline between phases $\sim 0.6 < \phi < \sim 0.9$ is indicative of reflection effect (compare, for example, Ruciński 1969; Vaz 1985).

The occurrence of a significant reflection effect in the light curve indicates the presence of a hot (and young?) star. This assumption is also strengthened by the slight eccentricity of the orbit and the relatively short orbital period; an aged system should—under normal circumstances—likely be showing a near-perfect circular orbit.

Additionally, the system is situated well inside the boundaries of a galactic HII region (G291.1-00.8; #999 of Paladini *et al.* 2003) which—according to the aforementioned authors—is centered on the coordinates R.A. $11^h\ 10^m\ 14.8^s$ Dec. –61° 19' 30" (J2000) and has an angular diameter of 4.4 arc minutes. Thus, OGLEII CAR-SC3 83135 is situated only about 47 arc seconds from the center of G291.1-00.8. An inspection of the corresponding sky region on ESO R-plates using ALADIN (Bonnarel *et al.* 2000) shows that the variable is actually embedded in nebulosity (see Figure 3), although it is impossible to tell if the star is associated with the HII region or a foreground object.

On grounds of the above-mentioned suppositions, we have chosen to base our model on the assumption of the presence of at least one young and hot star which is well inside its Roche lobe. From our computed model, which produces a very good fit to the observed light curve, we derive a mass ratio near 0.5 (according to BM3 convention, the mass ratio is always reported as the less massive star over the more massive one, thus resulting in less than unity),

Table 1. Essential data on the eclipsing binaries studied in this paper, sorted by right ascension.

Identifiers	*R.A. (J2000)* h m s	*Dec. (J2000)* ° ′ ″	*Type*	*Range (I_c)*	*Period (d)*	*Epoch (HJD)*	*J–K*[3]
OGLEII CAR-SC3 83135[2]	11 10 13.570	–61 20 17.27	EA	16.29–16.55	1.599808	2451264.680	0.932
USNO-B1.0 0286-0280163							
2MASS J11101357-6120172							
OGLEII CEN-SC1 63647[2]	13 57 43.249	–62 55 34.70	EA	14.40–14.64	3.609794	2451288.65	0.388
USNO-B1.0 0270-0493821							
2MASS J13574324-6255346							
UCAC4 136-105327							
OGLEII SCO-SC3 44645[2]	16 42 55.835	–44 35 49.79	EA	15.35–15.80:	2.736872	2451256.781	0.797
USNO-B1.0 0454-0511525							
2MASS J16425583-4435497							

Notes: 1. Positional data from UCAC4 (Zacharias et al. *2012); 2. Positional data from 2MASS (Skrutskie* et al. *2006); 3. From 2MASS (Skrutskie* et al. *2006).*

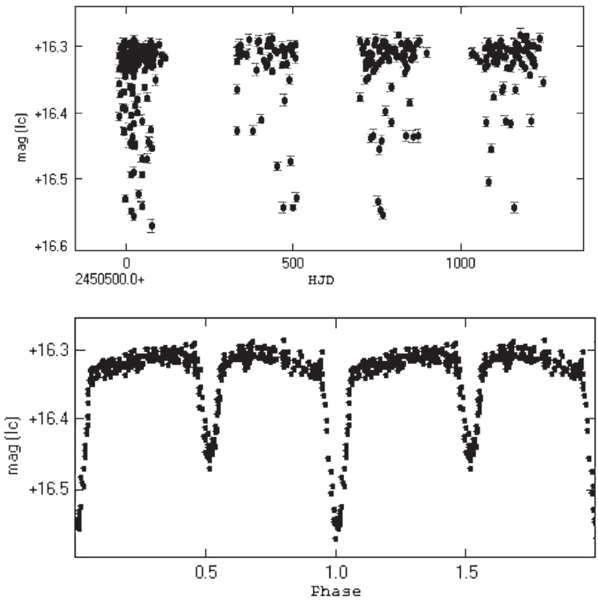

Figure 1. Light curve and phase plot (P = 1.599808 d) of OGLEII CAR-SC3 83135, based on OGLE-II data.

Table 2. BM3-derived parameters for OGLEII CAR-SC3 83135.

Parameter	*Value*
MASS_RATIO	0.5081
FILLOUT_G	–0.322
FILLOUT_S	–0.302
TEMPERATURE_1	11380 K
TEMPERATURE_2	8380 K
GRAVITY_1	1.0
GRAVITY_2	1.0
LIMB_1	0.225
LIMB_2	0.376
REFLECTION_1	1.0
REFLECTION_2	1.0 (1.22, see Figure 4)
THIRD_LIGHT	no evidence
INCLINATION	77.08
SPOTS	no evidence
DISK	no evidence
ECCENTRICITY	0.02

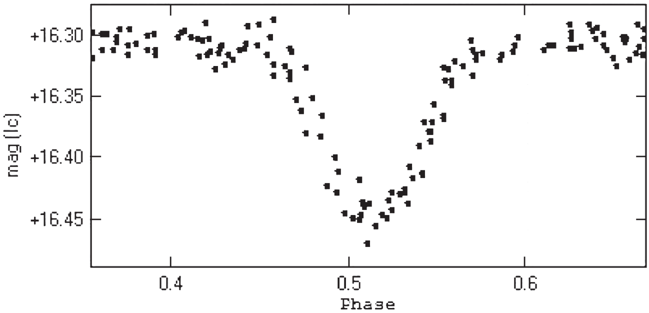

Figure 2. Phase plot of OGLEII CAR-SC3 83135 (detail), illustrating the slight displacement of the secondary minimum which occurs at phase $\phi = 0.52$.

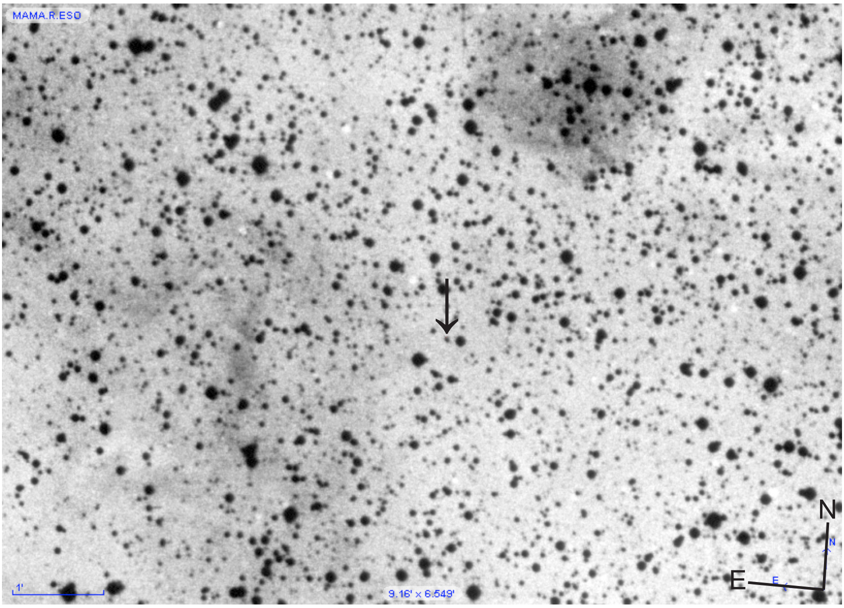

Figure 3. OGLEII CAR-SC3 83135 and its surrounding sky field on an ESO MAMA/CAI R image (accessed via ALADIN). The variable is marked with an arrow. The image is 9.16' × 6.549'. North is up and East is towards the left.

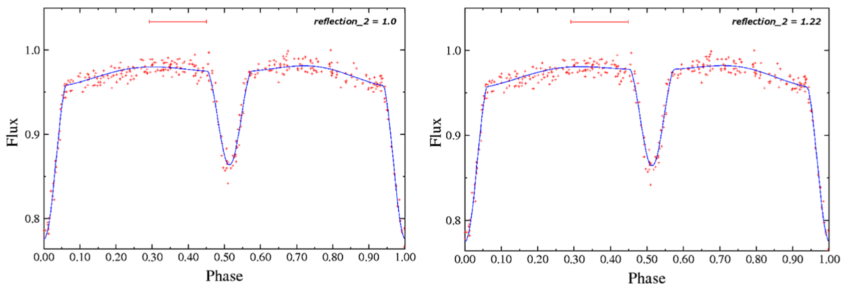

Figure 4. Phase plots of OGLEII CAR-SC3 83135 (crosses) and model fits assuming a value of REFLECTION_2 = 1.0 (solid line, left panel) and REFLECTION_2 = 1.22 (solid line, right panel). Notice the better fit to the observed light curve between phases ~0.3 < ϕ < ~0.45 (marked in the plot) in the right panel.

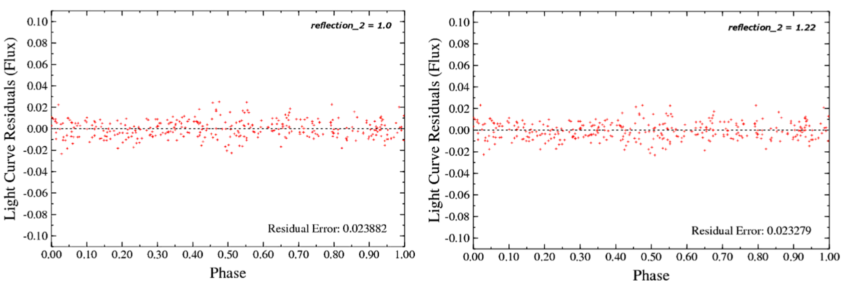

Figure 5. Residual plots of OGLEII CAR-SC3 83135, based on solutions assuming a value of REFLECTION_2 = 1.0 (left panel) and REFLECTION_2 = 1.22 (right panel).

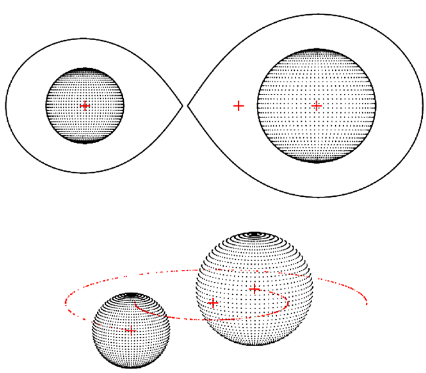

Figure 6. Three-dimensional model and outline of the equipotential surfaces for OGLEII CAR-SC3 83135. The crosses indicate the barycenter of each star and the barycenter of the system, respectively. The circles indicate the orbit of each star.

an inclination of 77.08 degrees, and an eccentricity of only 0.02. Detailed information on the derived BM3 parameters can be found in Table 2.

It is important to note that the best solution was obtained by raising the reflection coefficient REFLECTION_2 to a value of 1.22, which resulted in a noticeably better fit to the observed light curve, in particular between phases $\sim 0.3 < \phi < \sim 0.45$, and a decrease of the O–C (observed versus computed) error of ~2%. However, a value in excess of 1 is not allowed according to the theory of Ruciński (1969) as a value of 1 already implies that 100% of the flux striking the star is absorbed and re-emitted. This star is embedded in nebulosity, however (see Figure 3), and there could be extra light flux creating this effect. Regardless, as this could not be verified, we have chosen to restrict the corresponding value to 1, which still results in a very good model fit. Figure 4 gives phase plots and model fits for both solutions; the corresponding residual plots are shown in Figure 5. Figure 6 illustrates the corresponding three-dimensional model and the outline of the equipotential surfaces.

We have also computed a solution based on the surmise of a hot spot which also produces a reasonable though slightly inferior fit. However, at this point, we do not see evidence for spot activity in the light curve. Above that, it has to be kept in mind that—because of the data source consisting of information in only one passband—it is to be expected that there will be alternative models producing reasonable accordance with the observed light curves, which also holds true for the other stars presented in this paper.

A brief explanation of the parameters used in these models is necessary (for a far more detailed account see Bradstreet 2005). As mentioned previously, mass ratio q is defined as $Q = M_2/M_1$ where—according to BM3 convention —M_2 is the mass of the less massive and cooler star. The fillout parameter indicates how much of the inner Lagrangian surface of a star is filled by the gas envelope. Negative values indicate that the star does not fill the inner Lagrangian surfaces and correspond to detached systems; positive values indicate (over)contact. Temperature values describe the surface temperatures of the system's components.

Gravity brightening coefficients are used to indicate whether a star is in convective or radiative regime. For a derived surface temperature of $T \leq 7200$ K, stars are treated as convective and a gravity brightening coefficient of 0.32 is assumed. Higher surface temperatures are mostly indicative of radiative stars, in which case a coefficient of 1.00 is standard. Limb darkening parameters are used to evaluate the fading of the surface brightness towards the edges or limbs of the stars. These values are wavelength dependent and are tabulated in the BM3 manual. The reflection parameters have already been discussed above; for radiative stars ($T > 7200$ K), these parameters are usually equal to 1.

3.2. OGLEII CEN-SC1 63647

Due to differences in coverage of the various OGLE-II fields, there are only

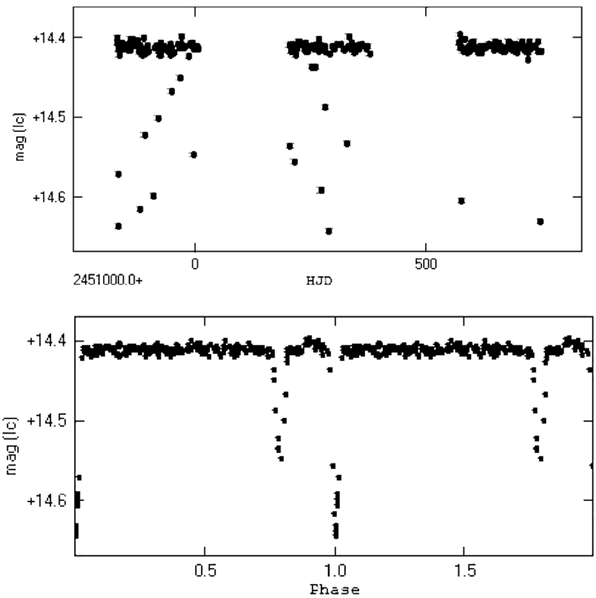

Figure 7. Light curve and phase plot (P = 3.609794 d) of OGLEII CEN-SC1 63647, based on OGLE-II data.

235 observations for this object which were collected over a time span of 915 days. Light curve and phase plot of OGLEII CEN-SC1 63647 (P = 3.609794 days and e = 0.45735) are shown in Figure 7.

Even from a casual inspection of the light curve, the pronounced eccentricity of this system is readily visible, with the secondary minimum occurring at phase $\phi = 0.79$. Additionally, there is a noticeable "hump" between secondary and primary minimum ($\sim 0.83 < \phi < \sim 0.96$). This is obviously due to the tidal distortion of the stars near periastron, when the observer from Earth sees a larger surface (as, for example, in W Ursae Majoris-type variables) and therefore a brighter object. The stars will only be of ellipsoidal shape when near periastron, as in their eccentric orbit they will otherwise be too far apart to be influenced by each other and just be spherical. The amplitude of this effect amounts to ~0.15 mag (I_c), which puts additional constraints on modelling attempts.

We have based our model on the assumption of two hot and young stars because a configuration like this (high eccentricity, relatively short orbital period) would be difficult to explain otherwise. Assuming stars well within their Roche lobes, we were able to compute a model for OGLEII CEN-SC1 63647 which produces a solid fit to the observed light curve. From this, we derive a mass ratio of 0.761, an inclination of 82.1 degrees, and the very high eccentricity of 0.45735. However, further uncertainties—especially concerning the exact shape of the minima—are introduced due to the sparse data for this

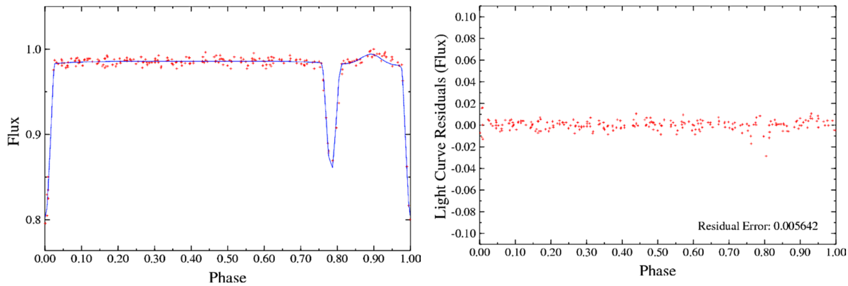

Figure 8. Left panel shows phase plot of OGLEII CEN-SC1 63647 (crosses) and model fit (solid line). Right panel shows the corresponding light curve residuals.

Table 3. BM3-derived parameters for OGLEII CEN-SC1 63647.

Parameter	*Value*
MASS_RATIO	0.761
FILLOUT_G	-0.321
FILLOUT_S	-0.437
TEMPERATURE_1	13485 K
TEMPERATURE_2	11080 K
GRAVITY_1	1.0
GRAVITY_2	1.0
LIMB_1	0.3
LIMB_2	0.23
REFLECTION_1	1
REFLECTION_2	1
THIRD_LIGHT	no evidence
INCLINATION	82.1
SPOTS	no evidence
DISK	no evidence
ECCENTRICITY	0.45735

binary system, to which we attribute the increased scatter seen in the residuals plot around secondary minimum (compare Figure 8, right panel).

Table 3 gives an overview of the BM3 parameters used to produce the present model. Model fit and residual plot are shown in Figure 8. Figure 9 illustrates the corresponding three-dimensional model and the outline of the equipotential surfaces at apastron and periastron, respectively.

3.3. OGLEII SCO-SC3 44645

This particular system exhibits eccentricity that is in between the two

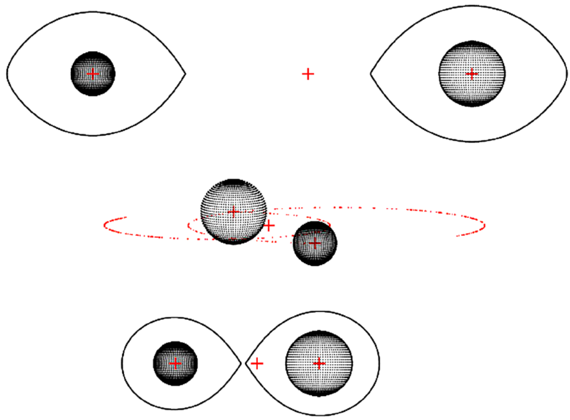

Figure 9. Three-dimensional model and outline of the equipotential surfaces for OGLEII CEN-SC1 63647. The top part shows the equipotential lines at apastron, the bottom part at periastron. The crosses indicate the barycenter of each star and the barycenter of the system, respectively. The circles indicate the orbit of each star.

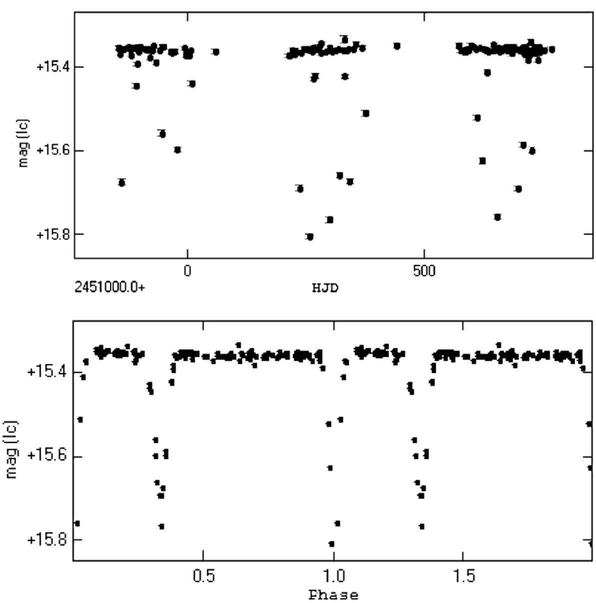

Figure 10. Light curve and phase plot (P = 2.736872 d) of OGLEII SCO-SC3 44645, based on OGLE-II data.

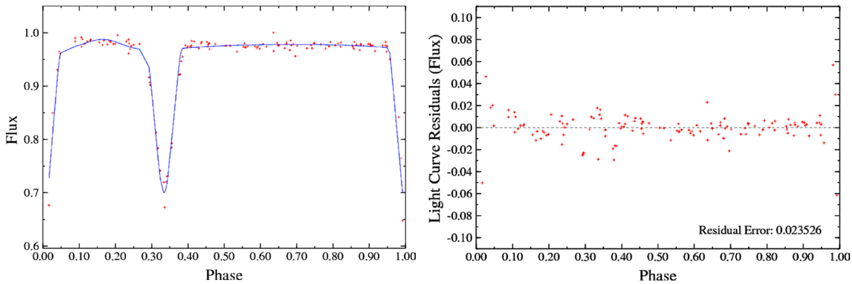

Figure 11. Left panel shows phase plot of OGLEII SCO-SC3 44645 (crosses) and model fit (solid line). Right panel shows the corresponding light curve residuals.

extremes shown before. Unfortunately, it was covered even more scantily; the OGLE-II database comprises only 135 observations taken over the course of 911 days, which adds considerable uncertainty to the derived model solution. Light curve and phase plot of OGLEII SCO-SC3 44645 (P = 2.736872 days and e = 0.2666) are shown in Figure 10; note the weak coverage of minima.

Given the large eccentricity (the secondary minimum occurs at phase $\phi \approx 0.33$), assumptions were made in similar vein to the previous system and the presence of fairly young stars were assumed; with such eccentricity, this system would be hard to conceive otherwise. From our computations, which produce a solid fit to the observations, we derive a mass ratio of 0.601, temperatures of 8115 K and 8305 K for the component stars, an inclination angle of 84.4 degrees, and an eccentricity of 0.2666.

Table 4 gives an overview of the parameters determined in BM3; model fit and residual plot are shown in Figure 11. Figure 12 illustrates the corresponding three-dimensional model and the outline of the equipotential surfaces at apastron and periastron, respectively.

4. Conclusion

We have identified three new eclipsing binary systems in the OGLE-II database which exhibit various degrees of eccentricity. We have computed models for all systems using BINARYMAKER3 which have been based on the assumption of young and hot stars. We present model fits to the observed light curves, residual plots, and basic parameters of the stars which have been derived during the modelling process. Our models—which produce good fits to the observed OGLE-II light curves—provide starting points for further (multicolour photometric and spectroscopic) observations of these interesting binary systems.

Table 4. BM3 derived parameters for OGLEII SCO-SC3 44645.

Parameter	*Value*
MASS_RATIO	0.601
FILLOUT_G	-0.2255
FILLOUT_S	-0.263
TEMPERATURE_1	8115 K
TEMPERATURE_2	8305 K
GRAVITY_1	1.0
GRAVITY_2	1.0
LIMB_1	0.24
LIMB_2	0.38
REFLECTION_1	1.0
REFLECTION_2	1.0
THIRD_LIGHT	no evidence
INCLINATION	84.4
SPOTS	no evidence
DISK	no evidence
ECCENTRICITY	0.2666

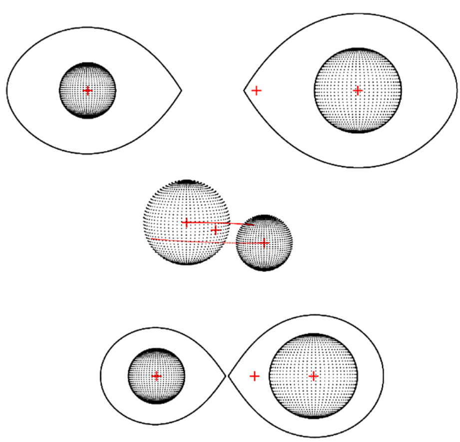

Figure 12. Three-dimensional model and outline of the equipotential surfaces for OGLEII SCO-SC3 44645. The top part shows the equipotential lines at apastron, the bottom part at periastron. The crosses indicate the barycenter of each star and the barycenter of the system, respectively. The circles indicate the orbit of each star.

References

Bonnarel, F. *et al.* 2000, eprint arXiv:astro-ph/0002109.
Bradstreet, D. H. 2005, SASS-24, 23.
Bradstreet, D. H., and Steelman, D. P. 2004, BINARYMAKER3, Contact Software (http://www.binarymaker.com).
Ciocca, M. 2013, *J. Amer. Assoc. Var. Star Obs.*, **41**, 267.
Hümmerich, S., and Bernhard, K. 2012, Perem. Zvezdy, Prilozh., **12**, 11.
Lenz, P., and Breger, M. 2005, *Commun. Asteroseismology*, **146**, 53.
Paladini, R., Burigana, C., Davies, R. D., Maino, D., Bersanelli, M., Cappellini, B., Platania, P., and Smoot, G. 2003, *Astron. Astrophys.*, **397**, 213.
Ruciński, S. M. 1969, *Acta Astron.*, **19**, 245.
Skrutskie, M. F., *et al.* 2006, *Astron. J.*, **131**, 1163.
Szymański, M. K. 2005, *Acta Astron.*, **55**, 43.
Udalski, A., Kubiak, M., and Szymanski, M. 1997, *Acta Astron.*, **47**, 319.
Vanmunster, T. 2011, PERANSO period analysis software (http://www.peranso.com).
Vaz, L. P. R. 1985, *Astrophys. Space Sci.*, **113**, 349.
Zacharias, N., Finch, C., Girard, T., Henden, A., Bartlett, J., Monet, D., and Zacharias, M. 2012, *The Fourth US Naval Observatory CCD Astrograph Catalog* (UCAC4; http://arxiv.org/abs/1212.6182).

The Light Curve and Period of MT696

Steven P. Souza
Department of Astronomy, Williams College, Williamstown, MA 01267; ssouza@williams.edu

Gillian Beltz-Mohrmann
Department of Astronomy, Wellesley College, Wellesley, MA 02418; gbeltzmo@wellesley.edu

Mona Sami
Department of Astronomy, Williams College, Williamstown, MA 01267; Mona.Sami@williams.edu

Received January 27, 2014; revised February 6, 2014; accepted February 6, 2014

Abstract We have obtained four-year narrowband light curves at 645 nm and 656 nm of the massive eclipsing binary star #696 in the Massey and Thompson (1991) study of massive stars in the Cygnus OB2 association. MT696 is a near-contact binary with components of near-equal temperature. We refine its orbital period to 1.46919 ± 0.00006 days. There is no convincing evidence of a change in period, and the 645-nm and 656-nm light curves are indistinguishable.

1. Introduction

The Cygnus OB2 Association (Cyg OB2) is home to an extraordinary number of massive stars (Massey and Thompson 1991; Camerón and Pasquali 2012), a high proportion of which are multiple (Kiminki *et al.* 2007; Kiminki *et al.* 2012). Massey and Thompson (1991) identified star #696 in their enumeration (hereafter "MT696"), also known as star No. 27 in Schulte (1956), as an O9.5V star. Rios and DeGioia-Eastwood (2004) found this star to be a double-lined spectroscopic and eclipsing binary, consisting of late O and early B components and having an orbital period of 1.46 days. Kiminki *et al.* (2007) spectroscopically determined a mass ratio of 0.7 and deduced a B1-B2V type for the secondary. Kiminki (2010) then found a spectroscopic period of 1.4694 ± 0.002 days, later refined to 1.4692 ± 0.0005 days and a mass ratio of 0.85 by Kiminki *et al.* (2012). Further, they observe no Balmer emission, which along with early spectral types and a period > 1 day leads them to suggest that it may be of β Lyr rather than W UMa type.

2. Observations and reduction

Since 2010 we have been monitoring Hα emission variability in massive stars in open clusters (Souza *et al.* 2011, Souza *et al.* 2013) via imaging through

Table 1. Identifications and basic observational data for MT696. Identifications and positions are from VizieR (Ochsenbein *et al.* 2000); magnitudes are from NOMAD (Zacharias *et al.* 2004) as accessed through VizieR.

Parameter	*Value*
USNO B1.0 identifier	1312-0390508
NOMAD identifier	1312-0408466
GSC 2.3 identifier	N31A000744
2MASS identifier	20335952+4117354
UCAC4 identifier	657-088171
R.A. (J2000)	$20^h 33^m 59.513^s$
Dec. (J2000)	+41° 17' 35.63"
B	13.18
V	12.38
R	10.61

5 nm-wide filters centered on continuum (645 nm) and Hα (656 nm) at the 0.6-m DFM Engineering telescope at Williams College. In the course of this work we have accumulated 106 pairs of observations of the central 20 × 20 arc minutes of Cyg OB2 during the 2010, 2011, 2012, and 2013 Cygnus observing seasons. Observing methods and reductions are as described in Souza *et al.* (2013) and Souza (2013), except that during the 2010, 2011, and 2012 seasons we used our original (Astrodon Imaging) filter pair, while during the 2012 and 2013 seasons we used a new filter pair from Custom Scientific, with parallel observations during the 2012 season for continuity. The new filters have similar bandpasses but better uniformity than the original set. Basic observational data for MT696, including alternate identifications, are shown in Table 1. A finding chart for MT696, including the star BD+40 4227 for reference, is shown in Figure 1.

The extraction of light curves from these less-than-homogeneous data is facilitated by inhomogeneous ensemble photometry (IEP; Honeycutt 1992; Bhatti *et al.* 2010; Richmond 2012) to correct for seeing, transparency, and airmass variations by using nearly all non-variable stars in the field as references. The IEP solution is a set of internally normalized time series, one per star. Putting these measurements on a standard magnitude scale requires comparison with at least several non-variable stars in the field, but this was not done because a) it is not needed for the desired orbital period estimate and normalized light curve, and b) these narrowband data are not readily comparable to the broadband magnitudes in the literature. Fortunately, in testing we found that IEP is effective in compensating for the slightly different characteristics of the two filter pairs, so all observations at each wavelength were combined for IEP solution.

Fourier-based period finding software such as VSTAR (Benn 2012) can have difficulty with eclipsing binaries, which proved to be the case for MT696. We

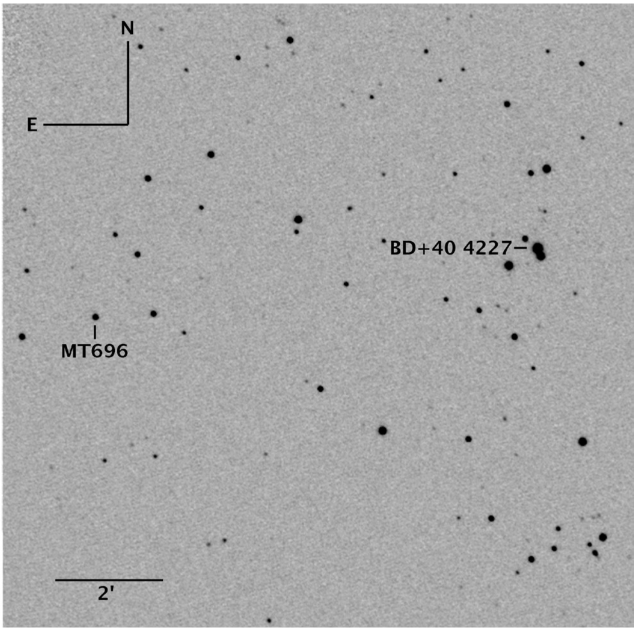

Figure 1. A portion of the Cyg OB2 field, from a 645-nm image taken on 2012 August 18. The position of MT696 is indicated, as is BD+40 4227 (the nominal center of Cyg OB2) for reference.

therefore used the NASA Exoplanet Archive Periodogram Service (Akeson *et al.* 2013) to determine the period and to phase the light curve. We selected the Plavchan *et al.* (2008) algorithm with a fixed period step of 0.00001 day, which is well suited to close eclipsing binaries. The uncertainty in the period was estimated from the half-width of the resulting periodogram peak.

3. Results and discussion

The orbital period of MT696 was derived from these data, grouped several ways (Table 2). The first (global) solution includes all the data from both filters combined, and should be considered our best estimate: 1.46919 ± 0.00006 days, which is in good agreement with but roughly an order of magnitude more precise than the best previously published estimate of 1.4692 ± 0.0005 days by Kiminki *et al.* (2012).

The resulting light curve is shown in Figure 2, plotted with mid-eclipse of the spectroscopic primary (Kiminki *et al.* 2012) at zero phase (epoch HJD 2456162.634). Data for the light curve are shown in Table 3, and are made available through the AAVSO ftp site at ftp:ftp.aavso.org/public/datasets/ssouzj421.txt. The shape of the light curve supports the identification of MT696 as a near-contact β Lyr type system, similar to BF Aur (Kallrath and

Table 2. Orbital period estimates for the MT696 system, derived from these data.

Data Grouping	*Period (days)*
All data	1.46919 ± 0.00006
645-nm only	1.46920 ± 0.00009
656-nm only	1.46920 ± 0.00006
2010–2011 only	1.46917 ± 0.00007
2012–2013 only	1.46920 ± 0.00009

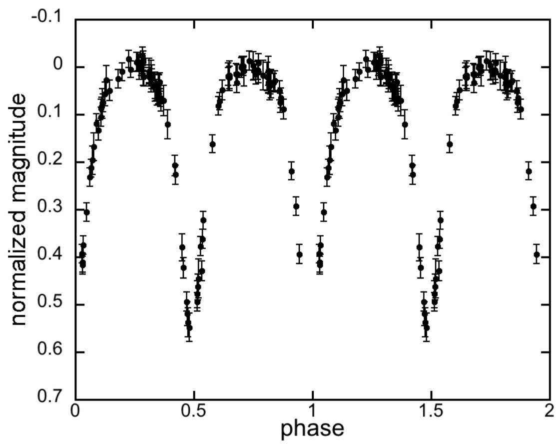

Figure 2. The phased light curve for MT696, using all 645-nm and 656-nm data. The magnitude is set to zero out of eclipse. The solution yields a period of 1.46919 ± 0.00006 days, plotted at an epoch of HJD2456162.634 to center on mid-eclipse of the spectroscopic primary.

Strassmeier 2000). From the nearly equal eclipses we deduce nearly equal surface temperatures, as expected. Correspondingly, the maximum eclipse depth of ~0.6 magnitude roughly corresponds to a minimum inclination of ~60 degrees, consistent with the estimate of 80 degrees by Kiminki *et al.* (2012) based on assumed stellar masses.

To check for filter dependence we computed separate period solutions for 645-nm and 656-nm data. They are consistent with one another and with the global solution, and their corresponding light curves are indistinguishable, as expected for a pair of hot main sequence stars with no Balmer emission.

Finally, we divided the combined data from both filters into early (2010–2011: 46 observations) and late (2012–2013: 50 observations) groups, effectively providing a two-year baseline. Though the later group gives a slightly longer period corresponding to a change of order 10^{-5}/yr, the periods agree to well within the stated uncertainty. However, the internal consistency of these solutions may indicate that our uncertainties are overestimated. If the actual uncertainty was

Table 3. Data for the MT696 light curve shown in Figure 2. Relative magnitude and magnitude uncertainty are from the IEP solution for all the data from both filters combined. Phase is from the NASA Exoplanet Archive Periodogram Service solution, adjusted for mid-eclipse of the spectroscopic primary (Kiminki *et al.* 2012) at zero phase.

HJD	*Relative Magnitude*	*Uncertainty*	*Phase*	*HJD*	*Relative Magnitude*	*Uncertainty*	*Phase*
2455403.726	0.379	0.028	0.451	2455823.709	0.021	0.020	0.312
2455404.649	0.168	0.029	0.079	2455843.641	0.089	0.021	0.878
2455404.703	0.075	0.018	0.116	2455844.614	0.323	0.019	0.540
2455405.653	0.016	0.020	0.763	2455871.533	0.049	0.020	0.862
2455405.694	0.018	0.031	0.791	2455872.524	0.362	0.020	0.537
2455407.631	0.088	0.020	0.109	2455878.560	0.021	0.030	0.645
2455407.683	0.049	0.022	0.144	2455906.484	0.018	0.031	0.652
2455408.669	0.033	0.021	0.815	2455907.497	0.048	0.022	0.342
2455416.629	0.005	0.018	0.234	2455909.463	0.016	0.023	0.679
2455416.683	0.000	0.026	0.270	2455914.484	0.134	0.021	0.097
2455437.611	0.495	0.019	0.515	2456118.721	0.084	0.020	0.110
2455438.613	0.010	0.019	0.197	2456118.727	0.077	0.031	0.114
2455472.608	0.041	0.030	0.336	2456147.703	0.034	0.019	0.837
2455472.687	0.121	0.031	0.389	2456147.708	0.029	0.021	0.841
2455477.720	0.034	0.021	0.815	2456148.641	0.538	0.030	0.476
2455480.595	0.011	0.023	0.771	2456148.647	0.548	0.030	0.480
2455482.664	0.025	0.020	0.180	2456158.643	–0.006	0.021	0.283
2455503.463	0.046	0.021	0.337	2456158.648	–0.013	0.020	0.287
2455503.640	0.423	0.022	0.457	2456158.697	0.035	0.018	0.320
2455512.676	0.072	0.018	0.607	2456158.703	0.016	0.021	0.324
2455514.620	0.293	0.019	0.931	2456158.754	0.065	0.019	0.359
2455514.639	0.394	0.020	0.944	2456158.760	0.072	0.021	0.363
2455733.675	0.412	0.021	0.030	2456161.585	0.020	0.018	0.286
2455743.660	0.036	0.030	0.826	2456161.591	0.021	0.019	0.290
2455743.722	0.065	0.021	0.868	2456162.675	0.393	0.019	0.028
2455744.672	0.478	0.029	0.515	2456162.681	0.417	0.019	0.032
2455748.733	–0.003	0.021	0.279	2456166.600	0.001	0.021	0.699
2455757.657	0.037	0.021	0.354	2456166.606	–0.002	0.020	0.703
2455758.698	0.232	0.019	0.062	2456173.609	0.494	0.020	0.470
2455759.687	–0.013	0.021	0.735	2456173.615	0.519	0.025	0.474
2455775.679	0.049	0.021	0.620	2456182.682	0.020	0.019	0.645
2455776.695	0.010	0.027	0.311	2456182.688	0.023	0.023	0.649
2455782.661	0.071	0.032	0.372	2456183.619	–0.022	0.020	0.283
2455797.691	0.082	0.020	0.602	2456183.625	–0.012	0.022	0.287
2455804.612	0.015	0.018	0.313	2456183.672	0.019	0.033	0.319
2455823.583	–0.016	0.018	0.226	2456183.678	0.025	0.021	0.323

Table continued on next page

Table 3. Data for the MT696 light curve shown in Figure 2, cont.

HJD	Relative Magnitude	Uncertainty	Phase	HJD	Relative Magnitude	Uncertainty	Phase
2456183.719	0.046	0.031	0.351	2456249.502	0.057	0.025	0.126
2456183.724	0.032	0.019	0.355	2456249.507	0.028	0.030	0.130
2456194.618	0.007	0.020	0.769	2456250.505	0.021	0.030	0.809
2456194.623	–0.008	0.021	0.773	2456250.513	0.008	0.030	0.814
2456212.638	0.375	0.020	0.035	2456275.497	0.041	0.029	0.820
2456213.586	0.033	0.021	0.680	2456275.503	0.034	0.023	0.824
2456213.591	0.016	0.021	0.683	2456463.690	0.219	0.019	0.912
2456213.628	–0.001	0.019	0.709	2456490.653	–0.011	0.020	0.265
2456213.634	0.009	0.031	0.713	2456500.681	0.119	0.021	0.090
2456213.689	–0.003	0.030	0.750	2456508.672	0.377	0.021	0.529
2456213.695	0.008	0.018	0.754	2456510.634	0.075	0.021	0.865
2456223.629	0.463	0.027	0.516	2456511.615	0.430	0.021	0.532
2456223.634	0.446	0.041	0.519	2456528.621	0.105	0.020	0.108
2456246.479	0.213	0.019	0.068	2456562.635	–0.010	0.020	0.259
2456246.484	0.196	0.030	0.072	2456564.573	0.162	0.019	0.578
2456248.463	0.207	0.021	0.419	2456600.521	0.306	0.020	0.046
2456248.469	0.227	0.020	0.423	2456621.529	0.057	0.024	0.345

about half that stated, these solutions would be marginally consistent with a period increase, but higher quality data over a longer baseline are needed.

4. Acknowledgements

We gratefully acknowledge support from the Division III Research Funding Committee of Williams College, the Office of the Dean of Faculty of Williams College, and the Keck Northeast Astronomy Consortium, supported by NSF grant AST-1005024 (partial support provided by the U.S. DoD's ASSURE program/NSF REU). This research was supported in part by NASA through the American Astronomical Society's Small Research Grant Program, and has made use of the NASA Exoplanet Archive, which is operated by the California Institute of Technology, under contract with the National Aeronautics and Space Administration under the Exoplanet Exploration Program. We thank the students who did some of the early observations: S. Wilson (Williams College), E. Boettcher (Haverford College), A. Davis (Williams College), Y. Teich (Vassar College). We thank an anonymous referee for several very helpful suggestions.

This work made use of the following software and internet resources: astrometry.net (Lang *et al.* 2010); APERTURE PHOTOMETRY TOOL 2.1.8 (Laher *et al.*

2012); ENSEMBLE 0.7 (Richmond 2012); NOMAD, U.S. Naval Observatory (http://www.nofs.navy.mil/nomad); VizieR catalog access tool, CDS, Strasbourg, France (http://vizier.u-strasbg.fr); NASA Exoplanet Archive Periodogram Service (http://exoplanetarchive.ipac.caltech.edu/cgi-bin/Periodogram/nph-simpleupload).

References

Akeson, R. L., *et al.* 2013, *Publ. Astron. Soc. Pacific*, **125**, 989.

Benn, D. 2012, *J. Amer. Assoc. Var. Star Obs.*, **40**, 852.

Bhatti, W. W., Richmond, M. W., Ford, H. C., and Petro, L. D. 2010, *Astrophys. J., Suppl. Ser.*, **186**, 233.

Comerón, F., and Pasquali, A. 2012, *Astron. Astrophys.*, **543A**, 101.

Honeycutt, R. K. 1992, *Publ. Astron. Soc. Pacific*, **104**, 435.

Kallrath, J., and Strassmeier, K. G. 2000, *Astron. Astrophys.*, **362**, 673.

Kiminki, D. C. 2010, Ph.D. Thesis, University of Wyoming.

Kiminki, D. C., *et al.* 2007, *Astrophys. J.*, **664**, 1102.

Kiminki, D. C., *et al.* 2012, *Astrophys. J.*, **747**, 41.

Laher, R. R., Gorjian, V., Rebull, L. M., Masci, F. J., Fowler, J. W., Helou, G., Kulkarni, S. R., and Law, N. M. 2012, *Publ. Astron. Soc. Pacific*, **124**, 737 (APERTURE PHOTOMETRY TOOL 2.1.8, http://www.aperturephotometry.org).

Lang, D., Hogg, D. W., Mierle, K., Blanton, M., and Roweis, S. 2010, *Astron. J.*, **139**, 1782 (astronomy.net, http://astrometry.net).

Massey, P., and Thompson, A. B. 1991, *Astron. J.*, **101**, 1408.

Ochsenbein, F., Bauer, P., and Marcout, J. 2000, *Astron. Astrophys., Suppl. Ser.*, **143**, 23.

Plavchan, P., Jura, M., Kirkpatrick, J. D., Cutri, R. M., and Gallagher, S. C. 2008, *Astrophys. J., Suppl. Ser.*, **175**, 191.

Richmond, M. 2012, ENSEMBLE 0.7 (http://spiff.rit.edu/ensemble).

Rios, L. Y., and DeGioia-Eastwood, K. 2004, *Bull. Amer. Astron. Soc.*, **36**, 1348 (9.05).

Schulte, D. H. 1956, *Astrophys. J.*, **123**, 250.

Souza, S. P. 2013, *J. Amer. Assoc. Var. Star Obs.*, **41**, 92.

Souza, S. P., Boettcher, E., Wilson, S., and Hosek, M. 2011, *Bull. Amer. Astron. Soc.*, **43**, 322.01.

Souza, S. P., Davis A. B., and Teich Y. G. 2013, *Bull. Amer. Astron. Soc.*, **45**, 354.22.

Zacharias, N., Monet, D. G., Levine, S. E., Urban, S. E., Gaume, R., and Wycoff, G. L. 2004, *Bull. Amer. Astron. Soc.*, **36**, 1418 (48.15).

125-Day Spectral Record of the Bright Nova Delphini 2013 (V339 Del)

Howard D. Mooers
Department of Geological Sciences, University of Minnesota Duluth, Duluth, MN 55812; send email correspondence to hmooers@d.umn.edu

William S. Wiethoff
SOLO Observatory, P. O. Box 88, Port Wing, WI 54865

Received March 7, 2014; revised March 31, 2014; accepted April 1, 2014

Abstract A 125-day spectral record of the evolution of Nova Delphini 2013 (V339 Del), which erupted on 2013 August 14 UT is presented. Spectra were acquired with a low-resolution, 100 line per millimeter grating. Records were acquired beginning one day after discovery and a total of forty-four spectra were analyzed. Despite the low resolution, major phases of evolution of this accreting-white-dwarf nova were recorded. These phases can be readily identified by the oxygen, iron, and nitrogen emission spectra within the range of most commercially available astronomical cameras (e.g. CCD and DSLR).

1. Introduction

The August 14 eruption of the bright Nova Delphini 2013 gave amateur astronomers a rare opportunity to study first-hand the evolution of novae. We present the results of 44 spectra gathered over 125 days with a 100 line per millimeter grating and an inexpensive, commercially-available CCD camera.

The nova was discovered August 14.5 UT by Itagaki (2013) and peaked on 2013 August 16.25 UT at an apparent visual magnitude of 4.3 (Munari *et al.* 2013a). Our first spectrum was acquired 2013 August 15.3 UT (-1 day relative to peak) and nightly thereafter through August 24 UT (+8 days). Additional spectra were acquired every clear night through 2013 December 19 UT (+125 days). After this time Delphinus was too low in the evening sky to image.

Spectra were acquired at SOLO (Studying Old Light Observatory) Observatory, located near Port Wing, Wisconsin. The observatory is a roll-off-roof type featuring a 14-inch Schmidt Cassegrain telescope on an equatorial mount. The system uses a Meade DSI Pro II monochrome CCD camera for image and spectra acquisition.

2. Methods

Spectra were acquired with a Star Analyzer® 100 (Paton Hawksley Education, Ltd. 2014), which is a 100 line per mm diffraction grating, mounted

70 mm from the CCD sensor, which yielded a dispersion of 13.75 Ångstroms/pixel. Dispersion was maximized by spacing the grating at a distance from the image sensor so the zero-order star and first-order spectrum extend across the full width of the sensor. The grating was rotated manually to adjust its horizontal alignment parallel to pixel rows to minimize geometrical artifacts. In addition, care was taken to orient the grating and imager to avoid field contamination from visible zero-order field stars.

The CCD camera was mounted at prime focus with no focal reducer. Images were shot at f/11 with a focal length of 4,086 mm. The CCD imaging camera is a 16-bit Meade DSI Pro II with a Sony ICX429ALL monochrome, front-illuminated, interline CCD image sensor with no coating or UV enhancement and has a sensitivity range of approximately 3900–10,000Å. Dimensions of the sensor are 752 (H) × 582 (V) effective pixels with pixel size of 8.6 (H) × 8.3 (V) µm, yielding a chip size of 7.4 × 5.95 mm and a plate scale of 0.429 arcsec per pixel.

Spectra were recorded by stacking 20 one-second exposures during the early phases of the nova evolution; as the magnitude faded exposure time was increased to 5.7 sec. All exposures were dark-frame subtracted. No bias or flat-field correction was done. After acquiring each spectrum the star 29 Vul, a type A0V star (strong H-Balmer absorption lines) located close to the nova, was imaged.

Spectra were analyzed with the RSPEC® software from Field Tested Systems, LLC (Field 2014), which when coupled with the Star Analyzer 100 provides an easy, very low-cost way for beginners to learn spectroscopy. Wavelength calibration was then done using a two-point method: the nova was used as the

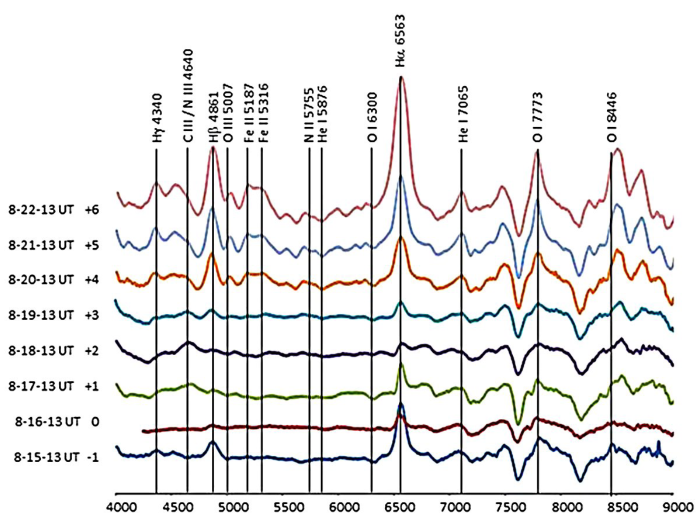

Figure 1. N Del 2013 spectra for days -1 through +6.

zero-order point and the hydrogen alpha emission line at 6563Å was used as the second point. Spectra were then corrected for instrument response using a reference curve generated from the star 29 Vul and were normalized for graphing.

Resolution (R) of the spectra is given by

$$R = \lambda/\Delta\lambda, \tag{1}$$

where λ is the wavelength of interest and $\Delta\lambda$ the smallest difference in wavelength that can be distinguished. The FWHM was determined for the Hβ line from several images and the average was 105Å. Using this value as $\Delta\lambda$ yields a spectral resolution of 46.3.

3. Results and discussion

The 44 normalized spectra were aligned, combined, and labeled in Universal Time and Day relative to peak magnitude of Nova Del 2013. These spectra are plotted for the interval 4000–9000Å and were combined into a single figure. This figure, although extremely helpful in characterizing the phases of evolution, is too large for the format or this journal but can be viewed at http://www.d.umn.edu/~hmooers/NovaDel2013CompositeSpectra.jpg.

Our spectra start at –1 day relative to maximum visible brightness (Munari *et al.* 2013a) during the fireball phase. At this time Hα and Hβ are the only prominent emission lines. By day +2, however, H emissions have all but disappeared but are again prominent by day +3 (Figure 1). On day +5, Fe II at 5187Å and 5316Å, He I at 7065Å, and O I at 7773Å appear.

By day +12, O I emission is increasing rapidly at 6300Å, 7773Å, and 8446Å and Fe II becomes more prominent (Figure 2). As the ejecta thins, however (Bhatia and Kastner 1995), O I 7773Å emission begins to drop and by day +52

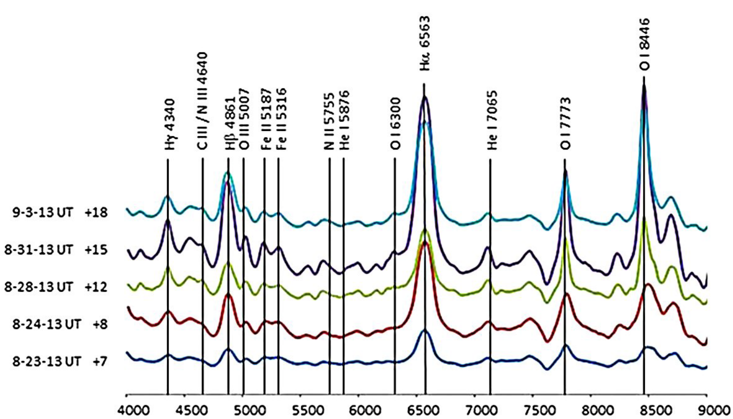

Figure 2. N Del 2013 spectra for days +7 through +18 with the appearance of neutral oxygen (8446Å) and strengthening of the iron lines.

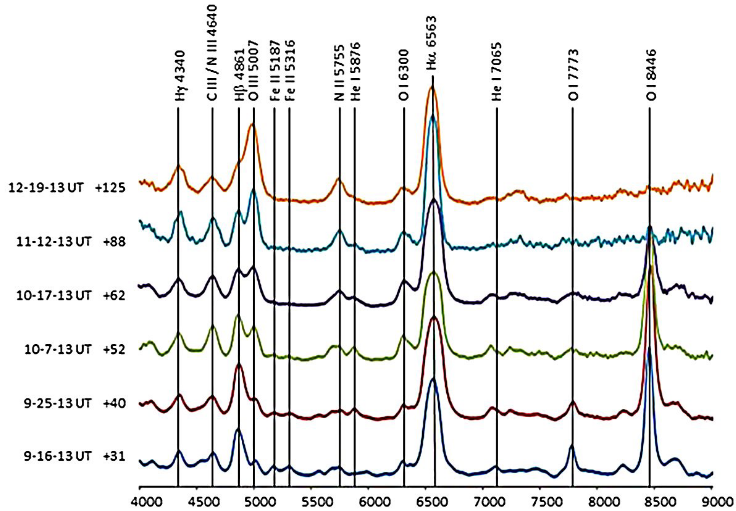

Figure 3. N Del 2013 spectra for days +31 through +125. The appearance of the forbidden lines of N II and O III accompany the disappearance of O I at the transition to the nebular phase.

is no longer discernible (Figure 3). Also at this time (day +52) the nebular lines of the C III/N III complex at 4640Å and particularly O III at 5007Å appear (Figure 3). The appearance of the forbidden transitions O III 5007Å and N II 5755Å accompany the thinning of outer ejecta, which is characteristic of the late stages of the expansion (Shore 2012, p. 10). By day +62 the O III 5007Å line has equaled Hydrogen β in intensity and corresponds to the flattening of the visible light curve around day +65 (Teyssier 2013) (Figure 3). The increasing intensity of OIII emission is commonly considered to be the beginning of the nebular phase (the optically thin regime of Munari *et al.* (2013b)). Fe II emissions are no longer discernible by this time (Figure 3).

The last several spectra (after day +62) acquired in this study show a curious upturn in the continuum above 9000Å and appear slightly noisier. We do not know the origin of these artifacts but speculate they may result from sky glow, because of the low altitude of Delphinus at this time (below 45° altitude) or other atmospheric effects. These artifacts do not, however, affect the overall utility of the spectra or the identification of emission lines.

4. Conclusions

Low resolution spectra obtainable by nearly any amateur astronomer with relatively modest equipment can be used to study the evolution of novae or investigate a host of other astronomical phenomena. Resolution of spectra is greatly improved by using larger imaging sensors but requires longer exposures because of decreased photon flux per pixel.

References

Bhatia, A. K., and Kastner, S. O. 1995, *Astrophys. J., Suppl. S.*, **96**, 325.

Field, T. 2014, Field Tested Software (http://www.rspec-astro.com).

Itagaki, K. 2013, IAU Cent. Bur. Astron. Telegrams Transient Object Followup Rep., 2013 08 14.584 (http://www.cbat.eps.harvard.edu/unconf/followups/J20233073+2046041.html).

Munari, U., Dallaporta, S., Cherini, G., Valisa, P., Cetrulo, G., Milani, A., and Ghirotto, L. 2013a, *Astron. Telegram*, No. 5304, 1 (http://www.astronomerstelegram.org).

Munari, U., Henden, A., Dallaporta, S., and Gherini, G., 2013b, *Inf. Bull. Var. Stars*, Nr. 6080, 1 (arXiv:1311.2788 [astro-ph.SR]).

Paton Hawksley Education, Ltd. 2014, The Star Analyser (http://www.patonhawksley.co.uk/staranalyser.html).

Shore, S. N. 2012, *Bull. Astron. Soc. India*, **40**, 185.

Teyssier, F. 2013, ARAS group (Astronomical Ring for Access to Astronomy), Nova Del 2013 = V339 Del (http://www.astrosurf.com/aras/novae/Nova2013Del-3.html).

New Observations of the Am Star BP Octantis

Terry T. Moon
Sydney Institute for Astronomy (SIfA), School of Physics, University of Sydney, NSW 2006, Australia; texmoon0@gmail.com

John L. Innis
Brightwater Observatory, 280 Brightwater Road, Howden, Tasmania 7054, Australia; jlinnis@gmail.com

Received January 21, 2014; revised February 19, 2014; accepted February 19, 2014

Abstract New observations are presented and analyzed for the Am star BP Oct. While a previously reported period of ~3 days cannot be unequivocally confirmed or dismissed, evidence is mounting that BP Oct is a binary and thus typical of Am stars. As light variations reported for BP Oct are no more than 0.03 magnitude, attempts to confirm or dismiss such variations remain challenging.

1. Introduction

Controversy has surrounded the variability of the Am star BP Oct (HR 5491) since Bessell and Eggen (1972) first reported a visual light range of around 0.03 magnitude with a period of about 0.08 day. Breger *et al.* (1972) observed BP Oct soon after but found no evidence of short-period variability in their one night of data. From the spectrum they confirmed that it was a classical Am star near the main sequence; additionally, they noted that there was no indication of spectral variation. When Eggen (1973) re-observed BP Oct he found it constant in light and so suggested its oscillations were multi-periodic, being at a low-amplitude phase at the time he re-observed it.

Coates *et al.* (1982) observed BP Oct on 15 nights during a period spanning more than 100 days, accumulating 95 measurements in total. There was no sign of short-period variability (< 0.3 day) in the data, indicating it is unlikely that BP Oct undergoes short-period oscillations greater than 0.01 magnitude in amplitude. There was, however, an indication of a possible 3-day variation of a little under 0.03 magnitude amplitude in V-band suggesting BP Oct is a binary. This would be consistent with observations that most, if not all, Am stars are members of binary systems (Eggen 1995; Smith 1996; Debernardi 2000). As the observations were made at two different sites with different equipment (Moon 1984), the two sets of observations were analyzed both as individual and combined datasets with appropriate corrections made for atmospheric extinction. Small differences that might arise from applying color corrections to the data (taken by the two different systems) were considered, noting that, while the comparison stars varied significantly in their colors, they did not show a similar variation to that observed for BP Oct. Color corrections alone would not account for the magnitude of the variations observed. A combined uncertainty of at least 0.01 magnitude, however, remains. Importantly, such an uncertainty significantly affects the estimated period for the small amplitude suggested.

Soon after, radial velocity measurements were attempted for different estimated phases (Moon 1984). Unfortunately poor weather and equipment failure resulted in only three usable measurements with a mean of $-7.2 \pm 3.6\,\mathrm{km s^{-1}}$. Gontcharov (2006) lists a mean value of $-14.5 \pm 2.9\,\mathrm{km s^{-1}}$ for BP Oct and Eggen (1998) a value of $-9\,\mathrm{km s^{-1}}$ with a note that it is variable. While listed as a bright star (Hoffleit and Warren 1991), BP Oct is within 2 degrees of the South celestial pole and has not been a popular candidate for long-term monitoring. It is thus not surprising that observations over the intervening years are sparse. New observations, along with an assessment of any other data taken in the intervening years, were thus in order. As an intensive observing program of BP Oct by Coates *et al.* (1982) provided no evidence that its light output varied on the timescale of hours, collection of new observations focused on investigating the reported 3-day variation.

2. Astrophysical significance of checking variability in Am stars

Kurtz (1989) discussed the observed properties of Am stars in the context of the underlying astrophysics at work. From his discussion the following are noted:

- A high proportion of normal A stars in the δ Scuti region (i.e. A stars later than about A2) exhibit oscillations with amplitudes above 0.01 magnitude.

- Most slowly-rotating A-type stars are Am stars.

- For classical Am stars the spectral classification based on the Ca II K-line and that based on metal lines differ by five or more sub-types.

- Most, if not all, classical Am stars are constant in their light output (to within 0.01 magnitude).

- There is strong evidence that the line strength anomalies observed in Am stars are due to atmospheric abundance peculiarities.

- The "diffusion" hypothesis is the prevailing explanation for the differences in the observed properties of Am and normal A-type stars. This hypothesis suggests that in the envelopes of Am stars, where a metal ion with many absorption lines is near its flux maximum, the radiation pressure drives the ion towards the star's surface. Where the absorption lines are not near their flux maximum (or are mostly saturated), those ions sink under their own weight in the layer of surrounding hydrogen. Slow rotation is seen as a necessary precursor to such diffusion, the result of which is the observed relative over- and under-abundances of various elements.

The measurement of the light of Am stars, particularly those reported as varying, remains important for understanding the astrophysical mechanisms at play, namely the hypothesized causal links among stellar rotation, diffusion, and pulsation.

3. New observations

3.1. V-band photoelectric photometry

Photometric observations of Am stars present some challenges which largely revolve around seeking to measure their light to an accuracy of 0.01 magnitude or better. These include:

- Precisely measuring and applying color corrections when stars are observed through air masses approaching 2. This is particularly problematic for BP Oct when observing it from latitudes typical of the populated land masses in the southern hemisphere where it will be observed at air masses around 2 all year round.

- Choice of non-variable comparison stars of similar spectral type. A high proportion of normal A-type stars vary by more than 0.01 magnitude, necessitating the choice of later or earlier spectral types for the comparison stars. Color corrections must then be applied but can give rise to greater uncertainties when data from different systems are combined.

- Changes in atmospheric extinction while observing.

- Searching for periodicities in low signal-to-noise data.

As indicated above, the choice of comparison stars for accurately measuring the constancy of the light output of Am stars poses a significant challenge. As a high proportion of normal A stars are variable at a greater than the 0.01 magnitude level, we chose comparison stars that were of a V magnitude similar to BP Oct with one being an earlier spectral type and the other a later type. Table 1 lists the adopted values of V and B–V, spectral type, and the source of those data for the comparison stars we chose. Neither was listed as being variable.

Table 2 presents 89 new V-band photometric measurements taken between 15 January 2004 and 17 November 2010 using the photoelectric photometer, equipment, and techniques described in Otero and Moon (2006). These data were corrected for atmospheric extinction and color corrections applied using coefficients that have been derived separately but shown to be stable for this equipment over the timescale of the observations made.

Table 1. Listed data for comparison stars used for new measurements of BP Oct.

Star	*V*[1]	*B–V*[1]	*Spectral Type*[2]	*Parallax*[2]
HR 6133	6.564	0.900	G4III	5.4 ± 0.38 mas
HIP 60041	6.630	–0.068	B9V	5.33 ± 0.39 mas

Notes: 1. Johnson V and B–V for HR 6133 from the General Catalogue of Photometric Data *(GCPD; Mermilliod* et al. *1997). As HIP 60041 is not listed in the GCPD, the values shown are from the Hipparcos catalogue (ESA 1997). 2. Spectral types and parallaxes from the Hipparcos catalogue (ESA 1997); values of parallax as reprocessed by van Leeuwin (2007).*

Table 2. New Johnson V-band photometry measurements of BP Oct.

Julian Date	*V*	*s. d.*	*Julian Date*	*V*	*s. d.*
2453020.040	6.496	0.005	2454609.915	6.481	0.009
2453022.993	6.490	0.007	2454618.986	6.454	0.002
2453025.008	6.461	0.012	2454632.976	6.465	0.011
2453026.991	6.496	0.010	2454641.940	6.475	0.004
2453028.988	6.493	0.003	2454659.974	6.484	0.006
2453031.008	6.488	0.008	2454674.911	6.484	0.009
2453031.989	6.480	0.009	2454713.981	6.437	0.009
2453034.983	6.495	0.007	2454728.010	6.484	0.005
2453046.994	6.519	0.01	2454741.992	6.539	0.006
2453047.973	6.486	0.011	2454747.997	6.499	0.011
2453053.983	6.490	0.016	2454755.001	6.506	0.006
2454462.017	6.486	0.006	2454769.966	6.451	0.012
2454467.010	6.477	0.009	2454816.006	6.464	0.007
2454478.995	6.490	0.014	2454818.002	6.472	0.011
2454482.988	6.477	0.008	2454834.010	6.468	0.012
2454489.993	6.476	0.005	2454845.004	6.469	0.011
2454493.995	6.522	0.006	2455112.943	6.504	0.008
2454496.998	6.486	0.009	2455122.978	6.482	0.007
2454503.996	6.484	0.008	2455125.953	6.472	0.004
2454507.989	6.504	0.014	2455131.980	6.448	0.014
2454520.983	6.438	0.011	2455245.986	6.497	0.005
2454521.992	6.476	0.006	2455249.990	6.460	0.007
2454541.965	6.476	0.012	2455250.997	6.481	0.009
2454549.944	6.489	0.006	2455256.992	6.472	0.006
2454571.000	6.477	0.007	2455257.979	6.481	0.010
2454571.990	6.494	0.007	2455258.961	6.464	0.005
2454573.969	6.484	0.004	2455265.955	6.467	0.006
2454574.932	6.479	0.009	2455270.942	6.468	0.006
2454595.977	6.465	0.011	2455274.962	6.479	0.008

Table continued on next page

Table 2. New Johnson V-band photometry measurements of BP Oct, cont.

Julian Date	*V*	*s. d.*	*Julian Date*	*V*	*s. d.*
2455276.933	6.496	0.008	2455379.912	6.471	0.005
2455277.980	6.464	0.007	2455382.902	6.450	0.004
2455278.929	6.465	0.004	2455401.989	6.484	0.006
2455285.942	6.475	0.011	2455402.918	6.480	0.007
2455297.931	6.466	0.011	2455437.957	6.485	0.005
2455298.967	6.494	0.005	2455447.969	6.492	0.007
2455300.914	6.470	0.005	2455464.988	6.460	0.007
2455308.006	6.495	0.004	2455474.922	6.485	0.006
2455324.992	6.470	0.007	2455477.940	6.501	0.003
2455325.961	6.473	0.007	2455489.991	6.494	0.005
2455329.967	6.502	0.002	2455493.952	6.479	0.008
2455337.910	6.482	0.005	2455494.972	6.454	0.004
2455349.930	6.463	0.007	2455504.990	6.478	0.009
2455350.966	6.522	0.015	2455505.957	6.484	0.008
2455361.921	6.474	0.005	2455517.981	6.467	0.007
2455374.006	6.477	0.006			

3.2. Radial velocity measurements

As only three useable Radial Velocity (RV) measurements were obtained in 1983 an attempt was made by one of us (JI) to obtain further measurements. Table 3 presents these unpublished RV data measurements including the three taken in 1983.

The RV observations from the mid-1980s (i.e. all but the last two entries in the table) were obtained with the Cassegrain echelle spectrograph on the 1.0-m Siding Spring reflector. Typically, exposures were made in the 5000- to 7000-Ångstrom region, and were usually around 2,000 seconds in duration. The resolution (two detector elements) was near 0.2 Ångstrom. Counts in the continuum pixels were around 200 to 1,000 depending on seeing and weather conditions. Velocity data were derived via digital cross-correlation of spectra of radial velocity standard stars, using the Mt. Stromlo PANDORA data-reduction package. Estimated total errors (statistical and systematic) are likely of the order $\pm 5\,\mathrm{kms}^{-1}$ for a given measurement.

The two most recent measurements were obtained through the UCLES (University College London Echelle Spectrograph) service observing program of the Anglo-Australian Telescope. Data reduction was carried out with the NOAO IRAF package, again via cross-correlation with spectra of radial velocity standard stars. Each measurement of these two recent data points represents the mean of three successive high signal-to-noise ratio exposures. Ten echelle orders in each spectrum were used. Internal errors are on the order of $0.4\,\mathrm{kms}^{-1}$. External errors are likely to be on the order $2\,\mathrm{kms}^{-1}$ or less.

Table 3. Previously unpublished radial velocity measurements of BP Oct.

HJD	*RV*$_{\odot}$ *(km/s)*	*HJD*	*RV*$_{\odot}$ *(km/s)*
2445509.973	–7.2	2445986.229	–16.3
2445566.939	–8.8	2446103.259	–7.8
2445568.072	–5.5	2446105.259	–10.3
2445928.018	–30.3	2446106.249	–21.1
2445981.187	–14.0	2446107.236	–26.0
2445982.145	–16.2	2446108.269	–24.9
2445984.229	–21.6	2452625.068	–26.0
2445985.229	–17.6	2452838.862	–26.9

While the data are consistent with previous published values (Gontcharov 2006; Eggen 1998), and clearly show some variation, we feel they are insufficient to determine periodicity.

4. Analyses

In addition to the new observations discussed above, we are aware of the following photometric datasets for BP Oct that have become available since the observations by Coates *et al.* (1982):

1. Hipparcos, HJD 2447871 to 2449048 (ESA 1997)

2. Tycho, HJD 2447871 to 2449014 (ESA 1997)

3. ASAS-3, HJD 2452439 to 2455111 (Pojmański and Maciejewski 2004)

The Tycho and ASAS-3 datasets have typical standard errors greater than the variation reported for this star so they were not considered for detailed period-search analysis. Standard errors were, however, generally less than 0.01 magnitude for Hipparcos data thus a period-search analysis was undertaken using the software PERSEA (Maciejewski 2005). The data downloaded were Hp magnitudes. As our focus was on looking for periodicities in the data, these were not corrected to V magnitudes. In the screen capture of the analysis of the Hipparcos data shown in Figure 1 there are no predominant peaks in the power spectrum over an interval of 1 to 100 days. PERSEA applies weightings relative to the standard error of each photometric measurement and also searches for the most significant periodicity in the data. Interestingly, PERSEA returned a "most significant" periodicity of around 3.5 days for these data. While the associated peak in the periodogram of Figure 1 is sharp and clearly visible, its power level is barely above a S/N of 2. Consequently we could not claim it to be significant with a degree of confidence.

Figure 2 gives a screen capture of the analysis and all the new observations given in Table 2 using PERSEA. As there was a significant gap in the observations

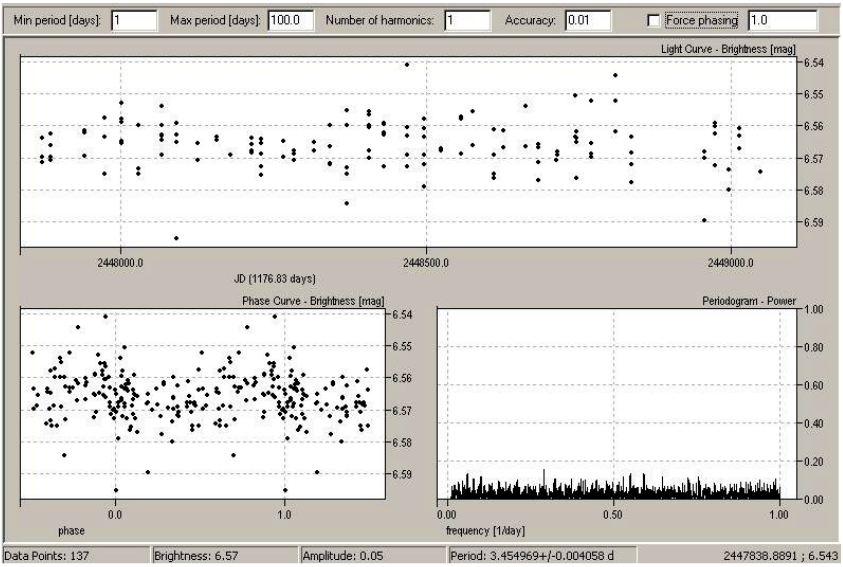

Figure 1. Screen capture of the analysis, using PERSEA, of the Hipparcos data for BP Oct. The periodogram is at bottom left.

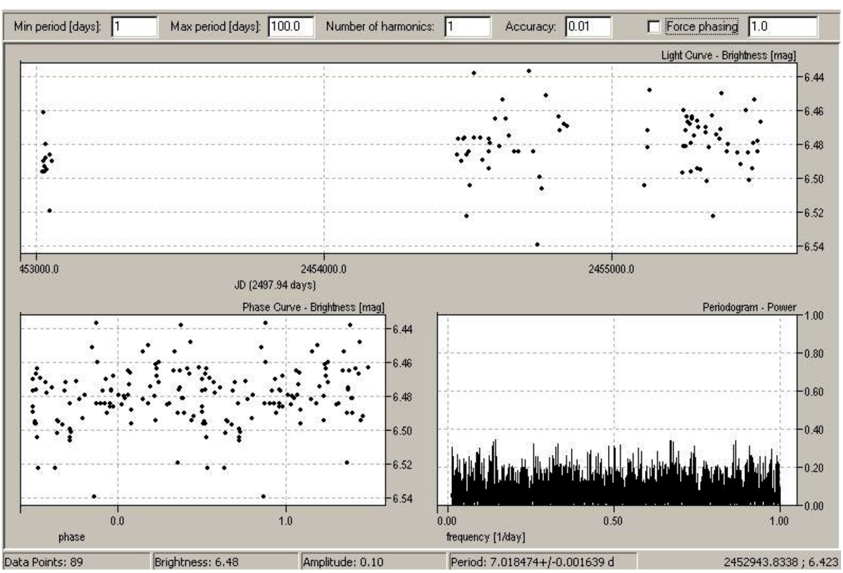

Figure 2. Screen capture of the analysis, using PERSEA, of BP Oct data taken at Blakeview.

between HJD 2453054 and 2454462 we also ran the software using only the data points collected after this gap. For both analyses we searched for periods from 1 to 100 days. Again there were no predominant peaks in the periodogram but interestingly PERSEA identified a "most significant" periodicity of 7 days; twice that for the Hipparcos data. For the periodogram of Figure 2 there is strong aliasing from the uneven distribution in the times the data were collected. The associated peak is thus less clearly defined than for the Hipparcos data and, with a S/N of barely 2, again we could not claim the period to be significant with any degree of confidence.

Period-search analyses were also undertaken on:

- Observations of the comparison star, HIP 60041, taken concurrently with the new observations of BP Oct

- Hipparcos data for HIP 60041

Neither analysis indicated any significant periodicities from 1 to 100 days.

Using the V magnitude for the first comparison star, HR 6133, as listed in the *General Catalogue of Photometric Data* (GCPD; Mermilliod *et al.* 1997; see Table 1), the mean magnitude for the second comparison star, HIP 60041, was calculated to be 6.624 ± 0.014. This value provides a precise reference for further measurements of BP Oct. The mean magnitude for the 89 measurements of BP Oct was calculated to be 6.480 ± 0.018, consistent with the value given in the GCPD.

5. Discussion

The entry for BP Oct in the *General Catalogue of Ap and Am Stars* (Renson and Manfroid 2009) lists its K line as indicating spectral class A3 and its metallic lines F2. This is consistent with a spectral type of A2mA7-F2 listed by Skiff (2009). It has been well established (Smith 1996; Koen *et al.* 1999; Debernardi 2000) that Am stars have low rotational velocities (vsini $\leq$ 100 kms^{-1}). Also, there is very little overlap in the vsini distributions of normal A and Am stars, which supports the hypothesis of slow rotation being a pre-condition for diffusion (Smith 1996), the result of which is the observed over- and under- abundance of metals that are characteristic of the spectra of Am stars. Głębocki and Gnaciński (2005) list a rotational velocity for BP Oct of $85.6 \pm 1.0\,kms^{-1}$, which is within the range of vsini measured for Am stars. The classical Am status of this star is thus not at issue.

Both Eggen (1995) and Smith (1996) note the high incidence of spectroscopic binaries among Am stars. Debernardi (2000) confirms this noting a range of periods from 0.77 to more than 1,000 days and the link to slow rotational velocities. Furthermore, in a study of 19 Am stars in the Praesepe and Hyades clusters, Debernardi *et al.* (2000) found that only two have no evidence of radial-velocity variations. This predominance of binarity in Am stars continues to be seen as explaining the reason for slow rotation of many Am stars, a binary companion providing a rotational "braking mechanism." Slow rotation then permits the onset of diffusion in the stellar envelope, resulting in observed over- and under-abundances of the specific elements that give rise to a star being categorized as Am.

Since the Hipparcos mission, a new method of detecting binaries has been developed (Wielen *et al.* 1999; Quist and Lindegren 2001). The method compares quasi-instantaneous measurements of proper motion from Hipparcos data (averaged over three years) with long-term averaged proper motions from ground-based data. Where the difference between these two measures is statistically significant with respect to the measurement errors, the star is designated as a "$\Delta\mu$ binary." The criterion for statistical significance was chosen by Wielen *et al.* (1999) to give a strong indication of binarity such that among 10,000 truly single stars only 27 would be wrongly classified as being $\Delta\mu$ binaries. A catalogue of $\Delta\mu$ binaries (Makarov and Kaplan 2005) was compiled and can be accessed at http://dc.zah.uni-heidelberg.de/dmubin/q/cone/info.

BP Oct is listed in this $\Delta\mu$ binary catalogue but is at the lower end of the threshold chosen for statistical significance. It should also be noted that its detection as a $\Delta\mu$ binary would not explain a 3-day variation in light as the $\Delta\mu$ binary technique only detects binaries with periods in the order of years.

6. Conclusions

We conclude that, through an analysis of the new observations presented here and Hipparcos data, the proposition of a faint companion to BP Oct giving rise to small variations in the measured light over a timescale of several days cannot be discounted. Furthermore, both datasets show no evidence of short-period variations (≤ 0.3 day) and little evidence of any other periodicity from 1 to 100 days. Coupled with the listing of BP Oct as a $\Delta\mu$ binary and the known high rate of binarity amongst Am stars, the hint of a 3.5-day period in the measured light of BP Oct supports the proposition of there being a binary companion. Variations of $\leq$ 0.03 magnitude, however, remain difficult to confirm, with any estimate of a period being highly uncertain. From the parallax of BP Oct (van Leeuwen 2007) we calculate an $M_V = 2.41 \pm 0.04$. A K-type dwarf with an M_V in the range 6.4 to 7.4 could then add ≤ 0.03 magnitude to the observed V magnitude of BP Oct.

Further observations to test a binary-star hypothesis for BP Oct would be challenging as they would require sustained, accurate observations over a long timescale. Both authors now live in Tasmania and would be able to regularly observe BP Oct (subject to the vagaries of weather) through air masses around 1.5, possibly increasing the accuracy of observations over those reported here and previously. A thorough observing program would, however, demand measurement on most available fine nights. For a variation of several hundredths of a magnitude any periodicity detected would continue to have a large uncertainty associated with it. Noting Debernardi's (2000) question "Are there any single Am stars," the question of the possible binary nature of BP Oct remains interesting and further studies important. BP Oct would then be most suited to observations by space-borne telescopes or from small telescopes located in Antarctica.

References

Bessell, M. S., and Eggen, O. J. 1972, *Publ. Astron. Soc. Pacific*, **84**, 72.

Breger, M., Maitzen, H. M., and Cowley, A. P. 1972, *Publ. Astron. Soc. Pacific*, **84**, 443.

Coates, D. W., Dieters, S., Innis, J. L., Moon, T. T., and Thompson, K. 1982, *Inf. Bull. Var. Stars*, No. 2233, 1.

Debernardi, Y. 2000, in *Birth and Evolution of Binary Stars, Poster Proceedings of IAU Symposium No. 200 on The Formation of Binary Stars*, ed. B. Reipurth and H. Zinnecker, 161.

Debernardi, Y., Mermilliod, J.-C., Carquillat, J.-M., and Ginestet, N. 2000, *Astron. Astrophys.*, **354**, 881.

Eggen, O. J. 1973, *Q. J. Roy. Astron. Soc.*, **14**, 426.

Eggen, O. J. 1995, *Astron. J.*, **110**, 823.

Eggen, O. J. 1998, *Astron. J.*, **116**, 284.

ESA. 1997, The Hipparcos Main Catalogue, Hipparcos Epoch Photometry (http://webviz.u-strasbg.fr/viz-bin/VizieR-5?-out.add=.&-source=I/239/hip_main&recno=39726).

Głębocki, R. and Gnaciński, P. 2005, in *Proceedings of the 13th Cambridge Workshop on Cool Stars, Stellar Systems and the Sun*, ed. F. Favata, G. A. J. Hussain, and B. Battrick, ESA SP-560, ESA Publications Division, Noordwijk, The Netherlands, 571.

Gontcharov, G. A. 2006, *Astron. Lett.*, **32**, 759.

Hoffleit, D., and Warren Jr., W. H. 1991, *The Bright Star Catalogue*, 5th rev. ed. (http://cdsarc.u-strasbg.fr/viz-bin/Cat?V/50).

Koen, C., van Rooyen, R., van Wyk, F., and Marang, F. 1999, *Mon. Not. Roy. Astron. Soc.*, **309**, 1051.

Kurtz, D. W. 1989, *Mon. Not Roy. Astron. Soc.*, **238**, 1077.

Maciejewski, G. 2005, "PERSEA 2.01, Period Search Program for Windows," (http://www.astri.umk.pl/~gm/SAVS/).

Makarov, V. V., and Kaplan, G. H. 2005, *Astron. J.*, **129**, 2420.

Mermilliod, J.-C., Mermilliod, M., and Hauck, B. 1997, "General Catalogue of Photometric Data (GCPD). II," *Astron. Astrophys., Suppl. Ser.*, **124**, 349 (http://obswww.unige.ch/gcpd/gcpd.html).

Moon, T. T. 1984, *Ultra Short Period Cepheids*, Ph.D. Thesis, Monash Univ., Australia.

Otero, S., and Moon, T. 2006, J. *Amer. Assoc. Var. Star Obs.*, **34**, 156.

Pojmański, G., and Maciejewski, G. 2004, *Acta Astron.*, **54**, 153.

Quist, C. F., and Lindegren, L. 2001, In *The Formation of Binary Stars*, ed. H. Zinnecker, R. D. Mathieu, IAU Symp. 200, Astronomical Society of the Pacific, San Francisco, 64.

Renson, P., and Manfroid, J. 2009, "General Catalogue of Ap and Am stars," *Astron. Astrophys. Suppl.*, **498**, 961 (VizieR On-line Data Catalog: III/260).

Skiff, B. A. 2009, General Catalogue of Stellar Spectral Classifications (Version 2009 February; http://vizier.u-strasbg.fr/viz-bin/VizieR?-source=B/mk).

Smith, K. C. 1996, *Astrophys. Space Sci.*, **237**, 77.

van Leeuwen, F. 2007, *Hipparcos, the New Reduction of the Raw Data*, Springer-Verlag, Berlin.

Wielen, R., Dettbarn, C., Jahreiß, H., Lenhardt, H., and Schwan, H. 1999, *Astron. Astrophys.*, **346**, 675.

Z Cam Stars in the Twenty-First Century

Mike Simonsen
AAVSO, 49 Bay State Road., Cambridge, MA 02138; mikesimonsen@aavso.org

David Boyd
5 Silver Lane, West Challow OX12 9TX, England; davidboyd@orion.me.uk

William Goff
13508 Monitor Lane, Sutter Creek, CA 95685; b-goff@sbcglobal.net

Tom Krajci
Center for Backyard Astronomy, P.O. Box 1351, Cloudcroft, NM 88317; tom_krajci@tularosa.net

Kenneth Menzies
318A Potter Road, Framingham MA, 01701; kenmenstar@gmail.com

Sebastián Otero
AAVSO, 49 Bay State Road, Cambridge, MA 02138; sebastian@aavso.org

Stefano Padovan
Barrio Masos SN, 17132 Foixà, Girona, Spain; stefano@stefanopadovan.com

Gary Poyner
67 Ellerton Road, Kingstanding, Birmingham B44 0QE, England; garypoyner@blueyonder.co.uk

James Roe
85 Eikermann Road-174, Bourbon, MO 65441; jim.roe@asemonline.org

Richard Sabo
2336 Trailcrest Drive, Bozeman, MT 59718; rsabo333@gmail.com

George Sjoberg
9 Contentment Crest, #182, Mayhill, NM 88339; george.y.sjoberg@gmail.com

Bart Staels
Koningshofbaan 51, Hofstade (Aalst) B-9308, Belgium; staels.bart.bvba@pandora.be

Rod Stubbings
2643 Warragul, Korumburra Road, Tetoora Road, VIC 3821, Australia; stubbo@sympac.com.au

John Toone
17 Ashdale Road, Cressage, Shrewsbury SY5 6DT, England; enootnhoj@btinternet.com

Patrick Wils
Aarschotsebaan 31, Hever B-3191, Belgium; patrickwils@yahoo.com

Received October 7, 2013; revised November 12, 2013; accepted November 12, 2013

Abstract Z Cam (UGZ) stars are a small subset of dwarf novae that exhibit standstills in their light curves. Most modern literature and catalogs of cataclysmic variables quote the number of known Z Cams to be on the order of thirty or so systems. After a four-year observing campaign and an exhaustive examination of the data in the AAVSO International Database (AID) we have trimmed that number by a third. One of the reasons for the misclassification of some systems is the fact that the definition of what a Z Cam is has changed over the last eighty-five years. This has caused many stars formerly assumed to be Z Cams or rumored to be Z Cams to be eliminated from the final list. In this paper we present the results of our investigation into sixty-five stars listed at one time or another in the literature as Z Cams or possible Z Cams.

1. Introduction

Dwarf novae (DNe), or U Geminorum (UG) systems, are a subclass of cataclysmic variable stars (CVs), semi-detached close binary systems in which a white dwarf (WD) accretes material from a Roche-lobe-filling secondary via an accretion disk (Warner 1995). They are called "dwarf novae" because DNe outbursts are smaller in amplitude and higher in frequency than classical novae eruptions.

DNe outbursts result from a temporary increase in the rate of accretion onto the WD. According to the thermal-viscous disc instability model, over time the mass of accreted material grows and the temperature of the disk rises, until it becomes sufficiently high to switch into a hot, highly viscous state. The disk becomes unstable and mass is dumped onto the surface of the WD after plowing through a violent transition region just above the surface of the WD called the "boundary layer," releasing copious amounts of energy from optical to X-rays.

DNe are classified into sub-groups based primarily on their light curves. SS Cygni stars (UGSS) brighten dramatically by 2 to 6 magnitudes in 1 to 2 days, and return to their original brightness after a period of several days to a week or more. Cycle times between outbursts range from 10 days to years. Orbital periods are usually longer than 3 hours. SU Ursae Majoris stars (UGSU) exhibit normal outbursts, but also have brighter and longer "superoutbursts." The cycle times of superoutbursts (super-cycle) are usually several times the length of time between normal outbursts and can be years or decades long. In general, the shorter the orbital period, the longer the super-cycle. Orbital periods are usually in the range of 75 minutes to 2 hours. Z Cam stars (UGZ) are DNe that exhibit normal UG-type outbursts, as well as random standstills. A standstill usually starts at the end of an outburst and consists of a period of relatively constant brightness 1 to 1.5 magnitudes below maximum light that may last from a few days to 1,000 days. The orbital periods of UGZ are all longer than 3 hours.

This classification system has evolved over time as our understanding of the physical processes behind the observed behaviors has grown. However, the changing definition of UGZ stars has created confusion in the literature and many stars that used to fit the definition no longer meet the requirements of membership in the Z Cam classification.

2. Origin and evolution of the Z Cam classification

The English astronomer J. R. Hind discovered U Gem on December 15, 1855. The speed and amplitude of its brightness variations attracted the attention of many of the leading observers of the day, and for over forty years it was the only star of its type known. Then, in 1896, Miss Louisa D. Wells discovered SS Cyg on plates taken at the Harvard College Observatory. The similarity between these two stars was noted immediately and the classification of U Gem stars was introduced. The early definition was based on light curves of stars that stayed at minimum for the majority of the time, but at intervals between 40 and 100 days erupted by 3 to 5 magnitudes (Toone 2012). By 1928 there were two dozen or more stars classified as UG or suspected of being UG.

Two stars, Z Cam and RX And, discovered in 1904 and 1905, respectively, were initially classified as UG, but years of close observation revealed these two stars to have much shorter periods (at that time, defined as the time between maxima) and they spent very little time at minimum. This caused A. A. Nijland to propose a new class of variable stars, the Z Cam type, of which he suggested X Leo and TW Vir might also be members (Nijland 1930). This new classification was further bolstered by support from Felix De Roy, Director of the British Astronomical Association-Variable Star Section (BAA-VSS), when he published a paper, “A New Variable Star Class, The Z Camelopardalis Type,” describing the state of knowledge of these stars to date (De Roy 1932).

The roots of some of the confusion on the classification of several stars can be traced back to this paper in which RX And, Z Cam, BI Ori, CN Ori, TZ Per, SV CMi, X Leo, and SU UMa are either included in the new class or suspected of membership and requiring further investigation.

It is also this paper that first defined the “crucial features for the Z Cam type.” In 1932 they were:

1. The short duration of minimum.

2. The irregularity of the light curve, described as rare for U Gem types and almost the norm for Z Cams.

3. The lesser amplitudes of variation compared to U Gems, 2.64 magnitudes for Z Cams versus 3.8 magnitudes for U Gems.

4. A "curious and very special feature" where the variable remains nearly constant at a magnitude in between the maximum and minimum.

Interestingly, it is mentioned that only Z Cam, TZ Per, and RX And exhibit this feature. At the time these "standstills," as they would come to be known, were not the primary feature of Z Cam stars, but more of a curiosity. It was the brief minima and short duration between maxima that set these stars apart initially.

Campbell and Jacchia (1941) note in *The Story of Variable Stars*, "from time to time they take a sort of vacation, and remain at almost constant brightness." But this is a footnote to the description based primarily on the hyperactive nature of Z Cams.

The standstills take on more prominence in Elvey and Babcock (1943) where they write, "Whenever they go through their regular variations, they behave similarly to the short period group of SS Cygni stars. However, these stars may remain for weeks at relatively constant brightness, approximately one-third from maximum to minimum brightness."

By 1971, the term "standstills" was in use and is described in *The Variable Star Observers Handbook* (Glasby 1971) as the main distinguishing feature of Z Cam type variables. "The major difference, and that which justifies their inclusion in a separate group, is the periods of standstill."

The modern day definition in the *General Catalogue of Variable Stars* (GCVS; Samus *et al.* 2007–2009) also stresses the importance of standstills as the determining characteristic of Z Cams:

> Z Camelopardalis type stars. These also show cyclic outbursts, differing from UGSS variables by the fact that sometimes after an outburst they do not return to the original brightness, but during several cycles retain a magnitude between maximum and minimum. The values of cycles are from 10 to 40 days, while light amplitudes are from 2 to 5 magnitudes in V.

This was the definition used when the Z CamPaign was launched in 2009 (Simonsen 2011), in order to differentiate between genuine Z Cam stars and their imposters. The criterion for inclusion in the Z Cam class was simply evidence of at least one standstill in the available data.

For many potential Z Cam stars, significant data exist in the AAVSO International Database which can be used to determine whether they belong to this class or not. For many others, the challenge has been to acquire enough data over a multi-year campaign to weed out the pretenders from the bona fide Z Cams.

3. Bona fide Z Cam stars

After four years of Z CamPaign observations and an exhaustive examination of the AAVSO International Database, nineteen bona fide Z Cam type systems have been identified out of the sixty-five stars listed in the literature at one time or another as Z Cam stars. Some of these have been known to be Z Cams for decades. Others are newly classified or re-classified as Z Cams.

All light curves (Figures 1–21) in this section were created using VSTAR (Benn 2012). Black dots are AAVSO visual data; green dots [gray in black/white version] are AAVSO Johnson V data (AAVSO 2013). Except for the prototype star Z Cam, the stars are listed here in order of R.A. Each star's position, maximum and minimum, and type is given in Table 1.

The entire set of AAVSO data for each star was downloaded and the light curve was examined visually, both in gross, multi-year displays and in close detail, cycle-by-cycle. Start dates of the data set and the beginnings and endings of outbursts and standstills could be determined by selecting individual data points on the VSTAR light curve and viewing the complete observational information on the VSTAR information screen.

Table 1: Bona fide Z Cam–type variable stars.

Name	*R.A. (2000)* h m s	*Dec. (2000)* ° ′ ″	*Max*	*Min*	*Type*
WW Cet	00 11 24.78	–11 28 43.1	10.4V	15.8V	UGZ
V513 Cas	00 18 14.91	66 18 13.6	14.9V	18.9V	UGZ*
IW And	01 01 08.91	43 23 25.7	13.8V	17.7V	UGZ*
RX And	01 04 35.54	41 17 57.8	10.2V	15.1V	UGZ
AY Psc	01 36 55.45	07 16 29.3	15.3V	17.0V	UGZ+E
TZ Per	02 13 50.97	58 22 52.3	12.0V	15.6V	UGZ
HL CMa	06 45 17.22	–16 51 34.7	10.6V	14.9V	UGZ*
BX Pup	07 54 15.57	–24 19 36.5	13.8V	18.0V	UGZ
Z Cam	08 25 13.20	73 06 39.2	10.0V	14.5V	UGZ*
AT Cnc	08 28 36.93	25 20 03.0	12.7V	15.2V	UGZ*
SY Cnc	09 01 03.32	17 53 56.2	11.1V	14.5V	UGZ
Leo5	10 28 00.08	21 48 13.7	15.2V	17.7V	UGZ+E*
ES Dra	15 25 31.81	62 01 00.0	14.1V	17.5V	UGZ
HP Nor	16 20 49.59	–54 53 22.9	12.8v	16.4V	UGZ
AH Her	16 44 10.01	25 15 02.0	11.3v	14.7V	UGZ*
UZ Ser	18 11 24.90	–14 55 33.9	12.4V	17.2V	UGZ*
EM Cyg	19 38 40.11	30 30 28.4	12.0V	14.3V	UGZ+E
VW Vul	20 57 45.07	25 30 25.7	13.1V	17.0V	UGZ
HX Peg	23 40 23.70	12 37 41.8	12.9V	16.6V	UGZ*

**Outbursts from standstills have been observed.*

Average cycle times were determined using a custom-designed tool in VSTAR. Maxima could be hand selected individually, and the mean magnitude and average time between selections were automatically calculated. The averages of the densest data sets were then calculated to derive the mean time between selections and the mean magnitude of maxima.

3.1. Z Cam (the prototype star)

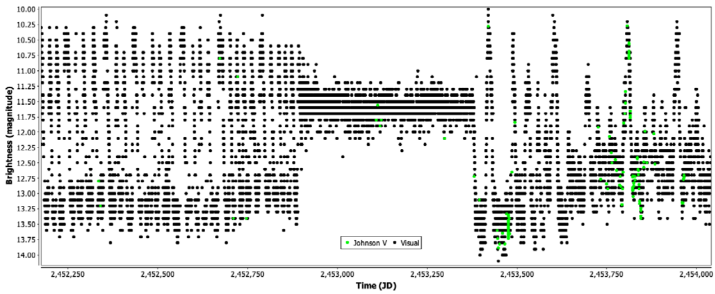

Figure 1.AAVSO light curve for Z Cam, the prototype of the class, showing the normal rapid succession of outburst to quiescence interrupted by a standstill from JD 2452896 to 2453381 (September 2003 to January 2005). There is then a drop to quiescence followed by an irregular pattern of outbursts.

3.2. WW Cet

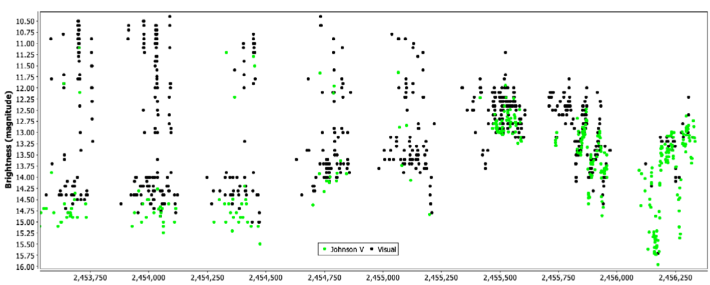

Figure 2. The AAVSO light curve of WW Cet shows a normal pattern of outbursts and minima, followed by the first standstill in AAVSO records, from JD 2455359 to 2455826 (June 2010 to September 2011). This is followed by a weaker pattern of outbursts with progressively fainter minima. Recently classified as Z Cam in Simonsen and Stubbings (2011).

3.3. RX And

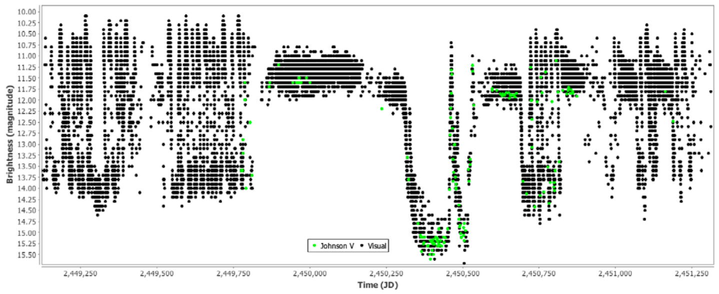

Figure 3. The AAVSO light curve for RX And, one of the first Z Cams classified as such (Nijland 1930; De Roy 1932), clearly shows a standstill from JD 2449843 to 2450315 (May 1995 to August of 1996), followed by a precipitous drop to an uncharacteristically faint minimum. This is followed by two brief outbursts, and then a series of standstills and outbursts.

3.4. AY Psc

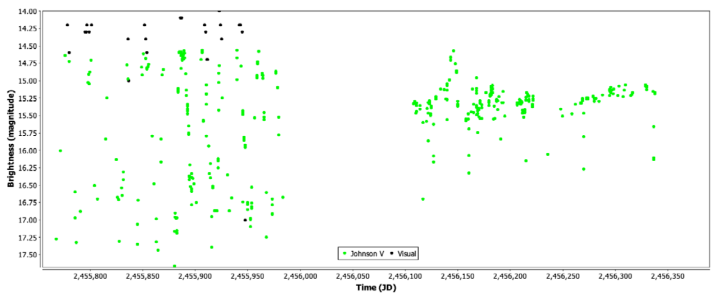

Figure 4. Classified as a Z Cam in Mercado and Honeycutt (2002), this AAVSO light curve for AY Psc shows a normal pattern of maximum and minimum cycles, then a seasonal gap in the data. This is followed by progressively brighter minima and a standstill from JD 2456163 to 2456335 (August 2012 to February 2013).

3.5. TZ Per

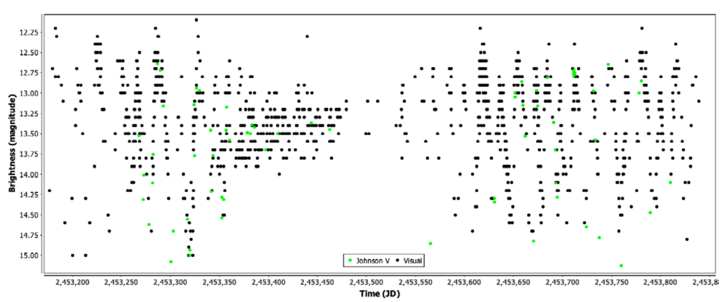

Figure 5. TZ Per is one of the original Z Cams classified in De Roy (1932). This AAVSO light curve shows a regular pattern of outbursts that is interrupted by a standstill from JD 2453394 to 2453511 (January to May 2005). This is followed by a seasonal gap, and then the resumption of normal maximum and minimum cycles.

3.6. HL CMa

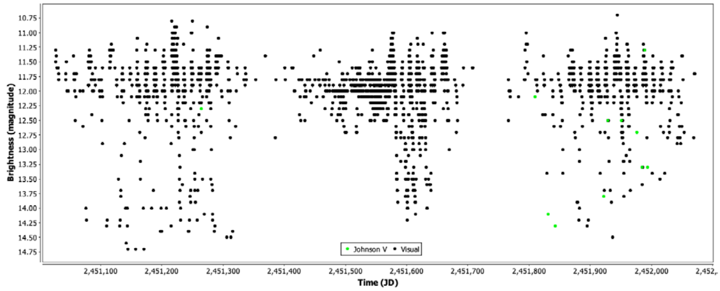

Figure 6. Classified as a Z Cam at least as early as Mansperger *et al.* (1994), this AAVSO light curve for HL CMa shows normal outburst cycles interrupted by a standstill from JD 2451386 to 2451574 (July 1999 to January 2000). This is followed by a rise to maximum before normal maximum and minimum cycles resume.

3.7. BX Pup

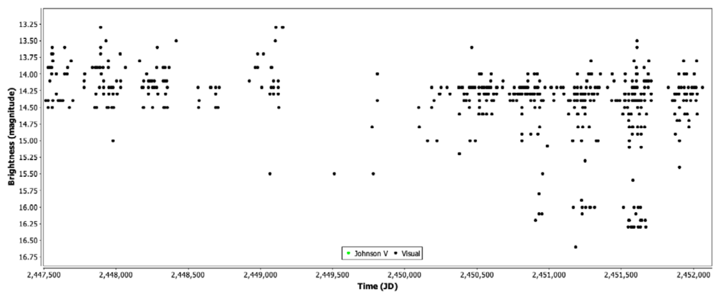

Figure 7. This AAVSO light curve of BX Pup, although sparse, does seem to indicate at least two standstills. The first from JD 2448569 to 2448713 (November 1991 to April 1992) and another more extended standstill from JD 2450097 to 2450904 (January 1996 to March 1998). There is another sparsely sampled standstill from JD 2452339 to 2452747 (April 2002 to April 2003) in the AAVSO data (Figure 8). This, coupled with observations of a 38-day standstill in Dirks (1941), leaves us to conclude that BX Pup is indeed a Z Cam.

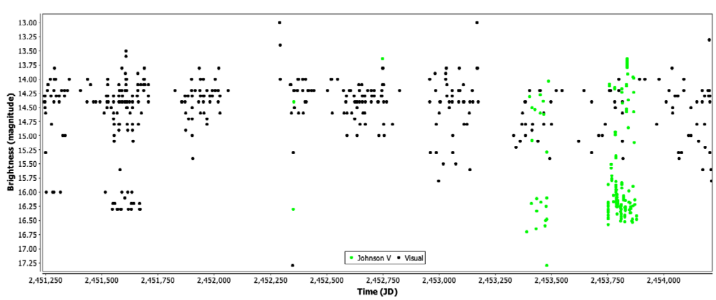

Figure 8. AAVSO light curve of BX Pup centered on the April 2002 to April 2003 standstill (JD 2452339 to 2452747).

3.8. AT Cnc

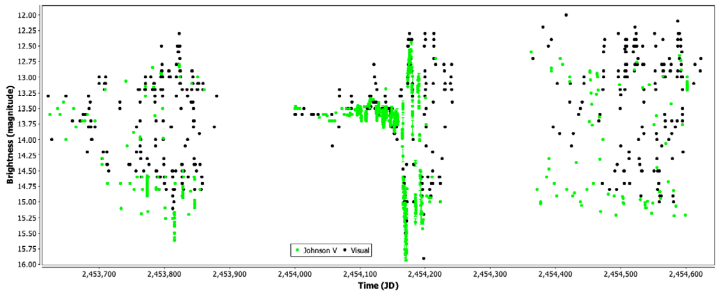

Figure 9. This AAVSO light curve of AT Cnc is a textbook example of a normal outburst cycle, followed by a seasonal gap, then an obvious standstill from JD 2453999 to 2454163 (September 2006 to March 2007), followed by a deep fade to minimum, then the resumption of normal maximum to minimum cycles.

3.9. SY Cnc

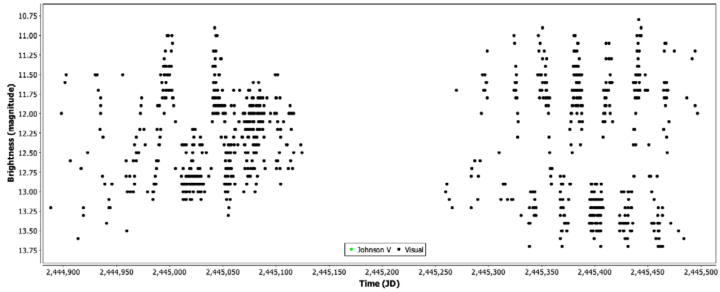

Figure 10. This standstill in SY Cnc, beginning on or around JD 2445069, lasts at least until JD 2445124 (April to June 1982). We don't know how long the standstill continued because the star is lost to the horizon and the seasonal gap. Though truncated by the seasonal gap, this is the only convincing evidence of a standstill in all the AAVSO data. However, there are tantalizing indications that several standstills may have taken place during other seasonal gaps.

3.10. Leo5

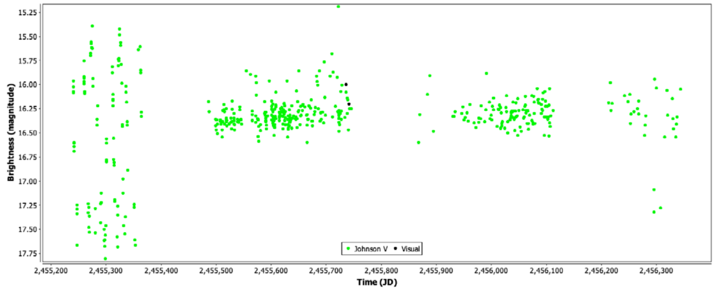

Figure 11. Leo5 is a newly classified Z Cam (Wils *et al.* 2011). AAVSO data for Leo5 show the normal outburst cycle, interrupted by a standstill beginning in October 2010 (JD 2455485), then a brief outburst from standstill in June 2011 (JD 2455721). The standstill then resumes, until it drops to minimum in January 2013 (JD 2456295).

3.11. AH Her

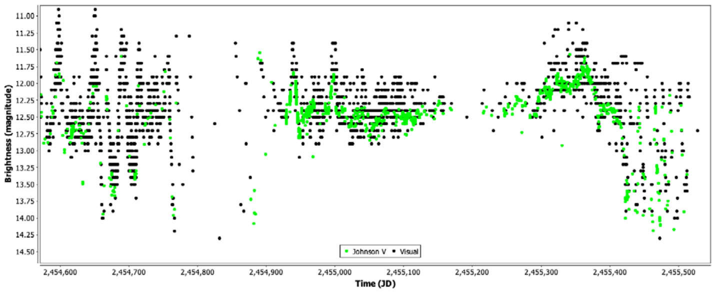

Figure 12. This AAVSO light curve of AH Her shows, in exquisite detail, the star settling into a standstill beginning on JD 2455005 (June 2009). It becomes slightly more chaotic, and then goes into outburst from standstill almost one year later on JD 2455363, before fading to progressively fainter minima.

3.12. UZ Ser

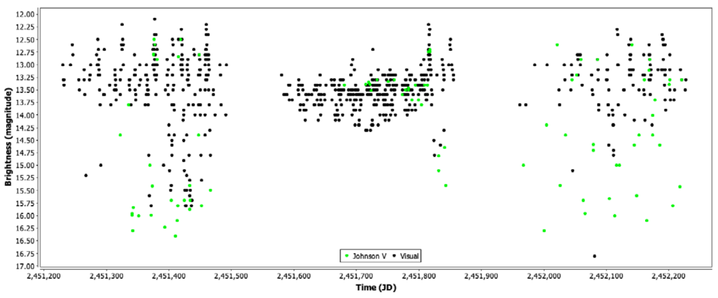

Figure 13. This AAVSO light curve clearly shows UZ Ser in a standstill beginning JD 2451580 (February 2000), followed by an outburst from standstill at JD 2451815 (September 2000). It then resumes more or less normal outburst cycles.

3.13. EM Cyg

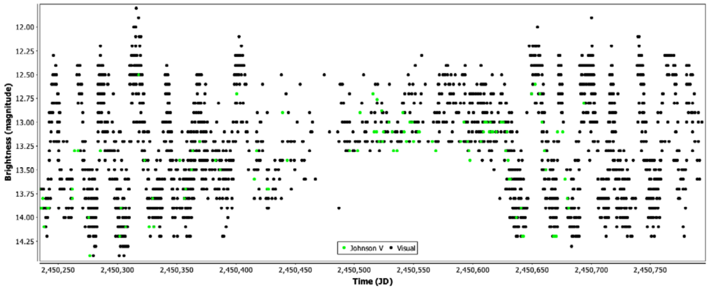

Figure 14. This AAVSO light curve shows EM Cyg in standstill from JD 2450454 to 2450636 (January to July 1997), preceded and followed by more or less normal outburst cycles.

3.14. VW Vul

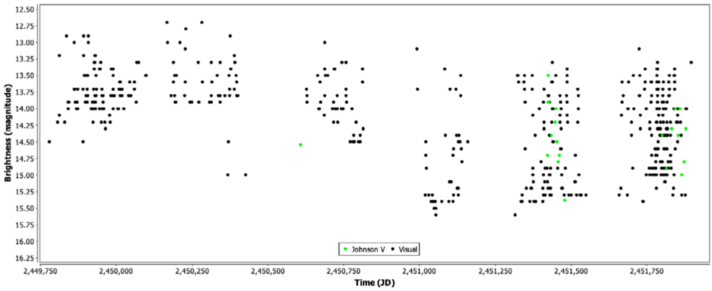

Figure 15. This AAVSO light curve shows VW Vul in standstill from JD 2450627 to 2450814 (June 1997 to January 1998).

3.15. HX Peg

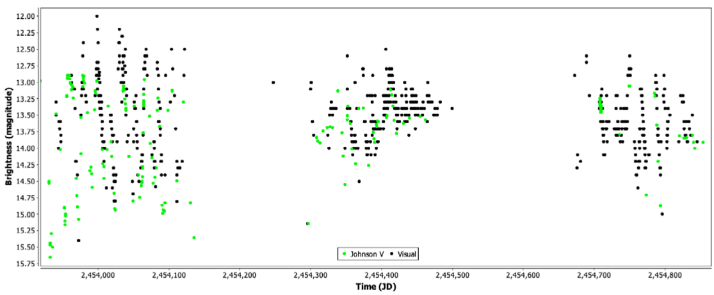

Figure 16. This AAVSO light curve of HX Peg shows it settling down to standstill on or around JD 2454423 (November 2007) until it is lost to the seasonal gap after JD 2454499 (February 2008).

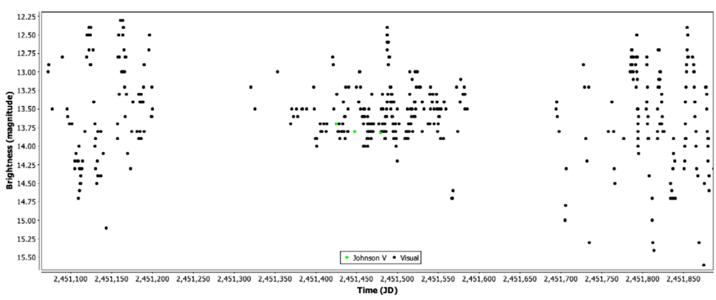

Figure 17. Here we see HX Peg go into outburst in November 1999 (JD 2451487) from standstill, then back into standstill at the end of 1999.

3.16. ES Dra

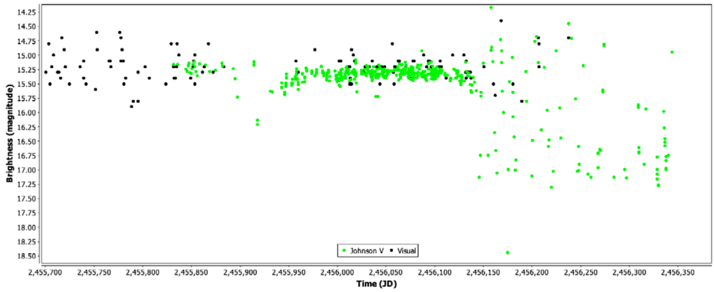

Figure 18. This AAVSO light curve shows the most recent standstill of ES Dra, from JD 2455931 to 2456167 (January to August 2012), firmly establishing ES Dra as a member of the Z Cam class. See also Ringwald and Velasco (2012).

3.17. HP Nor

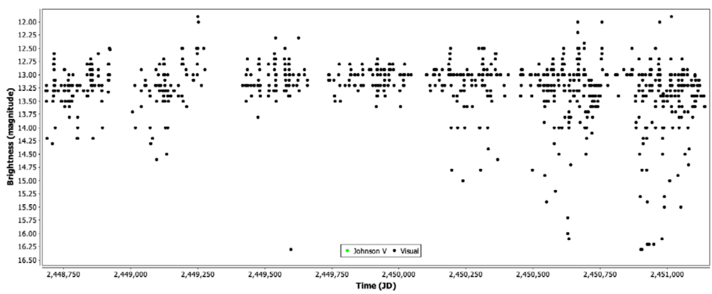

Figure 19. This AAVSO light curve of HP Nor shows a standstill beginning JD 2449737 (January 1995) and lasting until JD 2450161 (March 1996).

3.18. IW And

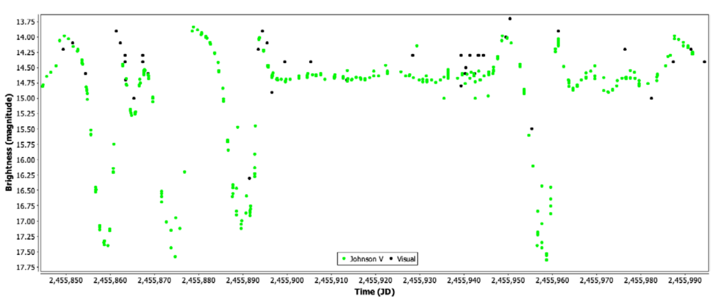

Figure 20. This AAVSO light curve shows IW And in a standstill December 1, 2011 (JD 2456263), followed by a rise to outburst on January 10, 2012 (JD 2456303). This is followed by a fade to minimum, a short outburst, and then another standstill—which is followed by yet another outburst.

3.19. V513 Cas

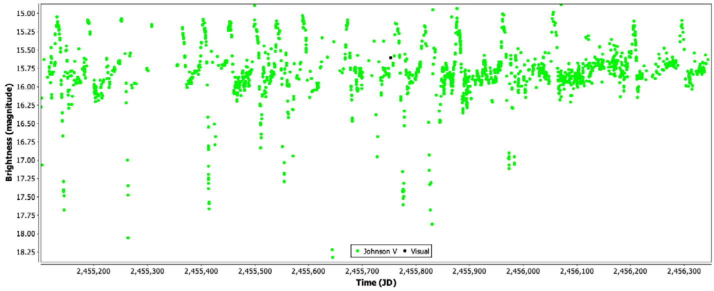

Figure 21. This AAVSO light curve shows the previously unknown, exotic nature of V513 Cas. Beginning in October of 2009 (JD 2455105) the system was observed with a pattern of outbursts every 51 days on average, punctuated by 20- to 30-day standstills, rise to outburst again, and then a deep fading episode roughly every other cycle. In February 2012 the pattern changed dramatically. Cycle time between outbursts stretched to an average of 83 days, the standstills were less chaotic, and there were no deep fades to 17th magnitude, resembling nova-like variable (NL) behavior.

4. Characteristics of true Z Cam stars

There are several other characteristics which many Z Cams share in addition to the modern defining characteristic of standstills.

4.1. Standstills

As the most significant characteristic of assigning membership to the Z Cam classification of DNe, it is appropriate to begin with our current understanding of Z Cam standstills.

The word "standstill" is somewhat misleading. Their light curves do not look like the flat line of an EKG graph of a patient whose heart has stopped beating. Indeed, Z Cams are quite lively even in standstill. Visual examination of the light curves of standstills reveals a remarkable amount of activity and "jitter." Szkody and Mattei (1984) showed erratic flare-ups with amplitudes up to several tenths of a magnitude in Z Cam standstills.

It is the cause of these episodes of more or less steady light fainter than maximum that has stirred the greatest amount of discussion. It is generally agreed nowadays that standstills are the result of a sudden increase in mass transfer, above the rate allowing for normal SS Cygni-type outburst cycles and below the rate that would cause the system to remain in a state of continuous outburst, like the nova-like stars. What causes this increase has been the subject of much debate for over thirty years.

Based on the disk-instability model, Meyer and Meyer-Hofmeister (1983) proposed that Z Cams normally have mass transfer rates slightly below the critical value that would keep their accretion rates stable. Irradiation of the secondary is given as a reason for the higher mass accretion rate seen in standstills than in outburst cycle phases. They suggest standstills occur when the mass transfer rate changes because of irradiation of the secondary, the mass transfer stream impacting the disk and tidal friction. They also suggest a "relaxation oscillation" cycle that happens as the mass transfer rate drops to lower levels, allowing the outburst cycle to begin again after a standstill.

Oppenheimer *et al.* (1998) argued that irradiation of the secondary does not play a significant role in the changes in mass accretion rates in Z Cams. If this were true, a standstill should accompany a bright quiescence, because an irradiated secondary should be brighter and lose more material into the bright spot. Their analysis showed that faint quiescences accompany standstill intervals. They suggest solar-type magnetic cycles and star spots as a plausible alternative mechanism. Smak (2004) also concludes that irradiation from the secondary is not a significant factor in enhanced mass transfer in Z Cam systems.

Stehle *et al.* (2001) explain standstills are fainter than outburst maxima because the gas stream from the donor star heats the disk, which lowers the threshold of mass transfer needed to keep the star from going back to quiescence. Their model predicts standstill luminosities to be about 40% less than the peak brightness of an outburst, which matches observations very well. Buat-Menard *et al.* (2001) also conclude that better agreement with the observations is obtained when one takes into account the energy released by the impact of the mass transfer stream onto the disk and by tidal torque dissipation.

The one thing none of the models explains is the underlying cause of this sudden shift in the mass transfer rate. What initiates it, and what makes it turn off, allowing the star to go back to quiescence, or in some cases, back into outburst?

An oft-quoted characteristic of Z Cams is that "standstills are always initiated by an outburst," and "standstills always end with a decline to quiescence" (Hellier 2001). However, there are at least nine Z Cam stars that have been shown since since 1959 (Collinson and Isles 1979) to go into outburst from standstill: Z Cam, HX Peg, AH Her, HL CMa, UZ Ser, AT Cnc, Leo5, V513 Cas, and IW And. This inconvenient truth raises even more questions about the cause of standstills. If it is true that the accretion disk has been drained in the plateau phase just before a standstill (as put forth in Oppenheimer *et al.* 1998), then what is the underlying cause of outbursts that occur immediately after standstills?

4.2. Orbital period

17 of the 19 bona fide Z Cams have orbital periods in the literature. All have periods from 3.048 hours (0.127d) to 8.4 hours (0.38d), the average being 5.272 hours (0.2196d). The distribution of orbital periods is shown in Figure 22.

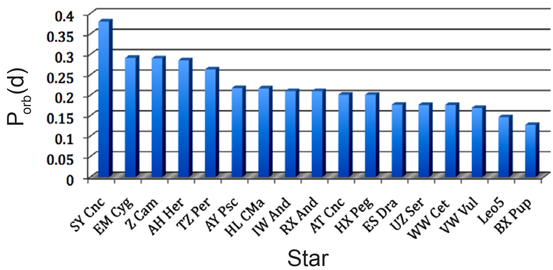

Figure 22. The distribution of orbital periods for 17 of the 19 confirmed Z Cams.

4.3. Outburst cycle

Z Cams are very active systems. Most have outburst cycles (the time between successive maxima) between 10 and 30 days. Their normal cycles between maxima and minima look very much like UGSS stars but they spend very little time at minimum.

4.4. Outburst amplitudes

Outburst amplitudes of Z Cam stars range from 2.3 to 4.9 magnitudes in V (Figure 23). The average amplitude is 3.7V. This is identical to the range of amplitudes seen in UGSS stars, so it cannot be used to distinguish them from these more common DNe. It does set them apart from NLs with smaller-amplitude changes and UGSU and WZ Sge stars with larger-amplitude outbursts.

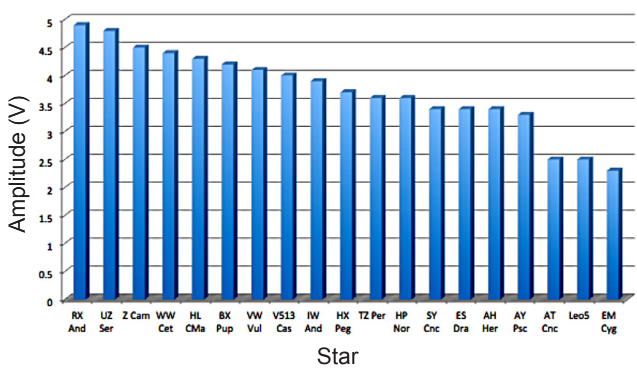

Figure 23. Outburst amplitudes (V magnitudes) for Z Cam stars.

4.5. VY Scl-like fading episodes

VY Sculptoris stars are CVs that behave much like NLs at maximum light; they may vary by up to one magnitude and they show no outbursts. Occasionally VY Scl stars undergo random fadings of two magnitudes or more. These episodes can last from days to years. Some Z Cam stars also exhibit dramatic fadings in their light curves, where they can bottom out at magnitudes fainter than their normal range (Figure 24).

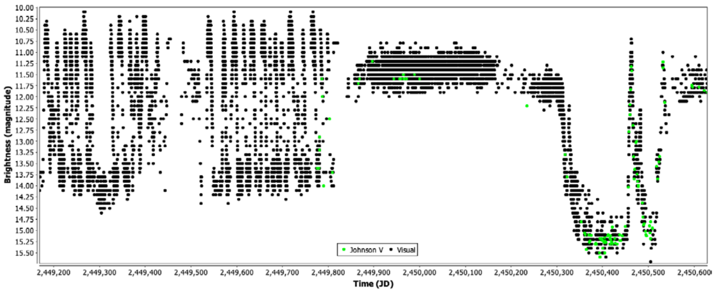

Figure 24. This AAVSO light curve of RX And shows two fading episodes. The short one (on the left) lasts about two months at about the normal magnitude range at minimum. The deeper fade (on the right) lasts 4.5 months and repeats after a brief outburst to maximum.

5. Misclassified Z Cams

The literature, CV catalogs, and the historical record are littered with stars classified as Z Cams or possible Z Cams, often based on slim, or no evidence. Some of these misclassified stars have been assumed to be Z Cams for a half-century or more. In fact, some have been touted as prototypical stars of the class and were used in studies characterizing the class of Z Cam stars. While many of these stars exhibit some of the characteristics, none of them are Z Cams.

As with the bona fide Z Cam stars, the entire sets of AAVSO data for each star were downloaded and the light curves were examined visually, both in gross, multi-year displays, and in close detail, cycle by cycle. Start dates of the data set and the beginnings and endings of outbursts could be determined by selecting individual data points on the light curve, displaying the detailed observational information in VSTAR.

Average cycle times were determined using a custom designed tool in VSTAR. Maxima could be hand-selected individually, and the average time between selections and mean magnitude were automatically calculated. The averages of the densest data sets were then calculated to derive the mean magnitude of maxima and the mean time between selections. The stars are listed below in order of R.A. Each star's position, maximum and minimum, and type are given in Table 2.

TW Tri There are no indications of standstills in the AAVSO data from August 1995 to the present. This star is a UGSS with an average cycle time of 22 days and amplitude of ~3.5 magnitudes in V.

KT Per Long considered a proto-typical Z Cam star, there are no indications of standstills in the AAVSO data from September 1967 to the present. This star is a UGSS with a ZZ Cet white dwarf. It has an average cycle time of 16.5 days and amplitude of ~4 magnitudes in V.

AM Cas There are no indications of standstills in the AAVSO data from September 1988 to the present. This star is a UGSS with an average cycle time of 21.4 days and amplitude of ~4 magnitudes in V.

Table 2: Variable stars misclassified as Z Cam–type in the historical record.

Name	*R.A. (2000)* *h m s*	*Dec. (2000)* ° ′ ″	*Max*	*Min*	*Type*
TW Tri	01 36 37.01	32 00 39.9	13.3p	17.0p	UGSS
KT Per	01 37 08.78	50 57 20.3	10.6V	16.1V	UGSS+ZZ
AM Cas	02 26 23.38	71 18 31.5	12.3p	15.2p	UGSS
FO Per	04 08 34.98	51 14 48.2	11.8V	16V	UGSS
AQ Eri	05 06 13.12	–04 08 07.3	12.5p	16.5p	UGSU
BI Ori	05 23 51.77	01 00 30.6	13.2p	16.7p	UGSS
FS Aur	05 47 48.36	28 35 11.1	14.4p	16.2p	UGSU:
CN Ori	05 52 07.79	–05 25 00.5	11.9v	16.3v	UGSS
V344 Ori	06 15 18.95	15 30 59.3	14.2p	17.5:p	UG
SV CMi	07 31 08.40	05 58 48.4	13.0p	16.9V	UGSS
UY Pup	07 46 31.25	–12 57 09.1	13.5V	15.8V	UG
SW Crt	11 52 25.41	–24 31 01.9	15.4CV	16.4CV	RRAB
CG Mus	12 20 13.08	–74 13 14.9	15.9p	17.0p	RRAB
V849 Her	16 35 45.72	11 24 58.1	15.0p	16.0p	NL
V391 Lyr	18 21 11.98	38 47 43.2	14.0p	17.0p	UG
V419 Lyr	19 10 13.91	29 06 14.0	14.4p	<17.5p	UGSU
V1504 Cyg	19 28 56.47	43 05 37.1	13.5p	17.4p	UGSU
FY Vul	19 41 29.95	21 45 59.0	13.4B	15.3B	NL
V1285 Cyg	19 44 49.51	35 59 34.4	13.1p	14.8p	SRB
AB Dra	19 49 06.51	77 44 22.9	12.3V	15.8V	UGSS
V1363 Cyg	20 06 11.53	33 42 37.6	13.0p	<17.6p	UGSU:
EV Aqr	21 06 17.87	00 52 43.9	11.3v	13.6V	SRA
BS Cep	22 29 05.43	65 14 41.9	13.9p	16.0p	UXOR
AY Oct	23 27 51.00	–75 40 40.7	15.0p	16.1p	RRAB

FO Per There are no indications of standstills in the AAVSO data from October 1956 to the present. This star is a UGSS with an average cycle time of 10.3 days and amplitude of ~5 magnitudes in V.

AQ Eri This star is a known UGSU with an orbital period of 0.06094 day (Thorstensen *et al.* 1996).

BI Ori There are no indications of standstills in the AAVSO data from November 1978 to the present. This star is a UGSS with an average cycle time of 16 days and amplitude of ~4 magnitudes in V.

FS Aur This star is a highly unusual CV, possibly a triple system with a magnetic and freely precessing white dwarf (Tovmassian 2010). It has an orbital period of 0.0595 day. It is not a Z Cam.

CN Ori Considered a typical Z Cam star for decades, there are no indications of standstills in the AAVSO data from January 1931 to the present. This star is a UGSS with an average cycle time of 16 days and amplitude of ~4 magnitudes in V.

V344 Ori There are no indications of standstills in the AAVSO data from October 1982 to the present. This star has a very long average cycle time of 443 days and an amplitude of ~5.5 magnitudes in V. This is either a UG or UGSU star.

SV CMi Classified as a Z Cam in nearly every CV catalogue, there are no indications of standstills in the AAVSO data from December 1961 to the present. This star is a UGSS with an average cycle time of 20-24 days and amplitude of ~4.5 magnitudes in V.

UY Pup There are no indications of standstills in the AAVSO data from February 1979 to the present. This star is a UGSS with an average cycle time of 57 to 60 days and amplitude of ~3.5 magnitudes in V.

SW Crt This is an RRAB variable with a period of 0.493164 day (Figure 25).

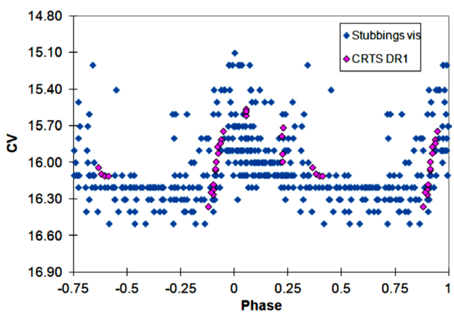

Figure 25. The light curve and period for SW Crt are from Otero (2012), derived from Rod Stubbings' visual data and the Catalina Real Time Survey data release 1 (Center for Advanced Computing Research 2013).

V849 Her This is a nova-like variable, possibly of the VY Scl sub-type. It has an orbital period of 0.1414 to 0.0030 day (Ringwald *et al.* 2012).

V391 Lyr There are no indications of standstills in the AAVSO data from April 1994 to the present. This star has a long average cycle time of ~110 days and an amplitude of ~4.2 magnitudes in V. V391 Lyr is a UG star.

V419 Lyr This star is a known UGSU with an orbital period of 0.0864 day.

V1504 Cyg This star is a known UGSU with an orbital period of 0.06951 day.

FY Vul This star has an amplitude of only 1.5 magnitudes in V and quasi-periodic modulations with peaks on average every 16 to 24 days. This star is a NL, not a Z Cam.

V1285 Cyg This is a red variable, spectral type M4IIIe, not a cataclysmic variable. It is a SRB varying irregularly between 13.1 and 14.8 p.

AB Dra This star has been touted as a prototypical Z Cam since the 1960s, but there are no indications of standstills in the AAVSO data from August 1938 to the present. This star is a UGSS with an average cycle time of 10.5 days and amplitude of ~3.5 magnitudes in V.

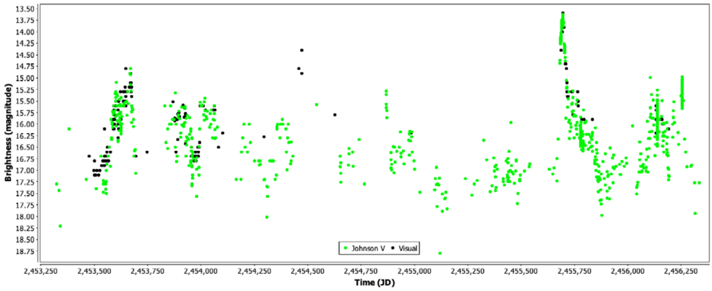

Figure 26. An AAVSO light curve of the long-term chaotic behavior of V1363 Cygni.

V1363 Cyg This is an intriguing UG with an amplitude of 4.5 magnitudes in V that may turn out to be a UGSU, but it is not a Z Cam star (Figure 26).

EV Aqr This is a red variable, a SRA varying between 11.2 and 13.8V with a period of 124.2 days.

BS Cep This star is an UXOR, spectral type Ae, varying irregularly between 13.9 and 16.0p. It is not a UGZ.

CG Mus Classified as a U Gem by Hoffmeister (1962) and as a possible UGZ in Downes and Shara (1993), this star was shown to be an RRAB with a period of 0.506815 day in Layden and Wachter (1997).

AY Oct Previously listed as a possible UGZ in Downes and Shara (1993), this variable was mentioned as a possible RRAB in Cieslinski *et al.* (1998), but the identification of the star was in question. It is fairly certain the RR Lyrae star in the field is AY Oct and it has a period of 0.589918 day.

6. Concluding remarks

Of the sixty-five stars variously listed in the literature and catalogs as Z Cams or possible Z Cams, nineteen have been positively confirmed as members of the class. Twenty-four have been eliminated from the list, leaving twenty-two stars that require further investigation. Of the remaining twenty-two stars, fourteen are very likely to be NL or UGSS, but they cannot be ruled out with the existing data (see Table 3). Further long-term observations will be required. The remaining seven hold some promise. PY Per and ST Cha both have intriguing light curves that need to be enhanced before a valid conclusion can be made. V426 Oph has many UGZ-like features in its light curve, but is probably an intermediate polar (Hellier *et al.* 1990; Homer *et al.* 2004; Ramsay *et al.* 2008). The remaining four stars, V868 Cyg, V1404 Cyg, V1505 Cyg, and MN Lac, are quite faint at minimum and will require extra effort to monitor deeply enough and densely enough to make a determination of their true nature and classification. From the data currently at hand in the AAVSO International Database, V868 Cyg looks like it could be another unusual star, similar to IW And and V513 Cas.

Table 3. Remaining Suspected Z Cams.

Name	*R.A. (2000)* h m s	*Dec. (2000)* ° ′ ″	*Max*	*Min*	*Preliminary Type*
HS 0139+0559	01 41 39.93	06 14 37.5	15.2	—	NL:
HS 0229+8016	02 35 58.20	80 29 44.2	13.7	15	NL:/VY:
V392 Per	04 43 21.39	47 21 25.8	15.2p	<17.5p	UG:
V368 Per	02 47 32.70	34 58 27.4	15.2p	<17.5p	UG:
PY Per	02 50 00.15	37 39 22.2	13.8p	16.5p	UGZ:
HS 0642+5049	06 46 19.60	50 45 49.3	15.6	—	NL
WZ CMa	07 18 49.20	–27 06 43.2	14.5p	18.3p	UGSS:
ST Cha	10 47 15.61	–79 28 06.9	12.4V	15.3V	UGZ:
V735 Sgr	17 59 51.83	–29 33 55.5	13.5p	16.5p	ISB:
V426 Oph	18 07 51.69	05 51 47.9	11.5V	13.5V	UGZ:/DQ:
BP CrA	18 36 50.89	–37 25 53.6	13.5v	15.9v	UGZ:
HS 1857+7127	18 57 20.36	71 31 18.8	13.9v	17.2V	UGSS+E:
V868 Cyg	19 29 04.50	28 54 26.0	14.3p	<17.8p	UGZ:
V1505 Cyg	19 29 49.00	28 32 54.0	15.2p	<17.5p	UGZ:
V991 Aql	19 35 34.84	06 33 45.8	14p	16p	UXOR:
V1101 Aql	20 13 04.07	15 35 46.8	14.3V	14.7V	CV:
IS Del	20 31 09.58	16 23 08.8	15.0p	<17.5p	UGSS:
TT Ind	20 33 37.08	–56 33 44.6	12.9V	18.3V	UG:
HS 2133+0513	21 35 59.30	05 27 00.0	15.2V	<19.9V	NL/VY
V1404 Cyg	21 57 16.39	52 12 00.5	15.1V	20.1:V	UGZ:
MN Lac	22 23 04.63	52 40 58.9	15.1p	<18.0p	UGZ:
HS 2325+8205	23 26 50.29	82 22 11.2	13.8V	17.8V	UG+E:/UGZ+E:

This study has weeded out the imposters from the real Z Cams often cited in the literature and CV catalogues of the past. It may now be worthwhile to re-investigate conclusions drawn in earlier studies of Z Cam characteristics based on samples that contained stars that were not Z Cam stars (Meyer and Meyer-Hofmeister 1983; Szkody and Mattei 1984; Shafter *et al.* 2005). Today's catalogues, such as Ritter and Kolb (2003), should be revised to reflect our current understanding of these fascinating and complex systems.

It is significant that we have reduced the number of known Z Cams from the often stated "30 members or so" (Buat-Menard *et al.* 2001) to less than twenty. This is an extremely small percentage of the thousands of known CVs, and may indicate that Z Cam stars represent a brief stage in CV evolution.

In the context of CV evolution, the "hibernation scenario" (Shara *et al.* 1986) suggests that all dwarf novae will eventually become classical novae or have already experienced a classical nova eruption in the past. It has now been shown that Z Cam and AT Cnc, both bona fide members of the Z Cam class, have classical nova shells (Shara *et al.* 2007, 2012a, 2012b), demonstrating that at least some classical novae have evolved into dwarf novae.

It is clear we still lack an explanation of the root cause of the increased mass accretion rates that trigger standstills, and what ends them. Perhaps with a more homogeneous sample to model, the answers will be found. Having cleared away the imposters, we can now more effectively redouble our observational energies on the genuine class members, and gather the remaining data needed to do a meaningful study of this small population of CVs, including orbital periods, spectra in high, low, and standstill states, masses and radii of the primary and secondary components of these systems, and the systematic search for other classical novae shells around Z Cam stars.

7. Acknowledgements

The authors acknowledge with thanks the variable star observations from the AAVSO International Database contributed by observers worldwide and used in this research. Special thanks go to David Benn for his technical assistance and support. The authors also wish to thank Arne Henden, Steve Howell, and Paula Szkody for their guidance and encouragement, and the anonymous referee whose helpful suggestions made the paper more complete.

References

AAVSO. 2013, observations from the AAVSO International Database (http://www.aavso.org).

Benn, D. 2012, *J. Amer. Assoc. Var. Star Obs.*, **40**, 852.

Buat-Menard, V., Hameury, J.-M., and Losota, J.-P. 2001, *Astron. Astrophys.*, **369**, 925.

Campbell, L., and Jacchia, L. 1941, *The Story of Variable Stars*, Blakiston Co., Philadelphia.

Center for Advanced Computing Research, California Institute of Technology, Pasadena. 2013, Catalina Real-Time Transient Survey (crts. caltech.edu).

Cieslinski, D., Steiner, J. E., and Jablonski, F. J. 1998, *Astron. Astrophys.*, **131**, 119.

Collinson, E. H., and Isles, J. E. 1979, *J. Br. Astron. Assoc.*, **89**, 169.

De Roy, F. 1932, *Gaz. Astron.*, **19**, 1.

Dirks, D. W. 1941, *Bull. Astron. Inst. Netherlands*, **9**, 197.

Downes, R. A., and Shara, M. M. 1993, *Publ. Astron. Soc. Pacific*, **105**, 127.

Elvey, C. T., and Babcock, H. W. 1943, *Astrophys. J.*, **97**, 412.

Glasby, J. 1971, *The Variable Star Observers Handbook*, Sedgwick and Jackson, London.

Hellier, C. 2001, *Cataclysmic Variable Stars*, Springer-Praxis, Chichester, U.K.

Hellier, C., O'Donoghue, D., Buckley, D., and Norton, A. 1990, *Mon. Not. Roy. Astron. Soc.*, **242**, 32.

Hoffmeister, C. 1962, *Z. Astrophys.*, **55**, 290.

Homer, L., *et al.* 2004, *Astrophys. J.*, **610**, 991.
Layden, A., and Wachter, S. 1997, *Publ. Astron. Soc. Pacific*, **109**, 977.
Mansperger, C. S., Kaitchuck, R. H., Garnavich, P. M., Dinshaw, N., and Zamkoff, E. 1994, *Publ. Astron. Soc. Pacific*, **106**, 858.
Mercado, L., and Honeycutt, R. K. 2002, *Bull. Amer. Astron. Soc.*, **34**, 1162.
Meyer, F., and Meyer-Hofmeister, E. 1983, *Astron. Astrophys.*, **121**, 29.
Nijland, A. A. 1930, *Bull. Astron. Inst. Netherlands*, **5**, 243.
Oppenheimer, B. D., Kenyon, S. J., and Mattei, J. A. 1998, *Astrophys. J.*, **115**, 1175.
Otero, S. 2012, private communication.
Ramsay, G., Wheatley, P., Norton, A. J., Hakala, P., and Baskill, D. 2008, *Mon. Not. Roy. Astron. Soc.*, **387**, 1157.
Ringwald, F. A., Rude, G. D., Roveto, J. J., and Khamvongsa, K. S. 2012, *New Astron.*, **17**, 570.
Ringwald, F. A., and Velasco, K. 2012, *New Astron.*, **17**, 108.
Ritter, H., and Kolb, U. 2003, *Astron. Astrophys.*, **404**, 301 (update RKcat7.18, 2012).
Samus, N. N., *et al.* 2007–2009, *General Catalogue of Variable Stars*, online catalogue (http://www.sai.msu.su/groups/cluster/gcvs/gcvs).
Shafter, A. W., Cannizzo, J. K., and Waagen, E. O. 2005, *Publ. Astron. Soc. Pacific*, **117**, 931.
Shara, M. M., Livio, M., Moffat, A. F. J., and Orio, M. 1986, *Astrophys. J.*, **311**, 163.
Shara, M. M., Mizusawa, T., Wehinger, P., Zurek, D., Martin, C. D., Neill, J. D., Forster, K., and Seibert, M. 2012a, *Astrophys. J.*, **758**, 121.
Shara, M., Mizusawa, T., Zurek, D., Martin, C. D., Neill, J. D., and Seibert, M. 2012b, *Astrophys. J.*, **756**, 107.
Shara, M. M., *et al.* 2007, *Nature*, **446**, 159.
Simonsen, M. 2011, *J. Amer. Assoc. Var. Star Obs.*, **39**, 66.
Simonsen, M., and Stubbings, R. 2011, *J. Amer. Assoc. Var. Star Obs.*, **39**, 73.
Smak, J. 2004, *Acta Astron.*, **54**, 181.
Stehle, R., King, A., and Rudge, C. 2001, *Mon. Not. Roy. Astron. Soc.*, **323**, 584.
Szkody, P., and Mattei, J. A. 1984, *Publ. Astron. Soc. Pacific*, **96**, 988.
Thorstensen, J. R., Patterson, J. O., Shambrook, A., and Thomas, G. 1996, *Publ. Astron. Soc. Pacific*, **108**, 73.
Toone, J. 2012, *BAA Var. Star Sect. Circ.*, No. 153, 23.
Tovmassian, G. 2010, arXiv1009.5813T.
Warner, B. 1995, *Cataclysmic Variable Stars*, Cambridge Univ. Press, Cambridge.
Wils, P., Krajci, T., and Simonsen, M. 2011, *J. Amer. Assoc. Var. Star Obs.*, **39**, 77.

ST Chamaeleontis and BP Coronae Australis: Two Southern Dwarf Novae Confirmed as Z Cam Stars

Mike Simonsen
AAVSO, 49 Bay State Road, Cambridge, MA 02139; mikesimonsen@aavso.org

Terry Bohlsen
Mirranook Observatory, Booroolong Road, Armidale, NSW, Australia; terry.bohlsen@bigpond.com

Franz-Josef (Josch) Hambsch
Oude Bleken 12, Mol, 2400, Belgium; hambsch@telenet.be

Rod Stubbings
2643 Warragul—Korumburra Road, Tetoora Road, Vic, Australia; stubbo@sympac.com.au

Received December 12, 2013; accepted January 20, 2014

Abstract Z Camelopardalis (Z Cam) stars are a subset of dwarf novae distinguished by the occurrence of “standstills”—periods of relative constant brightness one to one and a half magnitudes fainter than maximum brightness. As part of an ongoing observing campaign, the Z CamPaign, the authors focused attention on several Z Cam suspects in the southern hemisphere. Two stars, BP CrA and ST Cha, were found to exhibit standstill behavior in 2013, thus confirming them as Z Cam-type systems. This adds two more bona fide members to the nineteen confirmed Z Cams, bringing the total to twenty-one.

1. Introduction

Dwarf novae are a subset of cataclysmic variables, close binary pairs consisting of a white dwarf (WD) primary and a main sequence secondary. The primary accretes matter from the secondary star through the inner Lagrangian point, forming a disk around the WD primary in non-magnetic systems.

Z Cam stars are a subset of dwarf novae that, along with the typical dwarf nova outbursts and relatively brief periods of quiescence, occasionally display standstills in their light curves. It is these standstills that set the Z Cam stars apart from all other dwarf novae (Simonsen *et al.* 2014).

Since their discovery in the late 19th century, our understanding of dwarf novae has grown immeasurably. Along the way, our classifications and definitions have evolved to what they are today, causing some stars to be reclassified. This is especially true for the Z Cam stars whose definition has evolved considerably since being introduced over eighty years ago.

2. History

As with nearly all the bona fide and suspected Z Cams in the literature, the classifications of BP CrA and ST Cha have been the subject of confusion and debate for many years. This has been caused, in large part, by the evolution of the definition of Z Cams over time (Simonsen *et al.* 2014). In the case of many southern Z Cams and suspects there has historically been sparse coverage, which has led to misclassifications based on incomplete light curves and a lack of reliable information.

2.1. ST Cha

ST Cha was discovered in 1934 as an irregular variable (Luyten 1934). During the next seventy-nine years it became variously classified as rapidly irregular, RW Aur, IS, T Tau, and a dwarf nova. Included in a study of RW Aur stars in 1974 (Glass and Penston 1974), ST Cha was not detected in the JHKL infrared bands. However, it was not included in the list of stars considered not to be RW Aur stars in that paper. Still considered a pre-main sequence star in 1975, ST Cha was classified as a T Tau star (Mauder and Sosna 1975). UBVRI photometry obtained in 1986 (Cieslinski *et al.* 1998) suggested a dwarf nova classification. Downes and Shara adopted this classification in their *Catalog and Atlas of Cataclysmic Variables* (Downes *et al.* 2001). Another noteworthy CV catalog (Ritter and Kolb 2003) has it ambiguously classified as a possible nova-like variable or suspected dwarf nova that might be a Z Cam sub-type. The *General Catalogue of Variable Stars* (GCVS) still lists ST Cha as an IS type, a rapidly irregular variable not associated with nebulosity, as of December 2013 (Samus *et al.* 2007).

2.2. BP CrA

BP CrA was initially classified as an irregular variable of the SS Cyg (UGSS) type from plates from the Union Observatory, Johannesburg, South Africa (van Gent 1933). In 1960 it was suspected of being a Z Cam-type variable (Petit 1960), but in 1961 it was re-classified as a possible RW Aur-type variable by the same author (Petit 1961). It was later observed in a systematic attempt to determine which southern cataclysmic variables (CVs) might be binary stars by monitoring for eclipses (Mumford 1971). BP CrA is listed as a U Gem star in that paper. No eclipses were found. BP CrA's specific sub-classification remained unclear in papers published even after the nature of CVs was better understood, with some listing it as simply U Gem (Echevarria and Jones 1983) and others classifying it as a member of the Z Cam type (Vogt and Bateson 1982; Bruch 1983; Pretorius *et al.* 2006; Downes *et al.* 2001; Warner and Woudt 2006). The GCVS still classified BP CrA as a suspected Z Cam as late as 2013 (Samus *et al.* 2007). To this day, the orbital period of BP CrA is unknown.

3. Standstills of ST Cha and BP CrA

All observations in this paper are from the AAVSO International Database (AAVSO 2013). All ight curves were created using VSTAR (Benn 2012). Black dots are visual data, other dots are CCDV data.

3.1. ST Cha

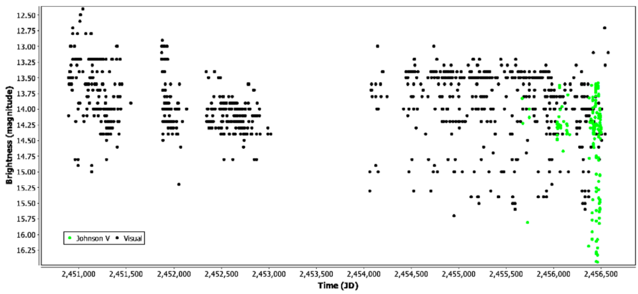

Figure 1. Long-term AAVSO light curve for ST Cha. It appears to show more-or-less common dwarf nova behavior from JD 2450892 to 2452134 (March 20, 1998–August 13, 2001). Then there is a period that could be interpreted as a standstill, or even nova-like behavior, from JD to 2452353 to 2453023 (March 17, 2002–January 18, 2004). After a significant gap in the data, typical dwarf nova behavior, with outbursts and quiescences, resumes from JD 2454062 (November 22, 2006) to the present.

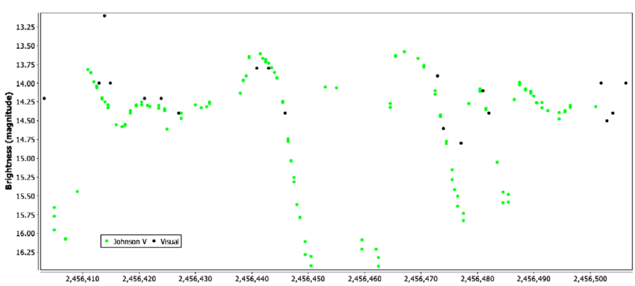

Figure 2. Embedded in the ST Cha light curve from 2013, the almost daily snapshot CCDV observations reveal a complex behavior featuring standstills followed by outbursts and minima in rapid succession, reminiscent of V513 Cas and IW And (Simonsen 2011; Szkody *et al.* 2013), confirming the Z Cam classification of ST Cha.

3.2. BP CrA

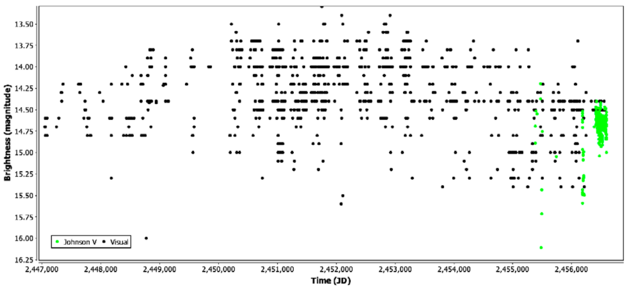

Figure 3. The long-term AAVSO light curve for BP CrA showing the spotty coverage dating back to 1987 and the recent concentrated effort beginning just before the first recorded standstill. There are no obvious standstills in the data until 2013 (beginning JD 2456362).

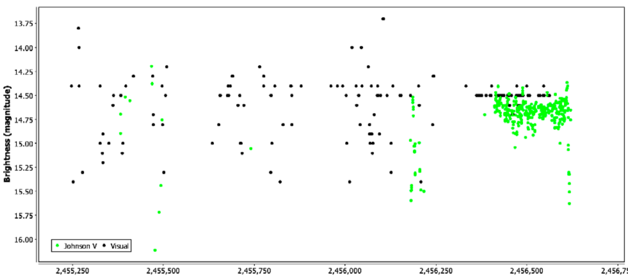

Figure 4. The more recent detailed AAVSO light curve, showing the first recorded standstill of BP CrA beginning JD 2456362 and ending JD 2456615 (March 10–November 18, 2013). This unambiguous example of a standstill confirms the status of BP CrA as a Z Cam dwarf nova.

4. Conclusions

Newly-acquired data clearly demonstrate the existence of standstills in the light curves of ST Cha and BP CrA, making them bona fide members of the Z Cam class of dwarf novae. This classification and their other known properties are listed in Table 1.

Table 1. Properties of two new Z Cam systems.

Name	*R.A. (2000)* *h m s*	*Dec. (2000)* ° ′ ″	*Max.*	*Min.*	*Type*	*Orbital period*
ST Cha	10 47 15.91	–79 26 07.2	12.4V	16.4V	UGZ	6.84 hrs
BP CrA	18 36 50.89	–37 25 53.6	12.7V	16.4V	UGZ	unknown

5. Acknowledgements

We acknowledge with thanks the variable star observations from the AAVSO International Database contributed by observers worldwide and used in this research. This research has made use of NASA's Astrophysics Data System.

References

AAVSO. 2013, observations from the AAVSO International Database (http://www.aavso.org).

Benn, D. 2012, J. Amer. Assoc. Var. Star Obs., **40**, 852.

Bruch, A. 1983, *Inf. Bull. Var. Stars*, No. 2287, 1.

Cieslinski, D., Steiner, J. E., and Jablonski, F. J. 1998, *Astron. Astrophys., Suppl. Ser.*, **131**, 119.

Downes, R. A., Webbink, R. F., Shara, M. M., Ritter, H., Kolb, U., and Duerbeck, H. W. 2001, *Publ. Astron. Soc. Pacific*, **113**, 764.

Echevarria, J., and Jones, D. 1983, *Rev. Mex. Astron. Astrofis.*, **5**, 301.

Glass, I. S., and Penston, M. V. 1974, *Mon. Not. Roy. Astron. Soc.*, **167**, 237.

Luyten, W. J. 1934, *Astron. Nachr.*, **253**, 135.

Mauder, H., and Sosna, F. M., 1975, *Inf. Bull. Var. Stars*, No. 1049, 1.

Mumford, G. 1971, *Astrophys. J.*, **165**, 369.

Petit, M. 1960, *J. Obs.*, **43**, 17.

Petit, M. 1961, *J. Obs.*, **44**, 6.

Pretorius, M. L., Warner, B., and Woudt, P. A. *Mon. Not. Roy. Astron. Soc.*, 2006, **368**, 361.

Ritter, H., and Kolb, U. 2003, *Astron. Astrophys.*, **404**, 301 (updated RKcat7.20, 2013).

Samus, N. N., et al. 2007–2009, *General Catalogue of Variable Stars*, online catalogue (http://www.sai.msu.su/groups/cluster/gcvs/gcvs).

Simonsen, M. 2011, *J. Amer. Assoc. Var. Star Obs.*, **39**, 66.

Simonsen, M., *et al.* 2014, *J. Amer. Assoc. Var. Star Obs.*, **42**, 177.

Szkody, P., *et al.* 2013, *Publ. Astron. Soc. Pacific*, **125**, 1421 (arXiv1311.1557).

van Gent, H. 1933, *Bull. Astron. Inst. Netherlands*, **7**, 21.

Vogt, N., and Bateson, F. M. 1982, *Astron. Astrophys., Suppl. Ser.*, **48**, 383.

Warner, B., and Woudt, P. A. 2006, *Mon. Not. Roy. Astron. Soc.*, **367**, 1562.

OQ Carinae—A New Southern Z Cam-Type Dwarf Nova

Rod Stubbings
Tetoora Road Observatory, 2643 Warragul-Korumburra Road, Tetoora Road 3821, Victoria, Australia; stubbo@sympac.com.au

Mike Simonsen
AAVSO, 49 Bay State Road, Cambridge, MA 02138; mikesimonsen@aavso.org

Received February 19, 2014; revised March 3, 2014; accepted March 3, 2014

Abstract Long-term optical monitoring of the dwarf nova OQ Car has been conducted to study the previously unknown behavior of this star system. The observations have shown OQ Car to have frequent dwarf nova outbursts and revealed the first recorded standstill of this star system. Based on this, we conclude that OQ Car is a new member of the Z Cam type of dwarf novae.

1. Introduction

Z Camelopardalis (Z Cam) stars are known for random standstills midway between their outburst and quiescence states. The defining features show a fairly large degree of constant brightness, around 1 to 1.5 magnitudes below the outburst state. The standstills can last for a few days, months, or years. The orbital periods of Z Cams are shown all to be over 3 hours (Simonsen *et al.* 2014b).

Z Cam stars appear to be a relatively rare group as there are currently only 21 known confirmed systems (Simonsen *et al.* 2014a).

2. History

Spectroscopic observations established OQ Car to be a cataclysmic variable (CV). A dwarf nova classification was suggested due to the variation seen the UBVRI data (Cieslinski *et al.* 1998). There was no period found up to 6 hours. This could be due to the low inclination of the system or the orbital period may exceed 6 hours. It was noted that the mean average magnitude from those observations was 15.8V (Woudt *et al.* 2005).

OQ Car is classified as a UG star in the AAVSO International Variable Star Index (VSX) (Watson *et al.* 2013) with a range of 14.5–17p. No previous long term monitoring of this object has been undertaken.

3. Observations

Close monitoring of the unstudied dwarf nova OQ Car commenced in July 2000 to establish the characteristics of this object. The observations have shown

OQ Car to be a very-frequently outbursting dwarf nova. Light curve analysis has shown an average outburst cycle of 14.9 days, which suggests little time is spent at minimum. The author's data have been uploaded to the AAVSO International Database (AAVSO 2013–2014).

The average cycle time was determined using a custom designed tool in VSTAR (Benn 2012). Maxima were hand selected individually, and the average times between selections were automatically calculated. The averages of the densest data sets were then calculated to derive the mean time between selections.

The brightest maxima observed reach magnitude 13.6 visual, which exceeds the VXS range of 14.5–17p. The minima were not observed directly in this study, as the visual observations extend only to a depth of 15.8 (Figure 1).

In January 2014, following a normal outburst, OQ Car failed to return to its faint state and entered into a standstill (Figure 2). The standstill, with a mean magnitude of 14.7 has lasted over 38 days so far.

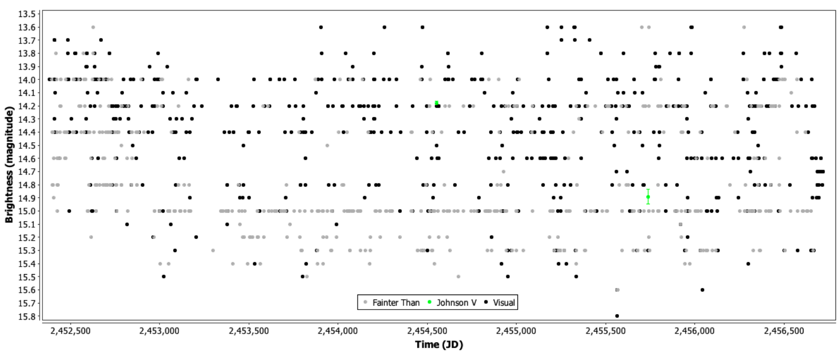

Figure 1. AAVSO historical data for OQ Car JD 2452383–2456717 (April 18, 2002–March 1, 2014) showing the normal, active dwarf nova behavior of this star. Black dots are visual data, green (with error bars) are Johnson V, and blue are upper limits.

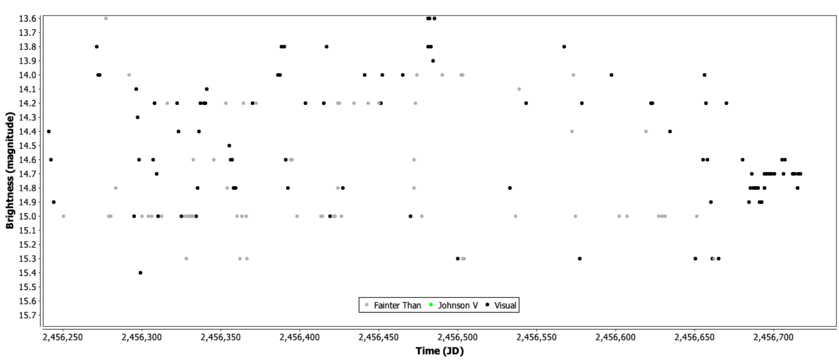

Figure 2. AAVSO visual data for OQ Car, showing the first known standstill of this star (far right), beginning JD 2456679, through JD 2456717 (January 22, 2014–March 1, 2014). Black dots are visual data, blue are upper limits.

4. Conclusion

The first long-term optical monitoring of OQ Car over fourteen years has revealed a very active dwarf nova with an outburst cycle of 14.9 days and an amplitude of 13.6v–17p. The orbital period remains unknown. The January 2014 standstill is a unique feature that has not been previously observed. Approximately 1 magnitude fainter than maximum, the current standstill has well exceeded the outburst cycle of 14.9 days, lasting over 38 days so far. We conclude that this confirms OQ Car to be a Z Cam-type dwarf nova.

5. Acknowledgements

This research has made use of the AAVSO International Variable Star Index (VSX) database, operated at AAVSO, Cambridge, Massachusetts. The authors wish to thank the anonymous referee whose comments and suggestions made this a better paper.

References

AAVSO. 2013–2014, observations from the AAVSO International Database (http://www.aavso.org).

Benn, D. 2012, *J. Amer. Assoc. Var. Star Obs.*, **40**, 852.

Cieslinski, D, Steiner, J. E., and Jablonski, F. J. 1998, *Astron. Astrophys., Suppl. Ser.*, **131**, 119.

Simonsen, M., Bohlsen, T., Hambsch, J., and Stubbings, R. 2014a, *J. Amer. Assoc. Var. Star Obs.*, **42**, 199.

Simonsen, M., *et al.*, 2014b, *J. Amer. Assoc. Var. Star Obs.*, **42**, 177.

Watson, C., Henden, A. A., and Price, A. 2013, AAVSO International Variable Star Index VSX (Watson+, 2006–2013; http://www.aavso.org/vsx).

Woudt, P. A., Warner, B., and Spark, M. 2005, *Mon. Not. Roy. Astron. Soc.*, **364**, 107.

The Ellipsoidal Variable b Persei

Steven L. Morris
Los Angeles Harbor College, Physics Dept., Wilmington, CA 90744; MorrisSL@lahc.edu

Received February 26, 2014; revised March 19, 2014 and April 4, 2014; accepted May 1, 2014

Abstract The bright (V = 4.6) ellipsoidal variable b Persei is unique, as it is a triple system that experiences an eclipse of the primary and secondary stars every 701.76 days by the tertiary component. This paper analyses the ellipsoidal light variations to show that the mass ratio is q = 0.28 ± 0.02 and the inclination is i = 43 ± 3°. Modeling the system with the Wilson-Devinney computer code leads to similar values of q = 0.25 ± 0.03 and i = 49 ± 10°.

1. Introduction

The star b Persei should not be confused with the better-known β Persei (= Algol = HR 936), which is 15.3° southwest of b Persei and is the prototype of the Algol eclipsing variable stars. The star b Persei (= HR 1324) consists of a bright primary star close to a faint, unseen secondary star in an orbital plane that does not generate eclipses. This close pair is orbited by a faint, distant tertiary star that is now known to eclipse the inner pair.

Ellipsoidal variable stars are close binaries whose components are distorted by their mutual gravitation. Though physically similar to eclipsing binaries with out-of-eclipse light variations, they have orbital inclinations that are too small to create eclipses, resulting in light variations that are typically only a few hundredths of a magnitude.

The slight light variations and the paucity of information that can be obtained from them have left the ellipsoidal variables as a neglected class of variable stars. Morris (1985) presents tables of confirmed, suspected, and rejected ellipsoidal variables, and describes a method of combining photometric and spectroscopic information to determine the physical parameters of such systems.

2. Previous work

Until recently, b Persei shared in this general neglect, despite its brightness (V = 4.6), short period (P = 1.5273639 days), and its accessibility to northern observers (δ = +50°). Stebbins (1923) discovered the variability of this star and published a good but unfiltered photoelectric light curve. The only other published light curve is by Duerbeck and Schettler (1979) who found, after their observations were obtained, that their DC amplifier was unstable.

Their published normal points are too noisy to be of much use in analyzing this system. A good comprehensive study of the radial-velocity data of this single-lined spectroscopic system is by Hill *et al.* (1976), who found that this is a triple system, with the tertiary star orbiting the close binary with a period of 701.76 days. They noted that five spectrographic plates taken on 1973 October 3 showed discrepant velocities that could be due to a partial eclipse by the tertiary star.

This system is of particular interest because it belongs to the small class of close binary systems with weak, non-periodic, non-thermal radio emission flares. Hjellming and Wade (1973) discovered the intermittent emission at 8.085 GHz, and Spangler *et al.* (1977) lists a possible detection at 5.0 GHz. Gibson and Hjellming (1974) modeled this radio emission as due to gravitational energization of matter flowing from one star to the other through the inner Lagrangian point of the system. This provides an important constraint in modeling b Persei, by forcing either the primary or secondary star to be close enough to filling its inner Lagrangian surface that the star provides enough matter to generate detectable radio emission flares.

The projected rotational velocity of the primary also provides a valuable constraint on models of the system, as short-period binaries are expected to be in synchronous rotation. Published values of vsini range from 70 km/s (Abt and Morrell 1995) to 98 ± 4 (Olson 1968). Hill *et al.* (1976) use vsini = 87 ± 3 km/s in their analysis, and this value is adopted for the present paper.

A study of the system's radial velocities by Hill *et al.* (1976) determined a mass function f(m) = 0.00966 $M_{\odot}$ for the single-lined spectroscopic binary formed by the primary and secondary stars, and a mass function f(m) = 0.0987 $M_{\odot}$ formed by the inner pair and the tertiary star. More recent work has not substantially altered these values.

One other constraint on the entire system is the separation of the tertiary star from the inner pair. Halbwachs (1981) calculated a maximum separation of 0.044 seconds of arc, so it is not surprising that the system has only recently been resolved by Hummel *et al.* (2013) with the Navy Precision Optical Interferometer, at a separation of 0.0095 seconds of arc.

In February 2013, Collins (2013) observed an eclipse of the ellipsoidal pair by the tertiary star of this system. Thus, b Persei in future may provide a unique light curve of two primary eclipses, distorted by the rapidly-changing positions of the inner pair. The parameters of this inner pair are now of considerable interest, and a high-quality, modern light curve is needed. In the meantime, photometry obtained in the 1980's and not previously published are here presented, along with an analysis.

3. Observations

The b Persei system was observed by the author on eight photometric nights at the Kitt Peak #4 16-inch reflector during February 1981. λ Persei was used as the comparison star because it is similar in color and magnitude to b Persei, and because it was the comparison star used by Stebbins (1923). An RCA gallium arsenide model #C31034A-02 photomultiplier tube was used in conjunction with a set of Johnson UBVRI filters as described by Bessell (1979), and in conjunction with a glass neutral-density filter (3.00 magnitudes in the V bandpass) because of the brightness of these stars. On each night, two blue and red pairs of standard stars were observed at small and large airmass to obtain the nightly extinction and transformation coefficients. These standard stars were taken from the lists of Crawford *et al.* (1971) and Barnes and Moffett (1979).

The times of primary minimum (assuming a circular orbit) are calculated from the elements of Hill *et al.* (1976) to be Min. I (hel.) = 2440001.49 + 1.5273639E. Radial velocities indicate that this occurs when the primary (A2 V) star is farthest from the observer. The original 132 data points per filter may be seen in the light curves of Morris (1983).

4. Analysis

All available b Persei light curves were fitted by least-squares to obtain discrete Fourier series coefficients, to compare the light curves with each other and to derive parameters of the binary system by using the method of Morris (1985). Sine terms, and cosine terms higher than $4\pi\times\varphi$ were found to be insignificant and were discarded, and the coefficients of the significant terms are given in Table 1. The mean magnitudes of b Persei on the Johnson UBVRI system were found to be 4.644 ± 0.004, 4.655 ± 0.005, 4.622 ± 0.003, 4.506 ± 0.004, and 4.524 ± 0.004, respectively.

A comparison between the C_0 values shows that Stebbins' unfiltered system is most closely approximated by Johnson's B bandpass, and a comparison of

Table 1. The coefficients fitting $C_0+C_1\cos(2\pi\times\varphi)+C_2\cos(4\pi\times\varphi)$ to the differential light curves, with λ Persei as the comparison star. The values in parentheses are the uncertainties of the last one or two digits.

Source	*Bandpass*	C_0	C_1	C_2
This paper	U	0.487(4)	0.009(2)	0.032(2)
	B	0.382(5)	0.003(2)	0.023(2)
	V	0.327(3)	0.007(1)	0.028(2)
	R	0.289(4)	0.010(2)	0.024(2)
	I	0.241(4)	0.015(2)	0.029(2)
Duerbeck & Schettler (1979)	U	0.491(8)	0.006(11)	0.034(12)
	B	0.368(10)	–0.008(15)	0.042(15)
	V	0.325(11)	–0.003(15)	0.038(16)
Stebbins (1923)	~B	0.374(1)	0.004(1)	0.024(1)

the C_1 and C_2 values indicate that the light curves have remained stable for several decades. The uncertainties of the C_1 and C_2 coefficients of Duerbeck and Schettler's data are so great that it seems reasonable to exclude them from further analysis.

The contributions to the luminosity of the system by the secondary and tertiary stars can be taken into account before modeling the variability of the primary. The secondary and tertiary lines are not clearly seen in the spectrum, but Hill *et al.* (1976) analyzed both the distortions in the hydrogen lines due to blending and the thirteen-color photometry of Mitchell and Johnson (1970) to find that the secondary and tertiary are best modeled as F0 V stars, with $\Delta B \sim 3.1$ between both the primary and secondary stars and the primary and tertiary stars.

5. System parameters

As previously mentioned, b Persei exhibits weak, non-periodic, non-thermal radio emission flares, and Gibson and Hjellming (1974) have modeled such radio emission as due to matter flowing through the inner Lagrangian point. The magnitude range of 0.057 ± 0.004 in the V bandpass is much too large to be due to variability of the faint secondary star, so it must be the primary that is filling, or close to filling, its inner Lagrangian surface. As shown below, the lack of eclipses indicates that the secondary star is indeed too small to fill its own inner Lagrangian surface.

If the primary star is assumed to fill its inner Lagrangian surface and to have a mass of $2.25M_{\odot}$ estimated from its spectral classification, the method of analysis in Morris (1985) determines that the system's mass ratio is $q = 0.28 \pm 0.02$, its inclination is $i = 43 \pm 3°$, and its projected rotational velocity is $v\sin i = 91 \pm 7$ km/s, which is reasonably close to the value of 87 ± 3 km/s from Hill *et al.* (1976). The radius of the primary star would be $4.1 \pm 0.2\ R_{\odot}$, which is larger than expected for an A2 V star, but may be justified by the primary's recent reclassification as A1 III by Abt (2009). The inclination is larger than the maximum value of 34.45° for a non-eclipsing contact system (Morris 1999), implying that the secondary star does not fill its inner Lagrangian surface.

The Wilson-Devinney computer code as described by Wilson and Devinney (1971) was also used to analyze this system, and it was found that the values of the mass ratio are tightly constrained, as $q < 0.20$ generates eclipses and $q > 0.29$ creates overflow of the primary star's inner Lagrangian surface. The normals (binned averages) of the data points are presented in Table 2, and Figure 1 shows the V light curve normals, symmetric around $\varphi = 0.50$. If the primary star's temperature is assumed to be $T_1 = 9000$ K based on its spectrum, then the most probable model of the system has $T_2 = 5500 \pm 500$ K, $q = 0.25 \pm 0.03$, $i = 49 \pm 10°$, $R_1 = 3.4 \pm 0.4\ R_{\odot}$ and, $R_2 = 2.1 \pm 0.3\ R_{\odot}$.

Table 2. Normals of the Johnson UBVRI photoelectric photometry of b Persei obtained in February 1981. The phases are calculated from Primary Minimum = HJD 2440001.49 + 1.5273639E.

Phase	*U*	*Phase*	*B*	*Phase*	*V*	*Phase*	*R*	*Phase*	*I*
0.0566	4.670	0.0452	4.699	0.0579	4.642	0.0425	4.502	0.0475	4.563
0.0973	4.668	0.0779	4.664	0.1000	4.635	0.0754	4.527	0.0875	4.538
0.1181	4.657	0.1128	4.664	0.1217	4.633	0.1122	4.519	0.1163	4.536
0.1384	4.642	0.1327	4.661	0.1437	4.621	0.1322	4.517	0.1374	4.532
0.1569	4.628	0.1529	4.647	0.1602	4.612	0.1526	4.503	0.1565	4.516
0.1728	4.631	0.1680	4.644	0.1774	4.611	0.1676	4.501	0.1721	4.523
0.1952	4.624	0.1889	4.639	0.2008	4.604	0.1883	4.494	0.1941	4.515
0.2240	4.616	0.2165	4.632	0.2288	4.594	0.2151	4.485	0.2222	4.509
0.2527	4.620	0.2437	4.628	0.2609	4.593	0.2434	4.483	0.2551	4.496
0.3239	4.617	0.3049	4.635	0.3311	4.600	0.3052	4.489	0.3217	4.485
0.3679	4.631	0.3596	4.657	0.3668	4.610	0.3569	4.489	0.3634	4.500
0.4010	4.648	0.3926	4.667	0.3928	4.616	0.3896	4.497	0.3961	4.510
0.4219	4.653	0.4176	4.666	0.4170	4.630	0.4164	4.514	0.4207	4.527
0.4402	4.661	0.4345	4.664	0.4342	4.635	0.4338	4.508	0.4392	4.535
0.4623	4.659	0.4574	4.666	0.4575	4.641	0.4577	4.517	0.4627	4.539
0.4787	4.667	0.4756	4.673	0.4757	4.643	0.4755	4.526	0.4800	4.543
0.4919	4.668	0.4912	4.671	0.4913	4.647	0.4916	4.519	0.4939	4.542

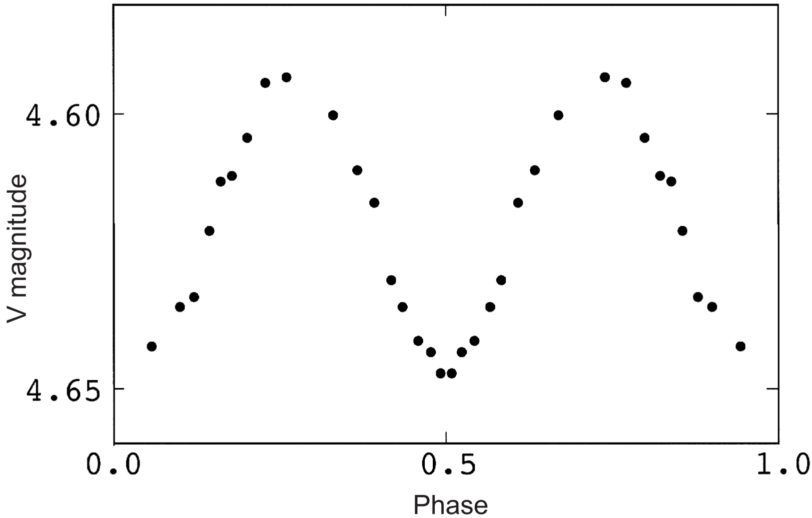

Figure 1. The light curve of b Persei (= HR 1324), symmetric around Phase = 0.5. The data for these normals were obtained in February 1981.

While these two different analyses are in reasonable agreement, a more accurate determination must await better light curves, a definitive value of vsini, and a mass ratio of the ellipsoidal pair, perhaps taken during mid-eclipse by the tertiary star.

6. Acknowledgements

The author thanks Dr. Eugene Milone for his assistance at all stages of his Ph.D. dissertation. The author also thanks Dr. Bruce Hrivnak for his assistance in learning how to use the Wilson-Devinney computer program.

References

Abt, H. A. 2009, *Astrophys. J., Suppl. Ser.*, **180**, 117.
Abt, H. A., and Morrell, N. I. 1995, *Astrophys. J., Suppl. Ser.*, **99**, 135.
Barnes, T. G., and Moffett, T. J. 1979, *Publ. Astron. Soc. Pacific*, **91**, 289.
Bessell, M. S. 1979, *Publ. Astron. Soc. Pacific*, **91**, 589.
Collins, D. F. 2013, *J. Amer. Assoc. Var. Star Obs.*, **41**, 391.
Crawford, D. L., Golson, J. C., and Landolt, A. U. 1971, *Publ. Astron. Soc. Pacific*, **83**, 652.
Duerbeck, H. W., and Schettler, A. 1979, *Acta Astron.*, **29**, 225.
Gibson, D. M., and Hjellming, R. M. 1974, *Publ. Astron. Soc. Pacific*, **86**, 652.
Halbwachs, J. L. 1981, *Astron. Astrophys., Suppl. Ser.*, **44**, 47.

Hill, G., Aikman, G. C. L., Cowley, A. P., Bolton, C. T., and Thomas, J. C. 1976, *Astrophys. J.*, **208**, 152.

Hjellming, R. M., and Wade, C. M. 1973, *Nature*, **242**, 250.

Hummel, C. A., Zavala, R. T., and Sanborn, J. 2013, *Cent. Eur. Astrophys. Bull.*, **37**, 127.

Mitchell, R. I., and Johnson, H. L. 1970, *Commun. Lunar Planet. Lab.*, **8**, 1.

Morris, S. L. 1983, *The Ellipsoidal Variable Stars*, Ph.D. dissertation, University of Calgary, 57–59.

Morris, S. L. 1985, *Astrophys. J.*, **295**, 143.

Morris, S. L. 1999, *Astrophys. J.*, **520**, 797.

Olson, E. C. 1968, *Publ. Astron. Soc. Pacific*, **80**, 185.

Spangler, S. R., Owen, F. N., and Hulse, R. A. 1977, *Astron. J.*, **82**, 989.

Stebbins, J. 1923, *Astrophys. J.*, **62**, 1.

Wilson, R. E., and Devinney, E. J. 1971, *Astrophys. J.*, **166**, 605.

Detecting Problematic Observer Offsets in Sparse Photometry

Tom Calderwood
1184 NW Mt. Washington Drive, Bend, OR 97701; tjc@cantordust.net

Received January 20, 2014; revised April 15, 2014; accepted April 23, 2014

Abstract A heuristic method, based upon histogram analysis, is presented for detecting offsets pervasive enough to be symptoms of problematic observing technique or calibration. This method is illustrated by a study of scatter in AAVSO photoelectric photometry (PEP) for five well-observed variable stars.

1. Data

The PEP data (Table 1) were obtained from the AAVSO International Database (AID; AAVSO 2014a). PEP magnitudes are established differentially from a single comparison star, including a correction for differential extinction. Only V band observations processed by the AAVSO reduction software, PEPHQ (AAVSO 2014b), with transformations to standard magnitudes were considered. W Boo, RS Cnc, P Cyg, V441 Her, and R Lyr had the most observations on record which qualified. B–V colors for the stars range from 0.339 to 1.662, and delta B–V from –0.813 to 1.265. The median magnitude error for observations of any one star was 3 or 4 mmag. The data were taken between JD 2445380 and 2456598, inclusive.

Table 1: Star Data.

Star	*Number Observations*	*Number Observers*	*Pairs*	*First Pair JD*	*Last Pair JD*	*Var B–V*	*Δ B–V*
W Boo	1410	29	237	2446945	2456478	1.662	0.608
RS Cnc	1031	26	109	2446881	2455261	1.625	1.265
P Cyg	1155	20	127	2446287	2456223	0.412	0.498
V441 Her	1156	20	168	2446953	2456171	0.339	–0.813
R Lyr	1571	26	283	2447387	2455124	1.588	0.546

2. Method

For a given star, pairs of magnitudes measured the same night by different observers were selected. It was uncommon for these stars to have more than two observations on a single night; those nights with three observations were split into three pairs. Repeat observations by the same observer were not paired for examination. From a star's set of pairs, a list is made of observers consistently brighter above a threshold, *T*, than other observers. A second list, based on the same threshold, is made of consistently dim observers. From these two lists, a "sore-thumb" observer, *S*, appearing the most times above a threshold, *N*, in either list is assumed to posses a systematic offset, and that offset value is estimated. This is done by histogramming the differences between *S*'s measurements and those of other observers. The histogram is evaluated by median and interquartile range (IQR). The magnitude difference of *S* from some observer *O* for one observation, i, is computed as:

$$\Delta V_i = V_{Si} - (V_{Si} / \sigma_{Si}^2 + V_{Oi} / \sigma_{Oi}^2) \times \left[(\sigma_{Si}^2 \times \sigma_{Oi}^2) / (\sigma_{Si}^2 + \sigma_{Oi}^2)\right] \quad (1)$$

A search is conducted over a range of hypothetical offsets, *o*, so that the absolute value of the median, $\kappa = |\mu_{1/2}|$, is minimized:

$$d(\kappa(\{\Delta V_i - o\})) = 0 \quad (2)$$

If a minimal median is attained over a range of offsets, the center of this range is taken to be the offset. Once observer *S*'s magnitudes have been adjusted to minimize κ, the process is repeated to find other observers with offsets.

3. Examples

The following procedure was used to find highly-offset observers for RS Cnc, with $T = 30$ mmag and $N = 10$. Table 2 gives histogram parameters for key observers before adjustments were made; Table 3 gives the dim/bright summary. Of these observers, E is most frequently offset. E's histogram is shown in Figure 1. The offset is sought via a simple incremental search in both directions from 0, in steps of 1 mmag. E is found to have an offset value of –28. E's magnitudes are then adjusted by this offset, and a new list of dim/bright observers is created (Table 4). An offset is now estimated for B, and found to be 67. Because adjusting B will likely change E's histogram, it is necessary

Table 2: Selected histograms before adjustments (mmag.).

Observer	*Median*	*IQR*	*Pairs*
A	8	13	13
B	53.5	67	22
E	–12	35	53

Table 3: Frequently-offset observers, first iteration.

Observer	*Bright or Dim*	*Frequent Counterparts*
A	dim 11 times	E
B	dim 17 times	C, D, E
E	bright 27 times	A, B

Table 4: Frequently-offset observers, second iteration.

Observer	*Bright or Dim*	*Frequent Counterparts*
B	dim 17 times	C, D, E
E	bright 16 times	A, B

Table 5: Histograms after adjustments (mmag.).

Observer	*Median*	*IQR*	*Δ IQR*
A	3	5	62%
B	0	28	58%
E	0	21	40%

Table 6: Sore-thumb observers and their offsets (mmag).

Star	S_1	S_2	*Δ B-V*
W Boo	A: 64	B: -49	0.608
RS Cnc	E: -25	B: 70	1.265
P Cyg	—	—	0.498
V441 Her	A: -41	E: 11	–0.813
R Lyr	A: 34	—	0.546

to iterate finding offsets for the two observers, and they converge to –25 for E and 70 for B. Once E and B have been adjusted, no other observers qualify as sore thumbs. The histogram improvements for A, B, and E are summarized in Table 5; E's final histogram is shown in Figure 2. Only one observer of R Lyr qualified as a sore thumb and none qualified for P Cyg (Table 6). Two observers each from V441 Her and W Boo qualified. If looser selection criteria for choosing outlying observers are permitted, allowing more adjustments to be made, the iteration process to establish stable offsets for all of them may not converge. From Table 6, it can be concluded that observers A and E have color correction (ε_V) errors. The signs of their offsets for each star either correlate or anti-correlate with the signs of the respective Δ B–V values.

4. Assumptions and limitations

The values of T and N were chosen to be conservative, but are otherwise arbitrary. No attempt was made to involve airmass in this analysis. Airmass data are not readily available for PEP observations in the AAVSO International Database (by convention, measurements are supposed to be taken at an airmass of 2 or less). The PEPHQ software approximates the first-order extinction

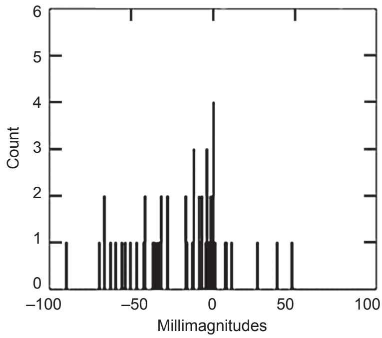

Figure 1. Observer E histogram before adjustment.

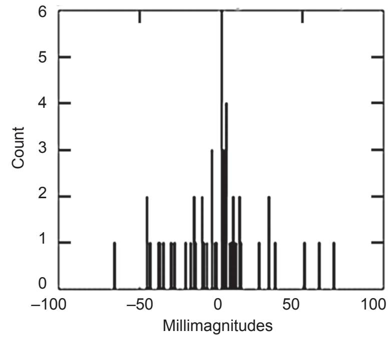

Figure 2. Observer E histogram after adjustment.

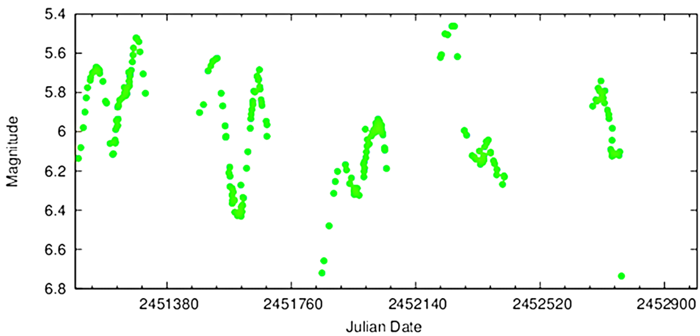

Figure 3. AAVSO light curve for RS Cnc, containing a moderately offset observer (highlighted in next figure).

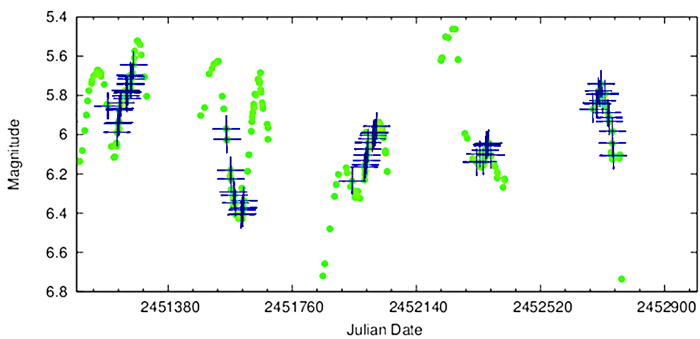

Figure 4. AAVSO light curve for RS Cnc, containing a moderately offset observer (identified by crosses).

coefficient, k_V, as a constant, 0.25. The observers found to have large offsets were, largely, active in disjoint time periods. Whether this technique would work with two or more highly-offset observers active simultaneously is unclear.

5. Conclusion

The method of this paper is simplistic, but the technique clearly detects observers with systematic offsets where limited data are available. While very large observer offsets may be readily apparent by visual inspection of a light curve, Figures 3, 4, and 5, illustrate a curve where the presence of a moderately offset observer (E), detected by this method, is not obvious.

6. Acknowledgements

Histograms in this paper were generated with MATPLOTLIB, a python graphics package developed by John Hunter (2012).

References

AAVSO. 2014a, observations from the AAVSO International Database (http://www.aavso.org).
AAVSO. 2014b, PEPHQ data reduction software.
Hunter, J. 2012, MATPLOTLIB graphics software (http://matplotlib.org/).

Analysis of Seven Years of Globe at Night Data

Jennifer J. Birriel
Department of Mathematics, Computer Science and Physics, Morehead State University, Morehead KY 40351

Constance E. Walker
National Optical Astronomical Observatory, 950 N. Cherry Avenue, Tucson, AZ 85719

Cory R. Thornsberry
Department of Mathematics, Computer Science, and Physics, Morehead State University, Morehead KY (current Address, Department of Physics and Astronomy, University of Tennessee, Knoxville TN 37996)

Received April 27, 2012; revised November 4, 2013, November 18, 2013; accepted November 19, 2013

Abstract The Globe at Night (GaN) project website contains seven years of night-sky brightness data contributed by citizen scientists. We perform a statistical analysis of naked-eye limiting magnitudes (NELMs) and find that over the period from 2006 to 2012 global averages of NELMs have remained essentially constant. Observations in which participants reported both NELM and Unihedron Sky Quality Meter (SQM) measurements are compared to a theoretical expression relating night sky surface brightness and NELM: the overall agreement between observed and predicted NELM values based on the reported SQM measurements supports the reliability of GaN data.

1. The Globe at Night (GaN) project

The faint band of the Milky Way as seen under a dark sky is very much a part of humanity's cultural and natural heritage. More than one-fifth of the world population, two-thirds of the United States population, and one-half of the European Union population have already lost naked-eye visibility of the Milky Way (Cinzano *et al.* 2001). This loss is caused by light pollution. Light pollution is artificial night sky brightness, directed up toward the sky and wasted. The International Dark-Sky Association estimates that one-third of outdoor lighting escapes unused into space, causing light pollution (IDA 2012). Under an unpolluted sky we ought to see a few thousand stars, yet we see only a couple hundred from most suburban areas. Light pollution is a serious and growing issue that impacts astronomical research, the economy, ecology, energy conservation, human health, public safety, and our shared ability to see the night sky. For this reason, the National Optical Astronomy Observatory has taken a lead in promoting activities on dark skies awareness by getting people worldwide involved in programs like the Globe at Night campaign (GaN 2013, http://www.globeatnight.org).

The campaign is easy and fun to do. First, you match the appearance of the campaign's constellation (Orion in the January, February, and March campaign and Leo in the March and April campaign, and so on) with simple star maps of progressively fainter stars. If you have a handheld, digital sky brightness meter known as a "Sky Quality Meter" or SQM (Unihedron 2013, http://www.unihedron.com/projects/darksky/), you have an opportunity to take more precise measurements of the night sky. With either or both of these measurements, you then submit them online, including the date, time, and location of your observation. If people have smart mobile phones or tablets, they can submit their measurements in real time. To do this, you can use the web application at www.globeatnight.org/webapp/. With smart phones and tablets, the location, date, and time are put in automatically. And if you do not have a smart phone or tablet, there are user-friendly tools on the Globe at Night report page to find latitude and longitude.

After all the campaign's measurements are submitted, the project's organizers release a map of light-pollution levels worldwide. Over the first seven annual campaigns, volunteers from more than 115 nations contributed 83,000 measurements. The data can be downloaded from www.globeatnight.org/analyze.html for comparisons with a variety of other data sets. (For an example, see this article's summary.) The formats for the GaN data files include csv, text, excel, (Google) kmz, ESRI geodatabase, and shape files.

2. Theoretical background

Night sky brightness as observed from the ground can be measured via a variety of methods. Semi-quantitative measures use the binocular vision of the unaided human eye: these include the naked-eye limiting magnitude, the Bortle Scale (Bortle 2001), and the visibility of the Milky Way (Moore 2001). All of these methods depend to some degree on observer age, visual acuity, and experience. Quantitative measures of night sky surface brightness include photographic or CCD photometry. The newly developed Unihedron Sky Quality Meter (SQM) is a portable, hand-held photometric device about the size of a deck of cards that contains a small CCD chip and on-board processor. The SQM is an extremely portable and inexpensive (less than $150) device designed to take quick and accurate (±0.10 magnitudes per square arcsecond) measurements of night sky surface brightness. Globe at Night participants can submit either naked-eye limiting magnitude (NELM) measurements or a combination of NELM and SQM measurements. (There are two models of SQM: the original model which has a FOV of ±40 degrees at FWHM, and the SQM-L which is equipped with a lens that reduces the FOV to ±10 degrees FWHM. The latter is primarily used now and is best used in cities where most of the Globe data come from.)

A theoretical relationship between naked-eye limiting magnitudes and night sky surface brightness was developed by Schaefer (1990) from empirical curves derived by Knoll *et al.* (1946). The relationship converted from Schaefer's equations 2, 16, and 17 is given by

$$\mathrm{NELM} = 7.93 - 5*\log(10^{(4.316 - (B/5))} + 1), \tag{1}$$

where B is the sky brightness in magnitudes per square arcsecond and NELM is simply the naked-eye limiting magnitude. This expression assumes binocular vision, natural pupils, and no atmospheric absorption; in addition, the observer was free to pick her/his own point of fixation. This relationship is utilized in the sky brightness nomogram on the Dark Skies Awareness (2011) website (http://www.darkskiesawareness.org/nomogram.php). Below, we will use Equation 1 as to evaluate the reliability of GaN data.

3. Statistical analysis of GaN data

One simple approach to using the Globe at Night data involves looking at global trends in NELMs over time. We might expect an overall increase in light pollution globally with increased industrialization or a decrease resulting from light pollution abatement programs in Europe and the Americas (for example, Dick (2000, 2010); Smith *et al.* (2006); Zitelli *et al.* (2001). Using a spreadsheet program, we plotted the relative frequencies of NELMs 1 through 7 from 2006 until 2012 (Figure 1). The general shape and centroid of each histogram varies slightly from year to year, but the centroids are clustered around 3–4. In any given year, the vast majority of measured naked eye limiting magnitudes lie between 3 and 5. Given that participants must choose which of the seven charts best fit her/his view of a given constellation, the uncertainty in measurements is, at best, ±0.5 magnitude and likely as high as ±1 magnitude. One could argue that the small changes observed in relative frequencies of NELM from 2006 to 2012 result from observational uncertainties and not from any real change in global NELMs. In an alternative approach, we plot all the NELM data from 2006 to 2012 on the same chart (Figure 2). Looking at the individual NELMS, it appears that there is a general upward trend in reported NELMs 1 through 3, indicating that more observers were seeing brighter skies. The opposite appears to be true of NELMs 4 through 7: there appears to be a general downward trend in the number of observers reporting dark skies. One interpretation is it that skies have gotten brighter over the six years of GaN campaign, but is this really the case?

Statistical analysis of the data is easily done using a spread sheet. In Table 1, we summarize the descriptive statistics of the data for each year: counts (that is, the number of observations), mean, standard deviation, standard error, five

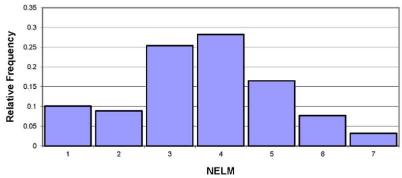

Figure 1a. 2006 frequency historgram.

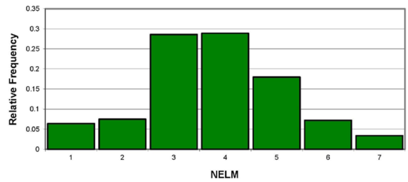

Figure 1b. 2007 frequency historgram.

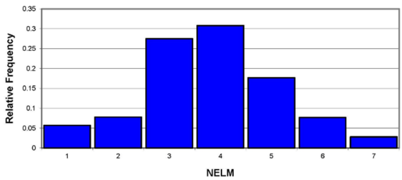

Figure 1c. 2008 frequency histogram.

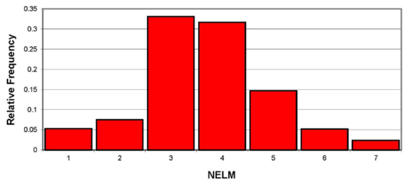

Figure 1d. 2009 frequency histogram.

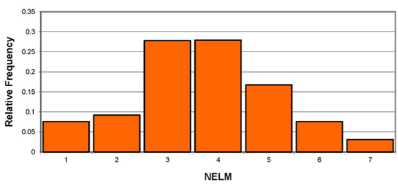

Figure 1e. 2010 frequency histogram.

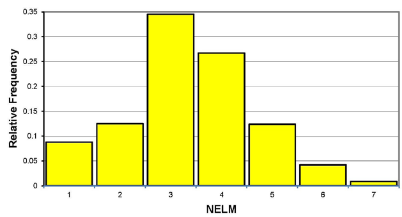

Figure 1f. 2011 frequency histogram.

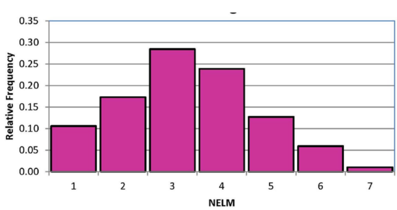

Figure 1g. 2012 frequency histogram.

Figure 1a–g. Frequency histograms of naked eye limiting magnitudes (NELMs) for Globe at Night data over the years 2006–2012. Given a reasonable uncertainty of ±1.0 associated with determining a matching chart for a given constellation, it appears that globally there has been no significant change in night sky brightness over the last six years.

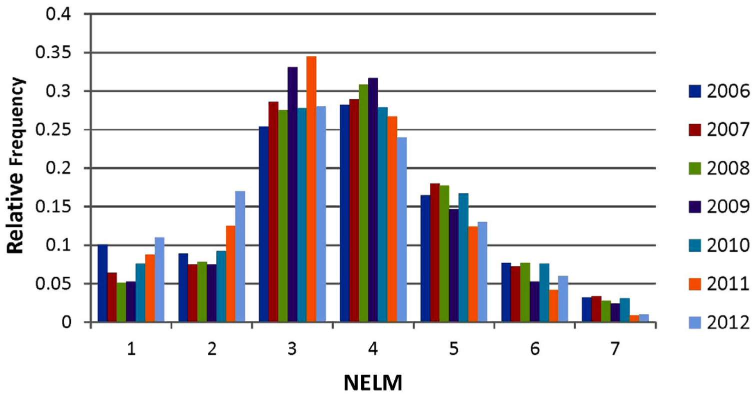

Figure 2. Naked-eye limiting magnitudes (NELMs) reported over the seven-year period of the Globe at Night project. Individual NELMs are plotted together and color coded by year. It appears that NELMs 1–3 exhibit a general upward slope, indicating that a larger fraction of observers reported brighter skies. NELMs 4–7, indicative of darker skies, appear to exhibit a general downward trend, indicating that a smaller fraction of participants reported darker skies.

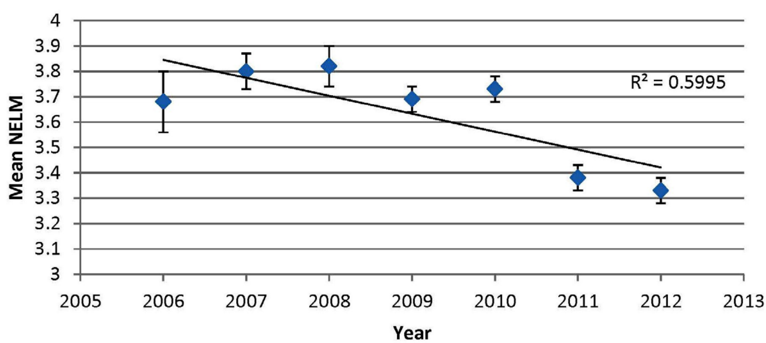

Figure 3. Mean global naked-eye limiting magnitudes (NELMs) reported over the seven-year period of the Globe at Night project. The error bars represent the five sigma confidence levels found in Table 1. A linear fit to the GaN data shows a weak trend toward brighter skies.

Table 1. Globe at Night NELM statistics.

Year	*Counts*	*Mean*	*Standard Deviation*	*Standard Error*	*5 Sigma Confidence*	*Skewness*
2006	3990	3.68	1.47	0.02	0.06	0.02
2007	7261	3.80	1.38	0.02	0.07	0.08
2008	5295	3.82	1.34	0.02	0.08	0.05
2009	14063	3.69	1.26	0.01	0.05	0.20
2010	14394	3.73	1.42	0.01	0.05	0.08
2011	12461	3.38	1.27	0.01	0.05	0.12
2012	14896	3.33	1.39	0.01	0.05	0.21

sigma confidence level, and skewness. The means are all relatively close and the data all exhibit a very small, but similar, skew. The mean NELM has remained relatively constant over the duration of the GaN project: for the first five years the mean has essentially remained constant at about 3.74 but in the last two years the average has dropped slightly to 3.36 (Figure 3).

Figure 3 exhibits a slight downward trend, indicating an overall brightening of skies over time. In keeping with a study of North America night sky brightness from 1947–2000 (Cinzano 2003) which determined that night sky brightness increased linearly over this period of time, we also adopt a linear fit to the GaN average NELM. However, with a correlation coefficient, that is, R^2, of 0.60 this corresponds to a 15 percent probability (Taylor 1997) that our seven NELM data points are uncorrelated with time. Therefore, we cannot argue conclusively that our skies are getting brighter. If we perform a one-tailed hypothesis test for the slope of the regression line, the null hypothesis is that the slope is zero and the alternative hypothesis is that the slope is less than zero; these correspond to the global average NELM being constant with time and decreasing with time, respectively. Using a spreadsheet to perform a regression analysis, the probability of the linear regression is 4.1%. Thus, we can reject the null hypothesis at the two sigma level but at the more rigorous three sigma level, we fail to reject the null hypothesis. We conclude that the global NELM appears to be constant over the seven years of Globe at Night campaigns.

According to urbanization data from the United Nations Department of Economics and Social Affairs (2013), there continues to be a world-wide trend toward urbanization. Over the period of the GaN project, this trend is strong in North America, South America, and Europe (http://esa.un.org/unup/Analytical-Figures/Fig_6.htm). If more Globe at Night observers are reporting from urban areas, the constant NELM values over time might actually be a sign of progress, in that we are not adding additional lighting to accommodate the increase in population in urban areas. This is an important question that future analyses of Globe at Night data may help answer as more data are added.

4. Observational errors: testing the reliability of GaN data

Many citizen science projects have individuals collecting data with little or no specialized scientific training. Most of these have been in the areas of biology and environmental studies (e.g. Rosales and Montan 2010, and references therein). In astronomy, the American Association of Variable Star Observers has led the promotion of public participation in the collection and reporting of astronomical data. Data collected by citizen volunteers have several advantages: they generally cover a larger geographic area, span a longer period of time, and are free. There has always been some concern regarding the quality of citizen science data. Fortunately, most studies show that well-trained volunteers do provide very reliable data (see, for example, Sachs *et al.* 2007; Alabri 2010; Malatesta *et al.* 2006; Cohn 2008).

How can we test the reliability of the Globe at Night data? Individual observations that include both a NELM and an SQM observation can be compared to the theoretical relationship in Equation 1. A couple of issues arose in the course of studying the reliability of the data that necessitated a "data filtering" stage. First, it was expected as part of the Globe at Night protocol that observers reporting SQM values were also to provide a simultaneous NELM value. This did not always happen: some SQM values were provided without a simultaneous NELM observation. To assess this, we removed all data that did not include both SQM and NELM values. In addition, sometimes the reported SQM and NELM values were grossly inconsistent; we used the sky brightness nomogram provided on the Dark Skies Awareness (2011) website (http://www.darkskiesawareness.org/nomogram.php) to remove data points that were clearly subject to high observational inaccuracy. An example of such a data point is a reported NELM of 2 when the SQM value is well above 19, indicating that the SQM reading was subject to either pointing error or shading due to buildings. In other instances, observers reported SQM values below 14 with NELM values well above the 0.5 expected from the sky brightness nomogram; this is likely the result of using an SQM too close to a nearby source of artificial light. The elimination rates for these apparent SQM pointing errors were between 1 and 3% for 2007 through 2010 and also in 2012. In 2011, the elimination rate was 9%. This relatively low elimination rate indicates at least nine out of ten SQM users appear to be using these devices correctly.

To test the reliability of the Globe at Night NELM data, we inserted the reported SQM values into Equation (1) and calculated the "expected" NELM value. We then plotted a frequency distribution of observed minus expected NELM values for all years of data from 2007 to 2012 (as per Schaefer 1990); the total number of data points was 6081. A histogram of the differences between observed and predicted NELMs based on reported SQM values is presented in Figure 4.

The histogram is essentially Gaussian in shape with a centroid of about –0.25 magnitude and a half-width-at half-maximum of about –1.0 magnitude. This half-width-at half-maximum is consistent with what we would expect for a reasonable limit on the uncertainty in observed NELM for an inexperienced observer. Note that a positive error value indicates that the observer saw fainter than expected based on the model, while a negative error indicates that the observer saw brighter than predicted.

We compared our results with that of Schaefer (1990), who developed a formula (which is different from Equation 1) for predicting telescopic limiting magnitudes based on zenith brightness. His group of 314 observations from 1990 shows a very similar qualitative distribution before correcting for observer experience. The centroid of his distribution is –0.24 with a half-width-half-

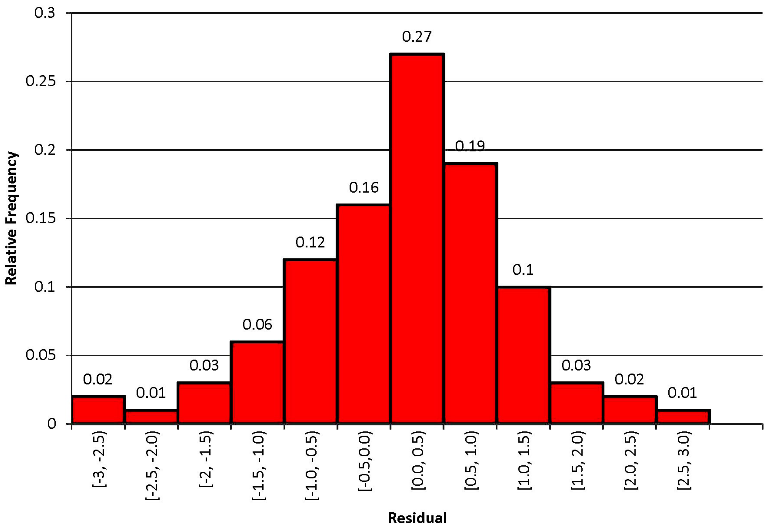

Figure 4. A histogram showing the distribution of observational errors for Globe at Night data. We plot observed minus predicted NELM values for 4,198 measured pairs of night sky bright using sky quality meters (in magnitudes per square arcsecond at zenith) and naked-eye limiting magnitudes for a given constellation (Orion, Leo, or Crux). The predicted values are calculated using Equation (1). A positive error value indicates that the observer saw fainter than expected. The histogram is roughly Gaussian in shape with a centroid of about –0.25 magnitude and a half-width-at half-maximum of about –1.0 magnitude.

maximum of 0.75. Schaefer's model was compared with 53 observations found in the astronomical literature, 17 observations made by himself and another professional astronomer, and 244 observations from a group of individuals who responded to a questionnaire Schaefer published in *Sky & Telescope* magazine. This group is therefore likely much more experienced than the GaN participants. The close agreement between Schaefer's distribution of errors and the GaN distribution is a good indicator that the GaN participants are submitting reliable data. Further support for the reliability of GaN data is the fact that the average GaN NELM correlates strongly with the light emitted upward as measured by the Defense Meteorological Satellite Program Operational Linescan System and with estimates of the World Atlas of Artificial Night SkyBrightness for European and North American skyglow (Kyba *et al.* 2013).

One interesting property of our distribution of errors is that the data appear to be weighted more on the side of positive errors than negative errors. In fact, for every positive error bin, the frequency is slightly higher than the corresponding negative error bin. Schaefer (1990) asked his participants to rate their experience level on a scale of 1 to 9 and was able to correct for observer experience. He found that more experienced observers tended to see fainter than less experienced observers. In fact, a very experienced observer might see a full magnitude fainter than an inexperienced observer. This could mean GaN observers tend to be a bit more optimistic and overestimate their NELMs. Alternatively, only about 6,000 of the total 62,682 reported observations have provided SQM values with corresponding NELMs. SQMs range in price from $120 to $135 plus taxes (U.S.) so, perhaps the group reporting SQM values represents a group of more experienced amateur astronomers and school teachers. GaN does not request information on observer experience, so at this point we do not have enough information to discriminate between these two possibilities.

5. Summary

The Globe at Night project was designed to increase public awareness of light pollution by having citizen-scientists around the world observe and report measured night sky brightness. It has evolved into a database of reliable measurements as demonstrated above. Our analysis of NELM data might seem to suggest that we have made little progress in decreasing light pollution on a global scale. On the other hand, the continuing urbanization of the global population with a nearly constant mean NELM seems to suggest some progress: we have not increased urban lighting to accommodate the additional urban inhabitants! Alternatively, perhaps we have simply gotten better at directing our light downward (Kyba et al. 2013). Determining the success of local or regional light pollution abatement projects will require a more sophisticated method of filtering data based on either identification of a city name or a restriction on the geographic coordinates.

6. Acknowledgements

The authors would like to thank the anonymous referee for many helpful suggestions that helped improve the focus and quality of this paper.

References

Alabri, A. 2010, *Bull. IEEE Tech. Committee Digital Libr.*, **6**, No. 2 (http://www.ieee-tcdl.org/Bulletin/v6n2/Alabri/alabri.html).

Bortle, J. E. 2001, *Sky & Telescope*, **101** (February), 126.

Cinzano, P. 2003, in *Light Pollution: The Global View*, ed. H. E. Schwarz, Cerro Tololo Inter-American Observatory, NOAO, La Serena, Chile, Astrophysics and Space Science Library 284, Kluwer Academic Publishers, Dordrecht, 39.

Cinzano, P., Falchi, F., and Elvidge, C. D. 2001, *Mon. Not. Roy. Astron. Soc.*, **328**, 689.

Cohn, J. P. 2008, *Bioscience*, **58**,192.
Dark Skies Awareness. 2011, Night Sky Nomogram (http://www.darkskiesawareness.org/nomogram.php), accessed August 8, 2011.
Dick, R. 2000, in *Amateur-Professional Partnerships in Astronomy*, ASP Conf. Ser. 220, eds. J. R. Percy, and J. B. Wilson, 221.
Dick, R. 2010, *J. Roy. Astron. Soc. Canada*, **104**, 257.
Globe at Night. 2013, website (http://www.globeatnight.org).
International Dark Sky Association. 2012, *Fighting Light Pollution: Smart Lighting Solutions for Individuals and Communities*, Stackpole Books, Mechanicsburg, PA, 9.
Knoll, H. A., Tousey, R., and Hulburt, E. O. 1946, *J. Opt. Soc. Amer.*, **36**, 480.
Kyba, C. C. M., Wagner, J. M., Kuechly, H. U., Walker, C. E., Elvidge, C. D., Falchi, F., Ruhtz, T., Fischer, J., and Hölker, F. 2013, *Sci. Rep.*, **3**, 1835 (http://www.ncbi.nlm.nih.gov/pmc/articles/PMC3655480/).
Malatesta, K. H., Beck, S. J., Menali, G., and Waagen, E. O. 2006, *J. Amer. Assoc. Var. Star Obs.*, **34**, 238.
Moore, C. A. 2001, *The George Wright Forum*, **18**, 46.
Rosales, J., and Montana, J. 2010, *Adirondack J. Environ. Sci.*, **16** (http://www.ajes.org/v16/rosal2010.php).
Sachs, S., Super, P. E., and Prysby, M. 2007, in *Protected Areas in A Changing World*, Proc. 2007 George Wright Soc. Conf., 281.
Schaefer, B. E. 1990, *Publ. Astron. Soc. Pacific*, **102**, 212.
Smith, M. G., Sanhueza, P., Schwarz, H. E., and Walker, A. R. 2006, *Bull. Amer. Astron. Soc.*, **38**, 1195.
Taylor, J. R. 1997, *An Introduction to Error Analysis: The Study of Uncertainties in Physical Measurements*, Univ. Science Books, Sausalito, CA, 290.
Unihedron. 2013, “Sky Quality Meter” (http://www.unihedron.com/projects/darksky).
United Nations Department of Urban Affairs. 2013, Urbanization data (http://esa.un.org/unup/Analytical-Figures/Fig_6.htm).
Zitelli, V., di Sora, M., and Ferrini, F. 2001, in *Preserving the Astronomical Sky*, IAU Symp.196, eds. R. J. Cohen, and W. T. Sullivan, 111.

Leslie Peltier: The World's Greatest Amateur Astronomer

Mike Simonsen
AAVSO Headquarters, 49 Bay State Road, Cambridge, MA 02138

One of the talks by AAVSO members who were past recipients of the Astronomical League's Peltier Award, presented at the 102nd Annual Meeting of the AAVSO, October 12, 2013; received November 19, 2013; accepted November 20, 2013

Abstract This paper is a brief account of the life of amateur astronomer Leslie C. Peltier, with reflections on how his astronomical accomplishments influenced the author's own involvement in variable star observing.

1. "The world's greatest non-professional astronomer"

"The world's greatest non-professional astronomer" is what Harlow Shapley called Leslie Peltier. If that is true, then why don't more people know about Peltier? I think the simple truth is he was a very private, soft-spoken man, who never sought the limelight and would have been embarrassed by all the attention he gets nowadays.


Leslie C. Peltier at the AAVSO Spring Meeting at Williams Observatory, Hood College, Frederick, Maryland, May 1932.

I've tried several times to write about Leslie Peltier, but every time before, I have begun thumbing through his classic book, *Starlight Nights*, for references and quotes and ended up reading the whole thing from cover to cover again instead of writing the piece that was my original intention. I'll never get tired of reading it. There are a lot of books that tell you how to observe the heavens and what you will find when you do, but this book always reminds me of why I love to be out under the stars at the eyepiece of a telescope, soaking in the sounds and smells of nature and admiring the majesty of the universe with my own eyes.

Born in January 1900 on a farm outside of Delphos, Ohio, Leslie grew up in a less complicated time, among the forests and farm fields of the area he lived in his entire life. If he was famous for anything, it was for his unwillingness to leave his home. He had everything he needed right there in Delphos—his family, his home, his gardens, and his observatories. Why would he want to leave any of that? So it was that later in his life people made the pilgrimage to come visit him. Leslie was not going to be making a public appearance anywhere near you. You had to go to the mountain.

As a boy Leslie was fascinated by the natural world around him. He read books from his family's home library and learned about the flora and fauna that appeared on and around his home in nature guides, such as *Wood's Natural History* and *Gray's Botany*. He thoroughly enjoyed identifying each new butterfly, bird, and flower. In 1977 he published *The Place On Jennings Creek*, a book relating twenty-five years of the gardens and critters that shared the natural setting of his home with him and his wife, Dorothy.

It's kind of surprising that it took Leslie until he was in high school to realize that his natural world extended upwards, over the tree tops, past the clouds, and out into the Universe into the night sky. He recalls in *Starlight Nights* the moment it dawned on him that he could name all the butterflies on his farm but didn't know the names of any of the stars in the heavens. He writes about that fateful May night:

> Something—perhaps it was a meteor—caused me to look up for a moment. Then, literally out of that clear sky, I suddenly asked myself: "Why do I not know a single one of those stars?"

Thus began an epic journey of discovery and observation that lasted the rest of his life. Peltier learned the stars on his own using only his eyes for the first year. He always felt this was the best way to learn the sky, as opposed to having someone teach the constellations or telescopic showpieces without investing the time and effort to become familiar with each one and its place in the heavens.

> Each star had cost an effort. For each there had been planning, watching and anticipation. Each one recalled to me a place, a time, a season. Each one now has a personality. The stars, in short, had become my stars.

His first telescope was purchased with earnings from picking strawberries. He had to pick 900 quarts at two cents a piece one summer to save up the $18.00 for his mail order 2-inch spyglass telescope. He made his own alt-azimuth mount for the telescope out of a left-over fencepost, an old grindstone, and discarded two-by-fours. This telescope served him well as he learned the sky and how to use a telescope to view the heavens.

His fatal attraction to variable stars and the AAVSO began when he wrote a letter to AAVSO founder William Tyler Olcott asking how he could contribute to science with his small telescope. Olcott wrote back explaining that observing variable stars was an exciting and scientifically useful way to spend one's time under the stars, and from the time Leslie was eighteen until his death in 1980 he never missed sending in a monthly report of variable star observations to AAVSO Headquarters in Cambridge, Massachusetts. His description of how variable star observing changed his life forever is something I have quoted often to many people.

> Life was never quite the same for me after that winter walk to town. The charts that I brought home with me were potent and ensnaring and I feel it my duty to warn any others who may show signs of star susceptibility that they approach the observing of variable stars with the utmost caution. It is easy to become an addict and, as usual, the longer the indulgence is continued the more difficult it becomes to go back to a normal life.

In 1919, Peltier was given the first of several telescopes that would be loaned or given to him outright based on his exceptional observing skills and perseverance. The AAVSO loaned him a 4-inch refractor with which to make variable star observations, and he immediately put it to good use by observing even fainter variable stars. Two years later, after enduring hundreds of nights in the dew and cold, his father suggested it was time they build a proper observatory for Leslie. This observatory soon housed an even larger telescope, the "Comet Seeker."

In 1925, he discovered his first comet, using the Comet Seeker, a 6-inch refractor on loan from Henry Norris Russell of Princeton University. He would go on to discover eleven more comets in his lifetime, the last one in 1954. He also discovered four naked-eye novae and made a habit of checking up on some old novae that still varied and occasionally had recurrent outbursts.

I think my favorite Leslie Peltier story is his experience with T CrB. He had faithfully observed T CrB every night for twenty-five years when finally in 1946 it rose once again for the first time in eighty years, and where was Leslie? Asleep in bed, thinking he might be coming down with a cold. And thus he missed the night of nights in the life of T Coronae Borealis.

> I alone am to blame for being remiss in my duties, nevertheless, I still have the feeling that T could have shown me more consideration. We had been friends for many years; on thousands of nights I had watched over it as it slept, and then it arose in my hour of weakness as I nodded at my post. I still am watching it but now it is with a wary eye. There is no warmth between us any more.

In 1959, life took a very unexpected turn when Miami of Ohio University offered to give Leslie their 12-inch Clark refractor, complete with observatory, dome, and transit room! The entire observatory was cut into sections and delivered 125 miles to the Peltier home, where it was re-assembled and served Leslie as he strove to observe the faint minima of many of the variables he followed for decades. With this telescope he could follow stars down to 15th or 16th magnitude, far fainter than his other telescopes would allow. In total, Leslie Peltier submitted over 132,000 variable star observations to the AAVSO, making him one of the all-time leading observers in history.

Peltier's life was a long, steady, calm procession of days and nights lived to the fullest and enjoyed for their blessings, punctuated by events like the appearance of a new comet or nova, or unexpected recognitions for doing what Leslie would have done even if no one had noticed.

Overcoming his lack of formal education (Leslie dropped out of school after the tenth grade to work on his father's farm), he received an honorary doctorate from Bowling Green State University in 1947. In 1965, a mountain in California, home of the AAVSO's Ford Observatory, was named Mt. Peltier in his honor. In 1975, he received an honorary high school diploma from his hometown's Delphos Jefferson High School.

In his obituary, written by friend and fellow AAVSOer Carolyn Hurless, she says,

> Leslie was able to accomplish all he did because he was a private person. He lived exactly as he wanted to. He did nothing he didn't wish to do and was able to say "no" very easily. He was very uncomfortable with those who sought him out because he was famous, but to those fellow variable star observers who visited, he was a warm and welcoming individual.

Shortly after his death in 1980, the Astronomical League established The Leslie C. Peltier Award "to be presented to an amateur astronomer who contributes to astronomy observations of lasting significance," and that is where our histories finally intersect. In July 2012, I became the 30th recipient of the Leslie Peltier Award at the Astronomical League Convention in Chicago, Illinois.

Finding myself uncharacteristically speechless and unprepared, this is what I wish I would have said when asked to say a few words.

> I've known about Leslie Peltier, the great amateur astronomer and variable star observer, for years. I've heard the reverence in people's voices when he is mentioned in conversation. I've read *Starlight Nights* more than any other book I can think of. And when I do, I'm always struck by the similarities in our experiences.

I too learned the sky and the names of all the stars and constellations on my own, through books and star charts borrowed from the library. I earned the money to buy my first telescope by getting up early in the morning and delivering papers door to door for far longer than I ever dreamed I could endure.

Peltier's story about seeing something in the sky he couldn't explain during the UFO-crazed 1950s—and the fact that it turned out to be geese flying in formation—is exactly like the story I have told my friends and will share with my grandchildren one day about a winter night in 1980.

My father helped me construct my first domed observatory and I still use the pier he welded for me to observe visually with my 12-inch Schmidt-Cassegrain.

I too, have received a telescope on loan from the AAVSO with which to observe variable stars. Even the opening paragraphs of *Starlight Nights*, where he describes walking down the path towards the two stark-white structures as night falls, reminds me of my walk to my observatories each clear night.

But when he writes about his love of variable stars, and how he gets excited each night, year after year, to go spend some time with his old friends, that is when I hear my passion and my words coming off the page. I am a hopeless variable star addict like Leslie, having now submitted over 85,000 observations of my own to the AAVSO, and indeed, my life will never be the same.

Awards and accolades are great, but like Leslie, I would have done it all anyway. I don't think I really had a choice.

It is because of who this award is named for that it means so very much to me. I'd like to thank my wife, Irene, for supporting me and enabling my addiction. Thank you to the Astronomical League for this very special and meaningful recognition. And thank you, Leslie Peltier, for being an inspiration and role model for amateur astronomers everywhere who want to reach for the stars and explore the Universe on their own terms, in their own time, and in their own way.

References

Peltier, L. C. 1965, *Starlight Nights: The Adventures of a Star-Gazer*, Harper & Row, New York.

Peltier, L. C. 1977, *The Place on Jenning's Creek*, Adams Press, Chicago.

Abstracts of Papers and Posters Presented at the 102nd Annual Meeting of the AAVSO, Held in Woburn, Massachusetts, October 11–12, 2013

Invited Guest Speaker

Dr. George R. Ricker
Massacuhsetts Institute of Technology, Cambridge, Massachusetts

The Transiting Exoplanet Survey Satellite Mission

Abstract The Transiting Exoplanet Survey Satellite (TESS) will discover thousands of exoplanets in orbit around the brightest stars in the sky. In a two-year survey of the solar neighborhood, TESS will monitor more than 500,000 stars for temporary drops in brightness caused by planetary transits. This first-ever spaceborne all-sky transit survey will identify planets ranging from Earth-sized to gas giants, around a wide range of stellar types and orbital distances.

TESS stars will typically be 30 to 100 times brighter than those surveyed by the Kepler satellite; thus,TESS planets will be far easier to characterize with follow-up observations. For the first time it will be possible to study the masses, sizes, densities, orbits, and atmospheres of a large cohort of small planets, including a sample of rocky worlds in the habitable zones of their host stars. All of the half-million plus TESS targets will be observed at a rapid cadence (1 minute or less). Hence, the brighter TESS stars will potentially yield valuable asteroseismic information. TESS will provide prime exoplanet targets for characterization with the James Webb Space Telescope (JWST), as well as other large ground-based and space-based telescopes of the future.

TESS will serve as the “People’s Telescope,” with data releases every 4 months, inviting immediate community-wide efforts to study the new planets. The TESS legacy will be a catalog of the nearest and brightest main-sequence stars hosting transiting exoplanets, which will endure as the most favorable targets for detailed future investigations.

TESS has been selected by NASA for launch in 2017 as an Astrophysics Explorer mission.

Paper Session: The Role of Amateur Astronomers in the Age of Large-Scale Surveys

Invited Talk: Photometry of Bright Variable Stars with the BRITE Constellation Nano-Satellites: Opportunities for Amateur Astronomers

Edward F. Guinan
Department of Astronomy and Astrophysics, Villanova University, Villanova, PA 19085; edward.guinan@villanova.edu

Abstract The BRIght Target Explorer (BRITE) is a joint Austrian-Canadian-Polish Astronomy mission to carry out high precision photometry of bright (mv < 4 mag.) variable stars. BRITE consists of a "Constellation" of 20 × 20 × 20-cm nano-satellite cubes equipped with wide field (20 × 24 deg.) CCD cameras, control systems, solar panels, onboard computers, and so on. The first two (of up to six) satellites were successfully launched during February 2013. After post-launch commissioning, science operations commenced during October 2013. The primary goals are to carry out continuous multi-color (currently blue and red filters) high-precision millimag (mmag) photometry in particular locations in the sky. Typically these pointings will last for two to four months and secure simultaneous blue/red photometry of bright variable stars within the field. The first science pointing is centered on the Orion region.

Since most bright stars are intrinsically luminous, hot O/B stars, giants, and supergiants will be the most common targets. However, some bright eclipsing binaries (such as Algol, β Lyr, ε Aur) and a few chromospherically-active RS CVn stars (such as Capella) may be eventually be monitored. The BRITE-Constellation program of high precision, two-color photometry of bright stars offers a great opportunity to study a wide range of stellar astrophysical problems. Bright stars offer convenient laboratories to study many current and important problems in stellar astrophysics. These include probing stellar interiors and pulsation in pulsating stars, tests of stellar evolution, and structure for Cepheids and other luminous stars.

To scientifically enhance the BRITE science returns, the BRITE investigators are very interested in securing contemporaneous ground-based spectroscopy and standardized photometry of target stars. The BRITE Ground Based Observations Team is coordinating ground-based observing efforts for BRITE targets. The team helps coordinate collaborations with amateur and professional astronomers. The ground-based coordinators are Thomas Eversberg (thomas.eversberg@dlr.de) and, for spectroscopy, Contanze Zwintz (konstanze@ster.kuleuven.be). Detailed information about the BRITE Mission is provided at: www.brite-contellation.at.

Using the Transient Surveys

Arne A. Henden
AAVSO Headquarters, 49 Bay State Road, Cambridge, MA 02138; arne@aavso.org

Abstract We are starting the era of all-sky surveys. While some, like APASS, have specific goals in mind (sky calibration, exoplanets, asteroids, and so on), others have begun releasing real-time alerts of interesting objects. The easily available surveys with alerts will be discussed, along with the kind of objects they are detecting and some hints about how to make use of the transient information.

Kepler and the RR Lyrae Stars

Katrien Kolenberg
Harvard-Smithsonian Center for Astrophysics, 60 Garden Street, Cambridge, MA 02138; kkolenb@cfa.harvard.edu

Abstract The spectacular data delivered by NASA's Kepler mission have not only boosted the discovery of planets orbiting other stars, but they have opened a window on the inner workings of the stars themselves. For the study of the RR Lyrae stars, Kepler has provided a breakthrough. To date, over fifty RR Lyrae stars are known in the Kepler field.

I will present some of the most interesting results on RR Lyrae stars obtained through Kepler so far. Though high-precision satellite data have led to new insights, amateur observations of these stars remain extremely valuable and can complement the space data.

A Study of RR1 Light Curve Modulation in OGLE-III Bulge Time-Series

Douglas L. Welch
100 Melville St., Dundas, Ontario L9H 2A3, Canada; welch@physics.mcmaster.ca

Abstract We report the preliminary results of our study of lightcurve modulation in a sample of 493 RR1 variables from the OGLE-III survey of galactic bulge fields. Each object in this list has 1,500 or more I-band observations. We have located a "modulated-Blazhko" RR1 variable, OGLE-BLG-RRLYR-03825, which is similar in many respects to LS Her, a galactic field RR1 star. OGLE-BLG-RRLYR-03825's photometric period is 0.2774114 d and it has a Blazhko period of 16.469 d which is, itself, modulated with a period of 339.2 d.

Using an application of the "sequential CLEANest" method, we find that 169 of the 493 RR1 lightcurves examined show a detectable peak within the amplitude spectrum near 0.63 times the photometric period. Our finding extends the detection of such a period ratio in the four known RR1 stars in the Kepler field by Moskalik *et al.* (2012). We discuss how the appearance of this apparently new mode correlates with photometric (first overtone) period in this sample.

Two Centuries of Observing R Coronae Borealis: What Will the Role of the AAVSO be in the Next Century?

Geoffrey C. Clayton
Department of Physics and Astronomy, Louisiana State University, Baton Rouge, LA 70803; gclayton@fenway.phys.lsu.edu

Abstract R Coronae Borealis was found to be variable in the year 1783, and was one of the first variable stars to be identified. Its class, the R Coronae Borealis (RCB) stars, are rare hydrogen-deficient carbon-rich supergiants. RCB stars undergo massive declines of up to 8 mag due to the formation of carbon dust at irregular intervals. Their rarity may stem from the fact that they are in an extremely rapid phase of evolution or in an evolutionary phase that most stars do not undergo. Several evolutionary scenarios have been suggested to account for the RCB stars, including a merger of two white dwarfs (WDs) or a final helium shell flash in a PN central star. The large overabundance of the rare isotope oxygen-18 found in most of the RCB stars favors the WD merger scenario while the presence of lithium in the atmospheres of five of the RCB stars favors the FF scenario. In particular, the measured isotopic abundances imply that many, if not most, RCB stars are produced by WD mergers, which may be the low-mass counterparts of the more massive mergers thought to produce Type Ia supernovae. Understanding these enigmatic stars depends to a large extent on continuous monitoring to catch their irregular but rapid variations due to dust formation, their variations due to stellar pulsations, and longterm changes that may occur over centuries. The AAVSO has been instrumental in this monitoring for over a century, but how will this change in the era of all-sky surveys?

General Paper Session

Unpredictable LPVs: Stars Dropped from the *AAVSO Bulletin*

Matthew R. Templeton
Elizabeth O. Waagen
AAVSO Headquarters, 49 Bay State Road, Cambridge, MA 02138; matthewt@aavso.org

Abstract A number of LPVs have been dropped from the *AAVSO Bulletin* over its history going all the way back to the days of Leon Campbell and Margaret Mayall. Many of these stars exhibit very interesting changes in behavior as recorded in their long-term visual light curves; they were dropped not for being uninteresting but simply for being too difficult to predict. We present highlights from this collection of stars and their light curves, with suggestions on what could be learned from both existing data and new observations.

Aperture Fever and the Quality of AAVSO Visual Estimates: μ Cephei as an Example

David G. Turner
Saint Mary's University, Department of Astronomy and Physics, 923 Robie Street, Halifax, NS B3h 3C3, Canada; turner@ap.smu.ca

Abstract At the limits of human vision the eye can reach precisions of 10% or better in brightness estimates for stars. So why did the quality of AAVSO visual estimates suddenly drop to 50% or worse for many stars following World War II? Possibly it is a consequence of viewing variable stars through ever-larger aperture instruments than was the case previously, a time when many variables were observed without optical aid. An example is provided by the bright red supergiant Cepheid variable μ Cephei, a star that has the potential to be a calibrating object for the extragalactic distance scale if its low-amplitude brightness variations are better defined. It appears to be a member of the open cluster Trumpler 37, so its distance and luminosity can be established provided one can pinpoint the amount of interstellar extinction between us and it. μ Cep appears to be a double-mode pulsator, as suggested previously in the literature, but with periods of roughly 700 and 1,000 days it is unexciting to observe and its red color presents a variety of calibration problems. Improving quality control for such variable stars is an issue important not only to the AAVSO, but also to science in general.

The Eggen Card Project

George Silvis
194 Clipper Road, Bourne, MA 02532; george@gasilvis.net

Abstract Olin Eggen, noted astronomer (1919–1998), left to us all his raw observation records recorded on 3×5 cards. The AAVSO has these cards on longterm loan from the Cerro Tololo Interamerican Observatory. This project is to make all these data available as an online resource. History and progress of the project will be presented. The 100,000 cards have been scanned and made into PDF files. The current phase of the project is to identify the star(s)

referenced on each card. This work is being done via crowdsourcing—you can help! Project details are available at: https://sites.google.com/site/eggencards/home. [*Ed note: see also Silvis' poster abstract, "Coding the Eggen Cards," in this issue.*]

AAVSO Visual Sunspot Observations vs. SDO HMI Sunspot Catalog

Rodney Howe
3343 Riva Ridge Drive, Fort Collins, CO 80526; ahowe@frii.com

Abstract The most important issue with regard to using the SDO HMI data from the National Solar Observatory (NSO, http://www.nso.edu/staff/fwatson/STARA) is that their current model for creating sunspot counts does not split in groups and consequently does not provide a corresponding group count and Wolf number. As it is a different quantity, it cannot be mixed with the data from our sunspot networks. Although, for the AAVSO, with about seventy stations contributing each day, adding HMI sunspot data would hardly change the resulting index.

Perhaps the best use of HMI data is for external validation, by exploiting the fact that HMI provides a series that is rather close to the sunspot number and is acquired completely independently. So, it is unlikely to suffer from the same problems (jumps, biases) at the same time. This validation only works for rather short durations, as the lifetime of space instruments is limited and aging effects are often affecting the data over the mission. In addition, successive instruments have different properties: for example, the NSO model has not managed yet to reconcile the series from MDI and HMI. There is a ~10–15% jump.

The first challenge that should be addressed by AAVSO using HMI data is the splitting in groups and deriving group properties. Then, together with the sunspot counts and areas per group, a lot more analyses and diagnostics can be derived (such as the selective disappearance of the smallest sunspots?) that can help interpreting trends in the ratio SSN/other solar indices and many other solar effects.

Identification of Cepheid Variables in ASAS Data (Poster abstract)

Vanessa Swenton
Department of Physics and Earth Sciences, Central Connecticut State University, 1615 Stanley Street, New Britain, CT 06053; address email correspondence to Larsen@ccsu.edu

Kristine Larsen
Department of Physics and Earth Sciences, Central Connecticut State University, 1615 Stanley Street, New Britain, CT 06053; Larsen@ccsu.edu

Abstract Through studying the characteristics of Cepheid variables, we can further understand the nature and evolution of stars, as well as the scale of the Universe (through the famous Leavitt period-luminosity relationship). Classical Cepheid stars, or Type I Cepheids, are radially-pulsating supergiants. Type II Cepheids are older and have lower mass than Type I Cepheids. They are rarer, and existing classifications of these stars have been shown to be erroneous at unusually high rates. Computerized automatic classification programs sift through the data of large photometric surveys to produce a list of (what the program recognizes as) Cepheid star candidates. Unfortunately, this automatic classification of light curves has been demonstrated to be ambiguous. Therefore, it takes a human to further sift through the list in order to come up with a more accurate (and, as a result, a more useful) list of probable Cepheids. This study was based on a list of 3,548 Cepheid candidates in the ASAS data provided by Patrick Wils (through Dr. Doug Welch). Patrick Wils had previously examined eighty-four stars on the spreadsheet and positively identified only five of these stars as Cepheids. The methodology of the current study was to use known properties of Cepheids, including available infrared photometry (2MASS), proper motion (PPMXL), and X-Ray emission (ROTSE) data (for which we received helpful guidance from Sebastian Otero), to cull the list to the most likely Cepheids. The ASAS light curves of these candidates were investigated to determine whether the shapes were truly consistent with those of Cepheids. This poster will summarize the methodology used and give examples of how individual Cepheid candidates were evaluated. Candidates of interest are currently being crosschecked for any updated information on VSX, and the light curves more closely analyzed using VStar. Results concerning the misidentification of candidate Cepheids will be reported to VSX and summarized in *JAAVSO*.

Identification of BY Draconis Variable Stars among ASAS Cepheid Candidates (Poster abstract)

Jessica Johnson
Department of Physics and Earth Sciences, Central Connecticut State University, 1615 Stanley Street, New Britain, CT 06053; address email correspondence to Larsen@ccsu.edu

Kristine Larsen
Department of Physics and Earth Sciences, Central Connecticut State University, 1615 Stanley Street, New Britain, CT 06053; Larsen@ccsu.edu

Abstract Cepheid variables are well-known to be important to astronomers, as their period-luminosity relationship (the Leavitt relationship) is used to determine the distances to galaxies. The unambiguous identification of newly discovered Cepheid variables in large photometric data sets is therefore of significance. A data set of 3,548 candidate Cepheid variable stars in the ASAS data was provided by Patrick Wils (through Dr. Doug Welch). A computer program had originally identified these candidates, however, Wils investigated a small subset of the data by hand and discovered that the vast majority of these stars were misidentified. The most common misidentification was of BY Draconis stars (rotating spotted K and M dwarfs). In a companion piece, Swenton and Larsen [see above] sought out the most likely Cepheid candidates in the data; the work discussed here is instead focused on looking at stars that had properties that were clearly different from Cepheids, more specifically properties likely to be seen in BY Dra stars. We are sorting the spreadsheet stars by characteristics in order to find as many BY Dra variables as possible (since they seem to be the most commonly misidentified stars). Resources for these characteristics include newly available infrared photometry (2MASS), proper motion (PPMXL), and X-Ray emission (ROTSE) data (for which we received helpful guidance from Sebastian Otero), as well as VSX information. The first 103 stars to be studied are those with the smallest range in magnitude (less than or equal to 0.1). An analysis of their light curves and other available data is being undertaken in order to determine whether or not they are indeed BY Dra-type variables. In doing so the goal is to be able to submit and publish the correct identifications for these stars to the International Variable Star Index (VSX) and *JAAVSO*.

Summer Student Solar Observing Project Determining the Sunspot Number (Poster abstract)

Brian Mason

Abstract While modern telescopes and instruments generate much more astrophysical data, the Wolf Index (established 1848) provides a very long term measure of Solar activity through the Sunspot count. Interns from the USNO have, since at least 2005, contributed to the mean Wolf Index calculated by the American Association of Variable Star Observers.

The DASCH Public Data Release (Poster abstract)

Edward J. Los
Harvard College Observatory, 60 Garden Street, Cambridge, MA 02138

Abstract The plate stacks of the Harvard College Observatory, one of the original large scale sky surveys, contains an estimated 30–50 × 10^9 star images spanning over 100 years. The Digital Access to a Sky Century @ Harvard (DASCH) is in the process of digitizing this archive and computing magnitudes for these images. This poster describes the public release of photometry data from approximately 29,000 scanned plates.

Coding the Eggen Cards (Poster abstract)

George Silvis
194 Clipper Road, Bourne, MA 02532; george@gasilvis.net

Abstract This poster presents a look at the Eggen Portal for accessing the Eggen cards, as well as a call for volunteers to help code the cards: 100,000 cards must be looked at and their star references identified and coded into the database for this to be a valuable resource. [*Ed. note: see also Silvis' talk abstract, "The Eggen Card Project," in this issue.*]

Observations of an Eclipse of Bright Star b Persei by the Third Star in February 2013: Erratum

Donald F. Collins
138 College View Drive, Swannanoa, NC 28778; dcollins@warren-wilson.edu

In the abstract "Observations of an Eclipse of Bright Star b Persei by the Third Star in February 2013" (*JAAVSO*, 2013, **41**, 149–150), the subject star name was incorrectly given in production. "β Persei" and "β Per" should read "b Persei" or "b Per". The same error was reproduced in the Author Index (page 211) and in the Subject Index (pages 403, 405, 406, 410, 413 (twice), 418, 420, 422, and 424).